Electronic Theses and Dissertations   Graduate School

1-1-2013

Molecular modeling and SAR studies of CDK5/p25 selective inhibitors

Arindam Chatterjee
University of Mississippi

MOLECULAR MODELING AND SAR STUDIES OF CDK5/p25 SELECTIVE INHIBITORS

A Dissertation
presented in partial fulfillment of requirements for the degree of
Doctor of Philosophy
in the Department of Medicinal Chemistry
The University of Mississippi

by

ARINDAM CHATTERJEE

November 2013

ABSTRACT

Alzheimer's disease (AD) is one of the most dreaded forms of progressive neurodegenerative diseases. The two main hallmarks of AD are the formation of amyloid senile plaques and neurofibrillary tangles. Cyclin dependent kinase 5 (CDK5) is a proline directed Serine/Threonine kinase, which expressed primarily in the central nervous system. In the biochemical process the CDK5-natural activator, p35 is cleaved by calpain to a shorter protein p25, which in turn hyperphosphorylates Tau, forms neurofibrillary tangles and causes AD. CDK5 deregulation is also indicated in other neurodegenerative diseases, such as Huntington's chorea, stroke, Parkinson's disease, amyotrophic lateral sclerosis, major depression and substance abuse.

We chose to design CDK5/p25 inhibitors as a target against neurodegeneration leading to Alzheimer's disease. One of our major goals was to design CDK5/p25 inhibitors selective over CDK2. Since we were targeting neurodegeneration we wanted to avoid any undesired cell cycle mediated apoptotic effects of CDK2 inhibition. The task was very challenging, because the two kinases possessed very high levels of sequence homology. In our approach we decided to achieve selectivity through structure based virtual screening strategy, validate the hits through biological screening and explore structure activity relationship (SAR) modifications around the lead structure.

To identify *de-novo* templates, we decided to use the structure based E-pharmacophore models coupled with docking based virtual screening workflow to screen a commercially available database containing 2.84 million compounds. The biological screening was performed

using radiometric filter binding assays with full length hCDK5/p25 and hCDK2/E kinases. An ATP non-competitive and selective inhibitor with ligand efficiency of 0.3 was identified as the lead molecule.

We developed an efficient six-step synthesis of a key intermediate starting from aniline utilizing a sequence of Friedel-Crafts, Vilsmeier-Haack, nucleophilic aromatic substitution and cyclization reactions. We also developed an easy derivatization approach utilizing convergent analog synthesis to study SAR around the lead structure.

Further SAR optimization led to the discovery of several low micromolar ATP non-competitive CDK5/p25 inhibitors with much greater CDK2/E selectivity. This new series of compounds can be further evaluated in *in-vitro* and *in-vivo* AD models to develop future drug candidates.

DEDICATION

To my mom, dad, loving wife and son

Whose every wishes came true in the pages of this dissertation

LIST OF ABBREVIATIONS

RAM = Random access memory

SAR = Structure activity relationship

LE = Ligand efficiency

AIBN = 2,2' Azobisisobutyronitrile

HBTU = N,N,N',N'-Tetramethyl-O-(1H-benzotriazol-1-yl)uronium hexafluorophosphate

ADME = Absorption, distribution, metabolism, and excretion

dppf = 1,1'-Bis(diphenylphosphino)ferrocene

DCM = Dichloromethane

THF = Tetrahydrofuran

EtOAc = Ethyl acetate

NaOEt = Sodium ethoxide

NaOAc = Sodium acetate

EtOH = Ethanol

PPA = Polyphosphoric acid

AcOH = Acetic acid

NBS = N-Bromosuccinimide

ACN = Acetonitrile

KOtBu = Potassium *tert*-butoxide

DMF = Dimethylformamide

KN(SiMe$_3$)$_2$ = Potassium bis(trimethylsilyl)amide

MeOH = Methanol

iPr$_2$Net = N,N-Diisopropylethylamine

POCl$_3$ = Phosphorus oxychloride

mw = Microwave

$cat.$ = Catalytic

K$_2$CO$_3$ = Potassium carbonate

$anhyd.$ = Anhydrous

GScore = Glide score

ACKNOWLEDGEMENTS

I would like to thank my two mentors and major professors Dr. John S. Williamson and Dr Stephen J. Cutler for their relentless guidance and support throughout this project. My heartiest gratitude goes to them for believing in me and making me grow into an independent researcher.

I am thankful to Dr. Robert J. Doerksen for sharing his knowledge and recommending me to preside a computational chemistry session at Indianapolis ACS meeting, 2013.

I am thankful to Dr. Avery for teaching two great courses on heterocyclic chemistry and total synthesis. Also I would like to thank him for allowing me to use his laboratory to pursue this project.

I am thankful to Dr. Ikhlas A. Khan for his help and encouragement during the difficult times of the project.

I am thankful to Dr. John M Rimoldi and Dr. Christopher R. McCurdy for allowing me to use the instruments in their labs.

I am extremely thankful to Dr. Ronald F. Borne for his encouragement throughout the program and his help in critically evaluating the manuscripts.

I would also like to thank Dr. Zia Shariat-Madar and Dr. Asok DasMahapatra for their help during the fluorescence based assay development.

I am thankful to Dr. Francisco Leon, Dr. Sridevi Ankisetty, Dr. Kuldeep K. Roy, Dr. Khaled Elokely and Mr. Frank Wiggers for their help and friendship.

TABLE OF CONTENTS

LIST OF TABLES

LIST OF FIGURES

LIST OF SCHEMES

CHAPTER 1: INTRODUCTION

1.1. Alzheimer's disease

Alzheimer's disease (AD) is one of the most dreaded forms of progressive neurodegenerative diseases. According to a recent report, AD is the sixth leading cause of death in United States and is estimated to affect about 14 million individuals by the year 2050.[1] The neuropathological hallmarks of AD were identified in 1906, when Dr Alois Alzheimer, a German physician, performed an autopsy on a cognitively impaired patient. The two main hallmarks leading to AD are the formation of amyloid senile plaques (SP) and neurofibrillary tangles (NFT).[2] SPs are extra-cellular and mainly composed of β-amyloid (Aβ) peptides, whereas intra-cellular NFTs are considered to be the downstream product of the hyper-phosphorylated tau, a microtubule associated protein.[2, 3]

The Aβ peptides are formed by the proteolytic cleavage of the amyloid precursor protein (APP) by a complex enzymatic action involving β-site amyloid precursor protein-cleaving enzyme 1 (BACE-1), a β-secretase and γ-secretase. In general, an imbalance between the clearance and production causes Aβ to accumulate and in the long run causes AD. On the other hand, the NFT formation occurs from taupathies.[4] Tau is a phospho-protein, which involves mainly in neuronal tubulin polymerization and microtubule stabilization. Tau phosphorylation occurs during the normal process of neuronal development and is regulated by several protein kinases and phosphatases. But in taupathies, normal tau phosphorylation is deregulated, which leads to hyperphosphorylation. To date at least 85 tau phosphorylation sites has been described and a number of protein kinases are involved in these processes.[5] Among them proline-directed kinases (PDPK), such as glycogen synthase kinase 3 (GSK-3), cyclin dependent kinase 5 (CDK 5) and mitogen-activated protein kinases (MAPK) account for the phosphorylation of the

residues around the tubulin-binding region of the tau protein. Some other non-PDPK group of kinases, such as tau-tubulin kinases (TTBK), protein kinase A (PKA), protein kinase C (PKC), casein kinase (CK), microtubule affinity-regulated kinases (MARK) and calcium/calmodulin-dependent protein kinases (CAMK) are involved in taupathies as well.

Most normal adult neurons are post mitotic and don't participate in cell cycle, while AD neurons re-enter the cell cycle but fail to complete mitosis and die. A recent theory hypothesizes neuronal cell cycle re-entry is the key step in the development of AD, which in turn produces Aβ accumulation through tau.[6] Some of the other popular theories include oxidative stress, mitochondrial dysfunction, disturbance in insulin-signaling pathway, vascular lesions, inflammation, elevated cytosolic calcium concentration, defective cholesterol metabolism etc. The currently available drugs, which can control the symptoms of cognitive impairment, are actylcholinesterase (ACh) inhibitors, such as aricept, exelon and razadyne. These drugs do not cure AD, but it improves the cognitive functions by increasing the ACh levels in the neurons. Currently there are several drugs undergoing clinical trials in AD patients, such as γ-secretase inhibitors, like semagacestat, avagacestat; β-secretase inhibitor like LY2886721 and Aβ immune-modulators like bapineuzumab and solanezumab. Unfortunately, these haven't demonstrated any successes so far.

One of the many mechanistic pathways leading to hyperphosphorylation of tau suggests the involvement of an atypical cyclin-dependent kinase (CDK), CDK5.[7-9] We concentrated our focus on CDK5 inhibitors as a target for AD.

1.2. Cyclin Dependent Kinase (CDK)

CDK5 is a proline-directed serine/threonine kinase (STK), belongs to a group of cyclin dependent kinase (CDK) family. To-date the CDK family consists of 20 CDKs (CDK1-20). CDKs are mainly involved in cell cycle process. The cell cycle of eukaryotic cells consist of four main successive phases: G1 phase (first gap), S phase (DNA synthesis), G2 phase (second gap) and M phase (mitosis) as described in Figure 1.1.
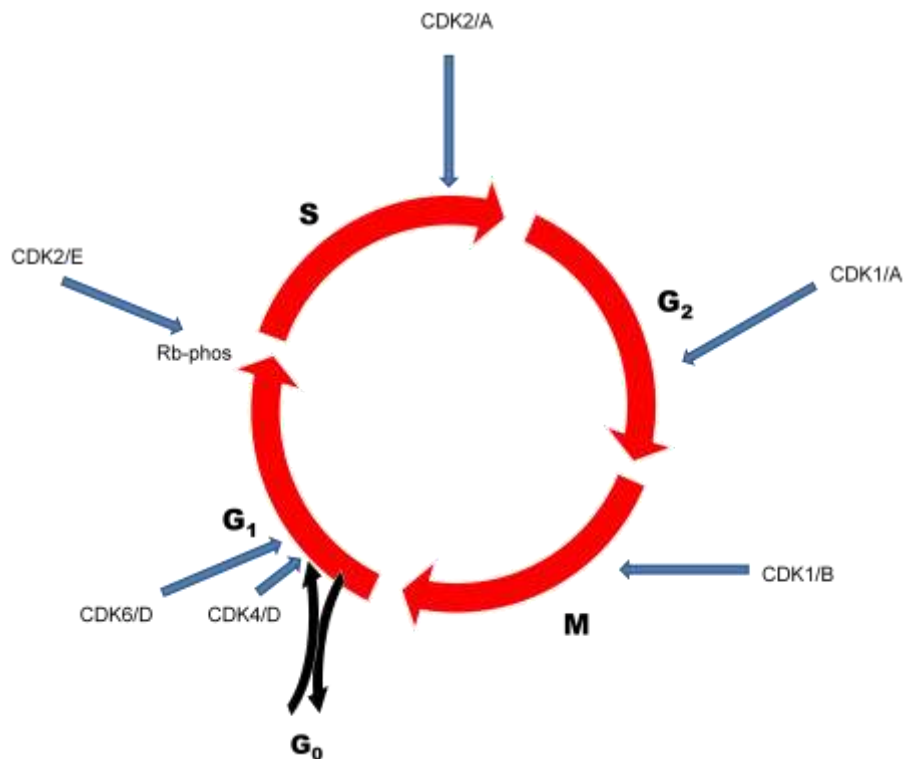
Figure 1.1.   Cell Cycle Process

During G1, the activation of CDK4 and CDK6 with cyclin D, phosphorylates retinoblastoma protein (Rb), and inhibits the binding of transcription factor E2F-1. The E2F-1 is released and participates in the transcription in the next stages. In the late phase of G1, activation of CDK2/E ensures the G1/S transition. Throughout the S phase, CDK2/A phosphorylates various substrate to proliferate DNA replication. The DNA replication ends at the S phase, and

cells enter G2 phase, where CDK1/A regulates the phosphorylation of the substrates. The CDK1/B activation occurs at the late G2 phase and triggers the G2/M transition. The cyclin D reactivates the CDK4 and CDK6 to initiate the next cycle. In M phase the cells separate into two daughter cells.

Because of their involvements in the cell-cycle, the major focus of the drug development from CDKs was in the area of anti-tumor or anti-cancer. Representative examples of various CDK inhibitors currently in different phases of clinical trial are described in Figure 1.2. Even though they belong to CDK group, most of these inhibitors are classified as pan-kinase inhibitors, since they lack selectivity and inhibit other kinases.
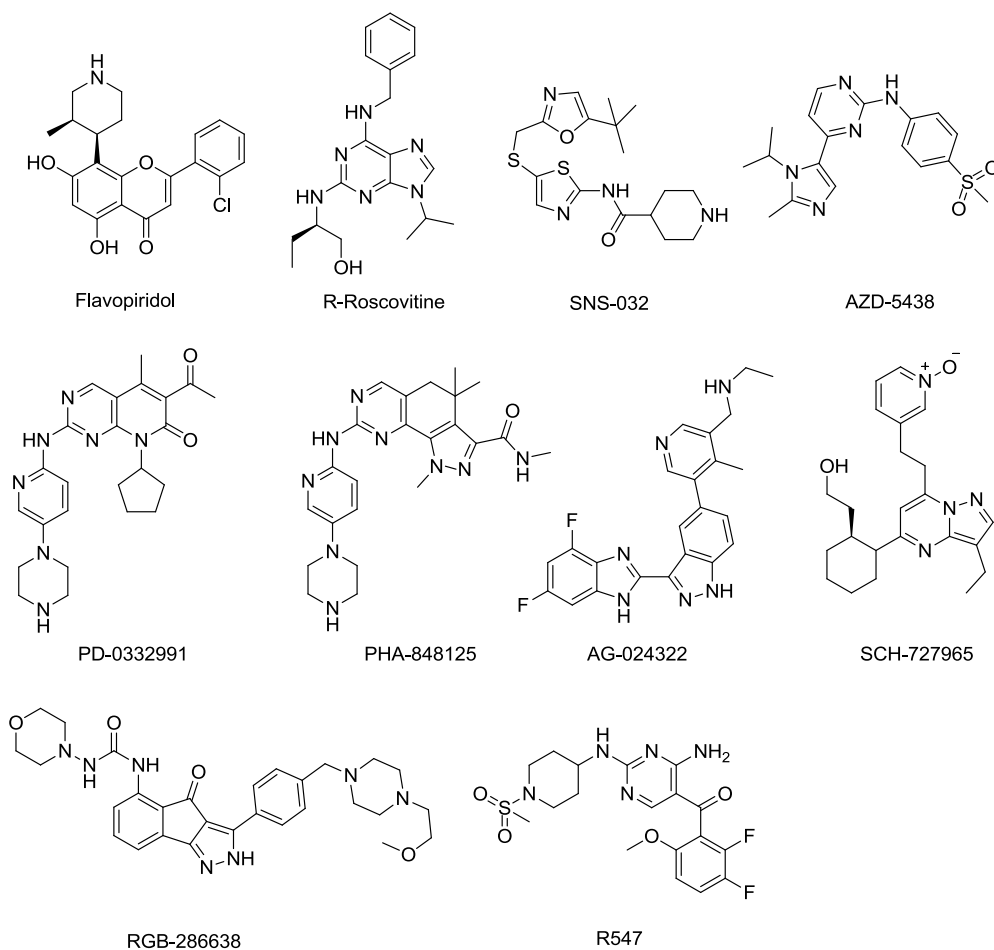
Figure 1.2.   Representative CDK inhibitors in different phases of clinical trials

5

As discussed before, several evidences point towards the involvement of cell cycle kinases in neurodegenerative processes. These findings suggest that anti-tumor drugs with cell cycle inhibition may find its application in neuro-degeneration as well. Following are a few examples of CDK inhibitors being evaluated for neurodegeneration leading to AD (Figure 1.3). All of these compounds inhibit CDK5 and GSK3β to some extents.
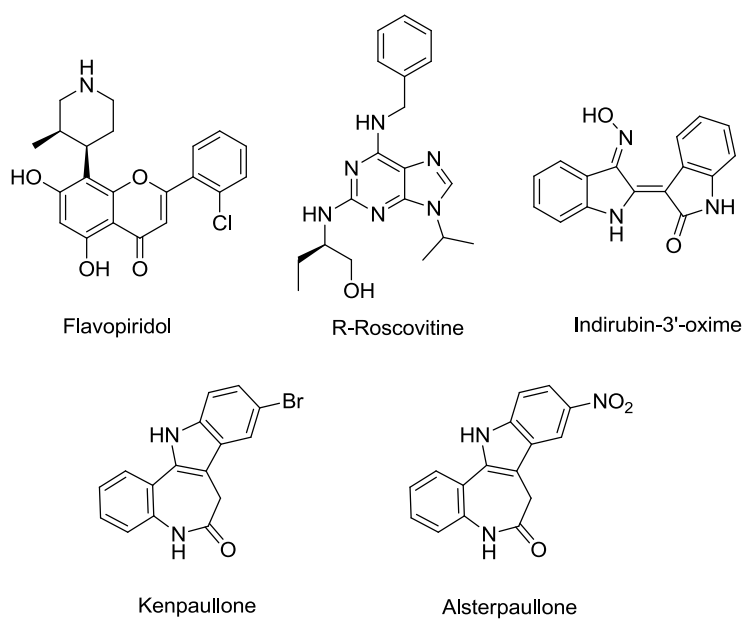
Figure 1.3. CDK inhibitors evaluated for neurodegenerative diseases

CDK5 is a unique member of the CDK family, which does not participate in cell division but it is important in neuronal tau phosphorylation leading to AD.

1.3.   Cyclin dependent kinase 5 (CDK5)

Since the discovery of CDK5 in early 1990s, a lot of progress has been made in determining its functions. CDK5 is also known as neuronal CDC2-like kinase (NCLK). It is a proline-directed serine/threonine kinase (STK), which is primarily expressed in neuronal and

testicular cells. It is essential for the development of neuronal cells and is involved in the regulation of neuronal cytoskeleton dynamics; neurite outgrowth; vesicular transport and synaptic functions. The major difference of CDK5 with its other mitotic counterparts is that it regulates neuronal development rather than cell division.[10, 11] The neuronal specificity is further established by the presence of its activators in the nervous system. It is primarily involved in neuronal migration, neuronal differentiation, synaptic functions and synapse development. Unlike other CDKs and STKs, it does not require 'T-loop' phosphorylation to achieve an active conformation.[10] It is also involved in post mitotic neuronal survival, migration and neurogenesis.[12] The post mitotic neuronal expression is marked by its activation by non-cyclin activators p35 and p39. However, it phosphorylates S/TPXK/R type motif as in other CDKs. Thus explains its inclusion in the CDK families.[13] Phosphorylation at threonine 14 and serine 159 produce inhibitory effects, whereas the activation is occurred by the phosphorylation at tyrosine 15.[14]

Oxidative or ischemic neuronal damages increase neuronal calcium influx and thereby activate the cysteine-protease calpain. The membrane bound natural precursor p35 is then cleaved by activated calpain to a longer lived cytosolic protein p25, leading to the formation of a hyperactive p25/CDK5 complex.[14] Such cleavage is reported as one of the key reasons for hyperphosphorylation of tau and subsequent NFT formation leading to AD.[7-9] CDK5 phosphorylates tau at 11 sites and all these phosphorylated sites exist in AD brain. CDK5 is also believed to be involved in the phosphorylation mediated activation of phosphatidylinositol-3-kinase (PI3K)-like kinase ATM (ataxia-telangiectasia mutated). The activated ATM causes DNA damage-induced cell cycle re-entry and subsequent apoptosis.[12]

A recent study with CDK5 knockout transgenic mouse has shown direct reduction of the NFT formation.[15] The *in-vitro* activity of CDK5/p25 inhibitors in Rat neuronal cells show dose-dependent inhibition of tau phosphorylation.[16] Inhibition of the p25-CDK5 complex is a viable target for AD, by blocking the hyperphosphorylation of tau and subsequent NFT formation. CDK5 deregulation is also indicated in other neurodegenerative diseases, such as Huntington's chorea, stroke, Parkinson's disease, amyotrophic lateral sclerosis (ALS), major depression and substance abuse.[7, 17-19] In non-neuronal systems it is indicated in the control of glucose metabolism in pancreatic beta cells[20] and tumorigenesis of the pancreas.[21] These therapeutic indications make it a very attractive target to investigate in depth.

We chose to design CDK5/p25 inhibitors as a target against neurodegeneration leading to Alzheimer's disease. One of our major goals was to design CDK5/p25 inhibitors selective over CDK2. Since we were targeting neurodegeneration we wanted to avoid any undesired cell cycle mediated apoptotic effects of CDK2 inhibition. The task is daunting, because the two kinases have about 60% sequence homology and commonality in the number of residues (27 out of 29) in the ATP binding domains. The only two differing amino acid residues in the catalytic domain for CDK5 are Cys83 and Asp84, whereas for CDK2 these are Leu83 and His84. Figure 1.4 explains the 3-dimentional (3-D) difference in the catalytic domain of the two kinases.
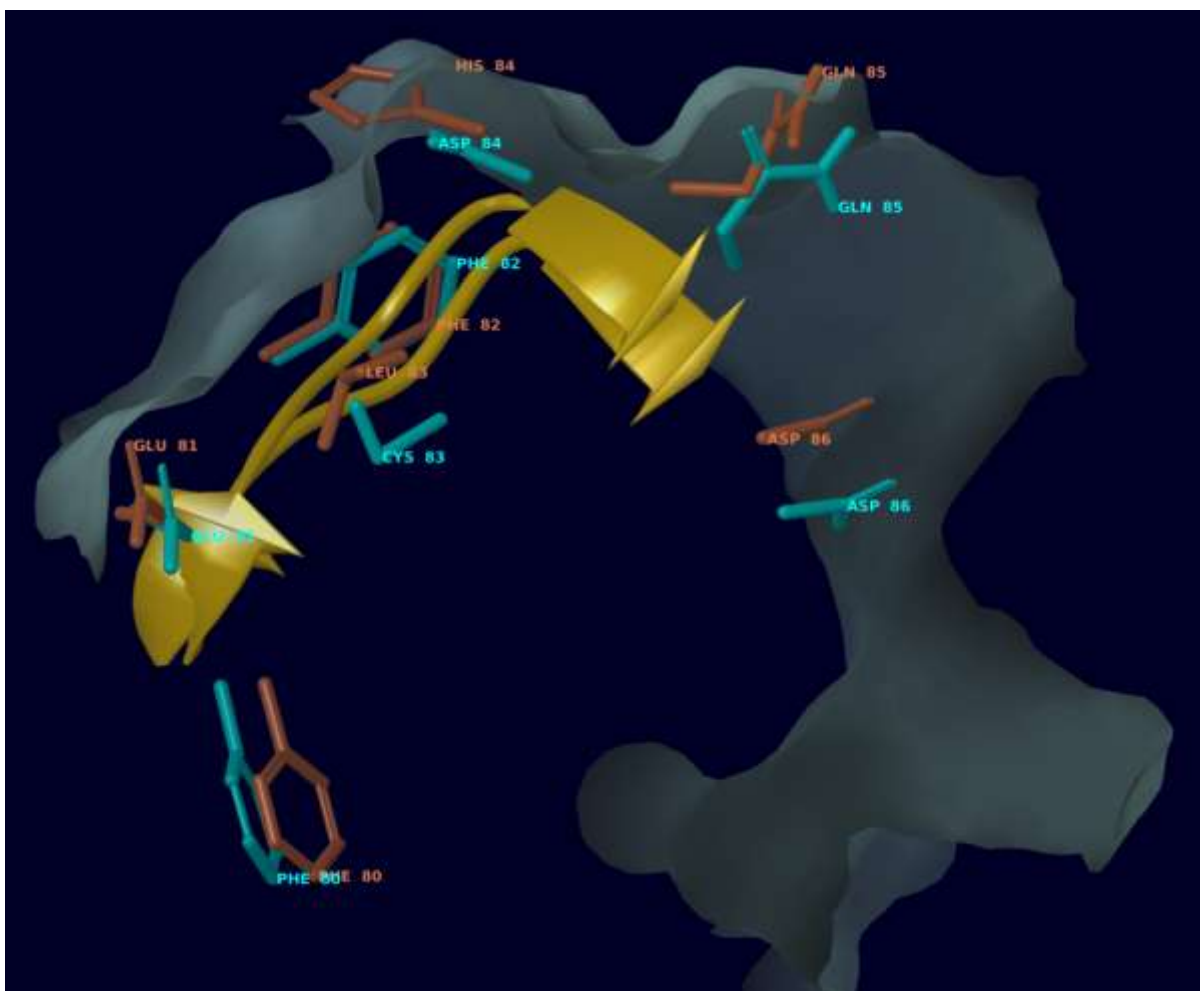
Figure 1.4. 3-D difference in catalytic domains of CDK5 (blue) and CDK2 (brown)

Even with these close sequential similarities some research groups have previously achieved the selectivity over CDK2 using homology model derived SAR studies. Three examples (**1.1**, **1.2** and **1.3**) in Figure 1.5 have selectivity values of 18-, 34- and 99- fold, respectively.[22-24]
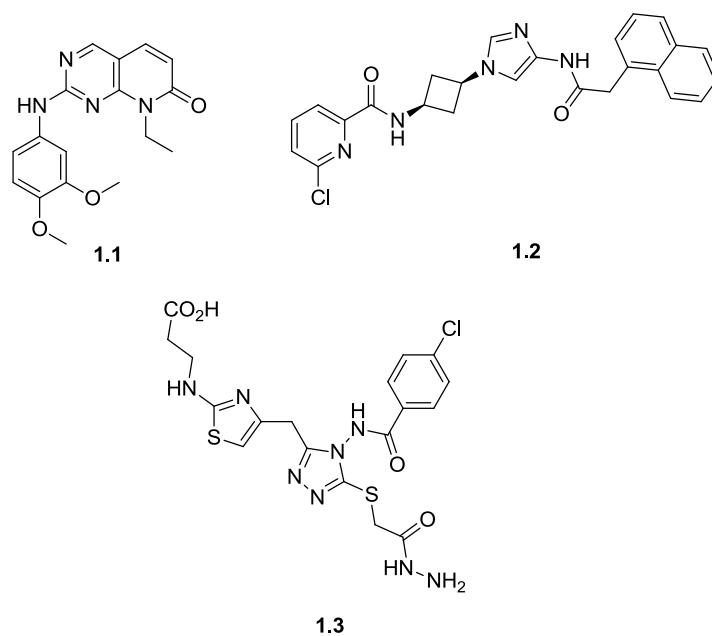
Figure 1.5. Structures of CDK5 selective compounds

In our approach we decided to achieve selectivity through structure based virtual screening strategy, validate the hits through biological screening and explore SAR modifications around the lead structure.

.

CHAPTER 2: VIRTUAL SCREENING METHODOLOGY TO FIND SELECTIVE AND POTENT CDK5/p25 INHIBITORS

2.1   Introduction

Inhibition of CDK5-p25 became a viable target for numerous acute and chronic neurodegenerative diseases; including Alzheimer disease. One of our major goals of designing selective CDK5/p25 inhibitors targeting neurodegeneration was to avoid any undesired mitotic side effects of CDK2. Even though R- roscovitine (**2.1**) had been explored as one of the kinase inhibitor for AD, it is not a selective CDK5/p25 inhibitor.[25] The task of finding selectivity became daunting, because the two kinases have very high levels (60%) of sequence homology and commonality in the number of residues (27 out of 29) in the ATP binding domains. The only two differing amino acid residues in the catalytic domain for CDK5 are Cys83 and Asp84, whereas for CDK2 these are Leu83 and His84.

Despite these similarities, the selectivity was achieved previously by different research groups, utilizing the ligand-based SAR strategies, where the lead compounds were identified by high throughput screening and were optimized by docking into homology models of CDK5/p25 derived from the X-ray structures of CDK2.[23, 26, 27]

The potential for structure-based inhibitor design received a shot in the arm with the availability of X-ray crystal structures of CDK5/p25.[10, 28, 29] The first apo-protein structure deposited in the RCSB protein data bank (PDB) had a PDB id: 1H4L, which was in its active conformation and showed no phosphorylation in the T-loop (specifically at Ser159).[10] Four other structures (PDB id: 3O0G, 1UNG, 1UNH and 1UNL)[29, 30] have ligands embedded and all are crystallized from the mutant CDK5/p25 form in which Asp144 of the wild form was mutated with Asn144. Structures of the known ligands with available PDB id are described in Figure 2.1.

Even with the availability of the crystal structures, to-date only a few groups have utilized structure-based design using simple docking protocols to identify leads.[5, 16, 31]
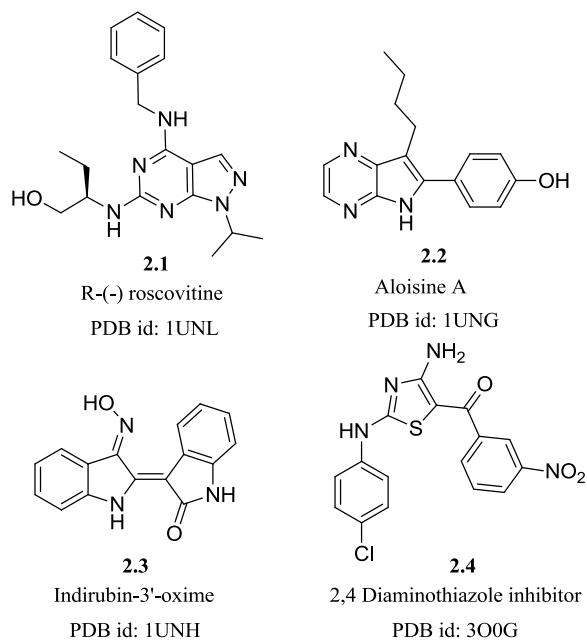
Figure 2.1.   Structures of known CDK5/p25 inhibitors with PDB id

Structure based virtual screening is a successful computational tool often used as complimentary to high throughput biological screening to identify hits.[32, 33] In view of the potential therapeutic importance and available crystal structures (PDB id: 1UNG, 1UNH, 1UNL and 3O0G),[29, 30] CDK5/p25 is an attractive target for structure based inhibitor design. However, no prospective virtual screening works have been reported to-date. A three dimensional quantitative structure-activity relationship (3D-QSAR) study[34] has been reported aimed towards understanding the SAR requirements of previously disclosed CDK5/p25 inhibitors.[24] Recently, a virtual screening effort[35] reporting the validity of the docking model of previously known inhibitors fell short of disclosing any new structural cores. In this current research an *in-silico* approach was used to identify novel selective CDK5/p25 inhibitors using structure-based virtual

screening. Usually, structure-based virtual screening studies use either docking-based screening or pharmacophore matching.[32, 33] To identify *de-novo* templates, we decided to use structure based E-pharmacophore models coupled with a docking-based virtual screening workflow to screen a commercially available database containing 2.84 million compounds with 4.28 million conformations. The computational approach can be divided into four distinct steps as described in the schematic representation (Figure 2.2).
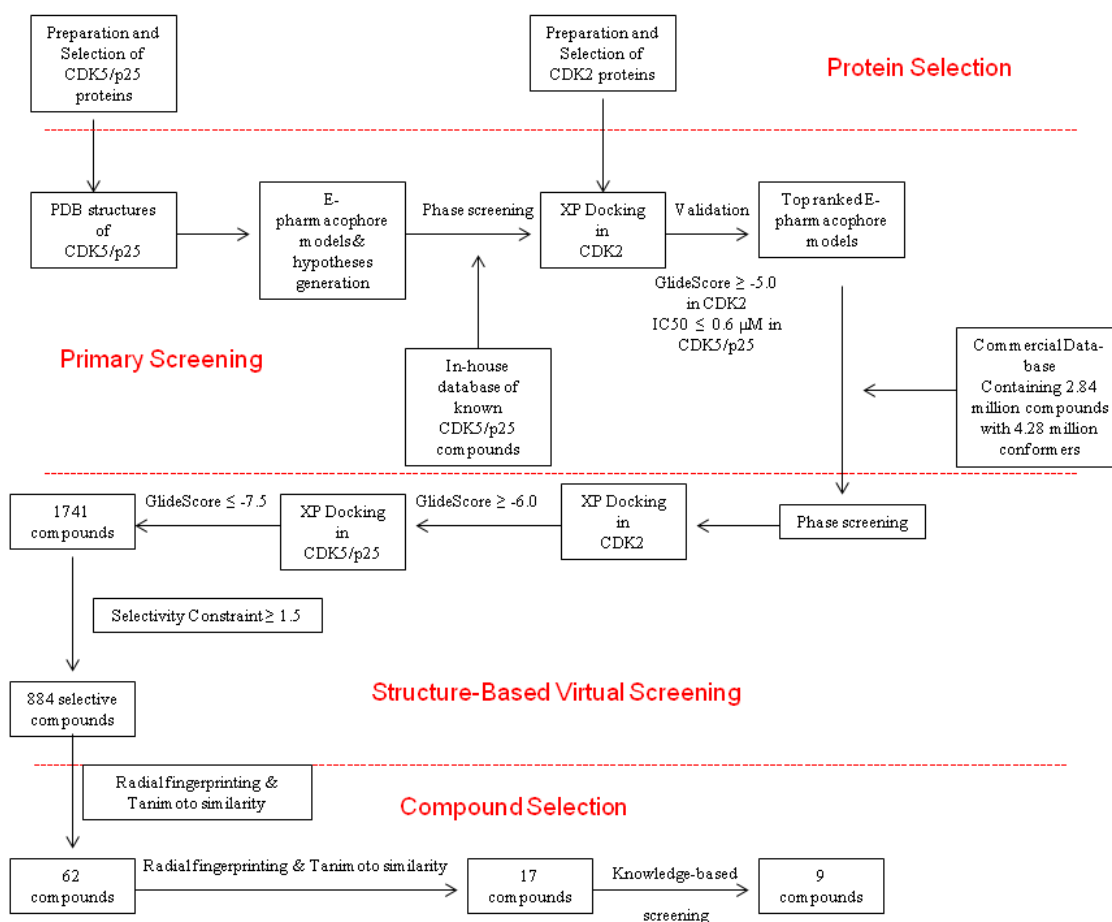
Figure 2.2.   *In-silico* scheme for virtual screening study

In this approach we further imposed a selectivity ratio constraint and subsequently used clustering and similarity analysis to identify nine compounds. Among these nine compounds, one was identified as the lead with a 0.3 LE and four-fold selectivity over CDK2/cyclin E.

2.2.   Methods

2.2.1.   General

All calculations were performed on a Linux workstation equipped with four parallel Intel Xenon X5460 processors (3.16 GHz) with 8GB total RAM. The pictures were generated using PyMol[36] and Maestro, *version 9.2.*[37]

2.2.2.   Ligand Preparation

LigPrep[38] was used to produce low energy 3D structures of compounds. The ionization/tautomeric states were generated using Epik. The chiralities of the compounds were retained from the original state. All the conformations were minimized using OPLS-2005 force field and at the most 32 conformations per ligands were generated.

2.2.3.   Protein Preparation

Each protein crystallographic structure was loaded from the RCSB Protein Data Bank (PDB) and prepared by using Protein Preparation Wizard.[39] For the dimer, the ligand bound fragment was selected for processing. It was then pre-processed by assigning the bond orders, adding hydrogen, and filling in the missing loops and the side chains using Prime.[40] The crystal

bound waters were deleted beyond 5Å from the ligand and ionization/tautomeric states were generated at pH 7.0±4.0 using Epik. Subsequently, the protein was refined by optimizing the hydrogen bonds (H bonds) and the sample water orientations. Finally the Impref-minimization was carried out using OPLS 2005 force field.

2.2.4. Hypothesis generation

The initial pharmacophoric hypotheses were generated from the PDB structures using E-Pharmacophore.[41] All the subsequent hypotheses were generated using Phase.[42, 43]

2.2.5. Phase database generation

A database was generated from known CDK5/p25 inhibitors,[27, 29, 30, 44-59] using Phase.[60] The ligand conformations were generated by Phase ligand processing using the following protocol. Different ionization/tautomeric states were generated at pH 7.0±2.0 using Epik and the high-energy states were removed. The stereochemical information was obtained from the 3D geometry of the ligands. For unspecified stereocenters, 4 low-energy stereo isomers were retained. For 5/6 membered rings the default value of up to 1 conformation per structure was retained. Duplicate structures were skipped. A default value of maximum number of 100 conformers was generated per molecule and up to 10 conformations were retained per rotatable bond.

2.2.6. Phase Database Screening

Both the Phase databases (the database built from known CDK5/p25 inhibitors and the commercial database) were screened to find pharmacophore matches[42, 43] using existing

conformers. For the database build from the known CDK5 inhibitors, the return limit was set as at most 1 hit per molecule and 1000 hits in total. On the other hand, for the commercial database the limit was set as, at most 1 hit per molecule and 10,000 hits in total. In both the cases, the hits with align scores >1.2, vector scores <-1.0 and volume scores <0.0 were rejected.

2.2.7. Ligand docking

All the docking calculations were performed with (extra precision) XP-Glide, because it was known to be more accurate and computationally intensive[61, 62] and run in the Virtual Screening Workflow framework. The ligands were pre-processed using LigPrep. Docking grids were generated by Glide using the co-crystallized ligand at the center of the grid box. The compounds were docked flexibly by using penalization for non-planar amide bond conformations and after docking 100% of the best compounds with all good scoring states were kept.

2.2.8. Fingerprinting, Similarity and Clustering Analysis

We performed the analysis of the virtual screening hits first by creating fingerprints using Radial fingerprinting.[63] Then the similarity analysis of the fingerprints was done using Tanimoto similarity[64] and hierarchical clustering by Ward's cluster linkage method[65] in Canvas.[66]

2.3.   Results and Discussion

2.3.1. Protein selection and evaluation of waters in crystal structures

Several previous computational studies have explored the importance of water molecules in the active site domains of proteins and showed that they were pivotal for ligand binding in virtual-screening frameworks.[67, 68] We first explored the significance of the water molecules in the crystal structures of CDK5/p25 (PDB id: 3O0G, 1UNL, 1UNG and 1UNH).[28, 29] In the protein preparation methodology we first considered keeping the highly conserved water molecules within 5Å of ligand binding distances. We also prepared the proteins without any water. Subsequently, the co-crystallized ligands were docked using Glide -XP to both the water-bound and the water-removed forms of the individual proteins. We observed that for all four cases the ligands showed better GlideScores with the water-bound forms (Table 2.1). This prompted us to prepare all proteins (both CDK5/p25 and CDK2) with conserved waters in the 5Å of their ligand binding domain.

Table 2.1.   XP-docking scores of ligands in water bound and no-water-bound proteins

CDK5/p25 Protein Structures	Status of water in crystal structure	GlideScores
3O0G	water bound	-10.570
	no water	-9.925
1UNL	water bound	-9.968
	no water	-9.554
1UNG	water bound	-9.208
	no water	-8.419
1UNH	water bound	-8.263
	no water	-7.441

In the ensemble-docking experiment of the CDK5/p25 crystal bound ligands we found that only co-crystallized ligands produced good GlideScores with the originating proteins (Table 2.2).

This made us believe that no single protein structure could be used to dock all the ligands and consequently we chose all four CDK5/p25 crystal structures for the virtual screening study.

Table 2.2.   Ensemble docking of CDK5/p25 crystal bound ligands

Protein PDB id	Crystal bound Ligands	GlideScores
3O0G	Ligand_3O0G	-10.570
	Ligand_1UNH	-8.542
	Ligand_1UNG	-8.401
	Ligand_1UNL	-5.530
1UNL	Ligand_1UNL	-9.968
	Ligand_1UNG	-8.498
	Ligand_3O0G	-8.325
	Ligand_1UNH	-7.678
1UNG	Ligand_1UNG	-9.208
	Ligand_1UNH	-6.737
	Ligand_1UNL	-4.612
	Ligand_3O0G	-3.912
1UNH	Ligand_1UNH	-8.263
	Ligand_3O0G	-6.594
	Ligand_1UNL	-5.999
	Ligand_1UNG	-5.883

With respect to CDK2, since 148 structures with a resolution of ≤ 2.5Å were available in the PDB between 1996-2011, we had to narrow down our selection through similarity searching,[64] followed by hierarchical clustering[65] to six structures (PDB id: 1AQ1, 2W17, 1OIT, 2A4L, 2VTP and 1R78).[69-74] While analyzing the data from ensemble-docking study of these six co-crystallized ligands, we found that all ligands docked reasonably well with 2VTP only (Table 2.3). Consequently, 2VTP was chosen as the CDK2 protein for the virtual screening work-flow.

Table 2.3.   Ensemble docking of CDK2 crystal bound ligands

| Protein Structures	Crystal bound Ligands	GlideScores
1AQ1	Ligand_1AQ1	-13.324
	Ligand_2VTP	-10.099
	Ligand_1OIT	-9.906
	Ligand_1R78	-8.256
	Ligand_2A4L	-8.117
	Ligand_2W17	-4.511
2W17	Ligand_2W17	-11.763
	Ligand_1OIT	-11.185
	Ligand_2A4L	-10.681
	Ligand_2VTP	-8.965
	Ligand_1R78	-6.146
	Ligand_1AQ1	-1.955
1OIT	Ligand_1OIT	-11.324
	Ligand_2W17	-10.102
	Ligand_1R78	-9.914
	Ligand_2VTP	-8.477
	Ligand_2A4L	-6.960
	Ligand_1AQ1	*
2A4L	Ligand_2W17	-10.450
	Ligand_1R78	-9.762
	Ligand_2A4L	-9.592
	Ligand_1OIT	-7.258
	Ligand_2VTP	-5.645
	Ligand_1AQ1	-3.240
2VTP	Ligand_1OIT	-11.279
	Ligand_2VTP	-10.470
	Ligand_2W17	-9.874
	Ligand_1R78	-9.102
	Ligand_2A4L	-7.590
	Ligand_1AQ1	-7.434
1R78	Ligand_2W17	-10.488
	Ligand_2A4L	-9.256
	Ligand_1OIT	-8.886
	Ligand_1R78	-8.724
	Ligand_2VTP	-8.418
	Ligand_1AQ1	-5.067

* Ligand did not dock in the selected grid

2.3.2. Primary screening and validation

For a rapid screening of a large database, we extracted the pharmacophoric features required for CDK5/p25 inhibition from the known x-ray structures (PDB id: 1UNL, 1UNH, 1UNG, 3O0G)[28, 29] and derived E-pharmacophore models[41, 75] using Maestro.[37] The structure-based pharmacophore model generated from 1UNL contained seven features: two hydrogen bond acceptors (A2, A4, red spheres), two hydrogen bond donors (D5, D6, blue spheres), one hydrophobic feature (H8, green sphere) and two ring aromatics (R11, R12, red rings) (Figure 2.3, generated by Maestro.[37]). Similar pharmacophore models were generated from 1UNH as A3D4H8R10; from 1UNG as A1A2D5H6R8R9; and from 3O0G as A1A2D3D4R7R8 (Figure 2.3).
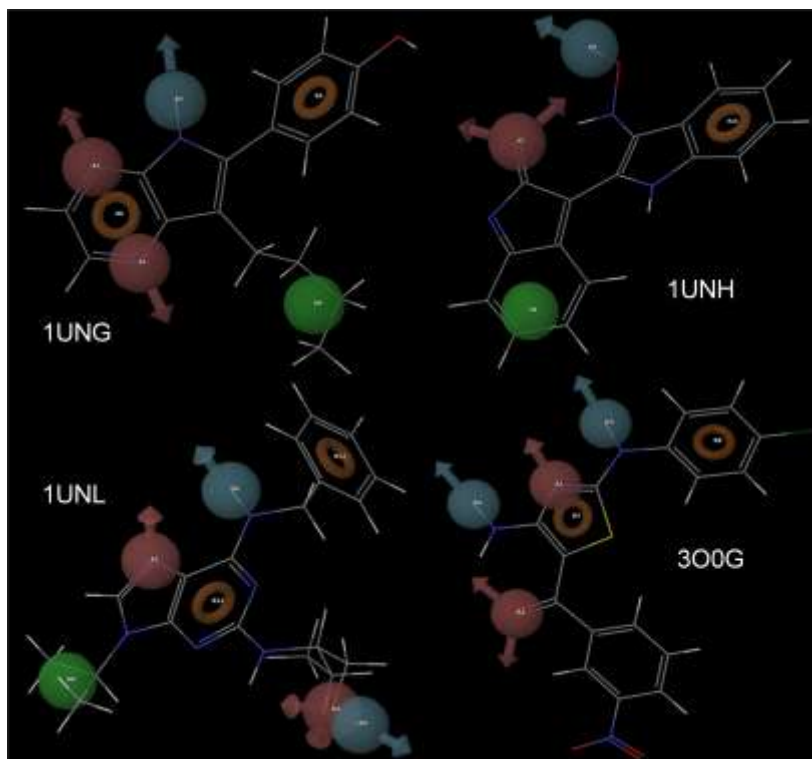
Figure 2.3. E-pharmacophoric features of 1UNG, 1UNH, 1UNL and 3O0G

In these e-pharmacophore models, some of the generated features did not comply with the original hydrogen bonding (H-boding) interactions of the ligands. The H-bonding interactions are shown in Figure 2.4 and the interaction diagrams were generated in the RCSB PDB by PoseView.[76-78] Considering these interactions we created a total of twelve hypotheses: five from the E-pharmacophore model of 1UNL, two from 1UNH, three from 1UNG and two from 3O0G (Table 2.4). The next goal was to validate and select a concise list from these twelve hypotheses for virtual screening study.
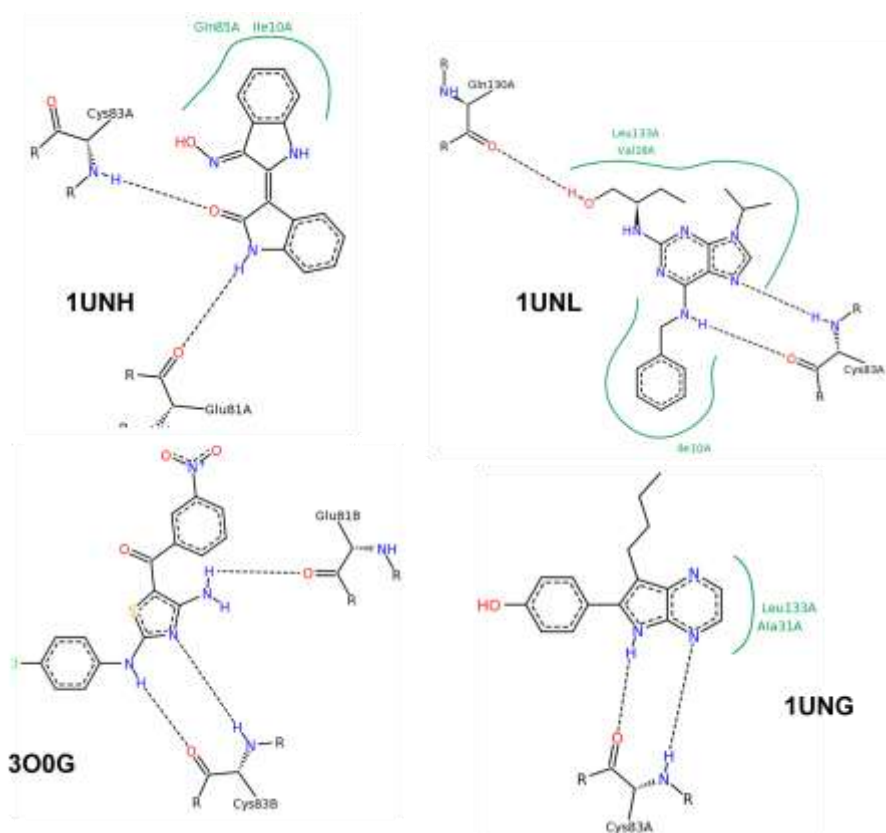

Figure 2.4.   H-bonding interaction diagrams of 1UNH, 1UNL, 3O0G and 1UNG

Table 2.4.   Hypotheses generated from E-pharmacophores

E-pharmacophore	Hypotheses	Pharmacophoric features
1UNG	1UNG_hypo 1	A1A2D5H6R8R9
	1UNG_hypo 2	A1A2D5R8R9
	1UNG_hypo 3	A2D5R8R9
1UNH	1UNH_hypo 1	A3D4H8R10
	1UNH_hypo 2	A1A3D4H8R10
1UNL	1UNL_hypo 1	A2D5D6R11R12
	1UNL_hypo 2	A2D6H8R11R12
	1UNL_hypo 3	A2A4H8D6R11R12
	1UNL_hypo 4	A2D5D6H8R11R12
	1UNL_hypo 5	A2A4D5D6H8R11R12
3O0G	3O0G_hypo 1	A1A2D3D4R7R8R9
	3O0G_hypo 2	A1A2D3D4R7R8

The validations of the hypotheses were done in two steps, first by Phase[60] screening of an in-house database containing known CDK5/p25 inhibitors,[27, 29, 30, 44-59] followed by Glide docking[61] of these screened hits in a CDK2 crystal structure (PDB id: 2VTP) using XP docking.[62] Number of compounds in each hypothesis with relatively poor GlideScores ($\geq$ -5.0) in CDK2 and good experimental activity ($IC_{50} \leq 0.6$ μM) in CDK5/p25 were identified (Figure 2.5).
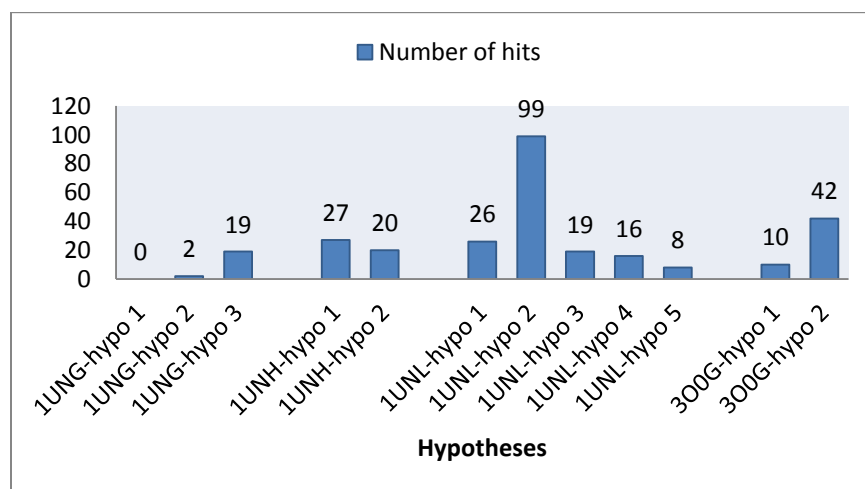
Figure 2.5.   Number of hits in each hypothesis

On the basis of their rank order, one hypothesis from each of 1UNH, 1UNG and 3O0G and three from 1UNL were selected, as described in Table 2.5.

Table 2.5.   Validated Hypotheses

Selected Hypotheses	Pharmacophoric Features
1UNG-hypo 3	A2D5R8R9
1UNH-hypo 1	A3D4H8R10
1UNL-hypo 1	A2D5D6R11R12
1UNL-hypo 2	A2D6H8R11R12
1UNL-hypo 3	A2A4H8D6R11R12
3O0G-hypo 2	A1A2D3D4R7R8

2.3.3. Structure-based virtual screening

In our virtual screening study we used a commercial database[79] containing 2.84 million compounds with 4.28 million conformations. We did not perform any further refinements of the database since the conformations were generated using ligprep,[38] Phase[60] and ADME property screens.[80]

As an initial step, we decided to use Phase based quick pharmacophore match[43] for the top six hypotheses as an alternative to the computationally exhaustive docking based virtual screening work-flow.

Subsequently, these six sets of hits were docked separately in CDK2 crystal structure (PDB id: 2VTP) using XP Glide.[61] In several previous studies, GlideScores had been used as a predictive tool to rank score compounds in virtual screening.[62, 81] We incorporated this predictive methodology in our scheme. We selected a cut-off CDK2 GlideScores ≥ -6.0 as a benchmark for compounds to be less active in CDK2. With this threshold in place we selected a total of 21,284 potential poor-CDK2-active compounds.

Compounds identified with the poor CDK2 GlideScores were docked into CDK5/p25 crystal structures (PDB id: 1UNL, 1UNH, 1UNG, 3O0G) using XP Glide. The set of compounds identified from the initial Phase screening of 1UNG-hypotheses, docked in 1UNG. The compounds identified from the other three protein-generated hypotheses were docked similarly. We used a cut-off GlideScores $\leq$ -7.5 to identify compounds as potential CDK5/p25 active compounds. Consequently, we identified 1741 potential CDK5/p25 selective compounds with poor CDK2 GlideScores ($\geq$ -6.0) and good CDK5/p25 GlideScores ($\leq$ -7.5). We further refined the selection of compounds by imposing a selectivity constraint ($\geq$ 1.5) as defined below:

$$\text{Selectivity Constraint} = \frac{\text{CDK5/p25 GlideScores}}{\text{CDK2 GlideScores}} \geq 1.5$$

In total we identified 884 computationally defined active CDK5/p25 compounds with selectivity against CDK2.

2.3.4. Selection of compounds

The selected 884 compounds were statistically analyzed using 2-dimesional (2-D) Radial fingerprinting,[63] in Canvas.[66] The hierarchical clustering of the fingerprints identified 49 diverse sets of clusters using Tanimoto similarity and Ward's cluster linkage method.[65] We eventually identified 62 compounds from these 49 diverse sets, which were further optimized through a second round of 2-D fingerprinting and clustering to a group of 17 compounds. Final selection of 9 compounds was done by knowledge-based screening. These selected nine compounds along with the carboxylic acid intermediate **3.14** are represented in Figure 2.6.

Commercial or in-house sources, docking scores and calculated properties of the compounds are listed in Table 2.6. Physicochemical and ADME properties, such as logP (octanol/water), logBB (log [brain]/[blood] (a predictor of a compound's ability to cross blood-

25

brain barrier) and number of metabolic sites (# metab) calculated by QikProp[80] are listed. The values of intermediate carboxylic acid (**2.14**) were also calculated and included in Table 2.6. The log BB for a good oral CNS drug usually is between -3.0 to 1.0. All the selected compounds showed good predicted blood-brain barrier (BBB) permeability.
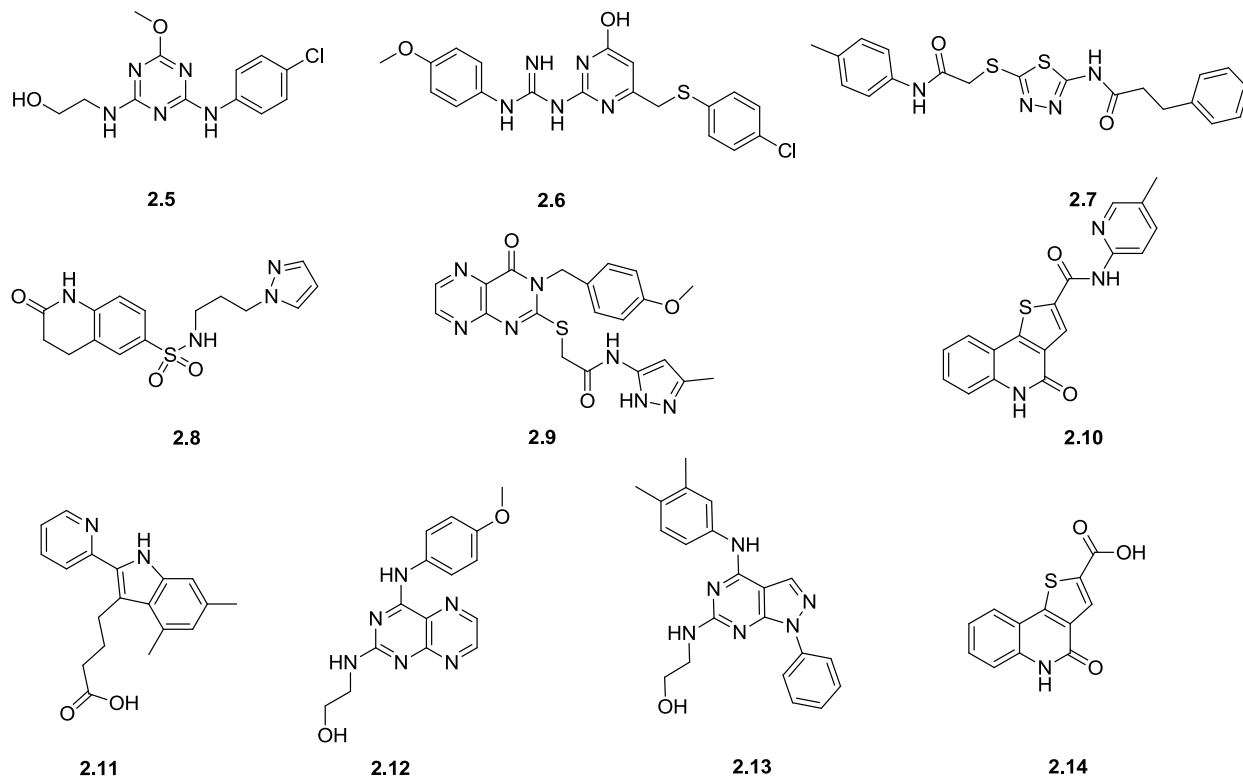
Figure 2.6. Selection of compounds from virtual screening study

Table 2.6. Calculated properties and sources of compounds selected in virtual screening

Compound #	CDK5/ p25 Glide Score	CDK2 Glide Score	Sources	MW	LogP (o/w)	LogBB	# Metab
2.5	-7.827	-3.673	Synthesized in-house	295.72	2.066	-0.823	2
2.6	-8.201	-4.069	Chem Bridge	415.90	4.071	-1.193	3
2.7	-9.221	-4.775	Ryan Sci.	412.53	3.685	-1.664	5
2.8	-7.582	-3.973	Ryan Sci.	334.39	1.233	-1.767	2
2.9	-8.007	-4.332	Chem Div	437.47	2.557	-2.107	6
2.10	-9.469	-5.539	Synthesized in-house	335.38	2.548	-1.020	4
2.11	-8.612	-5.240	Chem Bridge	308.37	4.134	-1.023	5
2.12	-8.908	-5.570	Ryan Sci.	312.33	1.522	-1.329	5
2.13	-7.864	-5.065	Chem Div	374.44	3.802	-1.115	3
2.14	-9.730	-8.117	Synthesized in-house	245.25	1.418	-1.027	2

2.4 Conclusions

A virtual screening work-flow comprised of pharmacophore matching, docking based screening methodology and constraint-based filtration was used to identify nine compounds from a commercial data-base containing 2.84 million compounds with 4.28 million conformers. This unique combination of e-pharmacophore matching and structure-based virtual screening was used to identify compounds with *de-novo* structural class. All the nine compounds showed excellent *in-silico* predicted blood-brain permeability. Along with these nine compounds the carboxylic acid intermediate (**2.14**) was also evaluated in *in-vitro* CDK5/p25 and CDK2/E kinase assays to find the validity of the model. The success rate of the model was defined by finding compounds with activity in CDK5/p25 and selectivity over CDK2/E. We found a 40% success

rate for the computational model with the identification of a lead with ligand efficiency (LE) of

0.3, as discussed in Chapter 6.

CHAPTER 3: SYNTHESIS OF STANDARDS AND 4-OXO-4,5 DIHYDROTHIENO[3,2-*c*]QUINOLINE-2-CARBOXYLIC ACID DERIVATIVES

3.1. Introduction

Because of high costs and long turn-around times, our initial focus was to prepare the 2,4-diaminothiazole standard (**2.4**) and the virtual screening hits (**2.5** and **2.10**). After the initial *in-vitro* assay of the identified hits from the virtual screening effort, we identified a lead molecule (**2.10**) in our effort with a ligand efficiency of 0.3. Consequently our effort in developing future SAR compounds around the lead also prompted us to develop an easy convergent synthesis.

We have noticed that in a previously reported method, synthesis of the 2,4-diaminothiazole derivative (**2.4**) was accomplished in two steps (Scheme 3.1).[16]
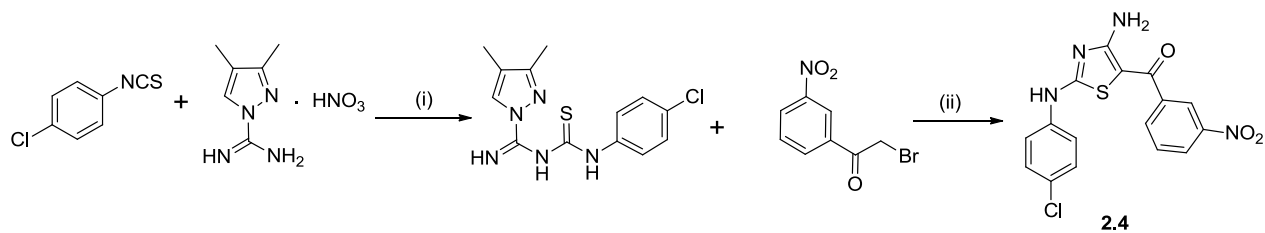
Laha *et al., Bioorg. Med. Chem. Lett.* **2011**, 21, 2098-2101

Scheme 3.1. Known synthesis of **2.4**

Reagents and conditions: (i) DIPEA or KOH, DMF, 50 °C, 2-16 h; (ii) DIPEA or TEA, DMF, 50-70 °C, 2-16 h

We observed that although the structures **2.5** and **2.10** were listed in SciFinder®, [82] there was no associated references. This motivated us to develop new and straight-forward strategies for the syntheses of the compounds. For synthesizing **2.10**, we searched for its closest intermediate, 4-oxo-4,5-dihydrothieno[3,2-*c*]quinoline-2-carboxylic acid (**2.14**). We found that the intermediate carboxylic acid (**2.14**) was also listed in SciFinder® [82] without any associated

references. This led us to develop a synthesis for the versatile intermediate **2.14** and rapid convergent synthesis of its derivatives for future SAR development.
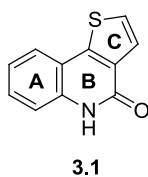

Figure 3.1.   Structure of the thieno[3,2-*c*]quinolin-4(5H)-one (**3.1**)

Several groups have explored the synthesis of the core structure (**3.1**) through free radical chemistry or transition metal mediated synthesis with varied yields ranging from 13-86% [83-86]. These palladium or copper mediated transition metal syntheses or the free radical chemistry are often hard to scale-up and pose issues relating purification and overall cost (Scheme 3.2). Only a few reports exist so far for the synthesis of the C-ring substituted derivatives of **3.1** (Scheme 3.2). Pierre *et al.* utilized palladium mediated cross coupling reaction and subsequent bromination to synthesize the 2-bromo derivative of **3.1** in very low yield. [85, 87] A ring expansion Beckmann rearrangement was used in a multi-step synthesis of 2-phenyl substituted derivatives of **3.1** in moderate yield [88] (Scheme 3.2). Efforts have also been made to synthesize N-alkylated derivatives of **2.14** [89-91]. However, difficulty in synthesizing the unstable α-chloro aldehyde (**3.2**) and subsequent cyclization barred any known synthesis available for C-ring substituted thienoquinolone moiety with free NH- lactam (**2.14**).
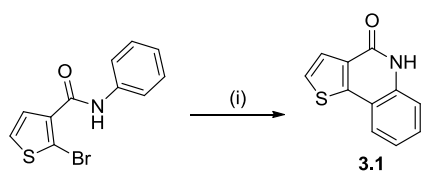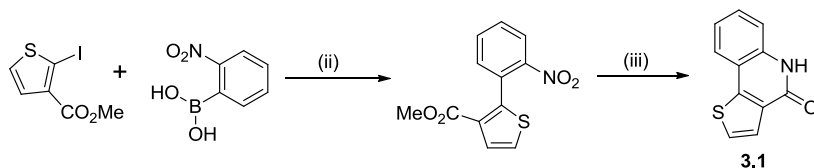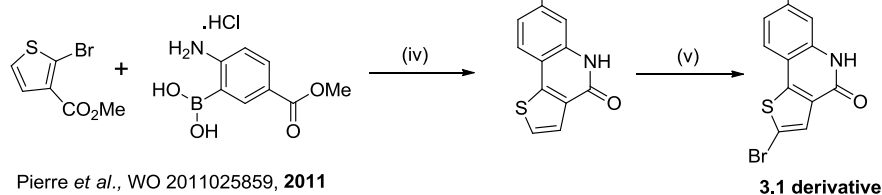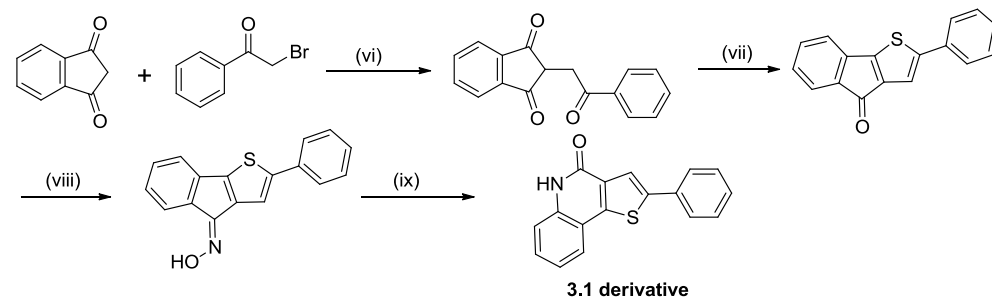
Scheme 3.2.   Known syntheses of core structure (**3.1**) and derivatives

Reagents and conditions: (i) AIBN, 1,10-phenanthroline, KO*t*Bu, benzene, 110 °C, 2-16 h; (ii) Pd(PPh$_3$)$_4$, Na$_2$CO$_3$, 1,2-dimethoxyethane, 120 °C, 5 h; (iii) Fe, AcOH, THF, 6 h; (iv) NaOAc, PdCl$_2$(dppf), DMF, *mw*, 120 °C, 10 min; (v) CHCl$_3$, AcOH, NBS, 70 °C, 16 h; (vi) NaOEt, EtOH, 100 °C, 30 min; (vii) Lawesson's reagent, toluene, 110 °C, 6 h; (viii) NH$_2$OH, NaOAc, 120 °C, 4 h; (ix) P$_2$O$_5$, H$_3$PO$_4$, 80-100 °C, 3 h.

Our proposed scheme starts with aniline (**3.4**) and utilizes a sequence of Friedel-Crafts, Vilsmeier-Haack, nucleophilic aromatic substitution (S$_N$Ar) and cyclization reactions to achieve the synthesis of the target compound (**2.14**). The retro-synthetic approach is described in Scheme 3.3.
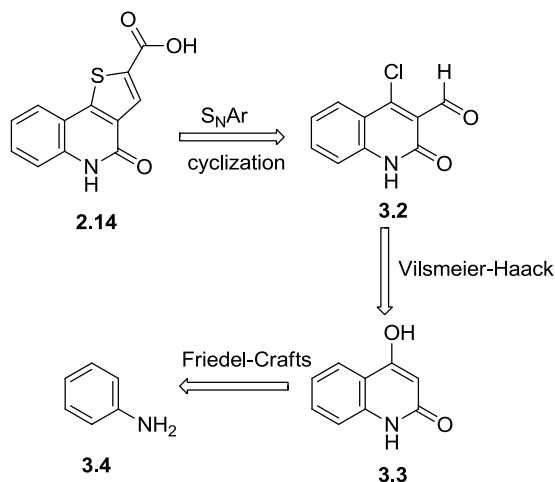
Scheme 3.3. Retro-synthetic approach for the synthesis of **2.14**

3.2. Results and Discussions

We developed an efficient one-pot condensation of (4-amino-2-((4-chlorophenyl)amino)thiazol-5-yl)(3-nitrophenyl) methanone (**2.4**). (Scheme 3.4) from cyanamide, a substituted phenyl isothiocyanate (**3.5**) and a β-halo acetophenone derivative (**3.6**).[92]
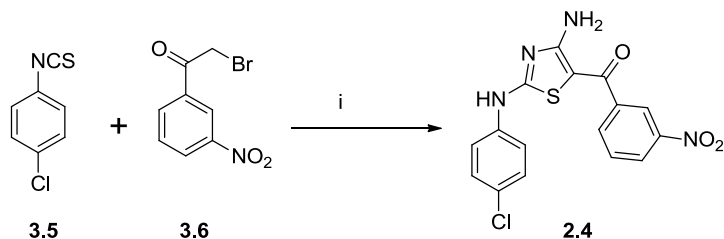

Scheme 3.4. One-pot synthesis of 2,4-diaminothiazole derivative (**2.4**)

Reagents and conditions: (i) Cyanamide, KO*t*Bu, ACN, *t*-BuOH, 30 °C, 2 h, 59%.

The synthesis of 2-((4-((4-chlorophenyl)amino)-6-methoxy-1,3,5-triazin-2-yl)amino)ethanol (**2.5**) was effectively achieved from 2,4-dichloro-6-methoxy-1,3,5-triazine

(**3.7**) by successive nucleophilic aromatic substitutions (S$_N$Ar) with 4-chloroaniline and ethanolamine in one-pot (Scheme 3.5).[93]
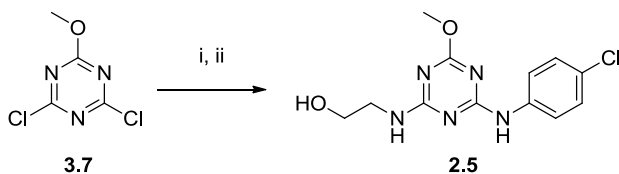
Scheme 3.5. One-pot synthesis of triazine derivative (**2.5**)

Reagents and conditions: (i) 4-Chloroaniline, *i*Pr$_2$NEt, DCM, 30 °C, 15 min; (ii) Ethanolamine, 30 °C, 5 h, 70%

In our synthetic approach for 4-oxo-4,5-dihydrothieno[3,2-*c*]quinoline-2-carboxylic acid (**2.14**), we first synthesized 4-hydroxyquinolin-2(1*H*)-one (**3.3**) starting from anthranilic acid (**3.8**) in three steps (Scheme 3.6).[94]
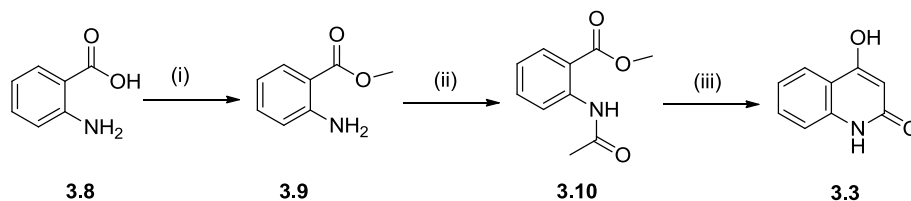
Scheme 3.6. Initial synthesis of 4-hydroxyquinolin-2(1*H*)-one (**3.3**)

Reagents and conditions: (i) MeOH, conc. H$_2$SO$_4$, 70 °C, 12h, 64%; (ii) Acetic anhydride, dioxane, 80 °C, 2h, 56%; (iii) KN(SiMe$_3$)$_2$, THF, -78 ° to 25 °C in 12h, 40%.

In order to optimize the yield we tried an alternate synthesis for **3.3**. We first attempted a direct microwave conversion of aniline (**3.4**) and diethylmalonate to 4-hydroxyquinolin-2(1*H*)-one (**3.3**).[95, 96]. Contrary to the reported findings, we could never repeat the direct synthesis of 4-hydroxyquinolin-2(1*H*)-one (**3.3**) as reported in the literature.[95, 96] Instead N^1,N^3-diphenylmalonamide (**3.8**) was obtained exclusively in 60% yield (Scheme 3.5). We optimized

34

the procedure by using a varied mix of aniline and diethylmalonate with catalytic amount of DMF in microwave and conventional heating as described in Table 3.1.

Table 3.1.   Optimization of the conversion of **3.4** to **3.8**

Entry	Aniline	Diethyl malonate	Heating condition	Time	Temperature (°C)	Isolated yield (%)
1	1 eq	1 eq	microwave	1h	80	34
2	2 eq	1 eq	microwave	1h	80	48
3	1 eq	1 eq	conventional	8h	80	34
4	2 eq	1 eq	conventional	8h	80	95

The optimum condition was the use of a (2:1) mixture of aniline and diethylmalonate with a catalytic amount of DMF at 140 °C for 8h to get **6** as a white solid in 95% yield. The structure of **3.11** was confirmed by comparing the ^{1}H NMR and melting point (mp) with the known literature values [97]. Finally, 4-Hydroxyquinolin-2(1*H*)-one (**3.3**) was obtained by intra molecular Friedel-Crafts acylation of **3.11** by heating it with polyphosphoric acid (PPA) at 150 °C for 3h [98]. Chromatographic purification was avoided by a simple acid-base workup, resulting in pure **3.3** in 74% yield. This alternate method improved the yield of **3.3** and reduced the number of steps used in Scheme 3.6. The improved synthesis is described in Scheme 3.7.
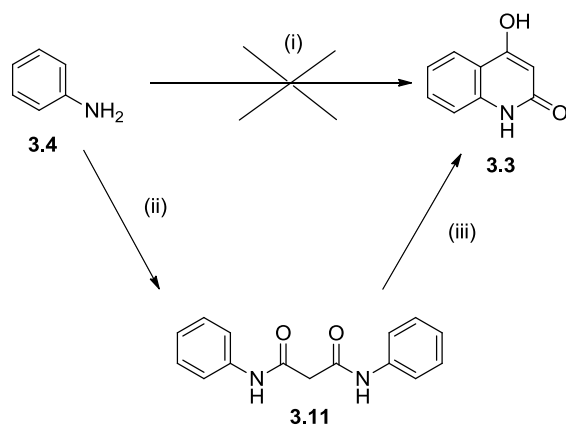
Scheme 3.7. A two-step synthesis of **3.3**

Reagents and conditions: (i) Diethyl malonate, *cat.* DMF, *mw*, 135 °C, 30 min; (ii) Diethylmalonate, cat. DMF, 140 °C, 8 h, 95%; (iii) PPA, 150 °C, 3 h, 70%.
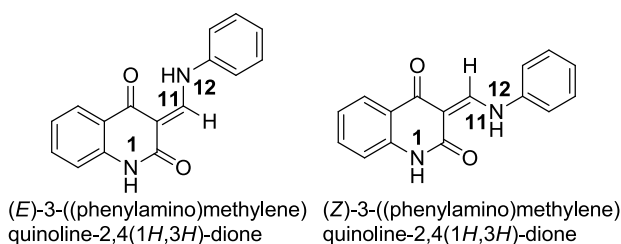
Our attempt to convert **3.3** directly to the α-chloro aldehyde (**3.2**) failed to yield the desired product [99]. However, we were able to convert **3.3** to an intermediate azomethine containing 3-((phenylamino)methylene)quinoline-2,4(1*H*,3*H*)-dione (**3.12**), which was easily converted to the α-chloro aldehyde (**3.3**) by a Vilsmeier-Haack reaction [100] (Scheme 3.8).
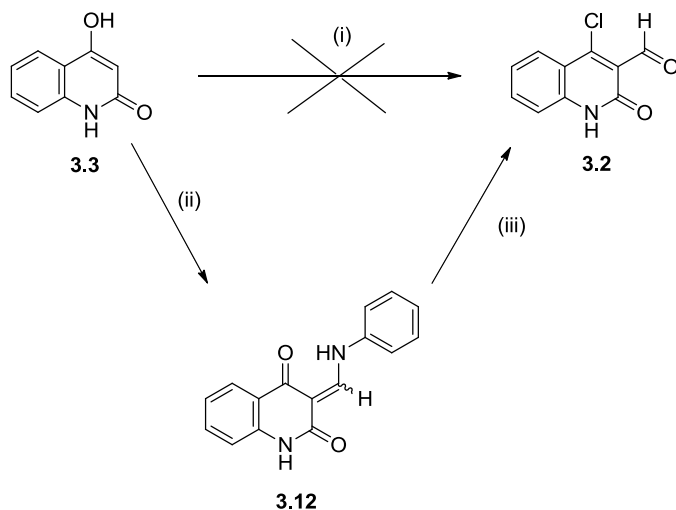
Scheme 3.8. Synthesis of α-chloro aldehyde, **3.3** -via- azomethine intermediate

Reagents and conditions: (i) POCl₃, DMF, 8h, no reaction; (ii) POCl₃, DMF, 8h, 90%; (iii) triethyl orthoformate, ethylene glycol, *mw*, 145 °C, 20 min, 82%.

36

While characterizing **3.12**, we noticed a striking difference between the reported ^{1}H-NMR chemical shifts [100] and our observed data. We observed two new chemical shifts at 13.70 (d, J = 12.5 Hz) and 12.81 (d, J = 12.5 Hz) ppm, which collectively integrated as one proton. We speculated that **3.12** exists as both the (*E*)- and (*Z*)- isomers as depicted in Figure 3.2, which were not reported either by Chilin *et al.* [100] or Fiala *et al.* [101].

(*E*)-3-((phenylamino)methylene)   (*Z*)-3-((phenylamino)methylene)
quinoline-2,4(1*H*,3*H*)-dione   quinoline-2,4(1*H*,3*H*)-dione

Figure 3.2.   (*E*) and (*Z*) isomers of **3.12**

In order to confirm our speculation, we first assigned the chemical shifts (δ in ppm) of A, B, C and D at 25 °C (Fig. 3.3), as follows. Three signals at 10.89 − 10.84 (m, 1H), 13.70 (d, J = 12.5 Hz) and 12.81 (d, J = 12.5 Hz) were exchanged by D_2O wash, confirming as -NH signals. By comparing the spectrum of **3.3**, the signal at 10.89-10.84 (m) was assigned to the lactam -NH. The doublet at 8.88 was assigned for H-$C_{11,}$ from COSY (see in appendices), which showed correlation of the peak only with the two exchangeable signals at 13.70 and 12.81. In summary, signal D at 8.88 (d, J = 12.0 Hz, 1H, H-C_{11}), signal C at 10.89 − 10.84 (m, 1H, H-N_1), signal B at 13.70 (d, J = 12.5 Hz, H-N_{12}) and signal A at 12.81 (d, J = 12.5 Hz, H-N_{12}) were assigned. Since COSY showed correlations of D (H-C_{11}) with both A (H-N_{12}) and B (H-N_{12}), we wanted to investigate further to confirm whether **3.12** is a mixture of tautomers or two geometric isomers (*E*- and *Z*-).
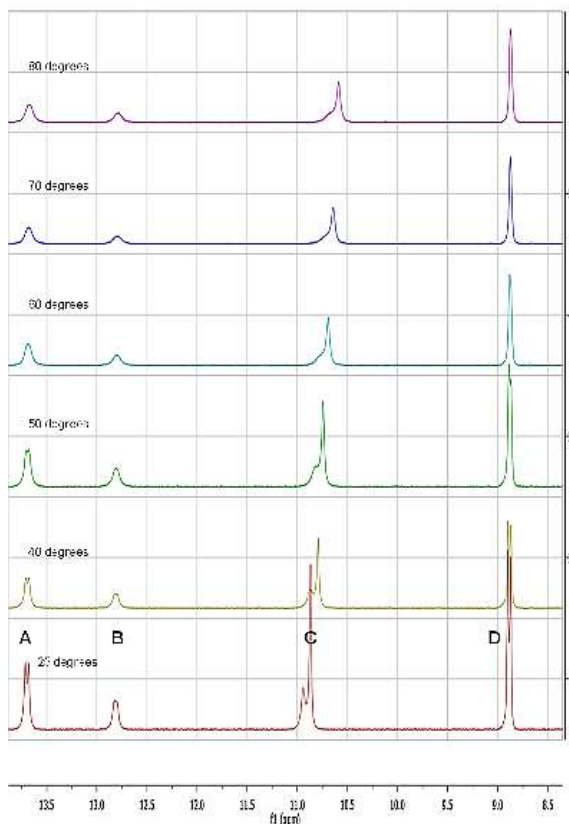
Figure 3.3. VTE of the azomethine intermediate **3.12**

We designed a variable temperature NMR experiment (VTE) from 25 °C to 80 °C and it was observed that each signal individually coalesced with the increase in temperature (Figure 3.3). But signals A and B never coalesced, confirming the presence of two different geometrical isomers (*E-* and *Z-*). In our modified conversion of **3.3** to **3.12** we used microwave irradiation at 140 °C for 40 min instead of conventional heating to obtain **3.12** as a mixture of the *E-* and *Z-*isomers in 82% yield. Compound **3.12** was subsequently stirred with 5 equivalents of phosphorous oxychloride in DMF at room temperature for 8h, followed by simple work-up to get 4-chloro-2-oxo-1,2-dihydroquinoline-3-carbaldehyde (**3.2**) as a white solid in 90% yield. We propose that the reaction proceeded through an intermediate iminium ion (**3.13**) formation by

38

initiating a regioselective electrophilic aromatic substitution at 4-position of **3.12**, followed by a S_NAr and elimination of DMF (Figure 3.4). Subsequent hydrolysis of **3.13** yielded the desired α-chloro aldehyde (**3.2**). The regioselectivity of the conversion was confirmed by IR, indicating the presence of a carbonyl stretching at 1646 cm^{-1} corresponding to the lactam. We found that **3.2** was unstable at room temperature, but could be stored at -20 °C under inert atmosphere for a period of over six months.
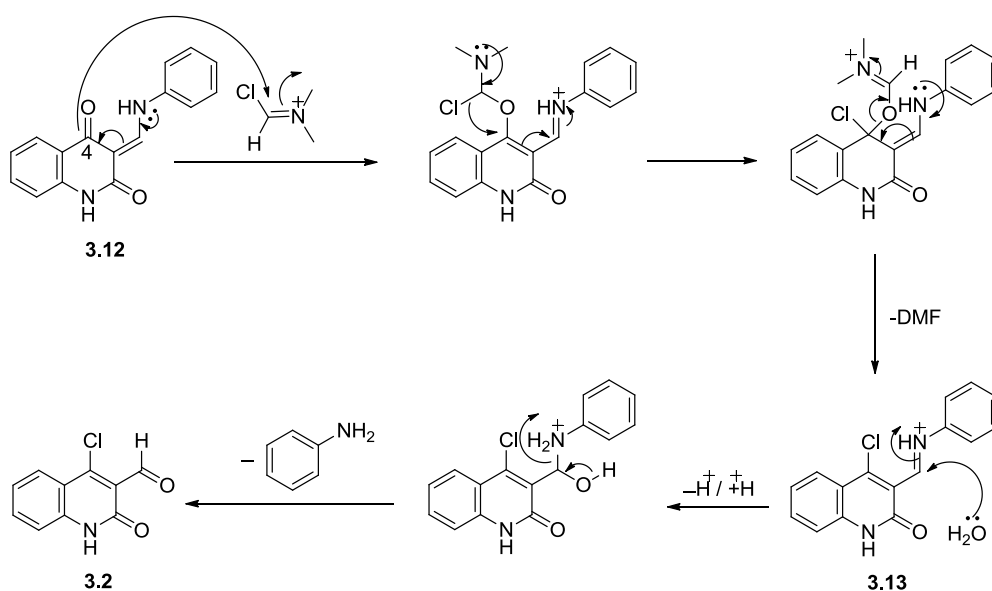
Figure 3.4.   Plausible mechanism for the formation of **3.2**

Next, to explore the possible synthesis of ethyl 4-oxo-4,5-dihydrothieno[3,2-c]quinoline-2-carboxylate (**3.14**), we evaluated the reaction of **3.2** and ethyl 2-mercaptoacetate. The result of using different bases with different reaction conditions is shown in Table 3.2.

Table 3.2.   Screening results of different bases for the synthesis of **3.14**
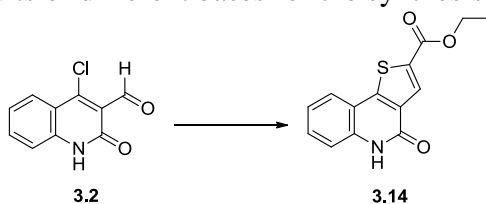
Entry	Solvent	Base	Time	Temperature (°C)	Isolated yield (%)
1	EtOH	NaOEt	3h	80	0
2	EtOH	Na$_2$CO$_3$	3h	80	48
3	EtOH	K$_2$CO$_3$	24h	30	22
4	EtOH	K$_2$CO$_3$	3h	80	88

We found that potassium carbonate (K$_2$CO$_3$) was the base of choice for the optimum conversion. Although the mechanism of this reaction has not been established experimentally, we believe the reaction went through a tandem S$_N$Ar / cyclization, followed by elimination of water (Figure 3.5). To the best of our knowledge, this is the first efficient tandem S$_N$Ar / cyclization reaction to synthesize a C-ring substituted thienoquinolone moiety containing a free – NH lactam. Hydrolysis of the ester (**3.14**) with lithium hydroxide and purification by a simple acid-base work-up produced the desired target 4-oxo-4,5-dihydrothieno[3,2-*c*]quinoline-2-carboxylic acid (**2.14**) in 96% yield. A detailed spectral characterization of **2.14** is established by using ^{1}H NMR, ^{13}C NMR, COSY, HSQC, HMBC, HRMS, IR and mp; purity is ascertained by HPLC analysis (see in appendices).
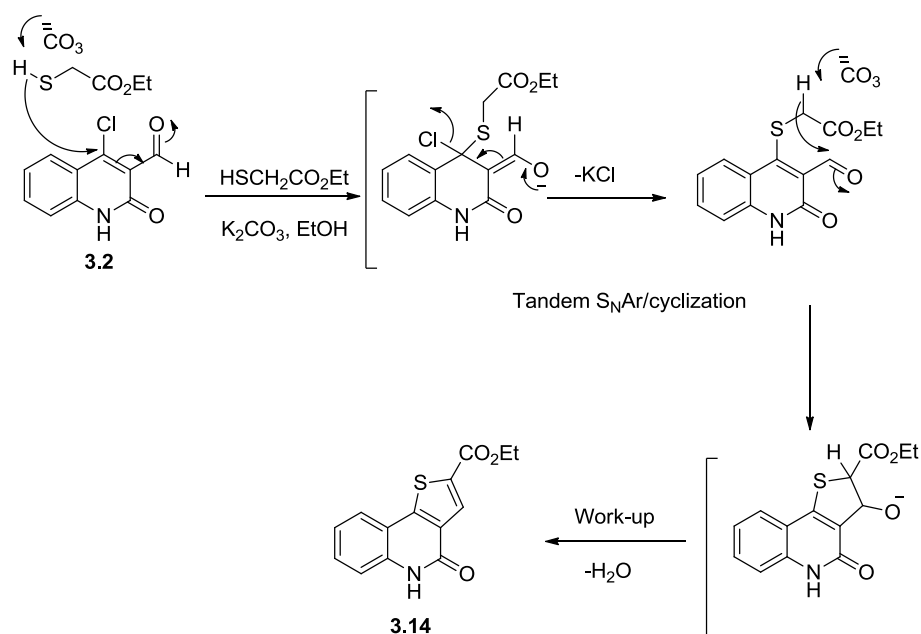
Figure 3.5. Plausible mechanism for tandem S_NAr/cyclization to synthesize **3.14**
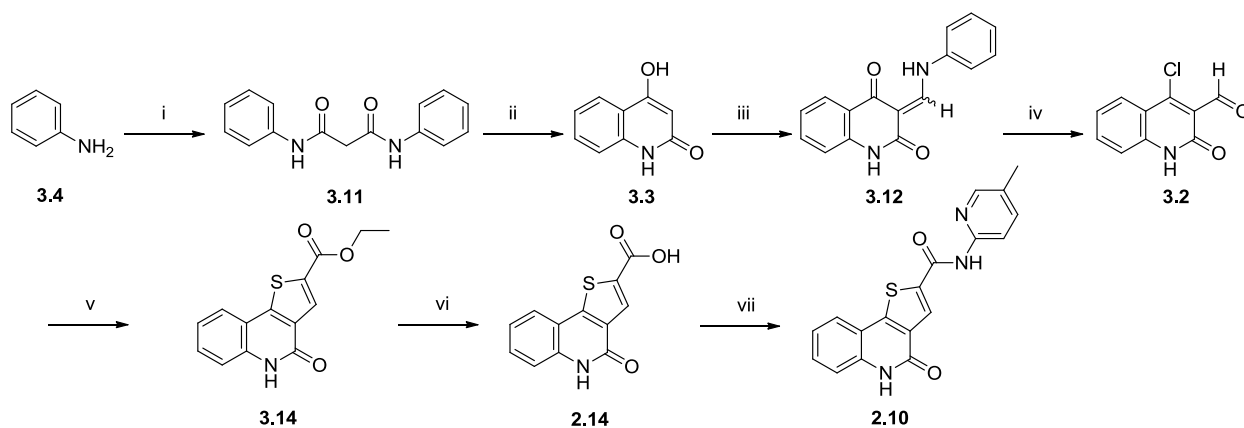
Scheme 3.9. Synthesis of **2.10** and **2.14**

Reagents and conditions: (i) Diethylmalonate, *cat.* DMF, 140 °C, 8 h, 95%; (ii) PPA, 150 °C, 3 h, 70%; (iii) Triethyl orthoformate, aniline, ethylene glycol, *mw*, 145 °C, 20 min, 82%; (iv) POCl₃, DMF, 8 h, 90%; (v) Ethyl 2-mercaptoacetate, K_2CO_3, *anhyd* EtOH, 80 °C, 3 h, 88%; (vi) LiOH, MeOH, H_2O, 12 h, 96%; (vii) 5-Methylpyridin-2-amine, HBTU, *i*Pr₂NEt, DMF, 30 °C, 12 h, 34%.

The overall syntheses of 4-oxo-4,5-dihydrothieno[3,2-c]quinoline-2-carboxylic acid (**2.14**) was achieved in six steps by using a sequence of Friedel–Crafts, Vilsmeier–Haack, S_NAr and cyclization reactions (Scheme 3.9).[102] We synthesized **2.10** by an activated ester coupling of **2.14** with 5-methylpyridin-2-amine. Compound **2.14** was used as a suitable precursor to access the functionalization of the C-ring by convergent analog synthesis. Since **2.14** was a key compound, we decided to fully assign the ^{1}H and ^{13}C chemical shifts (δ) from 1-D and 2-D NMR. The assignments are given in Table 3.3.

Table 3.3. ^{1}H and ^{13}C NMR assignments of **2.14**

2.14
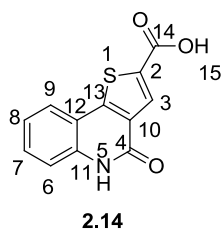
Position	δ_C (ppm)	δ_H (ppm)	Multiplicity (J-Values in Hz)	HMBC
2	133.88			C^2-HC^3
3	130.27	8.02	s, 1H	
4	157.78			C^4-HC^3
5		11.86	s, 1H, exchangeable	
6	116.38	7.41	d (8.4), 1H	C^6-HC^7, -HC^8, -HN^5
7	130.77	7.53	t (7.6), 1H	C^7-HC^9, -HC^6, -HC^8
8	122.65	7.24	t (7.6), 1H	C^8-HC^7, -HC^6
9	123.92	7.87	d (7.9), 1H	C^9-HC^7, -HC^8
10	130.94			C^{10}-HC^3, -HN^5
11	115.60			C^{11}-HC^6, -HN^5, -HC^8, -HC^9
12	137.14			C^{12}-HC^7, -HN^5, -HC^8, -HC^9
13	149.48			C^{13}-HC^3, -HC^9, -HC^6
14	162.52			C^{14}-HC^3
15		13.64	s, 1H, exchangeable	

The methyl ester (**3.15**) was synthesized by reacting **2.14** with TMS-diazomethane in 81% yield. The synthesis of the amide derivatives was achieved by reacting the acid chloride, generated in-situ with the corresponding amines.[102] We observed that a major by-product (**3.38**) was isolated in the reaction of the acid chloride with 2-aminopyridine (Scheme 3.10). This chlorinated product was observed only in case of the reaction with 2-aminopyridine, probably because of its strong basicity ($pK_a = 6.86$). In certain cases where the substituted amides contained Boc-protection (**3.23** and **3.25**), the deprotection was carried out with HCl in dioxane to yield the HCl salts (**3.24** and **3.26**). The free carboxylic acid derivatives (**3.34** and **3.36**) were prepared by the saponification of the methyl esters (**3.33** and **3.35**) with aqueous NaOH.

3.16-3.23, 3.25, 3.27-3.33, 3.35, 3.38

R substitutions as in Table 3.3
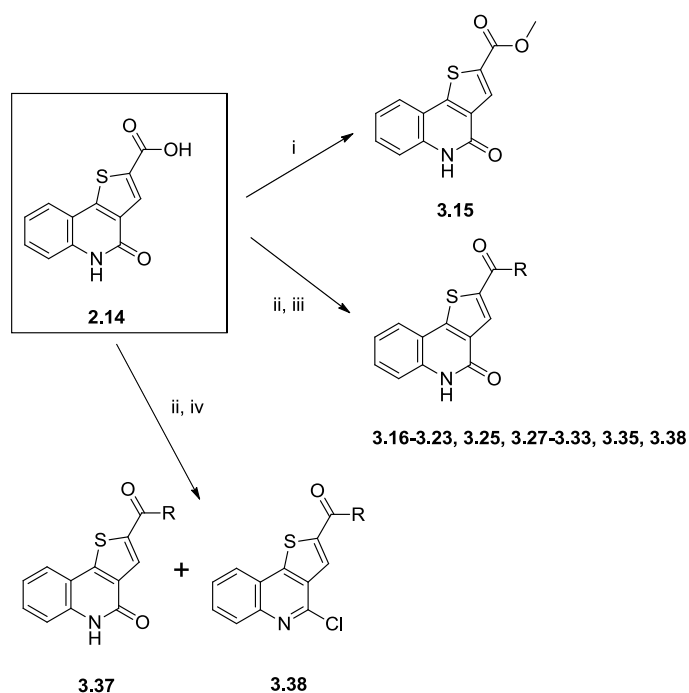
Scheme 3.10. Convergent syntheses of **3.15-3.39**
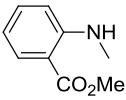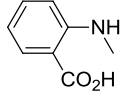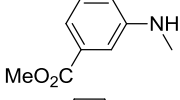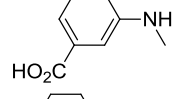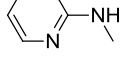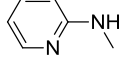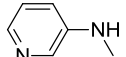
Reagents and conditions: (i) TMS diazomethane, CH_2Cl_2, MeOH, 81%; (ii) Oxalyl chloride, CH_2Cl_2, 3h, 0-30°C; (iii) Amines, Hunig's base, CH_2Cl_2, 8h, 23-86%; (iv) 2-aminopyridine, Hunig's base, CH_2Cl_2, 8h, 23-30%.

The R-substitutions and the yield of the convergent-synthesized amides are described in Table 3.4. All compounds were characterized by ^{1}H and ^{13}C NMR, and HRMS and the purities determined by HPLC (see in appendices).

Table 3.4. Isolated yield of the convergent syntheses amides
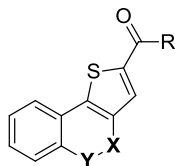
Compound	R	X	Y	% yield
3.16	-NH$_2$	C=O	NH	86
3.17	-NH(iPr)	C=O	NH	80
3.18	-NH(cyPr)	C=O	NH	71
3.19	-NH(cyHex)	C=O	NH	81
3.20	-NH(1-adamentyl)	C=O	NH	65
3.21	HO–CH$_2$CH$_2$–NH–	C=O	NH	83
3.22	HO–CH$_2$CH$_2$CH$_2$–NH–	C=O	NH	77
3.23	Boc-NH–CH$_2$CH$_2$–NH–	C=O	NH	65
3.24	H$_2$N–CH$_2$CH$_2$–NH–	C=O	NH	96[a]
3.25	Boc-NH–CH$_2$CH$_2$CH$_2$–NH–	C=O	NH	75
3.26	H$_2$N–CH$_2$CH$_2$CH$_2$–NH–	C=O	NH	92[a]
3.27	phenyl–NH–	C=O	NH	63
3.28	F–phenyl–NH–	C=O	NH	68
3.29	F–phenyl–NH–	C=O	NH	73
3.30	F,F–phenyl–NH–	C=O	NH	54
3.31	benzyl–HN–	C=O	NH	66
3.32	F–phenyl–CH$_2$CH$_2$–NH–	C=O	NH	58

44

3.33	2-(methylamino)phenyl, CO₂Me	C=O	NH	88
3.34	2-(methylamino)phenyl, CO₂H	C=O	NH	92[b]
3.35	3-(methylamino)phenyl, MeO₂C	C=O	NH	55
3.36	3-(methylamino)phenyl, HO₂C	C=O	NH	71[b]
3.37	2-(methylamino)pyridyl	C=O	NH	30
3.38	2-(methylamino)pyridyl	=C-Cl	N	23
3.39	3-(methylamino)pyridyl	C=O	NH	41

[a] Conversion yield represent the deprotection of the Boc- group from the preceding entries
[b] Conversion yield represent the hydrolysis of the methyl-esters from the preceding entries

3.3.   Conclusions

In summary, we developed an efficient one-step syntheses for 2,4-diamino thiazole derivative (**2.14**). We also developed one-step synthesis of the triazine derivative, **2.5**. The major achievement of the project was the development of a cost-effective and efficient synthesis of 4-oxo-4,5-dihydrothieno[3,2-*c*]quinoline-2-carboxylic acid (**2.14**) achieved in six steps. Some interesting features were highlighted: high yields with no chromatographic purification, operational simplicity and novelty. We also demonstrated the ease of derivatization of **2.14**, by synthesizing the convergent-synthesis analogs for SAR.

CHAPTER 4: EXPERIMENTAL OF THE SYNTHESIZED ANALOGS

Experimental Methods

General

Melting points were determined on an Opti-Melt automated melting point system (Stanford Research Systems) and are uncorrected. IR spectra were recorded using an Agilent model Cary 630 FT-IR. ^{1}H and ^{13}C NMR spectra were obtained on Bruker model AMX 500 and Avance 400 NMR spectrometers with standard pulse sequences, operating at 500 and 400 MHz for ^{1}H and 125 and 100 MHz for [13]C. The residual DMSO-d_6 solvent signals (DMSO-d_6: δ_H = 2.50 ppm and δ_C = 39.51 ppm) were used as an internal reference. The chemical shifts (δ) were expressed in ppm. Multiplicities were described as singlet (s), doublet (d), triplet (t), multiplet (m) and broad resonance (br). The coupling constants (J) were expressed in Hz. Low-resolution mass spectra (LRMS) were recorded on a Waters Micromass Quattro micro™ spectrometer with electro spray ionization (ESI) interface. High-resolution mass spectra (HRMS) were recorded on either a Bruker Daltonics micro-TOF mass spectrometer or a Micromass Q-TOF Agilent G1969A mass spectrometer with ESI interface. R (-) roscovitine (**1**) was purchased from Enzo Life Sciences (www.enzolifesciences.com). 1-(4-(((4-chlorophenyl)thio)methyl)-6-hydroxypyrimidin-2-yl)-3-(4-methoxyphenyl)guanidine (**6**) and 4-(4,6-dimethyl-2-(pyridin-2-yl)-1H-indol-3-yl)butanoic acid (**11**) were purchased from ChemBridge (www.chembridge.com) N-(5-((2-oxo-2-(p-tolylamino)ethyl)thio)-1,3,4-thiadiazol-2-yl)-3-phenylpropanamide (**7**), N-(3-(1H-pyrazol-1-yl)propyl)-2-oxo-1,2,3,4-tetrahydroquinoline-6-sulfonamide (**8**) and 2-((4-((4-methoxyphenyl)amino)pteridin-2-yl)amino)ethanol (**12**) were purchased from Ryan Scientific, Inc. (https://ryansci.com). 2-((3-(4-Methoxybenzyl)-4-oxo-3,4-dihydropteridin-2-yl)thio)-N-(3-methyl-1H-pyrazol-5-yl)acetamide (**9**) and 2-((4-((3,4-dimethylphenyl)amino)-1-phenyl-1H-

pyrazolo[3,4-d]pyrimidin-6-yl)amino)ethanol (**13**) were purchased from ChemDiv (www.chemdiv.com). All the purchased standards were characterized by ^{1}H NMR and HRMS. The purity was checked by HPLC and found to have purity of >95%. Column chromatography was carried out on silica gel (70-230 mesh, Merck). TLC was performed on silica gel 60 F$_{254}$ plates. Anhydrous DMF and CH$_2$Cl$_2$ were purchased in sure-seal® bottles from Aldrich. All the reagents were used without further purification unless otherwise noted. A Biotage® Initiator microwave was used for all microwave (*MW*) reactions. All the HPLC analysis were performed on Waters W2690/5, attached with a 996 PDA detector, using X-tera C-18, 3x100 column and using a gradient system (Table 3.1) consisting of water (0.1% formic acid) and acetonitrile (0.1% formic acid).

Table 4.1.   Gradient-mix used for HPLC purity determination

Time (min)	Flow (mL/min)	% water	% acetonitrile
0.00	0.30	90.0	10.0
2.00	0.30	90.0	10.0
22.00	0.30	5.0	95.0
23.00	0.30	0.0	100.0
25.00	0.30	0.0	100.0
27.00	0.30	90.0	10.0
42.00	0.30	90.0	10.0
43.00	0.00	90.0	10.0

Synthesis of (4-amino-2-((4-chlorophenyl)amino)thiazol-5-yl)(3-nitrophenyl) methanone (2.4).

2.4
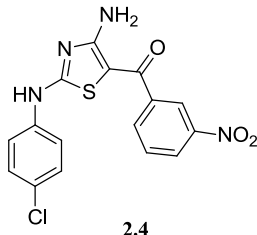
To a stirred suspension of cyanamide (0.0505g, 1.2 mmol) in 40 mL of CH$_3$CN was added 4-chlorophenyl isothiocyanate (**3.5**) (0.17 g, 1 mmol) in 5 mL of butanol and KOtBu (0.135 g, 1.2 mmol). The mixture was stirred at ambient temperature for 30 min and a suspension of 2-bromo-3′-nitroacetophenone (**3.6**) (0.6 g, 2.9 mmol) in 10 mL of CH$_3$CN was added and stirred for 2h. The precipitated solid was triturated with water, extracted with EtOAc and layers were separated. The organics were extracted with saturated brine, dried over anhydrous Na$_2$SO$_4$, filtered, and purified on silica gel using CH$_2$Cl$_2$:EtOAc (8:2) to yield the title compound as a yellow solid (0.22 g, 59%). ^{1}H NMR (400 MHz, DMSO) δ 11.02 (s, 1H), 8.45 (s, 2H, ex), 8.40 (s, 1H, ex), 8.35 (d, J = 8.3 Hz, 2H), 8.14 (d, J = 7.5 Hz, 1H), 7.80 (t, J = 8.0 Hz, 1H), 7.68 (d, J = 8.3 Hz, 2H), 7.42 (d, J = 8.4 Hz, 2H). ^{13}C NMR (100 MHz, DMSO) δ 179.42, 166.89, 166.27, 147.65, 142.74, 138.35, 133.20, 130.35, 128.96, 127.03, 125.07, 121.41, 120.48, 92.22. HRMS (ESI-TOF) m/z calcd for C$_{16}$H$_{10}$ClN$_4$O$_3$S [M-H]$^-$: 373.0162. Found: 373.0164. HPLC: retention time 19.27 min; purity >99%.

Synthesis of 2-((4-((4-chlorophenyl)amino)-6-methoxy-1,3,5-triazin-2-yl)amino) ethanol (2.5).

2.5
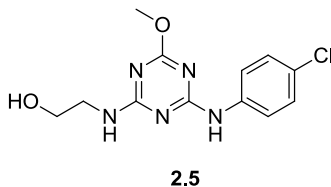
To a stirred solution of 2,4-dichloro-6-methoxy-1,3,5-triazine (**3.7**) (0.4 g, 2.22 mmol) and Hunig's base (0.43 g, 3.33 mmol) in 50 mL of CH$_2$Cl$_2$ at 0 °C was added 4-chloroaniline

(0.34 g, 2.66 mmol). The mixture was stirred at ambient temperature for 30 min and a solution of ethanol amine (212 µL, 2.66 mmol) and Hunig's base (0.43 g, 3.33 mmol) in 40 mL of CH_2Cl_2 was added to the reaction mixture. The mixture was stirred for 8h and monitored by TLC. It was then concentrated *in vacuo*, diluted with EtOAc and extracted with saturated $NaHCO_3$. The organics were extracted with saturated brine, dried over anhydrous Na_2SO_4, filtered, and purified over silica gel using CH_2Cl_2:EtOAc (8:2) to yield the title compound as a white solid (0.461 g, 70%). ^1H NMR (400 MHz, DMSO) δ 9.79 − 9.40 (m, 1H, ex), 7.77 (d, J = 8.7 Hz, 2H), 7.43 (brs, 1H), 7.31 (d, J = 8.7 Hz, 2H), 4.68 (d, J = 5.1 Hz, 1H, ex), 3.81 (s, 3H), 3.61 − 3.44 (m, 2H), 3.42 − 3.33 (m, 2H). ^{13}C NMR (100 MHz, DMSO) δ 170.36, 166.84, 165.10, 138.92, 128.23, 125.48, 121.15, 59.64, 53.58, 42.88. HRMS (ESI-TOF) *m/z* calcd for $C_{12}H_{13}ClN_5O_2$ [M-H]$^-$: 294.0758. Found: 294.0783. HPLC: retention time 13.57 min; purity >99%.

Synthesis of methyl 2-aminobenzoate (3.9)

3.9
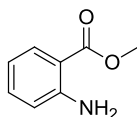
To a stirred suspension of anthranilic acid (**3.8**) (3.8 g, 27.7 mmol) in 50 mL of MeOH was added conc. H_2SO_4 (2 mL) and the mixture was refluxed for 12h and monitored by TLC. It was then concentrated *in vacuo*, diluted with EtOAc and neutralized with saturated $NaHCO_3$. The organics were separated and extracted with saturated brine, dried over anhydrous Na_2SO_4, filtered, and purified over silica gel using hexane:EtOAc (95:5) to yield the title compound as a white solid (2.69 g, 64%). ^1H NMR (400 MHz, DMSO-d_6) δ 7.69 (d, J = 8.0 Hz, 1H), 7.24 (t, J = 7.7 Hz, 1H), 6.76 (d, J = 8.3 Hz, 1H), 6.63 (s, 2H), 6.52 (t, J = 7.5 Hz, 1H), 3.78 (s, 3H). MS (ESI) *m/z* calcd for $C_8H_{10}NO_2$ [M+H]$^+$: 152.07. Found 152.41.

Synthesis of methyl 2-acetamidobenzoate (3.10)

3.10
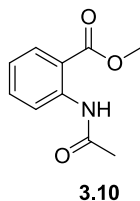
To a stirred solution of methyl 2-aminobenzoate (**3.9**) (1.0 g, 6.6 mmol) in 20 mL of dioxane was added acetic anhydride (10 mL) and the mixture was refluxed for 2h and monitored by TLC. It was then concentrated *in vacuo*, diluted with EtOAc and neutralized with saturated NaHCO$_3$. The organics were separated and extracted with saturated brine, dried over anhydrous Na$_2$SO$_4$, filtered, and purified over silica gel using hexane:EtOAc (95:5) to yield the title compound as a white solid (0.715 g, 56%). ^{1}H NMR (400 MHz, DMSO-d$_6$) δ 10.53 (s, 1H), 8.21 (d, J = 8.3 Hz, 1H), 7.89 (d, J = 7.9 Hz, 1H), 7.59 (t, J = 7.9 Hz, 1H), 7.18 (t, J = 7.6 Hz, 1H), 3.85 (s, 3H), 2.11 (s, 3H). MS (ESI) *m/z* calcd for C$_{10}$H$_{12}$NO$_3$ [M+H]$^+$: 194.08. Found 194.47.

Alternate synthesis of 4-hydroxyquinolin-2(1*H*)-one (3.3):

3.3
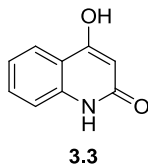
To a stirred solution of methyl 2-acetamidobenzoate (**3.10**) (0.7 g, 3.62 mmol) in 50 mL of THF was added a solution of potassium bis(trimethylsilyl)amide in toluene (20 mL, 10 mmol) at -78 °C under argon. The mixture was then allowed to warm to the ambient temperature for 12h. The mixture was quenched by pouring into ice-water. The aqueous layer was washed with EtOAc (10 mL). The aqueous fraction was acidified with 1N HCl to precipitate the desired product, which was filtered, washed with water and dried under vacuum to yield the title compound as a white solid (0.23 g, 40%). ^{1}H NMR (400 MHz, DMSO-d$_6$) δ 11.38 (s, 1H), 11.17

(s, 1H), 7.77 (d, J = 8.0 Hz, 1H), 7.48 (t, J = 7.7 Hz, 1H), 7.25 (d, J = 8.2 Hz, 1H), 7.13 (t, J =

7.6 Hz, 1H), 5.75 (s, 1H). MS (ESI) m/z calcd for $C_9H_8NO_2$ [M+H]$^+$: 162.05. Found 162.35.

m/z calcd for $C_9H_7NNaO_2$ [M+23]$^+$: 184.04. Found 184.33

Synthesis of N^1,N^3-diphenylmalonamide (3.11):

3.11
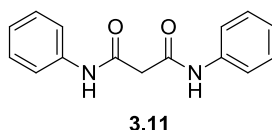
Catalytic amount of DMF was added to a stirred solution of aniline (**3.4**) (10 g, 108

mmol) and diethyl malonate (8.7 g, 54 mmol). The reaction mixture was heated at 140 °C for 8h.

The precipitated solid was filtered and washed with Et$_2$O to produce the title compound as a

white solid (13.03 g, 95%); mp 228-229 °C; FTIR ν_{max} (cm^{-1}): 3268, 3147, 1667, 1643, 1595,

1531, 1497, 1413, 1354, 1248, 1192, 979; ^{1}H- NMR (400 MHz, DMSO-d$_6$) δ 10.16 (s, 2H), 7.60

(d, J = 7.9 Hz, 4H), 7.32 (t, J = 7.9 Hz), 7.06 (t, J = 7.4 Hz), 3.47 (s, 2H). ^{13}C-NMR (100 MHz,

DMSO-d$_6$) δ 165.41, 138.95, 128.75, 123.37, 119.07, 45.94. HRMS (ESI-TOF) m/z calcd for

$C_{15}H_{15}N_2O_2$ [M+H]$^+$: 255.1134. Found: 255.1144.

Synthesis of 4-hydroxyquinolin-2(1H)-one (3.3):

3.3
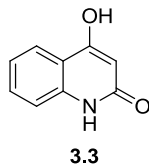
N^1,N^3-diphenylmalonamide (**3.11**) (12.76 g, 50 mmol) was added in portions to a stirred

solution of PPA (50 g) at 150 °C and stirred for 3h. It was then quenched by pouring onto ice-

water, resulting in precipitation. The solid was filtered and dissolved into 200 mL of 1N NaOH.

Any undissolved solid was removed by filtration. The filtrate was acidified with 1N HCl to

precipitate the desired product, which was filtered, washed with water and dried under vacuum to

yield the title compound as a white solid (6.01 g, 74%); mp 329-330 °C (dec); FTIR ν_{max} (cm^{-1}): 3090, 2984, 2854, 649, 1634, 1591, 1414, 1233, 860, 753; ^{1}H NMR (400 MHz, DMSO-d_6) δ 11.28 (br s, 1H), 11.18 (s, 1H), 7.77 (d, J = 7.8 Hz, 1H), 7.48 (t, J = 7.6 Hz, 1H), 7.25 (d, J = 8.2 Hz, 1H), 7.13 (t, J = 7.5 Hz, 1H), 5.73 (s, 1H). ^{13}C NMR (100 MHz, DMSO-d_6) δ 163.60, 162.47, 139.19, 130.84, 122.66, 121.05, 115.13, 115.02, 98.24, 83.17. HRMS (ESI-TOF) m/z calcd for $C_9H_8NO_2$ [M+H]$^{+}$: 162.0555. Found: 162.0550.

Synthesis of 3-((phenylamino)methylene)quinoline-2,4(1*H*,3*H*)-dione (3.12):

3.12
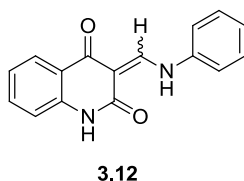
To a microwave vial containing aniline (0.38 g, 4.04 mmol) and triethylorthoformate (0.6 g, 4.04 mmol) in 10 mL of ethylene glycol was added 4-hydroxyquinolin -2(1*H*)-one (**3.3**). The reaction mixture was heated in a microwave at 140 °C for 40 min. The precipitated solid was filtered and washed with EtOH to produce the title compound as a mixture of *E*- and *Z*- isomers (0.87 g, 82%); ^{1}H NMR (400 MHz, DMSO- d_6) δ 13.70 (d, J = 12.5 Hz), 12.81 (d, J = 12.5 Hz), 10.94 (s), 10.87 (s), 8.88 (d, J = 12.0 Hz, 1H), 7.96 (d, J = 7.8 Hz, 1H), 7.63 – 7.43 (m, 5H), 7.30 (t, J = 6.9 Hz, 1H), 7.24 – 7.08 (m, 2H). ^{13}C NMR (125 MHz, DMSO- d_6) δ 181.72, 178.87, 165.85, 163.30, 152.96, 152.30, 141.27, 140.73, 138.44, 138.32, 133.79, 133.68, 129.92, 129.86, 126.40, 126.15, 125.97, 125.53, 121.70, 121.42, 120.35, 119.63, 118.66, 118.62, 118.49, 116.16, 115.87, 103.02, 102.32. HRMS (ESI-TOF) m/z calcd for $C_{15}H_{15}N_2O_2$ [M+H]$^{+}$: 265.0977. Found: 265.0949.

Synthesis of 4-chloro-2-oxo-1,2-dihydroquinoline-3-carbaldehyde (3.2):

3.2
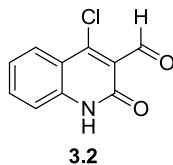
To a stirred solution of 3-((phenylamino)methylene)quinoline-2,4(1*H*,3*H*)-dione (**3.12**) (0.87 g, 3.29 mmol) in 10 mL of DMF at 0 °C was added POCl$_3$ (2.5 g, 16.5 mmol). The reaction mixture was stirred at 0 °C for 15 min and then stirred at ambient temperature for 8h. It was then quenched by pouring onto ice-water, resulting in precipitation. The solid was filtered, washed with Et$_2$O and dried under vacuum to yield the title compound as a yellow solid (0.61 g, 90%); mp 258-259 °C (dec); FTIR ν_{max} (cm^{-1}): 3156, 2981, 2854, 2716, 1701, 1646, 1612, 1587, 1538, 1479, 1436, 1235, 960, 750; ^{1}H NMR (400 MHz, DMSO-d_6) δ 12.42 (s, 1H), 10.29 (s, 1H), 8.06 (d, *J* = 8.3 Hz, 1H), 7.70 (t, *J* = 7.7 Hz, 1H), 7.50 – 7.26 (m, 2H); ^{13}C NMR (100 MHz, DMSO-d_6) δ 189.33, 160.37, 146.27, 139.54, 134.12, 126.66, 123.33, 122.71, 117.43, 115.92. HRMS (ESI-TOF) *m/z* calcd for C$_{10}$H$_5$ClNO$_2$ [M-H]$^-$: 206.0009. Found: 206.0071.

Synthesis of ethyl 4-oxo-4,5-dihydrothieno[3,2-*c*]quinoline-2-carboxylate (3.14):

3.14
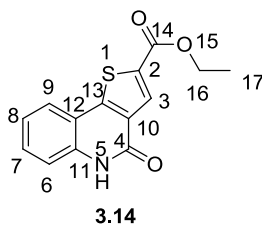
To a stirred suspension of K$_2$CO$_3$ (1.2 g, 8.7 mmol) in 20 mL of anhydrous EtOH, was added ethyl 2-mercaptoacetate (0.52 g, 4.35 mmol). The reaction was stirred for 10 min and a suspension of 4-chloro-2-oxo-1,2-dihydroquinoline-3-carbaldehyde (**3.2**) (0.6 g, 2.9 mmol) in 10 mL of EtOH was added and stirred at 80 °C for 3h. The precipitated solid was filtered, triturated with water, re-filtered, washed with EtOH and dried to yield the title compound as a white solid (0.7 g, 88%); mp 315-317 °C (dec); FTIR ν_{max} (cm^{-1}): 3020, 2875, 1711, 1655, 1589, 1513, 1467,

1366, 1284, 1246, 1153, 1071, 745; ^{1}H NMR (400 MHz, DMSO-d_6) δ 11.92 (s, 1H, H^5), 8.10 (s, 1H, H^3), 7.94 (d, J = 7.7 Hz, 1H, H^9), 7.57 (t, J = 7.3 Hz, 1H, H^7), 7.43 (d, J = 8.0 Hz, 1H, H^6), 7.27 (t, J = 7.1 Hz, 1H, H^8), 4.36 (q, J = 6.4 Hz, 2H, H^{16}), 1.35 (t, J = 6.7 Hz, 3H, H^{17}). ^{13}C NMR (100 MHz, DMSO-d_6) δ 160.79, 157.48, 149.53, 137.13, 131.91, 130.72, 130.58, 123.73, 122.48, 116.25, 115.33, 61.41, 13.87. HRMS (ESI-TOF) m/z calcd for C$_{14}$H$_{12}$NO$_3$S [M+H]$^+$: 274.0538. Found: 274.0536. HPLC: retention time 19.26 min; purity >99%.

Synthesis of 5-dihydrothieno[3,2-*c*]quinoline-2-carboxylic acid (2.14):

2.14
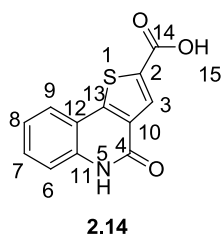
To a stirred suspension of ethyl 4-oxo-4,5-dihydrothieno[3,2-*c*]quinoline-2-carboxylate (**3.14**) (1.28 g, 4.68 mmol) in 50 mL of (1:1) MeOH-H$_2$O was added LiOH (0.5 g, 11.71 mmol). The mixture was stirred for 12h, filtered and the filtrate was concentrated *in vacuo* to evaporate the MeOH. Acidification with 6N HCl yielded the title compound as a white precipitate. The solid was filtered, washed with water and Et$_2$O and dried to yield the title compound as a white solid (1.1 g, 96%); mp 371 °C; FTIR ν$_{max}$ (cm^{-1}): 3090, 2983, 2067, 1685, 1644, 1587, 1541, 1404, 1159, 839, 743; ^{1}H NMR (400 MHz, DMSO-d_6) δ 13.64 (s, 1H, H^{15}), 11.86 (s, 1H, H^5), 8.02 (s, 1H, H^3), 7.87 (d, J = 7.9 Hz, 1H, H^9), 7.53 (t, J = 7.6 Hz, 1H, H^7), 7.41 (d, J = 8.4 Hz, 1H, H^6), 7.24 (t, J = 7.6 Hz, 1H, H^8). ^{13}C NMR (100 MHz, DMSO-d_6) δ 162.52 (C^{14}), 157.78 (C^4), 149.48 (C^{13}), 137.14(C^{12}), 133.88 (C^2), 130.94 (C^{10}), 130.77 (C^7), 130.27 (C^3), 123.92 (C^9), 122.65 (C^8), 116.38 (C^6), 115.60 (C^{11}). HRMS (ESI-TOF) m/z calcd for C$_{12}$H$_8$NO$_3$S [M+H]$^+$: 246.0225. Found: 246.0244. HPLC: retention time 12.58 min; purity >99%.

***N*-(5-methylpyridin-2-yl)-4-oxo-4,5-dihydrothieno[3,2-*c*]quinoline-2-carboxamide (2.10).**
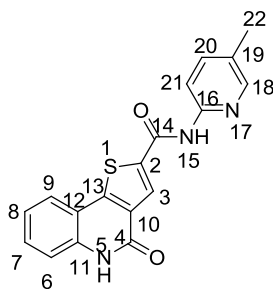
2.10

To a stirred suspension of 5-dihydrothieno[3,2-*c*]quinoline-2-carboxylic acid (**2.14**) (0.18 g, 0.73 mmol) in 10 mL of DMF was added HBTU (0.279 g, 0.73 mmol) and Hunig's base (0.472 g, 3.65 mmol). The mixture was stirred at ambient temperature for 30 min and a solution of 5-methylpyridin-2-amine (0.118g, 1.1 mmol) in 2 mL of DMF was added to the reaction mixture. The mixture was stirred for 8h and monitored by TLC. It was then concentrated *in vacuo* to a slurry, filtered through a Strata™ X-C pre-packed column and purified over silica gel using CH$_2$Cl$_2$:MeOH with 1% NH$_3$ (95:5) to yield the title compound as a white solid (0.083 g, 34%). ^{1}H NMR (400 MHz, DMSO) δ 11.83 (s, 1H, ex, H^5), 11.20 (s, 1H, ex, H^{15}), 8.75 (s, 1H, H^3), 8.25 (s, 1H, H^{18}), 8.03 (d, *J* = 8.4 Hz, 1H, H^9), 7.92 (d, *J* = 7.9 Hz, 1H, H^{21}), 7.67 (d, *J* = 8.4 Hz, 1H, H^{20}), 7.55 (t, *J* = 7.7 Hz, 1H, H^7), 7.43 (d, *J* = 8.3 Hz, 1H, H^6), 7.26 (t, *J* = 7.6 Hz, 1H, H^8), 2.29 (s, 3H, H^{22}). ^{13}C NMR (125 MHz, DMSO) δ 159.79, 157.93, 149.41, 148.80, 147.78, 138.92, 138.49, 136.97, 131.53, 130.57, 129.05, 127.65, 124.02, 122.60, 116.32, 115.66, 114.46, 17.30. HRMS (ESI-TOF) *m/z* calcd for C$_{18}$H$_{14}$N$_3$O$_2$S [M+H]$^+$: 336.0807. Found: 336.0818. HPLC: retention time 14.29 min; purity >99%.

Synthesis of methyl 4-oxo-4,5-dihydrothieno[3,2-*c*]quinoline-2-carboxylate (3.15):

3.15

56
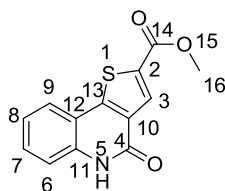
TMS-diazomethane (150 μL, 0.3 mmol) was added drop-wise to a stirred suspension of 5-dihydrothieno[3,2-c]quinoline-2-carboxylic acid (**2.14**) (0.025g, 0.1 mmol) in a mixture of 5 mL of CH_2Cl_2 and 1 mL of MeOH. The reaction mixture was stirred for 3h and monitored by TLC. It was then quenched with few drops of AcOH and stirred for an additional 2h, concentrated *in vacuo* to dryness and purified by column chromatography on silica gel to give the title compound as a white solid (0.021 g, 81%); mp 314-316 °C; FTIR ν_{max} (cm^{-1}): 2877, 1718, 1591, 1468, 1430, 1286, 1251, 1153, 1071, 702; ^{1}H NMR (400 MHz, DMSO-d_6) δ 11.91 (s, 1H, H^5), 8.08 (s, 1H, H^3), 7.91 (d, J = 7.9 Hz, 1H, H^9), 7.56 (t, J = 7.6 Hz, 1H, H^7), 7.42 (d, J = 8.2 Hz, 1H, H^6), 7.26 (t, J = 7.0 Hz, 1H, H^8), 3.90 (s, 3H, H^{16}). ^{13}C NMR (125 MHz, DMSO-d_6) δ 161.51, 157.72, 149.83, 137.28, 131.71, 131.10, 130.91, 124.09, 122.79, 116.46, 115.47, 52.85. HRMS (ESI-TOF) m/z calcd for $C_{13}H_8NO_3S$ [M-H]$^-$: 258.0225. Found: 258.0234. HPLC: retention time 14.60 min; purity >99%.

General procedure for synthesis of carboxamides (3.16-3.23, 3.25, 3.27-3.33, 3.35, 3.37-3.39):

To a stirred suspension of 5-dihydrothieno[3,2-c]quinoline-2-carboxylic acid (**2.14**) (0.025g, 0.1 mmol) in 5 mL of CH_2Cl_2 was added oxalyl chloride (0.02 g, 0.15 mmol) and 2 drops of DMF. The reaction mixture was stirred for 2h and then concentrated *in vacuo*. The dried suspension of the acid chloride in 10 mL of CH_2Cl_2 was added to a stirred solution of the respective amines (0.03 mmol) and Hunig's base (in 5 mL of CH_2Cl_2) and the reaction mixture was stirred for 12h. It was then concentrated to dryness and purified on silica gel column to give the title compounds.

4-Oxo-4,5-dihydrothieno[3,2-c]quinoline-2-carboxamide (3.16):
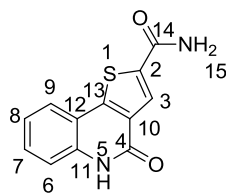
3.16

White solid (86%); mp 334 °C (dec); FTIR ν_{max} (cm^{-1}): 3206, 3086, 1662, 1616, 1518, 1423, 1374, 1106, 747; ^{1}H NMR (400 MHz, DMSO-d_6) δ 11.79 (s, 1H, H^5), 8.30 (s, 2H, H^{3,15}), 7.88 (d, J = 7.9 Hz, 1H, H^9), 7.66 (s, 1H, H^{15}), 7.53 (t, J = 7.7 Hz, 1H, H^6), 7.43 (d, J = 8.3 Hz, 1H, H^7), 7.25 (t, J = 7.6 Hz, 1H, H^8). ^{13}C NMR (125 MHz, DMSO-d_6) δ 162.38, 157.99, 148.12, 139.86, 136.79, 131.33, 130.30, 126.20, 123.81, 122.57, 116.30, 115.80. HRMS (ESI-TOF) m/z calcd for $C_{12}H_7N_2O_2S$ [M-H]$^-$: 243.0228. Found: 243.0248. HPLC: retention time 11.09 min; purity >99%.

_N_-Isopropyl-4-oxo-4,5-dihydrothieno[3,2-_c_]quinoline-2-carboxamide (3.17):
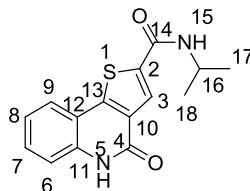
3.17

White solid (80%); ^{1}H NMR (400 MHz, DMSO-d_6) δ 11.77 (s, 1H, H^5), 8.62 (d, J = 8.1 Hz, 1H, H^{15}), 8.36 (s, 1H, H^3), 7.88 (d, J = 8.2 Hz, 1H, H^9), 7.53 (t, J = 8.0 Hz, 1H, H^7), 7.43 (d, J = 8.4 Hz, 1H, H^6), 7.25 (t, J = 7.9 Hz, 1H, H^8), 4.50 – 3.70 (m, 1H, H^{16}), 1.19 (d, J = 6.8 Hz, 6H, H^{17,18}). ^{13}C NMR (125 MHz, DMSO-d_6) δ 159.66, 158.06, 147.76, 139.99, 136.78, 131.29, 130.30, 125.43, 123.84, 122.64, 116.35, 115.86, 41.40, 22.27. HRMS (ESI-TOF) m/z calcd for $C_{15}H_{13}N_2O_2S$ [M-H]$^-$: 285.0698. Found: 285.0692. HPLC: retention time 13.70 min; purity >98%.

_N_-Cyclopropyl-4-oxo-4,5-dihydrothieno[3,2-_c_]quinoline-2-carboxamide (3.18):
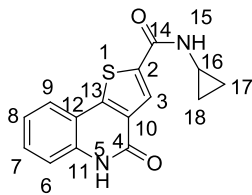
3.18

White solid (71%); ^{1}H NMR (400 MHz, DMSO-d_6) δ 11.77 (s, 1H, H^5), 8.81 (s, 1H, H^{15}), 8.28 (s, 1H, H^3), 7.89 (d, J = 8.1 Hz, 1H, H^9), 7.53 (t, J = 7.9 Hz, 1H, H^7), 7.43 (d, J = 8.4 Hz, 1H, H^6), 7.25 (t, J = 7.6 Hz, 1H, H^8), 2.94 - 2.76 (m, 1H, H^{16}), 0.82 - 0.50 (m, 4H, H^{17,18}). ^{13}C NMR (100 MHz, DMSO-d_6) δ 161.72, 158.00, 147.82, 139.47, 136.78, 131.28, 130.34, 125.54, 123.85, 122.63, 116.33, 115.80, 23.05, 5.72. HRMS (ESI-TOF) m/z calcd for $C_{15}H_{11}N_2O_2S$ [M-H]$^-$: 283.0541. Found: 283.0549. HPLC: retention time 14.19 min; purity >96%.

3.2.15.4. *N*-Cyclohexyl-4-oxo-4,5-dihydrothieno[3,2-*c*]quinoline-2-carboxamide (3.19):
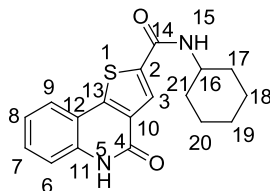
3.19

White solid (81%); ^{1}H NMR (400 MHz, DMSO-d_6) δ 11.77 (s, 1H, H^5), 8.62 (d, J = 8.0 Hz, 1H, H^{15}), 8.38 (s, 1H, H^3), 7.88 (d, J = 7.9 Hz, 1H, H^9), 7.53 (t, J = 7.7 Hz, 1H, H^7), 7.43 (d, J = 8.2 Hz, 1H, H^6), 7.25 (t, J = 7.6 Hz, 1H, H^8), 4.13 – 3.54 (m, 1H, H^{16}), 1.92 – 1.70 (m, 4H, H^{17,21}), 1.61 (d, J = 12.7 Hz, 1H, H^{19}), 1.40 – 1.22 (m, 4H, H^{18,20}), 1.21 – 1.09 (m, 1H, H^{19}). ^{13}C NMR (100 MHz, DMSO-d_6) δ 159.60, 158.07, 147.78, 140.01, 136.79, 131.31, 130.31, 125.49, 123.87, 122.64, 116.35, 115.87, 48.64, 32.38, 25.21, 24.86. HRMS (ESI-TOF) m/z calcd for $C_{18}H_{17}N_2O_2S$ [M-H]$^-$: 325.1011. Found: 327.1019. HPLC: retention time 15.16 min; purity >98%.

N-((3s,5s,7s)-Adamantan-1-yl)-4-oxo-4,5-dihydrothieno[3,2-c]quinoline-2-carboxamide (3.20):
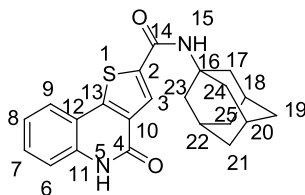
3.20

White solid (65%); ^{1}H NMR (500 MHz, DMSO-d_6) δ 11.76 (s, 1H, H^5), 8.44 (s, 1H, H^{15}), 8.07 (s, 1H, H^3), 7.87 (d, J = 7.8 Hz, 1H, H^9), 7.52 (t, J = 7.7 Hz, 1H, H^7), 7.42 (d, J = 8.1 Hz, 1H, H^6), 7.25 (t, J = 7.6 Hz, 1H, H^8), 2.23 – 1.99 (m, 9H, H$^{17,\ 18,20,22\text{-}24}$), 1.78 – 1.57 (m, 6H, H^{19,21,25}). ^{13}C NMR (125 MHz, DMSO-d_6) δ 159.99, 158.08, 147.63, 141.16, 136.75, 131.29, 130.24, 125.71, 123.86, 122.60, 116.31, 115.87, 52.16, 40.84, 36.00, 28.89. HRMS (ESI-TOF) m/z calcd for $C_{22}H_{21}N_2O_2S$ [M-H]$^-$: 377.1324. Found: 377.1317. HPLC: retention time 18.37 min; purity >99%.

N-(2-Hydroxyethyl)-4-oxo-4,5-dihydrothieno[3,2-c]quinoline-2-carboxamide (3.21):
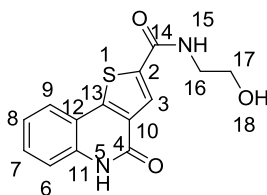
3.21

White solid (83%); mp 307-309 °C; FTIR ν_{max} (cm^{-1}): 3358, 2820, 1655, 1624, 1548, 1434, 1300, 1255, 1064, 903, 708; ^{1}H NMR (400 MHz, DMSO-d_6) δ 11.78 (s, 1H, H^5), 8.84 (s, 1H, H^{15}), 8.32 (s, 1H, H^3), 7.89 (d, J = 7.8 Hz, 1H, H^9), 7.53 (t, J = 7.6 Hz, 1H, H^7), 7.43 (d, J = 8.1 Hz, 1H, H^6), 7.25 (t, J = 7.4 Hz, 1H, H^8), 4.77 (t, J = 4.8 Hz, 1H, H^{18}), 3.53 (q, J = 5.1 Hz, 2H, H^{16}), 3.33 (q, J = 5.7 Hz, 2H, H^{17}). ^{13}C NMR (125 MHz, DMSO-d_6) δ 160.73, 158.07, 147.83, 139.73, 136.82, 131.34, 130.38, 125.54, 123.91, 122.67, 116.37, 115.85, 59.58, 42.30.

HRMS (ESI-TOF) m/z calcd for $C_{14}H_{13}N_2O_3S$ [M+H]$^+$: 289.0647. Found: 289.0627. HPLC: retention time 10.95 min; purity >99%.

**N-(3-Hydroxypropyl)-4-oxo-4,5-dihydrothieno[3,2-c]quinoline-2-carboxamide (3.22)**

3.22
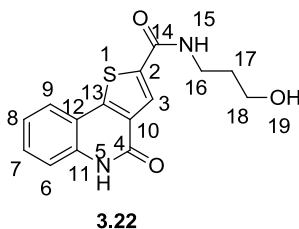
White solid (77%); ^{1}H NMR (400 MHz, DMSO-d_6) δ 11.69 (s, 1H, H^5), 8.81 (br s, 1H, H^{15}), 8.30 (s, 1H, H^3), 7.88 (d, J = 7.9 Hz, 1H, H^9), 7.53 (t, J = 7.8 Hz, 1H, H^7), 7.43(d, J = 8.3 Hz, 1H, H^6), 7.25 (t, J = 7.6 Hz, 1H, H^8), 4.48 (br s, 1H, H^{19}), 3.48 (m, 2H, H^{18}), 3.32 (overlapped, 2H, H^{16}), 1.70 (m, 2H, H^{17}). ^{13}C NMR (100 MHz, DMSO-d_6) δ 160.53, 158.00, 147.74, 139.72, 136.77, 131.29, 130.28, 125.31, 123.81, 122.60, 116.32, 115.81, 58.45, 36.66, 32.26. HRMS (ESI-TOF) m/z calcd for $C_{12}H_7N_2O_2S$ [M-H]$^-$: 301.0647. Found: 301.0640. HPLC: retention time 11.31 min; purity >99%.

tert-Butyl(2-(4-oxo-4,5-dihydrothieno[3,2-c]quinoline-2-carboxamido)ethyl) carbamate (3.23)

3.23
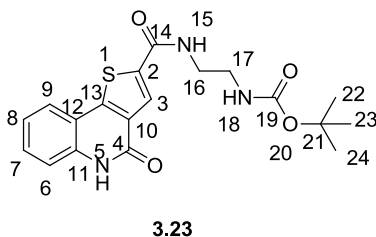
White solid (65%); ^{1}H NMR (400 MHz, DMSO-d_6) δ 11.78 (s, 1H, H^5), 8.82 (t, J = 5.9 Hz, 1H, H^{15}), 8.28 (s, 1H, H^3), 7.89 (d, J = 7.9 Hz, 1H, H^9), 7.53 (t, J = 7.7 Hz, 1H, H^7), 7.43(d, J = 8.3 Hz, 1H, H^6), 7.25 (t, J = 7.5 Hz, 1H, H^8), 6.92 (t, J = 6.1 Hz, 1H, H^{18}), 3.29 (overlapped, 2H, H^{17}), 3.12 (d, J = 6.4 Hz, 2H, H^{16}), 1.37 (s, 9H, H^{22,23,24}). ^{13}C NMR (125 MHz, DMSO-d_6) δ

160.74, 158.01, 155.68, 147.82, 136.80, 131.24, 130.34, 125.62, 123.85, 122.65, 116.35, 115.81, 77.72, 39.51 (overlapped), 28.22. HRMS (ESI-TOF) *m/z* calcd for $C_{12}H_7N_2O_2S$ [M-H]⁻: 386.1175. Found: 386.1171.

tert-butyl (3-(4-oxo-4,5-dihydrothieno[3,2-_c_]quinoline-2-carboxamido)propyl) carbamate (3.25)
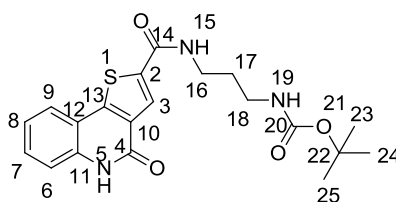
3.25

White solid (75%); ¹H NMR (400 MHz, DMSO-*d₆*) δ 11.78 (s, 1H, H⁵), 8.80 (t, *J* = 5.7 Hz, 1H, H¹⁵), 8.29 (s, 1H, H³), 7.89 (d, *J* = 8.0 Hz, 1H, H⁹), 7.53 (t, *J* = 7.7 Hz, 1H, H⁷), 7.43 (d, *J* = 8.3 Hz, 1H, H⁶), 7.25 (t, *J* = 7.6 Hz, 1H, H⁸), 6.82 (t, *J* = 6.1 Hz, 1H, H¹⁹), 3.27 (m, 2H, H¹⁸), 2.99 (m, 2H, H¹⁶), 1.65 (m, 2H, H¹⁷), 1.37 (s, 9H, H²³,²⁴,²⁵). ¹³C NMR (100 MHz, DMSO-*d₆*) δ 160.51, 158.00, 155.57, 147.78, 139.59, 136.79, 131.28, 130.31, 125.37, 123.82, 122.62, 116.33, 115.81, 77.48, 37.73, 37.14, 29.39, 28.24. HRMS (ESI-TOF) *m/z* calcd for $C_{12}H_7N_2O_2S$ [M-H]⁻: 400.1331. Found: 400.1320.

4-oxo-_N_-phenyl-4,5-dihydrothieno[3,2-_c_]quinoline-2-carboxamide (3.27):
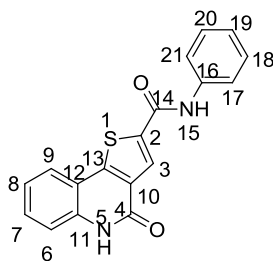
3.27

White solid (63%); mp 321-322 °C (dec); FTIR ν_max (cm⁻¹): 2728, 1638, 1536, 1512, 1321, 1254, 905, 749; ¹H NMR (400 MHz, DMSO-*d₆*) δ 11.83 (s, 1H, H⁵), 10.55 (s, 1H, H¹⁵), 8.64 (s, 1H, H³), 7.93 (d, *J* = 7.5 Hz, 1H, H⁹), 7.78 (d, *J* = 7.8 Hz, 2H, H¹⁷,²¹), 7.55 (t, *J* = 7.7 Hz,

1H, H[7]), 7.44 (d, J = 8.1 Hz, 1H, H[6]), 7.37 (t, J = 7.9 Hz, 2H, H[18,20]), 7.27 (t, J = 7.3 Hz, 1H, H[8]), 7.13 (t, J = 7.4 Hz, 1H, H[19]). ^{13}C NMR (100 MHz, DMSO-d_6) δ 159.33, 158.03, 148.54, 139.47, 138.50, 136.93, 131.36, 130.57, 128.74, 126.75, 123.99, 122.69, 120.21, 116.39, 115.74. HRMS (ESI-TOF) m/z calcd for $C_{18}H_{12}N_2O_2S$ [M-H]⁻: 319.0541. Found: 319.0539. HPLC: retention time 16.71 min; purity >99%.

**_N_-(4-fluorophenyl)-4-oxo-4,5-dihydrothieno[3,2-_c_]quinoline-2-carboxamide (3.28):**
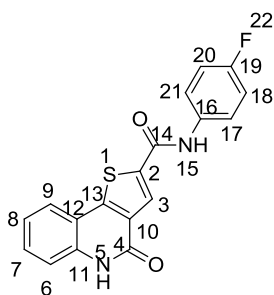
3.28

White solid (68%); ^{1}H NMR (400 MHz, DMSO-d_6) δ 11.84 (s, 1H, H[5]), 10.61 (s, 1H, H[15]), 8.61 (s, 1H, H[3]), 7.93 (d, J = 7.9 Hz, 1H, H[9]), 7.80 (dd, J = 8.7, 4.9 Hz, 2H, H[17,21]), 7.56 (t, J = 7.8 Hz, 1H, H[7]), 7.45 (d, J = 8.3 Hz, 1H, H[6]), 7.32 – 7.18 (m, 3H, H[8,18,20]). ^{13}C NMR (125 MHz, DMSO-d_6) δ 159.26, 158.01, 148.56, 139.22, 136.93, 134.86, 131.34, 130.59, 126.77, 124.01, 122.71, 122.09, 122.03, 116.39, 115.72, 115.45, 115.28. HRMS (ESI-TOF) m/z calcd for $C_{18}H_{10}FN_2O_2S$ [M-H]⁻: 337.0447 Found: 337.0455. HPLC: retention time 15.47 min; purity >97%.

_N_-(3-fluorophenyl)-4-oxo-4,5-dihydrothieno[3,2-_c_]quinoline-2-carboxamide (3.29):
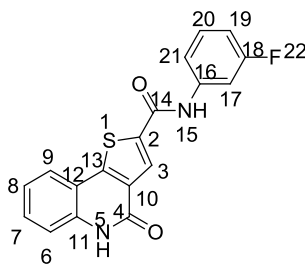
3.29

White solid (73%); ^{1}H NMR (500 MHz, DMSO-d_6) 11.87 (s, 1H, H^5), 10.72 (s, 1H, H^{15}),

8.64 (s, 1H, H^3), 7.94 (d, J = 7.9 Hz, 1H, H^9), 7.74 (d, J = 11.7 Hz, 1H, H^{17}), 7.62 – 7.52 (m, 2H,

H^{7,21}), 7.49 – 7.37 (m, 2H, H^{6,20}), 7.28 (t, J = 7.5 Hz, 1H, H^8), 6.97 (t, J = 8.5 Hz, 1H, H^{19}). ^{13}C

NMR (125 MHz, DMSO-d_6) 163.01, 161.09, 159.61, 158.04, 148.84, 140.32, 140.23, 138.92,

136.99, 131.35, 130.71, 130.48, 130.41, 127.16, 124.08, 122.76, 116.44, 115.89, 115.71, 110.56,

110.40, 107.01, 106.80. HRMS (ESI-TOF) m/z calcd for C$_{18}$H$_{10}$FN$_2$O$_2$S [M-H]$^-$: 337.0447

Found: 337.0450. HPLC: retention time 16.08 min; purity >97%.

N-(2,4-difluorophenyl)-4-oxo-4,5-dihydrothieno[3,2-c]quinoline-2-carboxamide (3.30):
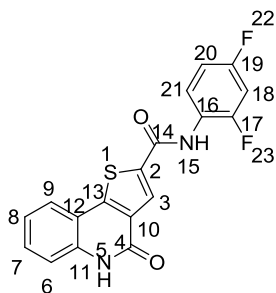
3.30

White solid (54%); ^{1}H NMR (500 MHz, DMSO-d_6) 11.85 (s, 1H, H^5), 10.53 (s, 1H, H^{15}),

8.56 (s, 1H, H^3), 7.93 (d, J = 7.9 Hz, 1H, H^9), 7.65 – 7.53 (m, 2H, H^{7,21}), 7.45 (d, J = 8.2 Hz, 1H,

H^6), 7.43 – 7.35 (m, 1H, H^{18}), 7.27 (t, J = 7.5 Hz, 1H, H^8), 7.15 (t, J = 8.7 Hz, 1H, H^{20}). ^{13}C

NMR (125 MHz, DMSO-d_6) 159.73, 158.04, 148.77, 138.21, 137.02, 131.40, 130.74, 128.65,

127.34, 124.12, 122.80, 116.46, 115.74, 111.53, 111.35, 104.79, 104.59, 104.39. HRMS (ESI-

TOF) *m/z* calcd for $C_{18}H_9F_2N_2O_2S$ [M-H]⁻: 355.0353 Found: 355.0351. HPLC: retention time 15.10 min; purity >97%.

***N*-benzyl-4-oxo-4,5-dihydrothieno[3,2-*c*]quinoline-2-carboxamide (3.31):**
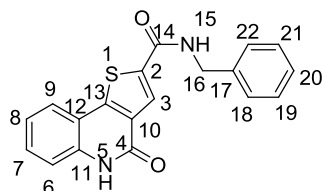
**3.31**

White solid (66%); ¹H NMR (400 MHz, DMSO-*d₆*) 11.79 (s, 1H, H⁵), 9.41 (s, 1H, H¹⁵), 8.37 (s, 1H, H³), 7.90 (d, *J* = 7.1 Hz, 1H, H⁹), 7.61 – 7.13 (m, 8H, H⁶⁻⁸,¹⁸⁻²²), 4.49 (d, *J* = 6.1 Hz, 2H, H¹⁶). ¹³C NMR (125 MHz, DMSO-*d₆*) 160.65, 158.02, 148.02, 139.33, 139.10, 136.86, 131.35, 130.42, 128.39, 127.38, 126.96, 125.74, 123.91, 122.67, 116.38, 115.81, 42.75. HRMS (ESI-TOF) *m/z* calcd for $C_{19}H_{13}N_2O_2S$ [M-H]⁻: 333.0698 Found: 333.0733. HPLC: retention time 13.76 min; purity >99%.

***N*-(2-fluorophenethyl)-4-oxo-4,5-dihydrothieno[3,2-c]quinoline-2-carboxamide (3.32):**
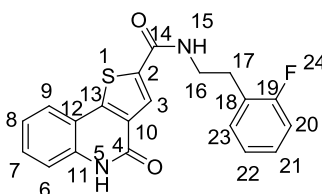
3.32

White solid (58%); ¹H NMR (400 MHz, DMSO-*d₆*) 11.79 (s, 1H, H⁵), 8.97 (m, 1H, H¹⁵), 8.25 (s, 1H, H³), 7.88 (d, *J* = 7.9 Hz, 1H, H⁹), 7.53 (t, *J* = 7.8 Hz, 1H, H⁷), 7.42 (d, *J* = 8.2 Hz, 1H, H⁶), 7.33 (m, 1H, H²⁰), 7.26 (d, *J* = 7.4 Hz, 2H, H⁸,²²), 7.14 (q, *J* = 8.6, 7.3 Hz, 2H, H²¹,²³), 3.50 (d, *J* = 6.8 Hz, 2H, H¹⁶), 2.90 (m, 2H, H¹⁷). ¹³C NMR (125 MHz, DMSO-*d₆*) δ 160.62, 158.07, 147.91, 139.50, 136.82, 131.28, 130.41, 128.46, 128.39, 125.95, 125.83, 125.46, 124.42, 123.89, 122.72, 116.39, 115.84, 115.25, 115.08, 28.48. HRMS (ESI-TOF) *m/z* calcd for

$C_{20}H_{14}FN_2O_2S$ [M-H]⁻: 365.0760 Found: 365.0790. HPLC: retention time 13.78 min; purity >99%.

Methyl 2-(4-oxo-4,5-dihydrothieno[3,2-*c*]quinoline-2-carboxamido)benzoate (3.33):
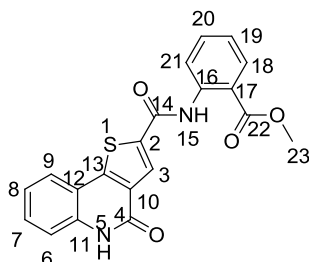
3.33

White solid (88%). ¹H NMR (400 MHz, DMSO-*d₆*) δ 11.85 (s, 1H, ex, H⁵), 11.60 (s, 1H, ex, H¹⁵),8.35 (d, *J* = 8.4 Hz, 1H, H⁹), 8.26 (s, 1H, H³), 8.00 (d, *J* = 7.9 Hz, 1H, H¹⁸), 7.93 (d, *J* = 7.9 Hz, 1H, H²¹), 7.68 (t, *J* = 8.0 Hz, 1H, H⁷), 7.55 (d, *J* = 7.7 Hz, 1H, H²⁰), 7.44 (d, *J* = 8.3 Hz, 1H, H⁶), 7.28 (t, *J* = 7.7 Hz, 2H, H⁸,¹⁹), 3.93 (s, 3H, H²³). ¹³C NMR (100 MHz, DMSO-*d₆*) δ 167.69, 158.93, 157.74, 148.81, 138.98, 136.92, 133.95, 131.16, 130.58, 125.83, 123.87, 122.60, 121.41, 118.25, 116.30, 115.52, 52.50. HRMS (ESI-TOF) *m/z* calcd for $C_{20}H_{13}N_2O_4S$ [M-H]⁻: 377.0596. Found: 377.0595. HPLC: retention time 18.32 min; purity >99%.

Methyl 3-(4-oxo-4,5-dihydrothieno[3,2-*c*]quinoline-2-carboxamido)benzoate (3.35):
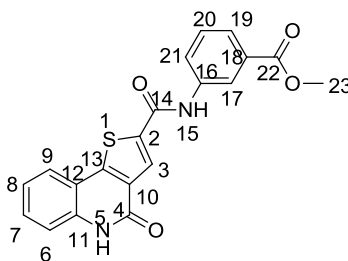
3.35

White solid (55%). ¹H NMR (400 MHz, DMSO-*d₆*) δ 11.84 (s, 1H, ex, H⁵), 10.75 (s, 1H, ex, H¹⁵), 8.66 (s, 1H, H³), 8.44 (s, 1H, H¹⁷), 8.11 (d, *J* = 8.3 Hz, 1H, H¹⁹), 7.93 (d, *J* = 7.9 Hz, 1H, H⁹), 7.71 (d, *J* = 7.7 Hz, 1H, H⁶), 7.61 – 7.49 (m, 2H, H⁷,²⁰), 7.45 (d, *J* = 8.3 Hz, 1H, H²¹),

7.27 (t, J = 7.6 Hz, 1H, H[8]), 3.88 (s, 3H, H[23]). ^{13}C NMR (100 MHz, DMSO-d_6) δ 166.01, 159.57, 158.01, 148.77, 138.98, 136.97, 131.39, 130.63, 130.12, 129.28, 127.12, 124.45, 124.05, 122.70, 120.57, 116.40, 115.70, 52.23. HRMS (ESI-TOF) m/z calcd for $C_{20}H_{13}N_2O_4S$ [M-H]$^-$: 377.0596. Found: 377.0596. HPLC: retention time 17.34 min; purity >99%.

4-oxo-N-(pyridin-2-yl)-4,5-dihydrothieno[3,2-c]quinoline-2-carboxamide (3.37):
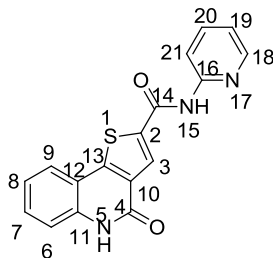
3.37

White solid (30%). ^{1}H NMR (500 MHz, DMSO-d_6) δ 11.84 (s, 1H, ex, H[5]), 11.29 (s, 1H, ex, H[15]), 8.79 (s, 1H, H[3]), 8.44 (d, J = 3.3 Hz, 1H, H[18]), 8.15 (d, J = 8.3 Hz, 1H, H[9]), 7.95 (d, J = 7.9 Hz, 1H, H[21]), 7.87 (t, J = 7.8 Hz, 1H, H[20]), 7.57 (t, J = 7.8 Hz, 1H, H[7]), 7.45 (d, J = 8.2 Hz, 1H, H[6]), 7.28 (t, J = 7.5 Hz, 1H, H[8]), 7.24 – 7.17 (m, 1H, H[19]). ^{13}C NMR (125 MHz, DMSO-d_6) δ 160.02, 157.94, 151.64, 148.94, 148.04, 138.76, 138.19, 137.01, 131.54, 130.64, 127.91, 124.06, 122.64, 120.06, 116.35, 115.65, 114.92. HRMS (ESI-TOF) m/z calcd for $C_{17}H_{10}N_3O_2S$ [M-H]$^-$: 320.0494. Found: 320.0498. HPLC: retention time 11.52 min; purity >99%.

4-chloro-*N*-(pyridin-2-yl)thieno[3,2-c]quinoline-2-carboxamide (3.38):
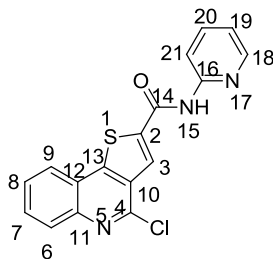
3.38

White solid (23%). ^{1}H NMR (400 MHz, DMSO-d_6) δ 11.55 (s, 1H, ex, H^{15}), 9.04 (s, 1H, H^3), 8.45 (d, J = 4.5 Hz, 1H, H^{18}), 8.35 (d, J = 8.0 Hz, 1H, H^9), 8.19 (d, J = 8.3 Hz, 1H, H^6), 8.10 (d, J = 8.3 Hz, 1H, H^{21}), 7.88 (t, J = 7.6 Hz, 2H, H^{7,20}), 7.78 (t, J = 7.5 Hz, 1H, H^8), 7.22 (dd, J = 7.3, 4.8 Hz, 1H, H^{19}). ^{13}C NMR (100 MHz, DMSO-d_6) δ 159.79, 151.59, 148.23, 148.10, 145.44, 143.24, 141.03, 138.32, 131.78, 130.77, 128.94, 128.32, 126.16, 124.10, 122.53, 120.21, 114.78. HRMS (ESI-TOF) m/z calcd for $C_{17}H_9ClN_3OS$ [M-H]$^-$: 338.0155. Found: 338.0158. HPLC: retention time 18.97 min; purity >97%.

4-oxo-N-(pyridin-3-yl)-4,5-dihydrothieno[3,2-*c*]quinoline-2-carboxamide (3.39):

3.39
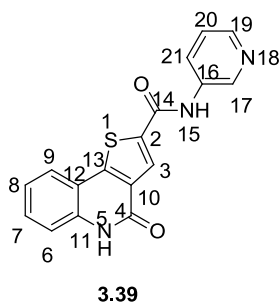
Yield: 41% of a white solid. ^{1}H NMR (400 MHz, DMSO-d_6) δ 11.83 (s, 1H, ex, H^5), 10.74 (s, 1H, ex, H^{15}), 8.95 (s, 1H, H^{17}), 8.64 (s, 1H, H^3), 8.34 (d, J = 4.6 Hz, 1H, H^{19}), 8.19 (d, J = 8.3 Hz, 1H, H^9), 7.94 (d, J = 7.9 Hz, 1H, H^{21}), 7.56 (t, J = 7.7 Hz, 1H, H^7), 7.49 – 7.38 (m, 2H, H^{6,20}), 7.28 (t, J = 7.5 Hz, 1H, H^8). ^{13}C NMR (125 MHz, DMSO-d_6) δ 159.78, 158.02, 148.85, 144.88, 141.75, 138.66, 137.01, 135.28, 131.37, 130.74, 127.31, 127.21, 124.10, 123.68, 122.76, 116.45, 115.69. HRMS (ESI-TOF) m/z calcd for $C_{17}H_{10}N_3O_2S$ [M-H]$^-$: 320.0494. Found: 320.0502. HPLC: retention time 10.97 min; purity >99%.

**Representative procedures for the synthesis of 3.24 and 3.26**

_N_-(2-aminoethyl)-4-oxo-4,5-dihydrothieno[3,2-c]quinoline-2-carboxamide (3.24):

3.24
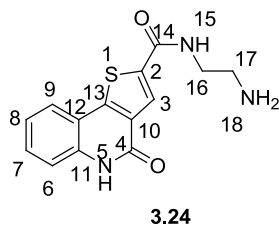
To a stirred suspension of *tert*-butyl (2-(4-oxo-4,5-dihydrothieno[3,2-*c*]quinoline-2-carboxamido)ethyl)carbamate (**3.23**) (0.03g, 0.075 mmol) in 5 mL of CH_2Cl_2 was added 4M HCl in dioxane (500 µL) and the mixture was stirred for 8h at ambient temperature. The precipitated solid was filtered, washed with Et_2O and dried under vacuum to yield the title compound as a white solid (0.024 g, 96%). ^{1}H NMR (400 MHz, DMSO-d_6) δ 11.84 (s, 1H, ex, H[5]), 9.08 (s, 1H, ex, H[15]), 8.35 (s, 1H, H[3]), 7.90 (d, J = 8.0 Hz, 3H, 2 ex, H[9,18]), 7.54 (t, J = 7.9 Hz, 1H, H[7]), 7.44 (d, J = 8.4 Hz, 1H, H[6]), 7.26 (t, J = 7.8 Hz, 1H, H[8]), 3.65 – 3.41 (m, 2H, H[16]), 3.00 (t, J = 6.6 Hz, 2H, H[17]). ^{13}C NMR (125 MHz, DMSO-d_6) δ 161.18, 157.93, 147.95, 138.85, 136.84, 131.21, 130.40, 126.18, 123.83, 122.61, 116.34, 115.71, 38.45, 37.13. HRMS (ESI-TOF) *m/z* calcd for $C_{14}H_{12}N_3O_2S$ [M-H]¯: 286.0650. Found: 286.0644. HPLC: retention time 8.46 min; purity >99%.

N-(3-aminopropyl)-4-oxo-4,5-dihydrothieno[3,2-*c*]quinoline-2-carboxamide (3.26):

3.26
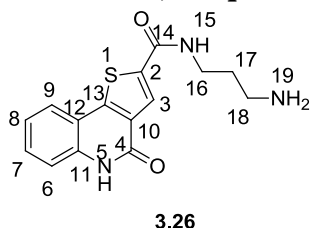
Yield: 92% of a white solid. ^{1}H NMR (400 MHz, DMSO-d_6) δ 11.82(s, 1H, ex, H[5]), 9.03 (s, 1H, ex, H[15]), 8.33 (s, 1H, H[3]), 8.06 – 7.70 (d, J = 7.9 Hz, 3H, 2 ex, H[9,18]), 7.53 (t, J = 7.7 Hz, 1H, H[7]), 7.44 (d, J = 8.3 Hz, 1H, H[6]), 7.25 (t, J = 7.5 Hz, 1H, H[8]), 3.43 – 3.33 (m, 2H, H[16]), 2.86 (t, J = 6.7 Hz, 2H, H[18]), 1.90 – 1.76 (m, 2H, H[17]). ^{13}C NMR (125 MHz, DMSO-d_6) δ 160.83, 157.97, 147.91, 139.23, 136.82, 131.27, 130.39, 125.69, 123.84, 122.64, 116.36, 115.76, 36.45,

36.06, 27.20. HRMS (ESI-TOF) m/z calcd for $C_{15}H_{14}N_3O_2S$ [M-H]⁻: 300.0807. Found: 300.0812. HPLC: retention time 8.71 min; purity >99%.

Representative procedures for the synthesis of 3.34 and 3.36

2-(4-Oxo-4,5-dihydrothieno[3,2-*c*]quinoline-2-carboxamido)benzoic acid (3.34):
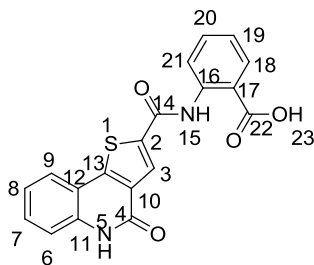
3.34

To a stirred suspension of methyl 2-(4-oxo-4,5-dihydrothieno[3,2-*c*]quinoline-2-carboxamido)benzoate (**3.33**) (0.025g, 0.066 mmol) in 5 mL of MeOH was added 1 N NaOH (1 mL) and the mixture was stirred for 30 min at ambient temperature. It was then quenched with 10% HCl. The precipitated solid was filtered, washed successively with H_2O and Et_2O and dried under vacuum to yield the title compound as a white solid (0.022 g, 92%). ^{1}H NMR (400 MHz, DMSO-d_6) δ 13.87 (s, 1H, ex, H^{23}), 12.48 (s, 1H, ex, H^5), 11.91 (s, 1H, ex, H^{15}), 8.51 (d, $J = 8.3$ Hz, 1H, H^9), 8.19 (s, 1H, H^3), 8.06 (d, $J = 7.8$ Hz, 1H, H^{18}), 7.95 (d, $J = 7.9$ Hz, 1H, H^{21}), 7.66 (t, $J = 8.0$ Hz, 1H, H^7), 7.57 (t, $J = 7.9$ Hz, 1H, H^{20}), 7.45 (d, $J = 8.3$ Hz, 1H, H^6), 7.32 – 7.19 (m, 2H, H^{8,19}). ^{13}C NMR (125 MHz, DMSO-d_6) δ 169.47, 158.52, 157.44, 148.48, 139.75, 138.71, 136.64, 133.74, 130.86, 130.36, 125.25, 123.62, 123.03, 122.34, 119.88, 117.10, 116.04, 115.24. HRMS (ESI-TOF) m/z calcd for $C_{19}H_{11}N_2O_4S$ [M-H]⁻: 363.0440. Found: 363.0443. HPLC: retention time 17.36 min; purity >99%.

3-(4-oxo-4,5-dihydrothieno[3,2-*c*]quinoline-2-carboxamido)benzoic acid (3.36):
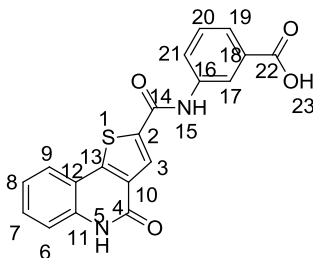
3.36

Yield: 71% of a white solid. ^{1}H NMR (400 MHz, DMSO-d_6) δ 13.04 (s, 1H, ex, H^{23}), 11.86 (s, 1H, ex, H^5), 10.74 (s, 1H, ex, H^{15}), 8.67 (s, 1H, H^3), 8.42 (s, 1H, H^{17}), 8.08 (d, J = 8.1 Hz, 1H, H^{19}), 7.95 (d, J = 7.9 Hz, 1H, H^9), 7.70 (d, J = 7.7 Hz, 1H, H^6), 7.61 − 7.41 (m, 3H, H^{7,20,21}), 7.28 (t, J = 7.6 Hz, 1H, H^8). ^{13}C NMR (125 MHz, DMSO-d_6) δ 167.05, 159.52, 158.00, 148.71, 139.08, 138.80, 136.96, 131.36, 130.61, 129.03, 127.05, 124.67, 124.08, 122.69, 120.86, 116.39, 115.70. HRMS (ESI-TOF) m/z calcd for C$_{19}$H$_{13}$N$_2$O$_4$S [M+H]$^+$: 365.0596. Found: 365.0591. HPLC: retention time 15.41 min; purity >99%.

CHAPTER 5: ATTEMPTED BIOLOGICAL EVALUATIONS OF THE VIRTUAL SCREENING HITS USING FLUORESCENCE RESONANCE ENERGY TRANSFER (FRET) BASED ASSAY

5.1. Introduction

5.1.1 FRET based kinase assay

Protein kinases act as phosphoryl transferases, which phosphorylate serine, threonine or tyrosine residues of a substrate by transferring the γ-phosphate group of an ATP and in turn convert ATP to ADP. There are several methods to assay this kinase activity. These methods involve the quantification of this phosphoryl transfer reaction by detecting the phosphorylated product or the change in the ratio of ATP to ADP. The detection can be done in following ways:

a) Radiometric assays

b) Fluorometric assay

c) Enzyme-linked immunosorbent assay (ELISA)

d) Luminescence assay

e) Mobility shift assay

One of the simplest methods is the fluorometric method, which uses non-radioactive material. So it has less liability in terms of handling or waste disposal. One of these methods uses fluorescence resonance energy transfer (FRET) between a donor (coumarin) and an acceptor (fluorescein). The commercially available assays include Invitrogen's Z'-Lyte™ assay, which can be used in any lab set-up to reliably screen potential kinase inhibitors in a two hour reaction at room temperature. The Z'-Lyte™ assay uses synthetic FRET-peptide substrates labeled with a donor (i.e., coumarin) and acceptor (i.e., fluorescein). The reaction occurs in two stages. Primarily in a kinase reaction, the kinase transfers the γ-phosphate of the ATP to a tyrosine, serine or threonine, but in presence of kinase inhibitor this phosphorylation reaction diminishes.

In a secondary reaction, with the addition of the development reagent, the development buffer quenches the kinase reaction and compared to the phosphorylated state, the non-phosphorylated state, gets cleaved faster by a protease, which disrupts the FRET pair. Thus produces less fluorescence. Better the inhibitor potential lower would be the number of FRET transfer. The FRET is expressed by calculating the emission ratio, which is defined as,

Emission ratio = coumarin emission/fluorescein emission.

The % phosphorylation is defined as,

% Phosphorylation = 100 X (1-(((emission ratio X $F_{100\%}$)/(($C_{0\%}$ - $C_{100\%}$) + (emission ratio X ($F_{100\%}$ - $F_{0\%}$)))))

Whereas the % inhibition is given as,

% Inhibition = 100 - % phosphorylation

5.1.2. Poor solubility issues

In general, kinase inhibitors are known to be insoluble compounds, because of the presence of number of hetero atoms or heterocycles in the molecules. Several groups have worked on solving the solubility problems in drug molecules, using different formulations containing mixtures of alcohols and emulsifiers. Cremophor EL is a non-ionic solubilizer and emulsifier often used for various poorly-water soluble drugs, including the anticancer agent paclitaxel (Taxol),[103] cyclosporine A[104] and Δ^9-tetrahydrocannabinol.[105]

5.2. Methods

5.2.1. General

Staurosporine, R-roscovitine standards were purchased from Enzo Life Sciences (www.enzolifesciences.com). CDK5/p25, CDK2/A, Z'-Lyte™ kinase assay kit-Ser/Thr 12 Peptide were bought from Invitrogen™, Life Technologies.[106] Cremophore EL was purchased from Sigma-Aldrich Corporation (www.sigmaaldrich.com). Perkin Elmer EnVision® multilabel Plate reader using Photometric 405 Excitation Filter and two Emission Filters (Photometric 450 and Fura2 510) was used to read 384-well black NBS™ coated plates from Corning Inc. (www.corning.com).

5.2.2. Compound stock solution preparation

All the compounds were dissolved in a mixture containing 1:1:18 (v/v/v) mixture of water with 10% DMSO : EtOH : cremophor EL at 1 mM concentration. 100 μM was the highest concentration, we screened for any compounds. Since we had to prepare 4X concentration, the 400 μM samples were prepared by diluting the stock solution with the same solvent mixture. We used the blank solvent mixture to do a baseline correction of the fluorescence reading.

5.2.3 CDK5/p25 and CDK2/A kinase assay

The method used is described as follows

1. 2.5 μL – 4X Test Compound

2. 5 μL – 2X Peptide/ specific Kinase Mixture

3. 2.5 μL – 4X ATP Solution

4. 30-second plate shake

5. 60-minute Kinase Reaction incubation at room temperature

6. 5 μL – Development Reagent Solution

7. 30-second plate shake

8. 60-minute Development Reaction incubation at room temperature

9. Read on fluorescence plate reader and analyzed the data

10. The EC_{50}/IC_{50} values were generated using GraphPad Prism.[107]

5.3.   Results and Discussions

Both staurosporine (**5.1**) and R-roscovitine (**2.1**) were used as the standards and analyzed first in the CDK5/p25 and CDK2/A assays. The structures of the staurosporine and R-roscovitine are given in Figure 5.1.
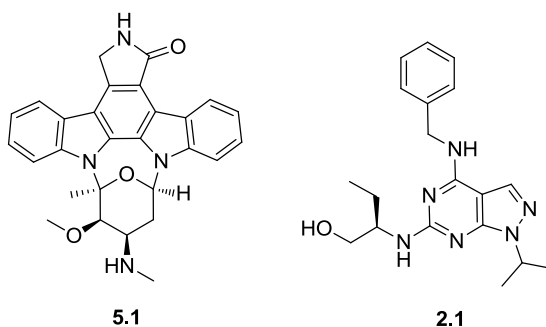
Figure 5.1.   Structures of staurosporine and R-roscovitine

The determined IC_{50} values for staurosporine and R-roscovitine are given as follows:

Staurosporine CDK5/p25 IC_{50} = 39 nM; CDK2/A IC_{50} = 7.7 nM

R-roscovitine CDK5/p25 IC_{50} = 1.34 μM; CDK2/A IC_{50} = 1.29 μM

The staurosporine IC50 in Z′-Lyte assay was reported as CDK5/p25 IC_{50} = 9.7 nM; CDK2/A IC_{50} = 5.88 nM in the Invitrogen Z'-Lyte manual.[108] We found out that the IC_{50} values obtained from the Z′-Lyte assay for staurosporine showed nanomolar potencies in both the kinases as reported. But the micromolar IC_{50} values of R- roscovitine in our assay deviated a lot from the sub-micromolar numbers reported earlier.[16] The IC50 curves for staurosporine and R-roscovitine are shown in Figure 5.2.

% Inhibition of Staurosporine in CDK5
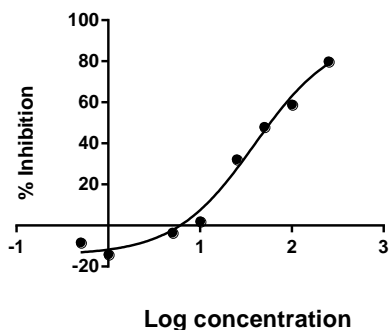
% Inhibition of Staurosporine in CDK2
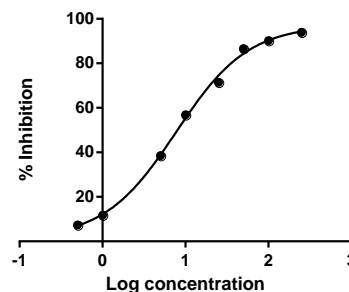
% Inhibition of Roscovitine in CDK5
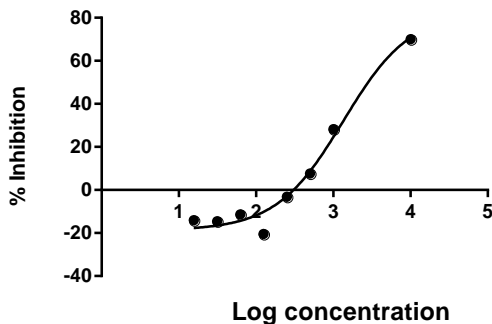
% Inhibition of Roscovitine in CDK2
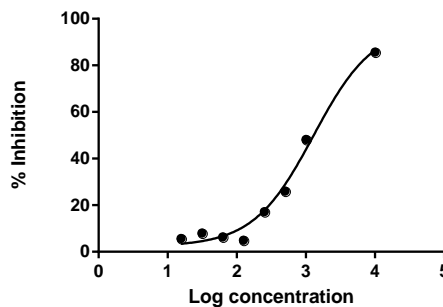
Figure 5.2. Z'-Lyte IC_{50} curves of staurosporine and R-roscovitne in CDK5/p25 and CDK2/A

We evaluated the selected hits from the virtual screening (Chapter 2) in our Z'-Lyte assay condition. A highest concentration of 100 µM was used for the compounds in the Z'-Lyte assays. We observed that the compounds did not produce reasonable IC_{50} curves in either CDK5/p25 or CDK2/A. Also the % inhibition did not reach to 50% mark for most of the compounds to produce meaningful IC_{50} values.

Following are the IC_{50} curves of **2.5** as described in Figure 5.3.
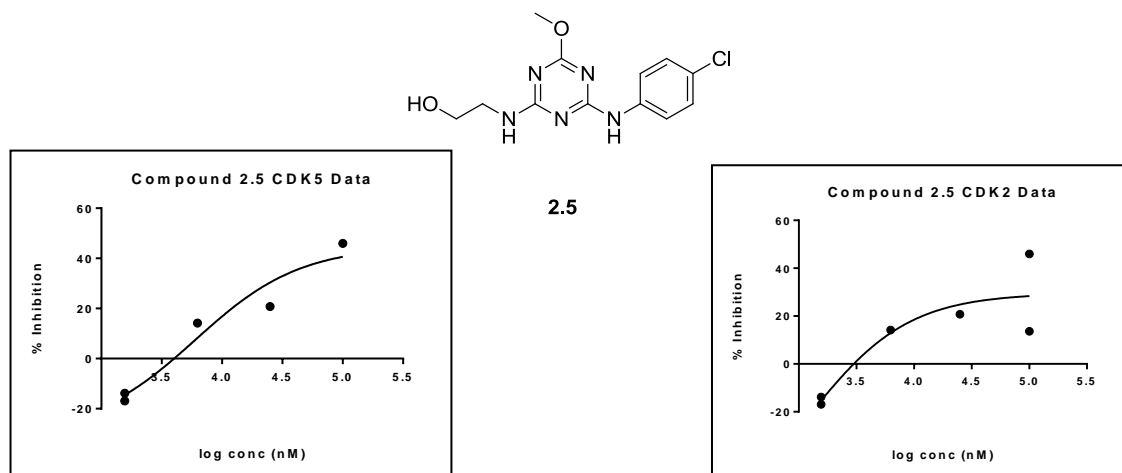
Figure 5.3. IC_{50} curves for **2.5** in CDK5/p25 and CDK2/A

The IC_{50} curves of **2.6** are given below in Figure 5.4
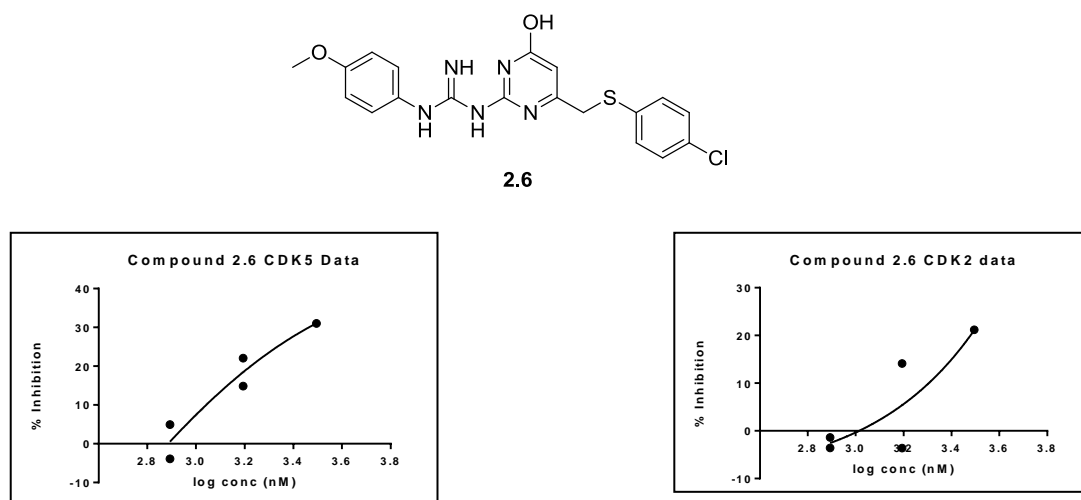
Figure 5.4. IC_{50} curves for **2.6** in CDK5/p25 and CDK2/A

The IC$_{50}$ curves of **2.7** are given below in Figure 5.5

2.7
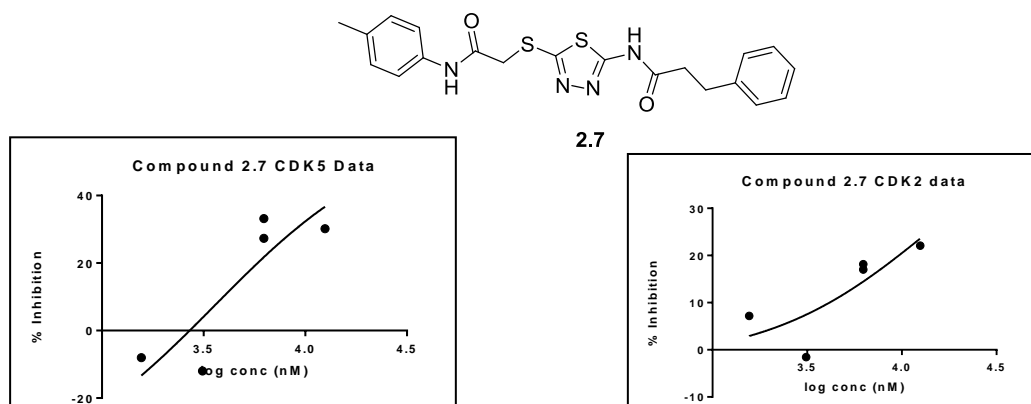
Figure 5.5.   IC$_{50}$ curves for **2.7** in CDK5/p25 and CDK2/A

The IC$_{50}$ curves of **2.8** are given below in Figure 5.6

2.8
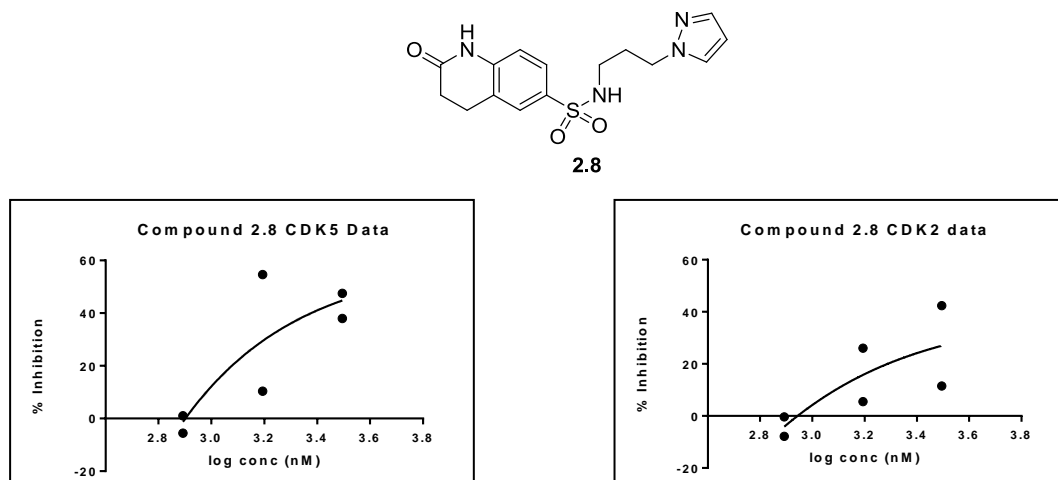
Figure 5.6.   IC$_{50}$ curves for **2.8** in CDK5/p25 and CDK2/A

The IC$_{50}$ curves of **2.9** are given below in Figure 5.7

2.9
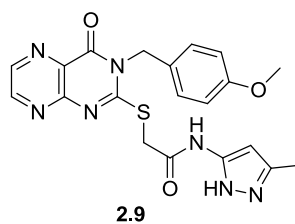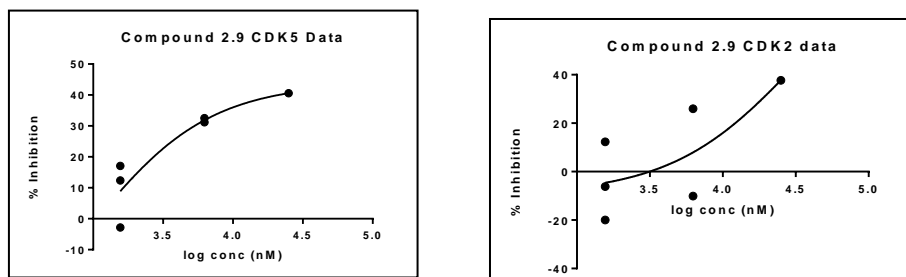
Figure 5.7. IC$_{50}$ curves for **2.9** in CDK5/p25 and CDK2/A

The IC$_{50}$ curves of **2.10** are given below in Figure 5.8

2.10
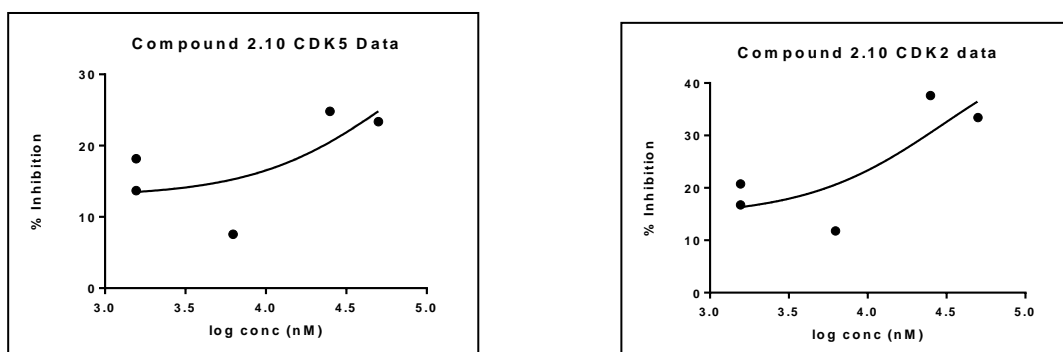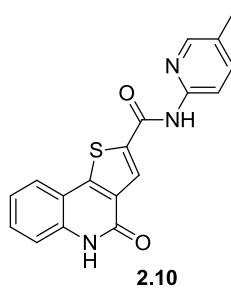
Figure 5.8. IC$_{50}$ curves for **2.10** in CDK5/p25 and CDK2/A

The IC$_{50}$ curves of **2.11** are given below in Figure 5.9

2.11
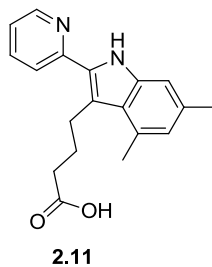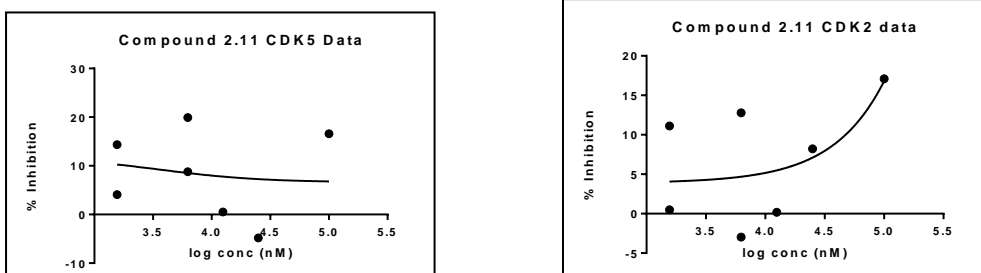
Figure 5.9. IC$_{50}$ curves for **2.11** in CDK5/p25 and CDK2/A

The IC$_{50}$ curves of **2.12** are given below in Figure 5.10
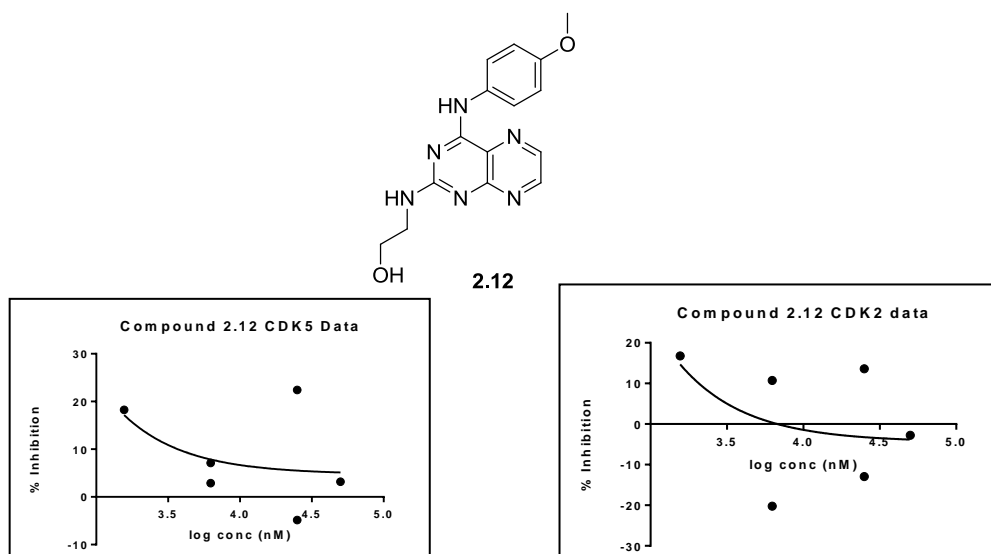
Figure 5.10. IC$_{50}$ curves for **2.12** in CDK5/p25 and CDK2/A

The IC$_{50}$ curves of **2.13** are given below in Figure 5.11
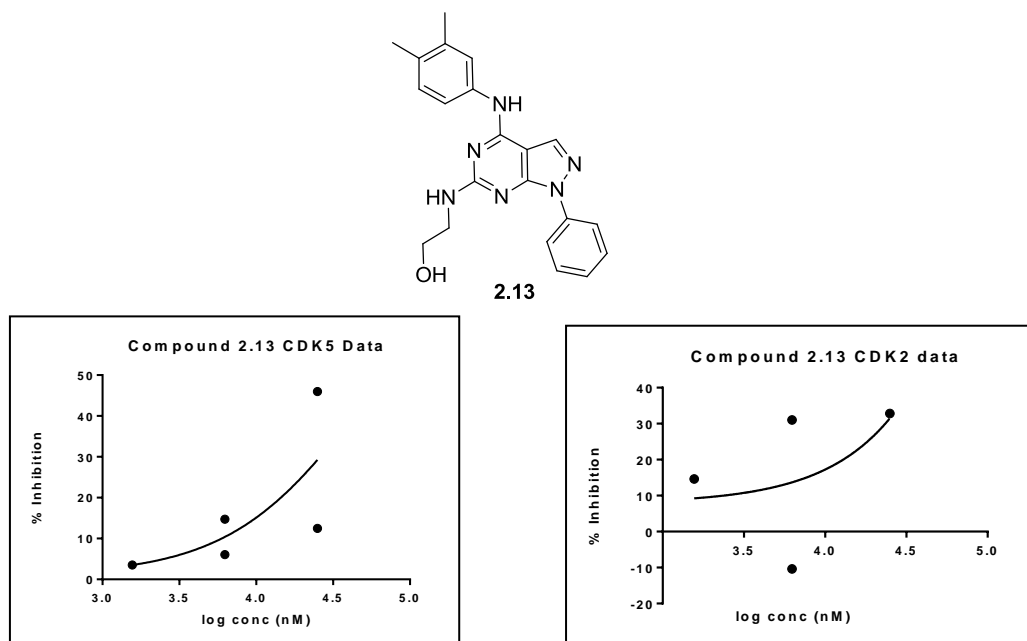
Figure 5.11.   IC$_{50}$ curves for **2.13** in CDK5/p25 and CDK2/A

The IC$_{50}$ curves of **2.14** are given below in Figure 5.12
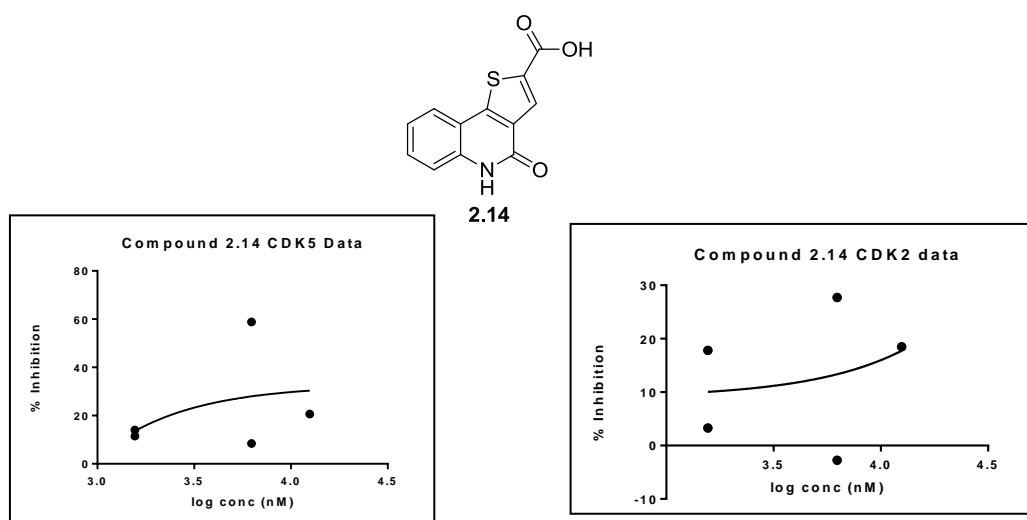
Figure 5.12.   IC$_{50}$ curves for **2.14** in CDK5/p25 and CDK2/A

5.4.   Conclusions

All the virtual screening compounds tested in Z'-Lyte assay did not generate reasonable IC_{50} curves in either CDK5/p25 or CDK2/A. The % inhibitions of some of the compounds did not reach the 50% mark for us to calculate a meaningful IC_{50} values. There could be a number of reasons for which we did not get 50% inhibition. Primarily, we could speculate about the poor solubility of the compounds. We have already encountered the poor solubility issues and used a 1:1:18 (v/v/v) mixture of water with 10% DMSO: EtOH: cremophor EL to dissolve the compounds at 1 mM concentration. The highest concentration tested was 100 µM, for which we had to prepare required 400 µM concentration (4X). But during the kinase reactions, compounds get diluted with the reaction buffer. The dilution with aqueous buffer may cause precipitation. Consequently, it will increase the absorbance reading and in turn the % inhibition number will go down. The poor performance of the assay was also reflected on the % inhibition value of the R-roscovitine. We observed that in the Z'-Lyte assay, the IC_{50} value of R-roscovitine was 10 fold less potent than the values reported in the literature. So hypothetically, if the tested compound would have a real IC_{50} value of 20 µM, in this assay, it will generate a 10 fold less potent number of 200 µM. And since the highest concentration we tested was 100 µM, we won't be able to get a meaningful IC_{50} curve for the hypothetical compound. All these data forced us to look for alternate assay methods to assay these compounds.

CHAPTER 6: BIOLOGICAL EVALUATION USING RADIOMETRIC ASSAYS AND SAR
ANALYSIS

6.1.   Introduction

Protein kinases act as phosphoryl transferases, which phosphorylate serine, threonine or tyrosine residues of a substrate by transferring the γ-phosphate group of the ATP and in turn convert ATP to ADP. Since our attempted biological evaluation in FRET based assay failed, we returned our focus on a robust assay method. Among many kinase assays, radiometric methods are the most reliable method of detecting kinase reactions.[109] In the P81 filter binding radiometric method, the homogeneous kinase reaction is performed in the presence of ATP, which is spiked with [γ-^{33}P] ATP and allowed to bind to the protein substrate. The incorporation of this radio-labeled phosphate to the filter bound substrate is then assayed after a series of binding and washing steps. The reaction data is then background subtracted by subtracting the signal obtained from control kinase reactions flooded with EDTA, which kills the kinase activity. The average signal from those EDTA wells is therefore set to kinase 0% activity. The average signal of DMSO only wells is set to 100% activity. Test compound data is then expressed within that signal range as percent residual kinase activity.   Then inhibition is measured using the following formula,

$$\% \text{ Inhibition} = 100 - \% \text{ activity.}$$

The target was to find active compounds for CDK5/p25. Compounds were also needed to be screened for selectivity against CDK2/E. The reason CDK2/E was chosen instead of CDK2/A, because cyclin E expression was identified in the post neuronal cytoplasm, where CDK5 plays an important part in AD pathogenesis.[110] The ATP binding rate for any particular kinase is half maximal at Michaelis-Menten constant (K_m) concentration. It is a true comparison

between any numbers of kinases if the assays are performed at ATP Km values, because all kinases are at half maximal rate.

For ATP competitive inhibition assay, the nature of the double reciprocal (Lineweaver-Burk) plot can express whether it is a competitive or non-competitive inhibition. For competitive binding the lines are going to merge on Y-axis. On the other hand, it is going to be a non-competitive binding, if the lines converge on X-axis. The Michaelis-Menten equation of reversible enzyme kinetics for mixed inhibitor can be represented as,

$$v = \frac{V_{max}.[S]}{K_m\left(1+\dfrac{[I]}{K_i}\right)+\left(1+\dfrac{[I]}{K_i'}\right)[S]}$$

Where v is velocity, [S] is substrate (ATP) concentration, [I] is inhibitor concentration, K_i is inhibitor affinity for enzyme, and K_i' is inhibitor affinity for enzyme/ATP complex.

The Lineweaver-Burk plot is a graphical plot of $1/v$ –vs– $1/[S]$.

Finally a panel of serine/threonine and tyrosine kinases is selected either on the basis of their existence in the CDK family or for their tau phosphorylation pathways.[111]

6.2. Methods

All the assays were performed at Reaction Biology Corp.[112] according to their standard procedure. The customer protocols are described below.

6.2.1. Radiometric CDK5/p25 and CDK2/E kinase assays

The phosphorylation of histone H1by ATP was conducted in a base buffer containing 20 mM Hepes (pH 7.5), 10 mM $MgCl_2$, 1 mM EGTA, 0.02% Brij35, 0.02 mg/ml BSA, 0.1 mM Na_3VO_4, 2 mM DTT, 1% DMSO at K_m ATP concentration (spiked with [γ-^{33}P] ATP).The

86

reactions were conducted in duplicate and initiated by the addition of hCDK5/p25 or hCDK2/E and the compounds dissolved in 4% DMSO solution. The reaction was incubated at room temperature for 120 min after which it was stopped by adding EDTA and filtered through P81 ion exchange paper. It was then washed with 0.75% phosphoric acid, which removed any free ^{33}P signal. The ^{33}P that was transferred onto the substrate however remained on the filter with the bound substrate. The signal intensities were recorded and the raw image data was converted into numbers. The reaction data was then background subtracted by subtracting the signal obtained from control kinase reactions flooded with EDTA, which killed the kinase activity. The average signal from those EDTA wells was considered to be the kinase 0% activity. The average signal of DMSO only wells was set to 100% activity. Test compound data was expressed between the 0-100% signal ranges as percent residual kinase activity. The IC_{50} for each compound was determined from dose-response curves ran at ATP (K_m) concentrations of 30 μM for CDK5/p25 and 65 μM for CDK2/E and at least two independent experiments were performed to generate the average numbers. Staurosporine was used as positive controls for the assays.

6.2.2. ATP competitive binding assay

ATP competitive binding assay was performed in the same manner as the radiometric filtration assay with different ATP concentrations of 10, 30, 75, 150 and 300 μM with hCDK5/p25. A 10 point IC50 curve was determined. The Ki was calculated using GraphPad Prism.[107]

6.2.3. Selectivity assay

The selectivity assays were performed the same way as the radiometric filter binding assay using full length human kinases with the appropriate co-factors as mentioned in the selected panel of kinases. All the assays were performed at ATP Km concentrations and 20 µM compound concentrations. At least two independent experiments were performed to generate the average % activity.

6.3. Results and Discussions

The identified nine compounds from the virtual screening were tested in the γ-^{33}P ATP filter binding assay using full length hCDK5/p25 and hCDK2/E at Reaction Biology Corp.[112, 113] The % inhibitions at 50 µM concentration were determined at 10 µM ATP and the compounds with greater than 50% inhibition were re-screened (at ATP K_m concentrations) for relevant % inhibitions or IC_{50} (generated from the dose-response curves). The intermediate carboxylic acid (**2.14**) was also tested and shown to be active at 50 µM concentrations. The *in-vitro* potencies of the selected compounds are reported in Table 6.1.

It was observed that among the tested compounds **2.5**, **2.7**, **2.8** were equipotent in both the enzymes, whereas **2.9** and **2.12** showed preferential activity towards CDK2/E. The success of the computational model was established by CDK5/p25 selectivity of compounds **2.6**, **2.10**, **2.11** and **2.13** making a 40% positive turnover rate for the model. The intermediate **2.14** also showed preferential activity towards CDK5/p25. We used **2.1** and **2.4** as the standards for the assay validation and found that both the compounds showed sub-micromolar activities for CDK5/p25 as reported earlier,[16, 28] but showed selectivity towards CDK2/E.

Compound **2.10** showed reasonably good potency for CDK5/p25 (IC_{50}=7 µM) and four fold selectivity over CDK2/E (IC_{50}=25 µM) with a calculated ligand efficiency[114] (LE) of 0.3.

The carboxylic acid (**2.14**) also showed moderate activity in CDK5/p25 (IC_{50}=52 μM) and good selectivity over CDK2/E (showed 14% inhibition @ 50 μM concentration).

Table 6.1.   In-vitro CDK5/p25 and CDK2/E assay

Compound #	CDK5/p25 % inhibition[a] @ 50 μM	CDK2/E % inhibition[a] @ 50 μM	CDK5/p25 IC_{50} (μM)[b]	CDK2/E IC_{50} (μM)[b]
2.5	20.0	24.2		
2.6	43.1	32.3		
2.7	23.6	29.9		
2.8	12.7	14.8		
2.9	25.2	38.7		
2.10	88.2	77.0	7.02	25.8
2.11	17.2	8.0		
2.12	48.3	58.2	107	81.7
2.13	14.7	5.3		
2.14	64.8	23.5	52.1	14.5% inh[c]
2.1			0.188	0.028
2.4			0.655	0.417

[a] Assays were performed in duplicate @ 10 μM ATP and 50 μM compound concentrations
[b] Assays were performed @ ATP (K_m) concentrations of 30 μM for CDK5/p25 and 65 μM for CDK2/E and at least two independent experiments were performed to generate the average numbers
[c] % inhibitions were generated @ 50 μM compound and ATP K_m concentrations

The selectivity of **2.10** can be explained by its docking pose in CDK5/p25 showing H-bonding interactions with Asp86 and Asn144 (Figure 6.1 A), whereas in CDK2, the only interaction existed was with water a molecule (represented by black dotted line in Figure 6.1 B). In CDK2 two other residues (Thr14 and Asp145) were at 3.5 Å distances (represented by red dotted line in Figure 6.1 B), which were only viable for very weak H-bonding with **2.14**. The selectivity of the carboxylic acid (**2.14**) can be explained by its H-bonding interactions with Cys83 and Lys33 in CDK5/p25 (Figure 6.1 C) compared to the only interactions with Leu83 in case for CDK2 (Figure 5.1 D). The diagrams in Figure 5.1 were generated by Pymol.[36]
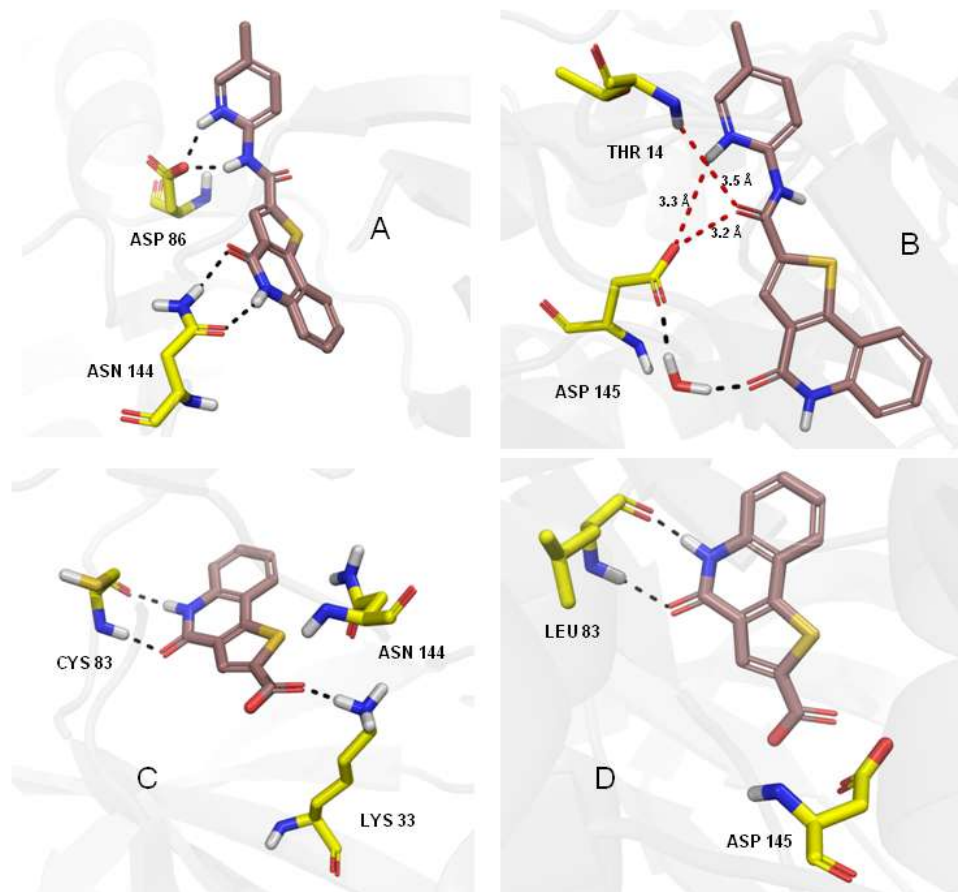
Figure 6.1. H-bonding interactions of **2.10** and **2.14** with CDK5/p25 (A, C) and CDK2 (B, D) Black dotted lines represent H-bonding interactions; Red dotted lines represent measured distances showing probable very weak H-bonding within 3.5 Å.

The identification of a novel thieno[3,2-*c*]quinolin-4(5H)-one derivative (**2.10**) with LE=0.3 from virtual screening and an intermediate (**2.14**) with moderate activity in the same series, led us to choose **2.10** as the lead molecule to proceed with mechanistic evaluation and further SAR development. In an ATP competitive binding assay, performed at Reaction Biology Corp.,[112] **2.10** showed non-competitive inhibition as represented by unchanged IC_{50} values with the increase in ATP concentrations (Figure 6.2 A). The convergence of all the lines on X-axis of

90

the double-reciprocal (Lineweaver-Burke) plot in Figure 6.2 B, reiterated the non-competitive

binding as well.

	10 uM ATP	30 uM ATP	75 uM ATP	150 uM ATP	300 uM ATP
HillSlope	-0.9769	-1.252	-1.046	-1.589	-1.827
EC50	5.444e-006	8.229e-006	5.853e-006	7.913e-006	8.127e-006

	DMSO	2.22 uM	6.67 uM	20 uM
Y-intercept when X=0.0	45.86 ± 0.1844	53.25 ± 1.742	76.73 ± 3.238	246.3 ± 25.53
X-intercept when Y=0.0	-0.08999	-0.06020	-0.07237	-0.07140
1/slope	0.001962	0.001131	0.0009431	0.0002899
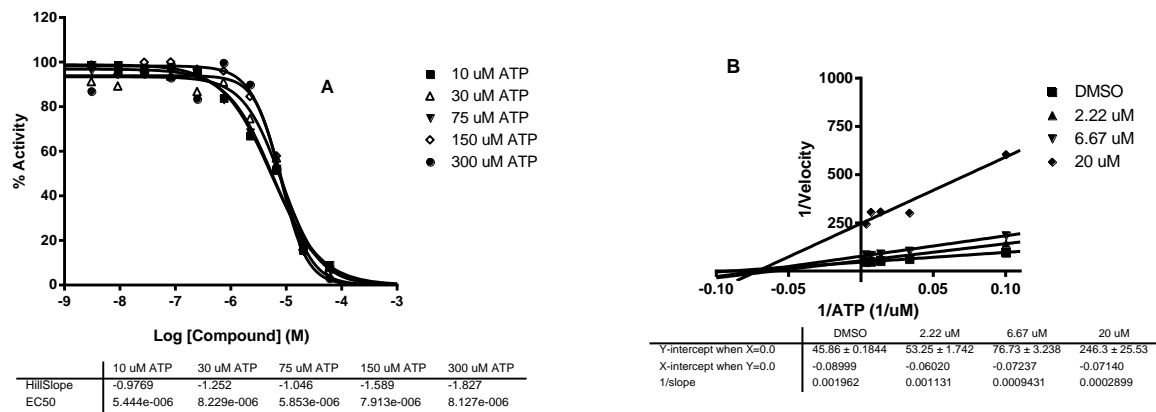
Figure 6.2. IC_{50} curves (A) and Lineweaver-Burk Plot (B) of **2.10** in CDK5/p25 at different ATP concentrations

	10 uM ATP	30 uM ATP	75 uM ATP	150 uM ATP	300 uM ATP
HillSlope	-0.8630	-0.6438	-0.7459	-0.2506	
EC50	4.806e-005	8.384e-005	0.0002765	0.02635	

	DMSO	26.7 uM	80 uM
Y-intercept when X=0.0	45.86 ± 0.1844	47.70 ± 2.929	44.44 ± 1.629
X-intercept when Y=0.0	-0.08999	-0.03756	-0.01690
1/slope	0.001962	0.0007875	0.0003802
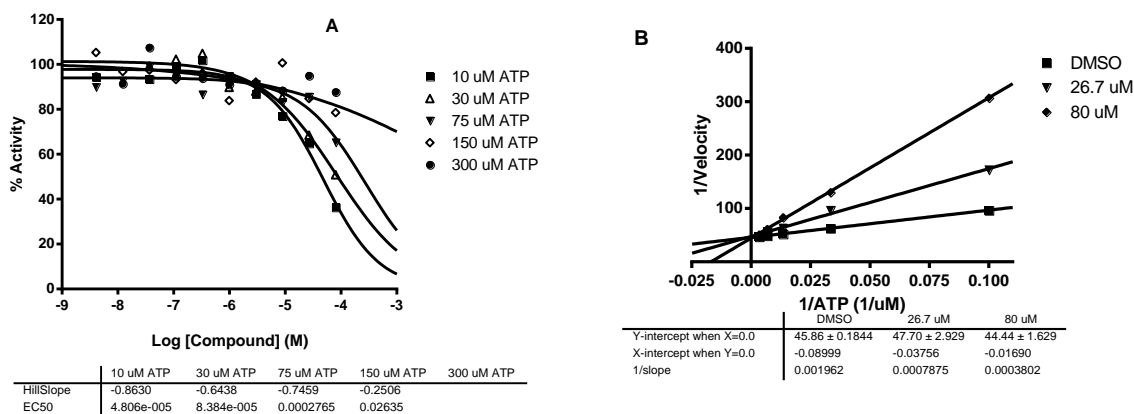
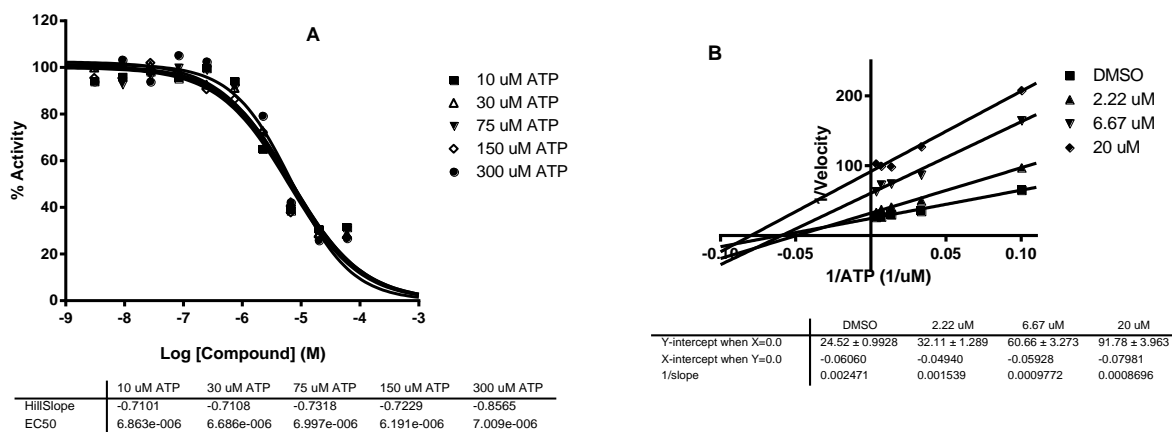**Figure 6.3.** IC_{50} curves (A) and Lineweaver-Burk Plot (B) of **2.14** in CDK5/p25 at different ATP concentrations

On the contrary when we tested the carboxylic acid, (**2.14**) we observed the apparent K_m

increased with the increase in inhibitor concentration and all lines were converged on the Y-axis

in the double-reciprocal plot (Figure 6.3 B), suggesting that the compound is competitive with

respect to ATP against CDK5/p25. In the plot of % enzyme activities at each ATP concentrations

-vs- compound concentration, the IC_{50} values were shifted higher with ATP concentration increase, as expected for competitive inhibitors (Figure 6.3 A). It was observed that at higher concentrations of ATP, the solubility of the compound falls off.

Non-competitive inhibition of (**2.10**) can be explained by a speculative hypothesis that in its protonated form the 2-pyridine amide was interacting with the Asp86 and pushed the rest of the molecule deep into the pocket to H-bond with Asn144 (Figure 6.1 A). On the other hand the carboxylic acid (**2.14**) failed to reach deep into the pocket and consequently showed competitive inhibition (Figure 6.1 C). To further test this hypothesis we synthesized several 2- (*ortho-*) substituted analogs exploiting this deep pocket interaction and we were pleased to observe the similar non-competitive inhibitions for these SAR compounds.

The primary goal of the SAR was to improve the activity of CDK5/p25 and selectivity against CDK2/E. We also synthesized several analogs exploiting the probable deep pocket H-bonding interactions to understand the ATP non-competitive binding of **2.10**.

In the SAR effort we focused our emphasis mainly on the C-ring substitutions as shown in Table 3.3. We utilized convergent analog synthesis to systematically explore different substitutions like esters, aliphatic amides, solubilizing groups, aromatic and hetero-aromatic amides as described in Chapter 3.

The ester (**3.15**) and the simple unsubstituted aliphatic amide (**3.16**) showed no significant activities either in CDK5/p25 or in CDK2/E assays. The same activity trend persisted as we screened more substituted aliphatic amides (**3.17-3.20**) or amides with water soluble groups (**3.21-3.26**). But the trend suddenly showed improvement as we started exploring aromatic amides (**3.27-3.36**). However, we have observed that the over-extension of the aromatics with linkers caused disruption of the aromatic stacking for **3.31** and **3.32**, which

resulted in no activity. It can be concluded that CDK5/p25 activity requires aromatic interactions of the amides. By Comparing **3.28** and **3.30**, we observed a drastic increase in CDK2/E selectivity for **3.30** from 5 fold to a greater than 10 fold, while slightly improving CDK5/p25 activity (IC_{50} = 3.6 µM). This can be explained by extra H-bonding of the *ortho-* F group in **3.30** as we observed previously with protonated 2-pyridyl of **2.10**. We prepared analogs **3.33** and **3.34** by exploiting this H-bonding interaction of the *ortho-* groups and we observed incresed selectivity for both compounds. **3.34** showed the best selectivity profile in the series (at least >13 fold selectivity) and a low micromolar activity in CDK5/p25 (IC50 = 4.3 µM). Both 2-pyridyl compounds (**3.37** and **3.38**) showed low micromolar activities in CDK5/p25 (for **3.37** IC_{50} = 4.3 µM; for **3.38** IC_{50} = 3.8 µM), with highly improved selectivty for the by-product thieno[3,2-*c*]quinoline derivative (**3.38**). The selectivity trend did not go beyond the *ortho-* substitutions, as observed for the 3- (*meta-*) substituted compounds (**3.29**, **3.35**, **3.36** and **3.39**) did not provide good selectivities. The *in-vitro* data of CDK5/p25 and CDK2/E assays for all the SAR compounds are described in Table 6.3.

Table 6.3.   In-vitro CDK5/p25 and CDK2/E assay of SAR compounds

Compound	CDK5/p25 inhibition @50μM[a]	CDK5/p25 IC$_{50}$ (μM)[a]	CDK2/E inhibition @50μM[a]	CDK2/E IC$_{50}$ (μM)[a]
3.15		58.1	7.9%	-
3.16	29.0%	-	21.8%	-
3.17	No inhibition	-	12%	-
3.18	No inhibition	-	10%	-
3.19	No inhibition	-	No inhibition	-
3.20	No inhibition	-	No inhibition	-
3.21	24.9%	-	15.9%	-
3.22	16.6%	-	8.8%	-
3.23	23.3%	-	12.3%	-
3.24	15.3%	-	4.9%	-
3.25	13.1%	-	6.5%	-
3.26	12.8%	-	3.7%	-
3.27		29.2		35.3
3.28		5.2		27.4
3.29		15.6		53.8
3.30		3.6		35.4
3.31	No inhibition	-	No inhibition	-
3.32	No inhibition	-	No inhibition	-
3.33		3.0		25.5
3.34		4.3	No inhibition	
3.35		1.6		6.3
3.36	27.4%	-	No inhibition	-
3.37		4.3		9.9
3.38		3.8	21.8%	-
3.39		10.6	36.7%	-

[a] Assays were performed @ ATP (K$_m$) concentrations of 30 μM for CDK5/p25 and 65 μM for CDK2/E and at least two independent experiments were performed to generate the average numbers

From the above SAR we have identified three compounds (**3.30**, **3.34** and **3.38**) with low micromolar potencies and improved selectivities for further evaluation in ATP competitive binding at Reaction Biology Corp.[112]

For **3.30** we observed that all the lines converged on the X-axis in the double-reciprocal plot (Figure 6.4 B), suggesting that the compound is noncompetitive with respect to ATP against CDK5/p25. When % enzyme activities of slopes relative to DMSO control at each ATP

concentration are plotted against compound concentration and IC_{50} curves were drawn, the IC_{50} values were unchanged significantly when ATP concentration was increased, as expected for noncompetitive inhibitors (Figure 6.4 A).

	10 uM ATP	30 uM ATP	75 uM ATP	150 uM ATP	300 uM ATP
HillSlope	-0.9278	-0.9563	-0.8668	-1.031	-1.059
EC50	6.433e-006	5.114e-006	4.003e-006	8.864e-006	6.805e-006

	DMSO	2.22 uM	6.67 uM	20 uM
Y-intercept when X=0.0	68.73 ± 1.464	93.73 ± 3.056	148.4 ± 26.90	233.1 ± 13.20
X-intercept when Y=0.0	-0.08840	-0.07094	-0.1013	-0.06550
1/slope	0.001286	0.0007569	0.0006826	0.0002810
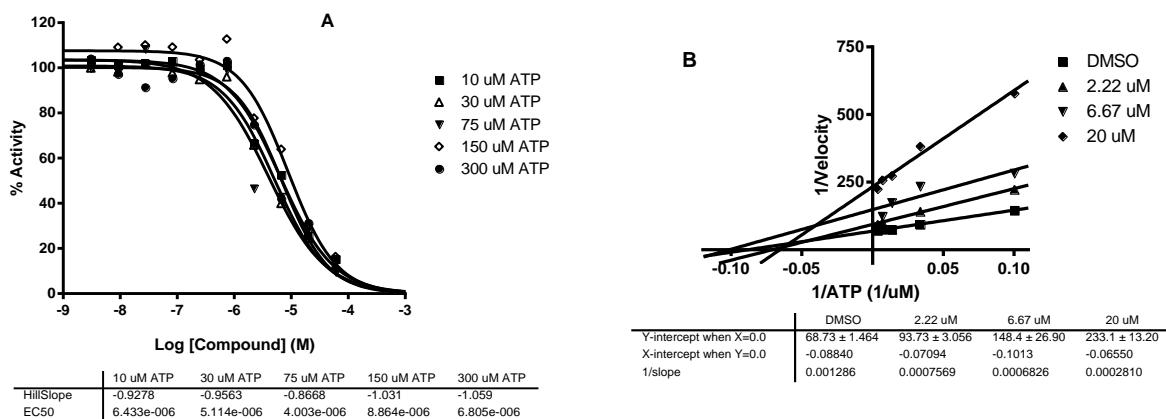
Figure 6.4. IC50 curves (A) and Lineweaver-Burk Plot (B) of **3.30** in CDK5/p25 at different ATP concentrations

	10 uM ATP	30 uM ATP	75 uM ATP	150 uM ATP	300 uM ATP
HillSlope	-1.017	-0.9749	-1.021	-1.067	-1.264
EC50	2.365e-006	1.907e-006	1.807e-006	2.814e-006	2.944e-006

	DMSO	0.62 uM	1.85 uM	5.6 uM
Y-intercept when X=0.0	75.74 ± 1.735	86.77 ± 5.961	154.3 ± 16.54	412.0 ± 30.56
X-intercept when Y=0.0	-0.09230	-0.09192	-0.09850	-0.1227
1/slope	0.001219	0.001059	0.0006381	0.0002978
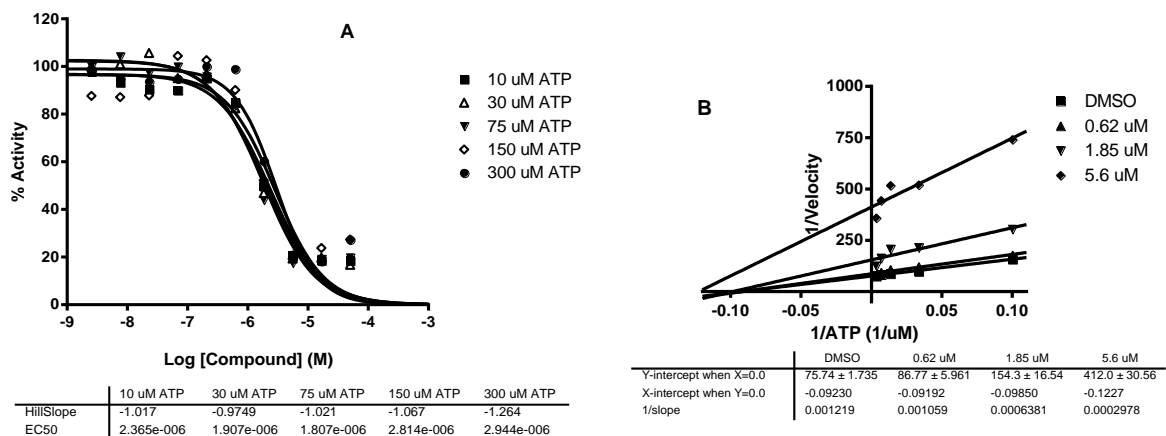
Figure 6.5. IC50 curves (A) and Lineweaver-Burk Plot (B) of **3.34** in CDK5/p25 at different ATP concentrations

In the ATP competitive binding assay for **3.34** we observed that when % enzyme activities of slopes relative to DMSO control at each ATP concentration are plotted against

compound concentration and IC_{50} curves were drawn, the IC_{50} values were unchanged significantly when ATP concentration was increased, as expected for noncompetitive inhibitors (Figure 6.5 A). Also we observed that all the lines converged on the X-axis in the double-reciprocal plot (Figure 6.5 B), suggesting that the compound is noncompetitive with respect to ATP against CDK5/p25.

For **3.38** the ATP competitive binding assay revealed that when % enzyme activities of slopes relative to DMSO control at each ATP concentration are plotted against compound concentration and draw IC_{50} curves, the IC_{50} values were unchanged significantly when ATP concentration was increased, as expected for noncompetitive inhibitors (Figure 6.6 A). Also we observed that all the lines converged on the X-axis in the double-reciprocal plot (Figure 6.6 B), suggesting that the compound is noncompetitive with respect to ATP against CDK5/p25.

	10 uM ATP	30 uM ATP	75 uM ATP	150 uM ATP	300 uM ATP
HillSlope	-0.7101	-0.7108	-0.7318	-0.7229	-0.8565
EC50	6.863e-006	6.686e-006	6.997e-006	6.191e-006	7.009e-006

	DMSO	2.22 uM	6.67 uM	20 uM
Y-intercept when X=0.0	24.52 ± 0.9928	32.11 ± 1.289	60.66 ± 3.273	91.78 ± 3.963
X-intercept when Y=0.0	-0.06060	-0.04940	-0.05928	-0.07981
1/slope	0.002471	0.001539	0.0009772	0.0008696

Figure 6.6.   IC50 curves (A) and Lineweaver-Burk Plot (B) of **3.38** in CDK5/p25 at different ATP concentrations

All three selected compounds showed non-competitive ATP binding, which proved our hypotheses of deep pocket interaction to produce non-competitive inhibition.

Since we are targeting CDK5/p25 inhibitors for AD, we calculated the predicted properties of these three identified compounds to profile their brain permeability, physico-chemical properties and metabolic liabilities using QikProp (Table 6.4).[80]. We found that all three compounds have good BBB permeabilities, low metabolic liabilities and good physico-chemical properties as predicted *in-silico*.

Table 6.4.   Calculated properties of compounds **3.30**, **3.34** and **3.38**

Compound #	Molecular weight	LogP (o/w)	LogBB	# Metab
3.30	356.346	3.202	-0.588	2
3.34	364.375	2.204	-1.655	3
3.38	339.798	3.79	-0.182	3

Finally, we screened these three most potent, selective and non-ATP competitive compounds for selectivity in several serine/threonine and tyrosine kinases (Table 6.4). The % inhibitions were determined at 20 μM of compound concentrations and at ATP Km concentrations of the recombinant human kinases. At least two independent experiments were performed to generate the average numbers

In general the three CDK5/p25 inhibitors showed selectivity over the cell cycle kinases, such as CDK1/B,CDK2/A, CDK2/E, CDK4/D1, CDK6/D1 and WEE1 (nuclear kinase). However, **3.30** and **3.34** showed some activity at few other kinases as described in Table 6.5. The best selectivity profile was observed for **3.38**, which showed only off-target activity in HER2 (Human Epidermal Growth Factor Receptor 2) among the tested kinases.

Table 6.5.   Selectivity profile (% inhibition at 20 μM)[a] of **3.30**, **3.34** and **3.38**

Kinases	3.30	3.34	3.38	ATP Km (μM)
CDK1/B	56	No inhibition	35	5
CDK2/A	58	50	45	10
CDK2/E	27	5	6	65
CDK4/D1	8	No inhibition	No inhibition	90
CDK6/D1	26	No inhibition	No inhibition	30
CK1a1	22	41	19	10
DYRK1/DYRK1A	12	23	4	30
ERBB2/HER2	79	82	77	50
GSK3α	65	79	22	30
GSK3β	53	81	41	5
KDR/VEGFR2	95	88	44	30
PKA	3	89	No inhibition	20
PKCα	8	No inhibition	1	10
PKCε	32	7	4	35
WEE1	11	No inhibition	2	50

[a] Assays were performed @ ATP (K_m) concentrations and at least two independent experiments were performed to generate the average numbers

6.4.   Conclusions

In summary, the identified hits from the virtual screening strategy were evaluated in radiometric filter binding assays in hCDK5/p25 and hCDK2/E. A novel thieno[3,2-c]quinolin-4(5H)-one lead (**2.10**) with 0.3 LE was identified by its modest potency (CDK5/p25 IC_{50} = 7.02 μM) and selectivity (4 fold) over CDK2/E. Mechanistic evaluation revealed the nature of the ATP non-competitive inhibition of **2.10**. This led us to develop a synthetic strategy to evaluate further SAR compounds. We developed a diverse SAR by using convergent analog synthesis strategy to achieve substituted C-ring analogs of thieno[3,2-c]quinolin-4(5H)-one (**3.1**). By analyzing the docked pose of **2.10**, we postulated two working hypotheses of ortho- substitution H-boding to produce selectivity and deep pocket interaction to generate ATP non-competitive

binding interaction. Subsequently, we identified three low micromolar ATP non-competitive CDK5/p25 inhibitors **3.30**, **3.34** and **3.38** with much greater CDK2/E selectivity. We screened the three identified compounds for broader selectivity in a panel of kinases. We observed all three compounds showed good selectivity over cell cycle kinases and among them **3.38** showed better overall selectivity across the selected panel with an off-target activity in HER2. This represents a new series of compounds with ATP non-competitive CDK5/p25 inhibitions. The results of this study may prove useful in the future optimization of this novel series of CDK5/p25 inhibitors.

Biochemically, there are clear indications about the involvement of CDK5/p25 complex in the hyperphosphorylation of tau leading to NFT formation leading to Alzheimer's disease.[7-9] The known kinase inhibitors selected to-date for evaluation in AD, such as R-(-) roscovitine, flavopiridol, indirubin-3′-oxime and kenpaullone showed lack of selectivity and are termed as pan-kinase inhibitors.[25] The three selective and non ATP-competitive CDK5/p25 inhibitors (**3.30**, **3.34** and **3.38**) identified from the dissertation research showed not only low micromolar activity in CDK5/p25, but also good selectivity against all the cell cycle kinases. Additionally, the good predicted BBB permeabilities, physicochemical properties and low metabolic liabilities generate real potential for the compounds to be evaluated in *in-vitro* and *in-vivo* models for AD. The identification of this new class of compounds show promise for future research for developing a candidate for AD.

BIBLIOGRAPHY

1. Association, Alzheimer's. 2013 Alzheimer's disease facts and figures. *Alzheimer's Dementia* **2013,** 9, 208-245.
2. Querfurth, H. W.; LaFerla, F. M. Alzheimer's Disease. *N. Engl. J. Med.* **2010,** 362, 329-344.
3. Dimakopoulos, A. C. Protein aggregation in Alzheimer's disease and other neuropathological disorders. *Curr. Alzheimer Res.* **2005,** 2, 19-28.
4. Froelich-Fabre, S.; Bhat, R. V. Mechanisms of tauopathies. *Drug Discovery Today: Dis. Mech.* **2004,** 1, 391-398.
5. Jain, P.; Flaherty, P. T.; Yi, S.; Chopra, I.; Bleasdell, G.; Lipay, J.; Ferandin, Y.; Meijer, L.; Madura, J. D. Design, synthesis and testing of an 6-O-linked eries of benzamidazole based inhibitors of CDK5/p25. *Bioorg. Med. Chem.* **2011,** 19, 359-373.
6. Seward, M. E.; Swanson, E.; Norambuena, A. s.; Reimann, A.; Cochran, J. N.; Li, R.; Roberson, E. D.; Bloom, G. S. Amyloid-b signals through tau to drive ectopic neuronal cell cycle re-entry in Alzheimer's disease. *J. Cell Sci.* **2013,** 126, 1278-1286.
7. Cruz, J. C.; Tsai, L.-H. Cdk5 derulation in the pathogenesis of Alzheimer's disease. *Trends Mol. Med.* **2004,** 10, 452-458.
8. Lee, S.; Hall, G. F.; Shea, T. B. Potentiation of tau aggregation by cdk5 and GSK3β. *J. Alzheimer's Dis.* **2011,** 26, 355-364.
9. Maccioni, R. B.; Otth, C.; Concha, I. I.; Munoz, J. P. The protein kinase Cdk5. *Eur. J. Biochem.* **2001,** 268, 1518-1527.
10. Tarricone, C.; Dhavan, R.; Peng, J.; Areces, L. B.; Tsai, L.-H.; Musacchio, A. Structure and Regulation of the CDK5-p25^{nck5a} Complex. *Mol. Cell* **2001,** 8, 657-669.
11. Tsai, L.-H.; Delalle, I.; Caviness Jr, V. S.; Chae, T.; Harlow, E. p35 is a neural-specific regulatory subunit of cyclin-dependent kinase 5. *Nature* **1994,** 371, 419-423.
12. Jessberger, S.; Gage, F. H.; Eisch, A. J.; Lagace, D. C. Making a neuron: Cdk5 in embryonic and adult neurogenesis. *Trends Neurosci.* **2009,** 32, 575-582.
13. Sharma, P.; Steinbach, P. J.; Sharma, M.; Amin, N. D.; Barchi Jr., J. J.; Pant, H. C. Identification of Substrate Binding Site of Cyclin-dependent Kinase 5. *J. Biol. Chem.* **1999,** 274, 9600-9606.
14. Dhavan, R.; Tsai, L.-H. A decade of CDK5. *Nat. Rev. Mol. Cell Biol.* **2001,** 2, 749-759.
15. Piedrahita, D.; Hernandez, I.; Lopez-Tobon, A.; Fedorov, D.; Obara, B.; Manjunath, B. S.; Boudreau, R.; Davidson, B.; LeFerla, F.; Gallego-Gomez, J. C.; Kosik, K. S.; Cardona-Gomez, G. P. Silencing of CDK5 Reduces Neurofibrillary Tangles in Transgenic Alzheimer's Mice. *J. Neurosci.* **2010,** 30, 13966-13976.
16. Laha, J. K.; Zhang, X.; Qiao, L.; Liu, M.; Chatterjee, S.; Robinson, S.; Kosik, K. S.; Cuny, G. D. Structure-activity reletionship study of 2,4-diaminothiazoles as Cdk5/p25 kinase inhibitors. *Bioorg. Med. Chem. Lett.* **2011,** 21, 2098-2101.
17. Cheung, Z. H.; Ip, N. Y. Cdk5: a multifaceted kinase in neurodegenerative diseases. *Trends Cell Biol.* **2012,** 22, 169-175.
18. Patzke, H.; Tsai, L.-H. Cdk5 sinks into ALS. *Trends Neurosci.* **2002,** 25, 8-10.
19. Shelton, S. B.; Johnson, G. V. W. Cyclin-dependent kinase-5 in neurodegeneration. *J. Neurochem.* **2004,** 88, 1313-1326.
20. Wei, F.-Y.; Nagashima, K.; Ohshima, T.; Saheki, Y.; Lu, Y.-F.; Matsushita, M.; Yamada, Y.; Mikoshiba, K.; Seino, Y.; Matsui, H.; Tomizawa, K. Cdk5-dependent regulation of glucose-stimulated insulin secretion. *Nat. Med.* **2005,** 11, 1104-1108.

21. Feldmann, G.; Mishra, A.; Hong, S.-M.; Bisht, S.; Strock, C. J.; Ball, D. W.; Goggins, M.; Maitra, A.; Nelkin, B. D. Inhibiting the Cyclin-Dependent Kinase CDK5 blocks pancreatic cancer formation and progression through the suppression of Ras-Ral signaling. *Cancer Res.* **2010,** 11, 4460-4469.

22. Booth, R. J.; Chatterjee, A.; Malone, T. C. Pyridopyrimidinone derivatives for treatment of neurodegenerative disease WO2001055148, 2001.

23. Helal, C. J.; Kang, Z.; Lucas, J. C.; Gant, T.; Ahlijanian, M. K.; Schachter, J. B.; Richter, K. E. G.; Cook, J. M.; Menniti, F. S.; Kelly, K.; Mente, S.; Pandit, J.; Hosea, N. Potent and cellularly active 4-aminoimidazole inhibitors of cyclin-dependent kinase 5/p25 for the treatment of Alzheimer's disease. *Bioorg. Med. Chem. Lett.* **2009,** 19, 5703-5707.

24. Shiradkar, M. R.; Padhalingappa, M. B.; Bhetalabhotala, S.; Akula, K. V.; Tupe, D. A.; Pinninti, R. R.; Thummanagoti, S. A novel approach to cyclin-dependent kinase 5/p25 inhibitors: A potential treatment for Alzheimer's disease. *Bioorg. Med. Chem.* **2007,** 15, 6397-6406.

25. Pallas, M.; Canudas, A. M.; Verdaguer, E.; Allgaier, C.; de Arriba, S. G.; Alvira, D.; Sureda, F. X.; Camins, A. Inhibitors of Cyclin-Dependent Kinases: Potential Drugs for the Treatment of Neurodegenerative Disorders? . *Curr. Med. Chem.: Cent. Nerv. Syst. Agents* **2005,** 5, 101-109.

26. Booth, R. J.; Chatterjee, A.; Malone, T. C. Pyridopyrimidinone derivatives for treatment of neurodegenerative disease WO2001055148, 2001.

27. Rzasa, R. M.; Kaller, M. R.; Liu, G.; Magal, E.; Nguyen, T.; Osslund, T. D.; Powers, D.; Santora, V. J.; Viswanadhan, V. N.; Wang, H.-L.; Xiiong, X.; Zhong, W.; Norman, M. H. Structure-activity relationships of 3,4-dihydro-1H-quinazolin-2-one derivatives as potential CDK5 inhibitors. *Bioorg. Med. Chem.* **2007,** 15, 6574-6595.

28. Ahn, J. S.; Radhakrishnan, M. L.; Mapelli, M.; Choi, S.; Tidor, B.; Cuny, G. D.; Musacchio, A.; Yeh, L.-A.; Kosik, K. S. Defining Cdk5 ligand chemical space with small molecule inhibitors of Tau phosphorylation. *Chem. Biol.* **2005,** 12, 811-823.

29. Mapelli, M.; Massimiliano, L.; Crovace, C.; Seeliger, M. A.; Tsai, L.-H.; Meijer, L.; Musacchio, A. Mechanism of CDK5/p25 Binding by CDK Inhibitors. *J. Med. Chem.* **2005,** 48, 671-679.

30. Meijer, L.; Borgne, A.; Mulner, O.; Chong, J. P. J.; Blow, J.; Inagaki, N.; Inagaki, M.; Delcros, J.-G.; Moulinoux, J.-P. Biochemical and cellular effects of roscovitine, a potent and selective inhibitor of the cyclin-dependent kinases cdc2, cdk2 and cdk5. *Eur. J. Biochem.* **1997,** 243, 527-536.

31. Nair, N.; Kudo, W.; Smith, M. A.; Abrol, R.; Goddard III, W. A.; Reddy, V. P. Novel purine-based fluoroaryl-1,2,3-triazoles as neuroprotecting agents: Synthesis, neuronal cell culture investigations, and CDK5 docking studies. *Bioorg. Med. Chem. Lett.* **2011,** 21, 3957-3961.

32. Andricopulo, A. D.; Salum, L. B.; Abraham, D. J. Structure-based drug design strategies in medicinal chemistry. *Curr. Top. Med. Chem.* **2009,** 9, 771-790.

33. Lyne, P. D. Structure-based virtual screening: an overview. *Drug Discovery Today* **2002,** 7, 1047-1055.

34. Haq, Z. U.; Uddin, R.; Wai, L. K.; Wadood, A.; Lajis, N. H. Docking and 3D-QSAR modeling of cyclin-dependent kinase 5/p25 inhibitors. *J. Mol. Model.* **2011,** 17, 1149-1161.

35.   Pitchuanchom, S.; Boonyarat, C.; Forli, S.; Olson, A. J.; Yenjai, C. Cyclin-dependent kinases 5 template: Useful for virtual screening. *Comput. Biol. Med.* **2012,** 42, 106-111.
36.   *The PyMOL Molecular Graphics System, Version 1.5.0.4 Schrödinger, LLC*, Schrödinger, LLC,: New York, NY, 2011.
37.   *Maestro, version 9.2, Schrödinger, LLC, New York, NY, 2011*, Schrödinger, LLC,: New York, NY, 2011.
38.   *LigPrep, version 2.5*, Schrödinger, LLC: New York, NY, 2011.
39.   *Schrödinger Suite 2011 Protein Preparation Wizard; Epik version 2.2, Impact version 5.7, Prime version 3.0,* Schrödinger, LLC, New York, NY, 2011.
40.   *Prime, version 3.0,* Schrödinger, LLC: New York, NY, 2011.
41.   Salam, N. K.; Nuti, R.; Sherman, W. Novel Method for Generating Structure-Based Pharmacophores Using Energetic Analysis. *J. Chem. Inf. Model.* **2009,** 49, 2356-2368.
42.   Dixon, S. L.; Smondyrev, A. M.; Knoll, E. H.; Rao, S. N.; Shaw, D. E.; Friesner, R. A. PHASE: a new engine for pharmacophore perception, 3D QSAR model development, and 3D database screening: 1. Methodology and preliminary results. *J. Comput.-Aided Mol. Des.* **2006,** 20, 647-671.
43.   Dixon, S. L.; Smondyrev, A. M.; Rao, S. N. PHASE: A Novel approach to Pharmacophore Modeling and 3D Database Searching. *Chem. Biol. Drug Des.* **2006,** 67, 370-372.
44.   Gompel, M.; Leost, M.; De Kier Joffe, E. B.; Puricelli, L.; Franco, L. H.; Palermo, J.; Meijer, L. Meridianins, a new family of protein kinase inhibitors isolated from the Ascidian Aplidium meridianum. *Bioorg. Med. Chem. Lett.* **2004,** 14, 1703-1707.
45.   Helal, C. J.; Sanner, M. A.; Cooper, C. B.; Gant, T.; Adam, M.; Lucas, J. C.; Kang, Z.; Kupchinsky, S.; Ahlijanian, M. K.; Tate, B.; Menniti, F. S.; Kelly, K.; Peterson, J. R. Discovery and SAR of 2-aminothiazole inhibitors of cyclin-dependent kinase 5/p25 as a potential treatment for Alzheimer's disease. *Bioorg. Med. Chem. Lett.* **2004,** 14, 5521-5525.
46.   Larsen, S. D.; Stachew, C. F.; Clare, P. M.; Cubbage, J. w.; Leach, K. L. A catch-and-release strategy fot the combinatorial synthesis of 4-acylamino-1,3-thiazoles as potential cdk5 Inhibitors. *Bioorg. Med. Chem. Lett.* **2003,** 13, 3491-3495.
47.   Ortega, M. A.; Montoya, M. E.; Zarranz, B.; Jaso, A.; Aldana, I.; Leclerc, S.; Meijer, L.; Monge, A. Pyrazolo[3,4-*b*]quinoxalines. A new class of cyclin-dependent kinases inhibitors. *Bioorg. Med. Chem. Lett.* **2002,** 10, 2177-2184.
48.   Polychronopoulos, P.; Magiatis, P.; Skaltsounis, A.-L.; Myrianthopoulos, V.; Mikros, E.; Tarricone, A.; Musacchio, A.; Roe, S. M.; Pearl, L.; Leost, M.; Greengard, P.; Meijer, L. Structural Basis for the Synthesis of Indirubins as Potent and Selective Inhibitors of Glycogen Synthase Kinase-3 and Cyclin-Dependent Kinases. *J. Med. Chem.* **2004,** 47, 935-946.
49.   Kaller, M. R.; Zhong, W.; Henley, C.; Magal, E.; Nguyen, T.; Powers, D.; Rzasa, R. M.; Wang, W.; Xiong, X.; Norman, M. H. Design and synthesis of 6-oxo-1,6-dihydropyridines as CDK5 inhibitors. *Bioorg. Med. Chem. Lett.* **2009,** 19, 6591-6594.
50.   Metty, Y.; Gompel, M.; Thomas, V.; Garnier, M.; Leost, M.; Ceballos-Picot, I.; Noble, M.; Endicott, J.; Vierfond, J.-m.; Meijer, L. Aloisines, a new family of CDK/GSK-3 inhibitors. SAR study, crystal structure in complex with CDK2, enzyme selectivity, and cellular effects. *J. Med. Chem.* **2003,** 46, 222-236.

51.   Shiradkar, M.; Akula, K. V.; Dasari, V.; Baru, V.; Chiningiri, B.; Gandhi, S.; Kaur, R. Clubbed thiazoles by MAOS: A novel approach to cyclin-dependent kinase 5/p25 inhibitors as a potential treatment for Alzheimer's disease. *Bioorg. Med. Chem.* **2007,** 15, 2601-2610.

52.   Zhong, W.; Liu, H.; Kaller, M. R.; Henley, C.; Magal, E.; Nguyen, T.; Osslund, T. D.; Powers, D.; Rzasa, R. M.; Wang, H.-L.; Wang, W.; Xiiong, X.; Zhang, J.; Norman, M. H. Design and synthesis of quinolin-2(1H)-one derivatives as potent CDK5 inhibitors. *Bioorg. Med. Chem. Lett.* **2007,** 17, 5384-5389.

53.   Becknell, N. C.; Hudkins, R. L. Fused [d]pyridazin-7-ones. US 20070299061, 2007.

54.   Ip, N. Y.-Y.; Ip, F. C.-F.; Fu, W. Y.; Fu, G. Cdk5 inhibitors and therapeutic uses thereof. WO/2011/069334, 2011.

55.   Luo, Y.; Shu, F.; Wang, S. Kinase inhibitors and their use as pharmaceutical agents. WO/2010/051781 2010.

56.   Machacek, M., R.; Ahearn, S., P. ; Romeo, E.; Siu, T.; Chichetti, S.; De Almeida, G.; Rivkin, A. Imidothiazole kinase inhibitors. WO/2011/037780 2011.

57.   Routier, S., César, Léonce; Guillaumet, G.; Boulahjar, R.; Meijer, L.; Chiurato, M. 10-Amino-1,2,3,4-tetrahydropyrido[2,1-a]isoindol-6(10b*H*)-one   derivatives,   method   for preparing same, and therapeutic uses thereof. WO/2010/103240 2010.

58.   Shiradkar, M.; Thomas, J.; Kanase, V.; Dighe, R. Studying synergism of methyl linked cyclohexyl thiophenes with triazole: Synthesis and their cdk5/p25 inhibition activity. *Eur. J. Med. Chem.* **2011,** 46, 2066-2074.

59.   Siu, T.; Dinsmore, C.; Kumarasinghe, S., E. Pyrazolo [3,4-b] pyridin-4-one kinase inhibitors. WO/2011/049722, 2011.

60.   *Phase, version 3.3,* Schrödinger, LLC, : New York, NY, 2011.

61.   *Glide, version 5.7,* Schrödinger, LLC: New York, NY, 2011.

62.   Friesner, R. A.; Murphy, R. B.; Repasky, M. P.; Frye, L. L.; Greenwood, J. R.; Halgren, T. A.; Sanschagrin, P. C.; Mainz, D. T. Extra precision Glide: Docking and scoring incorporating a model of hydrophobic enclosure for protein-ligand complexes. *J. Med. Chem.* **2006,** 49, 6177-6196.

63.   Duan, J.; Dixon, S. L.; Lowrie, J. F.; Sherman, W. Analysis and comparison of 2D fingerprints: Insights into database screening performance using eight fingerprint methods. *J. Mol. Graphics Modell.* **2010,** 29, 157-170.

64.   Willett, P.; Barnard, J. M.; Downs, G. M. D. Chemical similarity searching. *J. Chem. Inf. Model.* **1998,** 38, 983-996.

65.   Sastry, M.; Lowrie, J. F.; Dixon, S. L.; Sherman, W. Large-Scale Systematic Analysis of 2D Fingerprint Methods and Parameters to Improve Virtual Screening Enrichments. *J. Chem. Inf. Model.* **2010,** 50, 771-784.

66.   *Canvas, version 1.4,* Schrödinger, LLC: New York, NY, 2011.

67.   de Beer, S. B. A.; Vermeulen, N. P. E.; Oostenbrink, C. The Role of Water Molecules in Computational Drug Design. *Curr. Top. Med. Chem.* **2010,** 10, 55-66.

68.   Sastry, G. M.; Adzhigirey, M.; Day, T.; Annabhimoju, R.; Sherman, W. Protein and ligand preparation: parameters, protocols, and influence on virtual screening enrichments. *J. Comput.-Aided Mol. Des.* **2013,** 27, 221-234.

69.   Anderson, M.; Beattie, J. F.; Breault, G. A.; Breed, J.; Byth, K. F.; Culshaw, J. D.; Ellston, R. P. A.; Green, S.; Minshull, C. A.; Norman, R. A.; Pauptit, R. A.; Stanway, J.; Thomas, A. P.; Jewsbury, P. J. Imidazo[1,2-a]pyridines: A potent and selective class of

Cyclin-Dependent Kinase inhibitors identified through structure-based hybridisation. *Bioorg. Med. Chem. Lett.* **2003,** 13, 3021-3026.

70. de Azevedo Jr., W. F.; Leclerc, S.; Meijer, L.; Havlicek, L.; Strnad, M.; Kim, S.-H. Inhibition of cyclin-dependent kinases by purine analogues: crystal structure of human cdk2 complexed with roscovitine. *Eur. J. Biochem.* **1997,** 243, 518-526.

71. Jones, C. D.; Andrews, D. M.; Barker, A. J.; Blades, K.; Daunt, P.; East, S.; Geh, C.; Graham, M. A.; Johnson, K. M.; Loddicka, S. A.; McFarland, H. M.; McGregor, A.; Moss, L.; Rudge, D. A.; Simpson, P. B.; Swain, M. L.; Tam, K. Y.; Tucker, J. A.; Walker, M. The discovery of AZD5597, a potent imidazole pyrimidine amide CDK inhibitor suitable for intravenous dosing. *Bioorg. Med. Chem. Lett.* **2008,** 18, 6369-6373.

72. Lawrie, A. M.; Noble, M. E. M.; Tunnah, P.; Brown, N. R.; Johnson, L. N.; Endicott, J. A. Protein kinase inhibition by staurosporine revealed in details of the molecular interaction with CDK2. *Nat. Struct. Mol. Biol.* **1997,** 4, 796-801.

73. Luk, K.-C.; Simcox, M. E.; Schutt, A.; Rowan, K.; Thompson, T.; Chen, Y.; Kammlott, U.; DePinto, W.; Dunten, P.; Dermatakis, A. A new series of potent oxindole inhibitors of CDK2. *Bioorg. Med. Chem. Lett.* **2004,** 14, 913-917.

74. Wyatt, P. G.; Woodhead, A. J.; Berdini, V.; Boulstridge, J. A.; Carr, M. G.; Cross, D. M.; Davis, D. J.; Devine, L. A.; Early, T. R.; Feltell, R. E.; Lewis, E. J.; Mcmenamin, R. L.; Navarro, E. F.; O'Brien, M. A.; O'Reilly, M.; Reule, M.; Saxty, G.; Seavers, L. C. A.; Smith, D.; Squires, M. S.; Trewartha, G.; Walker, M. T.; Woolford, A. J. Identification of N-(4-Piperidinyl)-4-(2,6-dichlorobenzoylamino)-1H-pyrazole-3-carboxamide (AT7519), a Novel Cyclin Dependent Kinase Inhibitor Using Fragment-Based X-Ray Crystallography and Structure Based Drug Design. *J. Med. Chem.* **2008,** 51, 4986-4999.

75. Loving, K.; Salam, N. K.; Sherman, W. Energetic analysis of fragment docking and application to structure-based pharmacophore hypothesis generation. *J. Comput.-Aided Mol. Des.* **2009,** 23, 541-554.

76. *PoseView is developed at the Center for Bioinformatics Hamburg and jointly provided with BioSolveIT as a community service at the PDB.*

77. Stierand, K.; Maaß, P.; Rarey, M. Molecular Complexes at a Glance: Automated Generation of two-dimensional Complex Diagrams. *Bioinformatics* **2006,** 22, 1710-1716.

78. Stierand, K.; Rarey, M. From Modeling to Medicinal Chemistry: Automatic Generation of Two-Dimensional Complex Diagrams. *ChemMedChem* **2007,** 2, 853-860.

79. *CAC (2010);* Database of commercially available compounds as provided by Schrodinger, LLC, New York, NY, 2011.

80. *QikProp, version 3.4,* Schrödinger, LLC,: New York, NY, 2011.

81. Friesner, R. A.; Banks, J. L.; Murphy, R. B.; Halgren, T. A.; Klicic, J. J.; Mainz, D. T.; Repasky, M. P.; Knoll, E. H.; Shaw, D. E.; Shelley, M.; Perry, J. K.; Francis, P.; Shenkin, P. S. Glide: A New Approach for Rapid, Accurate Docking and Scoring. 1. Method and Assessment of Docking Accuracy. *J. Med. Chem.* **2004,** 47, 1739–1749.

82. Assays were performed at Reaction Biology Corp., PA, USA. In.

83. Bhakuni, B. S.; Kumar, A.; Balkrishna, S. J.; Sheikh, J. A.; Konar, S.; Sangit, K. KOtBu Mediated Synthesis of Phenanthridinones and Dibenzoazepinones. *Org. Lett.* **2012,** 14, 2838-2841.

84. Gorlitzer, K.; Gabriel, B.; Jomaa, H.; Wiesner, J. Synthesis of thieno[3,2-c]quinolin-4-ylamines and antimalarial activity. *Pharmazie* **2006,** 61, 278-284.

85. Pierre, F.; Haddach, M.; Regan, C. F.; Ryckman, D. M. Condensed Quiolines as Protein Kinase Modulators. WO 2011025859, 2011.

86. Rajeshkumar, V.; Lee, T.-H.; Chuang, S.-C. Palladium-Catalyzed Oxidative Insertion of Carbon Monoxide to N-Sulfonyl-2-aminobiaryls through C-H Bond Activation: Access to Bioactive Phenanthridinone Derivatives in One Pot. *Org. Lett.* **2013,** 15, 1468-1471.

87. Pierre, F.; Regan, C. F.; Chevrel, M.-C.; Siddiqui-Jain, A.; Macalino, D.; Streiner, N.; Drygin, D.; Haddach, M.; O'Brien, S. E.; Rice, W. G.; Ryckman, D. M. Novel potent dual inhibitors of CK2 and Pim kinases with antiproliferative activity against cancer cells. *Bioorg. Med. Chem. Lett.* **2012,** 22, 3327-3331.

88. Castle, L. W.; Elmaaty, T. A. A New Method for the Synthesis of Substituted Indeno[1,2-b]thiophene with Subsequent Ring Expansion to form Substituted Thieno[3,2-c]quinoline. *J. Heterocycl. Chem.* **2006,** 43, 629-631.

89. Jayashree, A.; Darbarwar, M. Synthesis of 4,5-dihydro-4(5*H*)-oxothieno[3, 2-c]quinoline-2-carboxylicacids and their alkyl esters. *Indian J. Chem.* **1994,** 33B, 676-678.

90. Majumdar, K. C.; Ghosh, M. Tandem cyclization: one pot regioselective synthesis of thieno[3,2-c]quinolin-4(5H)-one derivatives. *Tetrahedron* **2002,** 58, 10047-10052.

91. Ohashi, T.; Oguro, Y.; Tanaka, T.; Shiokawa, Z.; Shibata, S.; Sato, Y.; Yamakawa, H.; Hattori, H.; Yamamoto, Y.; Kondo, S.; Miyamoto, M.; Tojo, H.; Baba, A.; Sasaki, S. Discovery of pyrrolo[3,2-c]quinoline-4-one derivatives as novel hedgehog signaling inhibitors. *Bioorg. Med. Chem.* **2012,** 20, 5496-5506.

92. Ibrahim, P. N.; Cho, H.; England, B.; Gillette, S.; Artis, D. R.; Zuckerman, R.; Zhang, C. PDE4B inhibitors and uses therefor. US 20060041006, 2006.

93. Coburn, G., A.; Han, A., Qi; Provoncha, K., P.; Rotshteyn, Y. Triazines and related compounds having antiviral activity, compositions and methods thereof. WO/2009/091388, 2009.

94. Cai, S. X.; Zhou, Z.-L.; Huang, J.-C.; Whittemore, E. R.; Egbuwoku, Z. O.; Lu¨, Y.; Hawkinson, J. E.; Woodward, R. M.; Weber, E.; Keana, J. F. W. Synthesis and Structure-Activity Relationships of 1,2,3,4-Tetrahydroquinoline-2,3,4-trione 3-Oximes: Novel and Highly Potent Antagonists for NMDA Receptor Glycine Site. *J. Med. Chem.* **1996,** 39, 3248-3255.

95. Ahmed, N.; Brahmbhatt, K. G.; Sabde, S.; Mitra, D.; Singh, I. P.; Bhutani, K. K. Synthesis and anti-HIV activity of alkylated quinoline 2,4-diols. *Bioorg. Med. Chem.* **2010,** 18, 2872-2879.

96. Arya, K.; Agarwal, M. Microwave prompted multigram synthesis, structural determination, and photo-antiproliferative activity of fluorinated 4-hydroxyquinolinnes. *Bioorg. Med. Chem. Lett.* **2007,** 17, 86-93.

97. Sechi, M.; Azzena, U.; Delussu, M. P.; Dallocchio, R.; Dessì, A.; Cosseddu, A.; Pala, N.; Neamati, N. Design and Synthesis of Bis-amide and Hydrazide-containing Derivatives of Malonic Acid as Potential HIV-1 Integrase Inhibitors. *Molecules* **2008,** 13, 2442-2461.

98. Shobana, N.; Yeshoda, P.; Shanmugam, P. A convenient approach to the synthesis of prenyl-, furo- and pyrano-quinoline alkaloids of the Rutaceae. *Tetrahedron* **1989,** 45, 757-762.

99. Khan, K. A.; Shoeb, A. Chemistry of Carbostyril: Part I - Oxidation reactions of 4-hydroxy- & 4-hydroxy-1-methyl-2(1*H*)-quinolinones. *Indian J. Chem.* **1985,** 24B, 62-66.

100. Chilin, A.; Marzaro, G.; Marza, C.; Via, L. D.; Ferlin, M. G.; Pastorini, G.; Guiotto, A. Synthesis and antitumor activity of novel amsacrine analogs: The critical role of the

acridine moiety in determining their biological activity. *Bioorg. Med. Chem.* **2009,** 17, 523-529.

101. Fiala, W.; Stadlbauer, W. Nucleophilic Chlorination of 3-formyl-4-hydroxy-quinolin-2(1H)-ones. *J. Prakt. Chem./Chem.-Ztg.* **1993,** 335, 128-134.

102. Chatterjee, A.; Cutler, S.; Khan, I.; Williamson, J. Efficient synthesis of 4-oxo-4,5-dihydrothieno[3,2-c]quinoline-2-carboxylic acid derivatives from aniline. *Mol. Diversity* **2013,** (in press), DOI: 10.1007/s11030-013-9476-4.

103. Gelderblom, H.; Verweij, J.; Nooter, K.; Sparreboom, A. Cremophor EL: the drawbacks and advantages of vehicle selection for drug formulation. *Eur. J. Cancer* **2001,** 37, 1590-1598.

104. Veau, C.; Faivre, L.; Tardivel, S.; Soursac, M.; Banide, H.; Lacour, B.; Farinotti, R. Effect of Interleukin-2 on Intestinal P-glycoprotein Expression and Functionality in Mice. *J. Pharmacol. Exp. Ther.* **2002,** 302, 742-750.

105. Garzón, J.; de la Torre-Madrid, E.; Rodríguez-Muñoz, M.; Vicente-Sánchez, A.; Sánchez-Blázquez, P. Gz mediates the long-lasting desensitization of brain CB1 receptors and is essential for cross-tolerance with morphine. *Mol. Pain* **2009,** 5:11.

106. Life Technologies, Carlsbad, CA 92008; (www.lifetechnologies.com).

107. *GraphPad Prism version 6.02 for Windows*, GraphPad Software: La Jolla California, USA, www.graphpad.com, 2013.

108. *Z'-LYTE® Screening Protocol and Assay Conditions*, (www.lifetechnologies.com): Revised 30 April-2013.

109. Ma, H.; deacon, S. W.; Horiuchi, K. The challenge of selecting protein kinase assays for lead discovery optimization. *Expert Opin. Drug Discovery* **2008,** 3, 607-621.

110. Currais, A.; Hortobágyi, T.; Soriano, S. The neuronal cell cycle as a mechanism of pathogenesis in Alzheimer's disease. *Aging* **2009,** 1, 363-371.

111. Tell, V.; Holzer, M.; Herrmann, L.; Mahmoud, K. A.; Schächtele, C.; Totzke, F.; Hilgeroth, A. Multitargeted drug development: Discovery and profiling of dihydroxy substituted 1-aza-9-oxafluorenes as lead compounds targeting Alzheimer disease relevant kinases. *Bioorg. Med. Chem. Lett.* **2012,** 22, 6914-6918.

112. Reaction Biology Corp., Malvern, PA 19355; (www.reactionbiology.com).

113. Anastassiadis, T.; Deacon, S. W.; Devarajan, K.; Ma, H.; Peterson, J. R. Comprehensive assay of kinase catalytic activity reveals features of kinase inhibitor selectivity. *Nat. Biotechnol.* **2011,** 29, 1039-1045.

114. Hopkins, A. L.; Groom, C. R.; Alex, A. Ligand efficiency: a useful metric for lead selection. *Drug Discovery Today* **2004,** 9, 430-431.

LIST OF APPENDICES

APPENDIX A: SPECTRA OF SYNTHESIZED COMPOUNDS

¹H of NMR of **2.4**
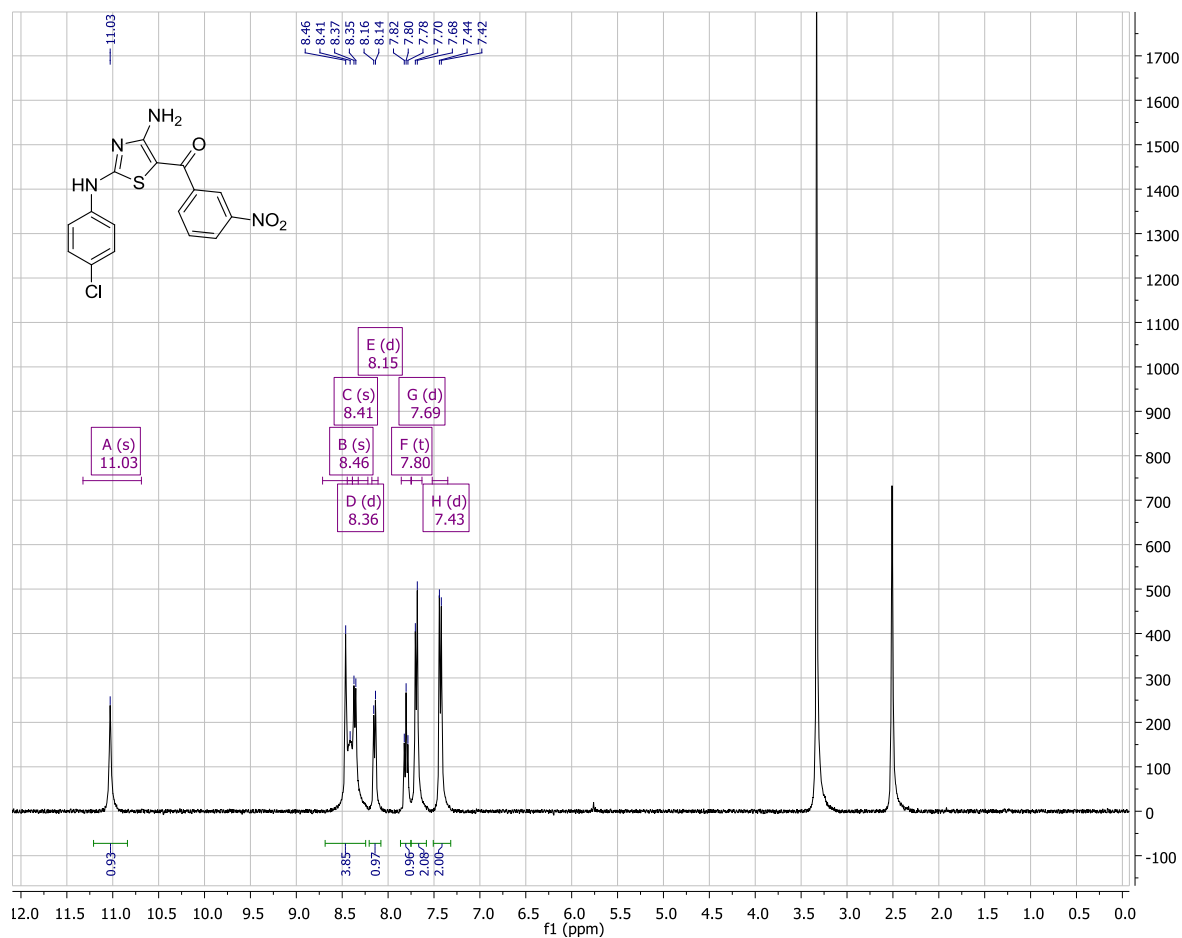
¹³C NMR of **2.4**
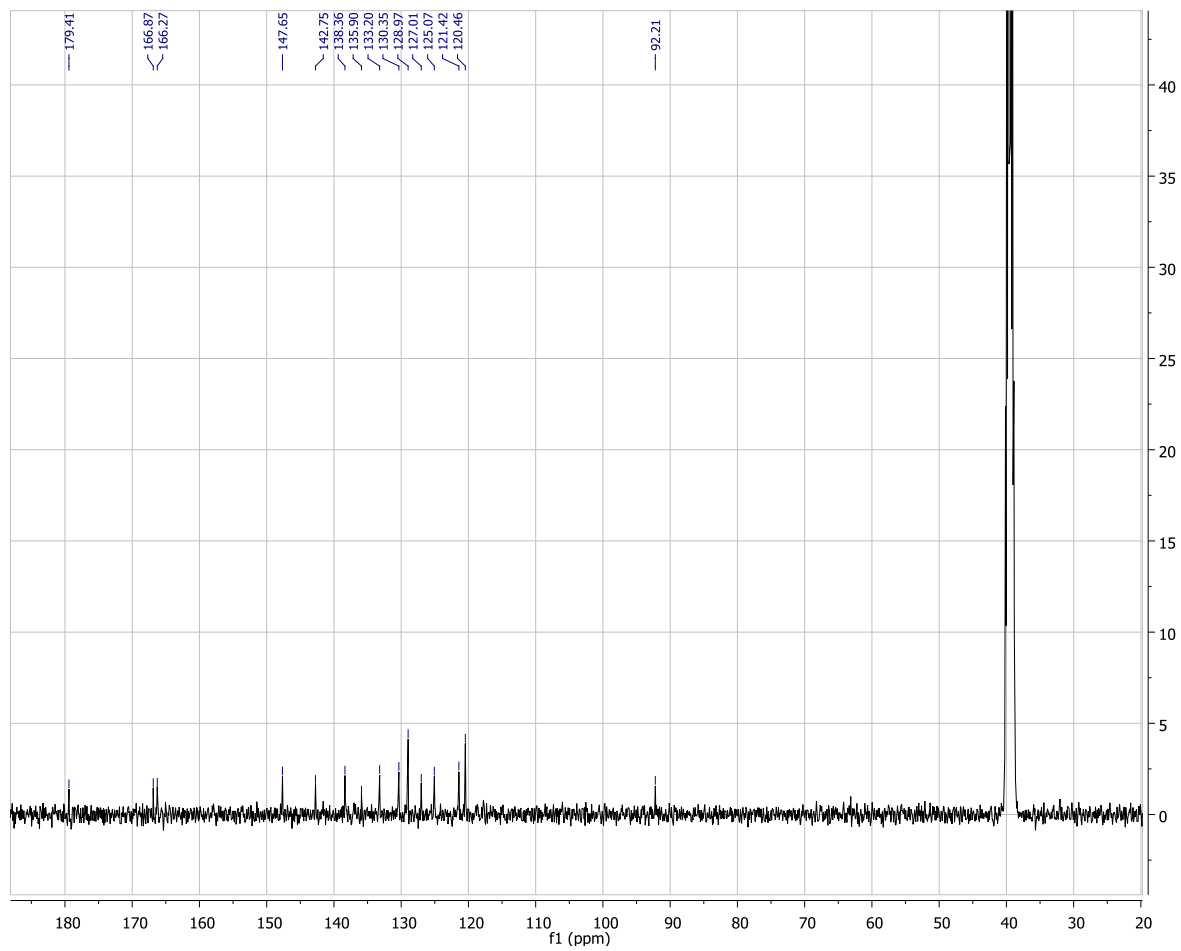
HRMS (ESI TOF) of Compound **2.4**
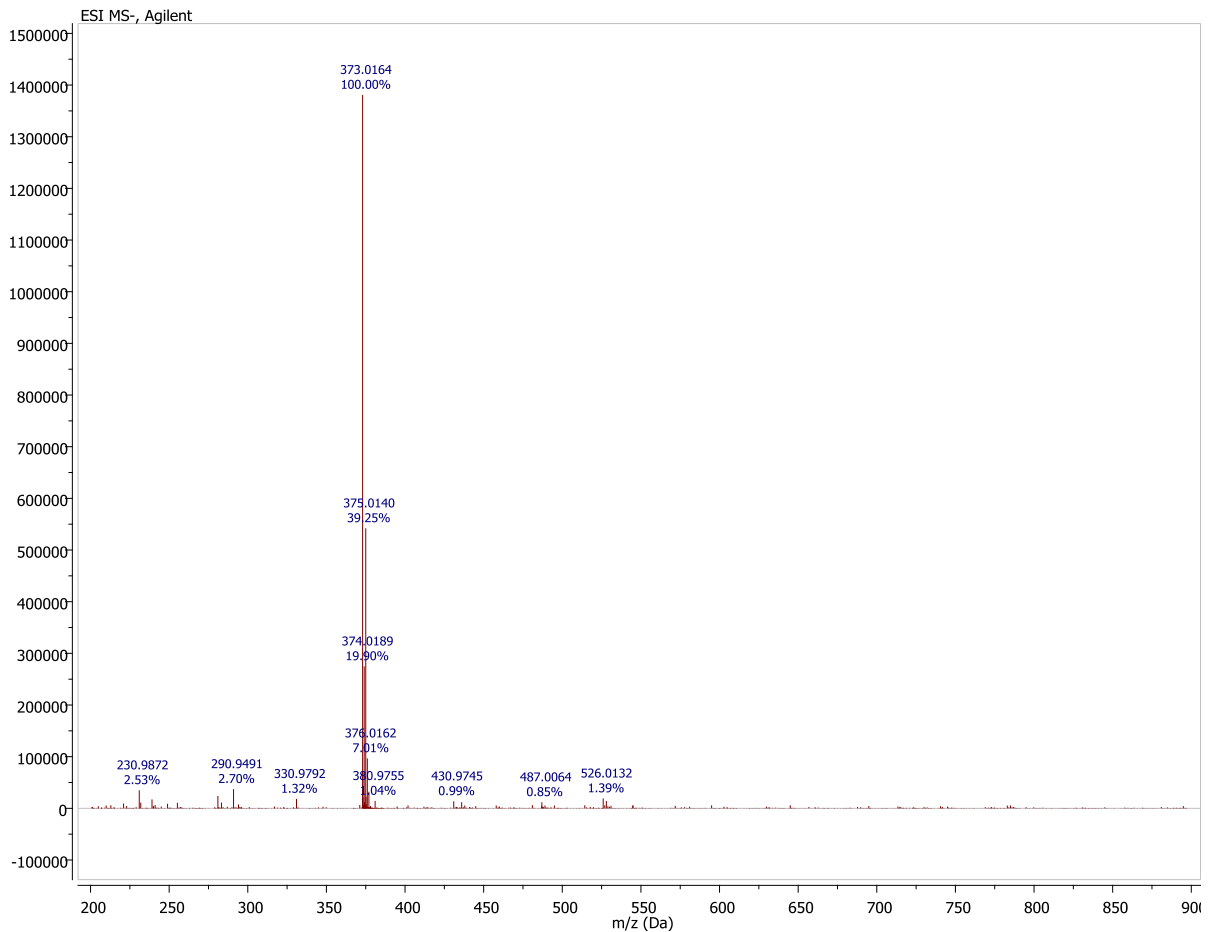
HPLC of **2.4**
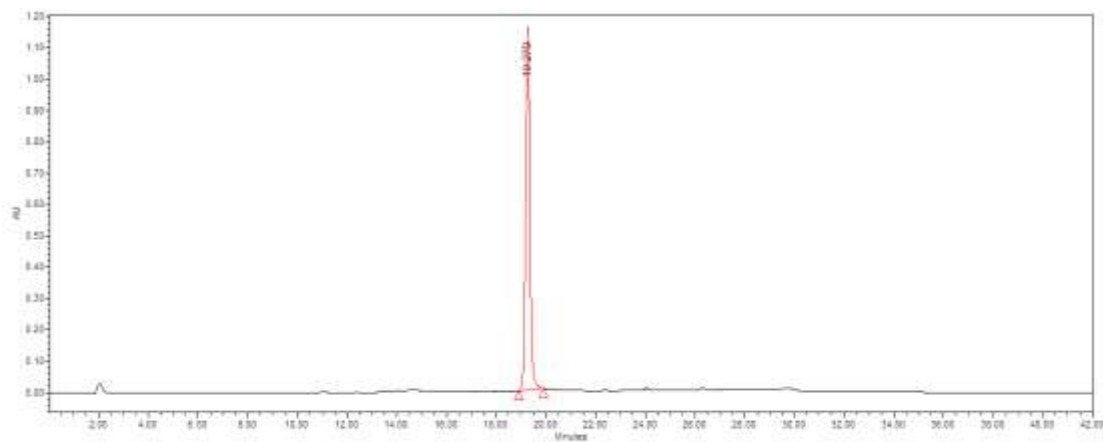
Retention time (min)	% Area
19.270	100

¹H NMR of **2.5**

^{1}H NMR of **2.5**
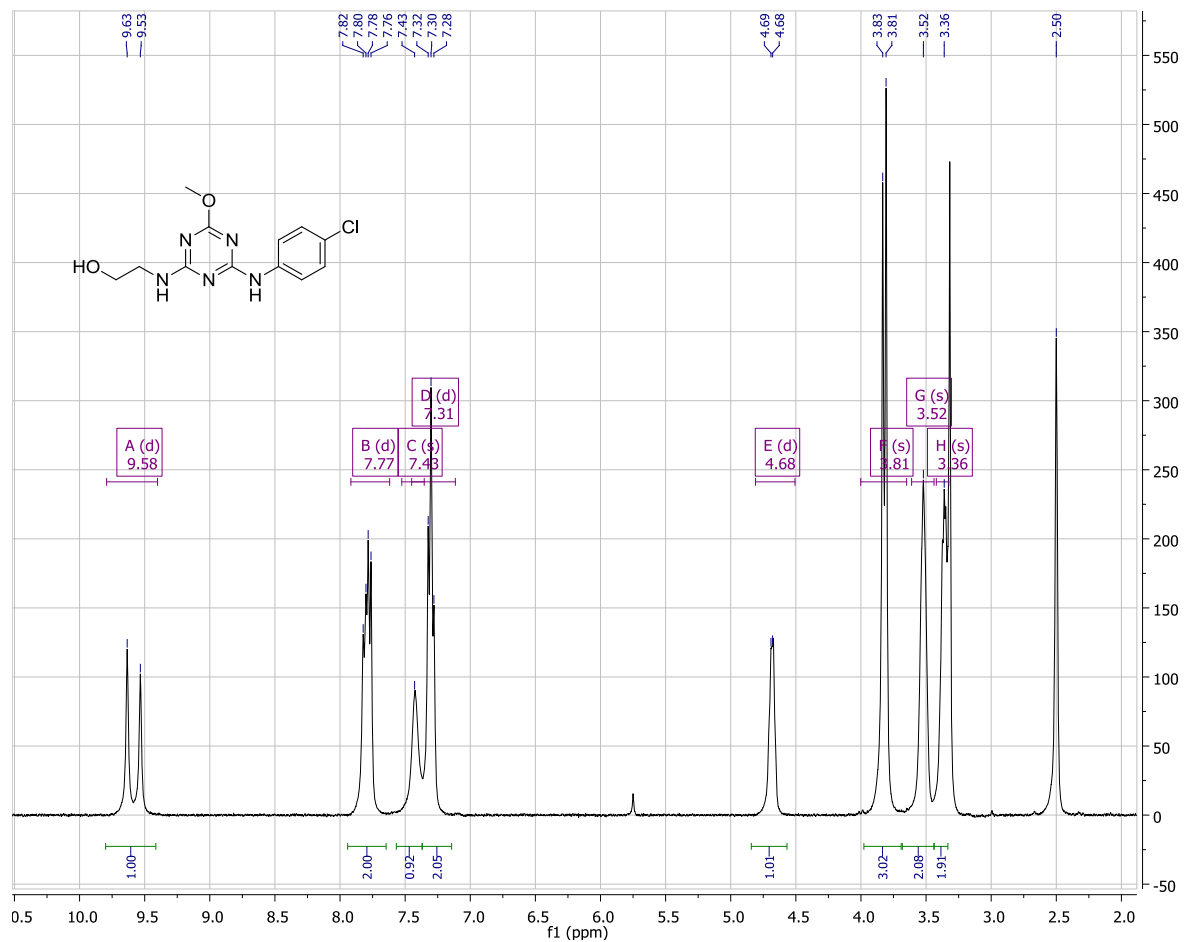
^{1}H NMR of **2.5**

^{13}C NMR of **2.5**
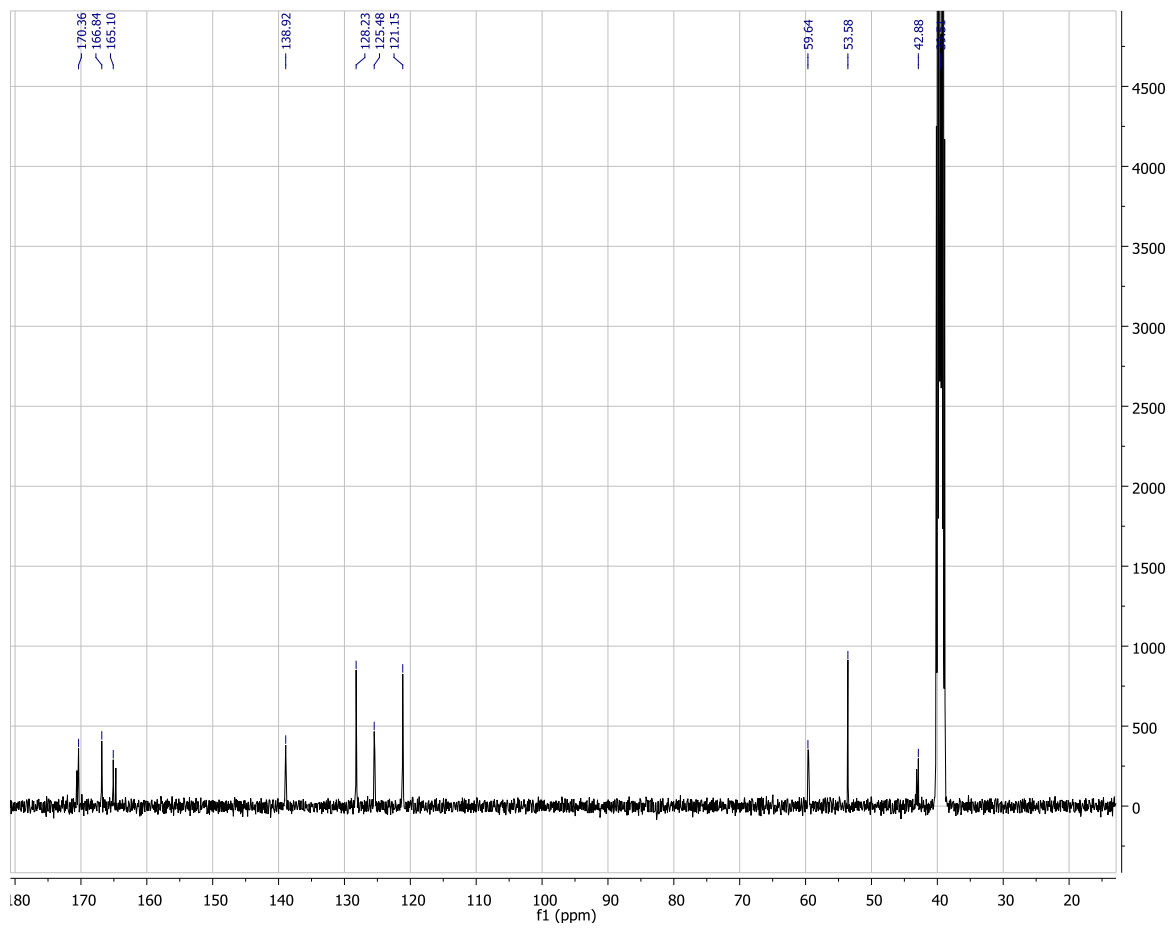
HSQC of **2.5**
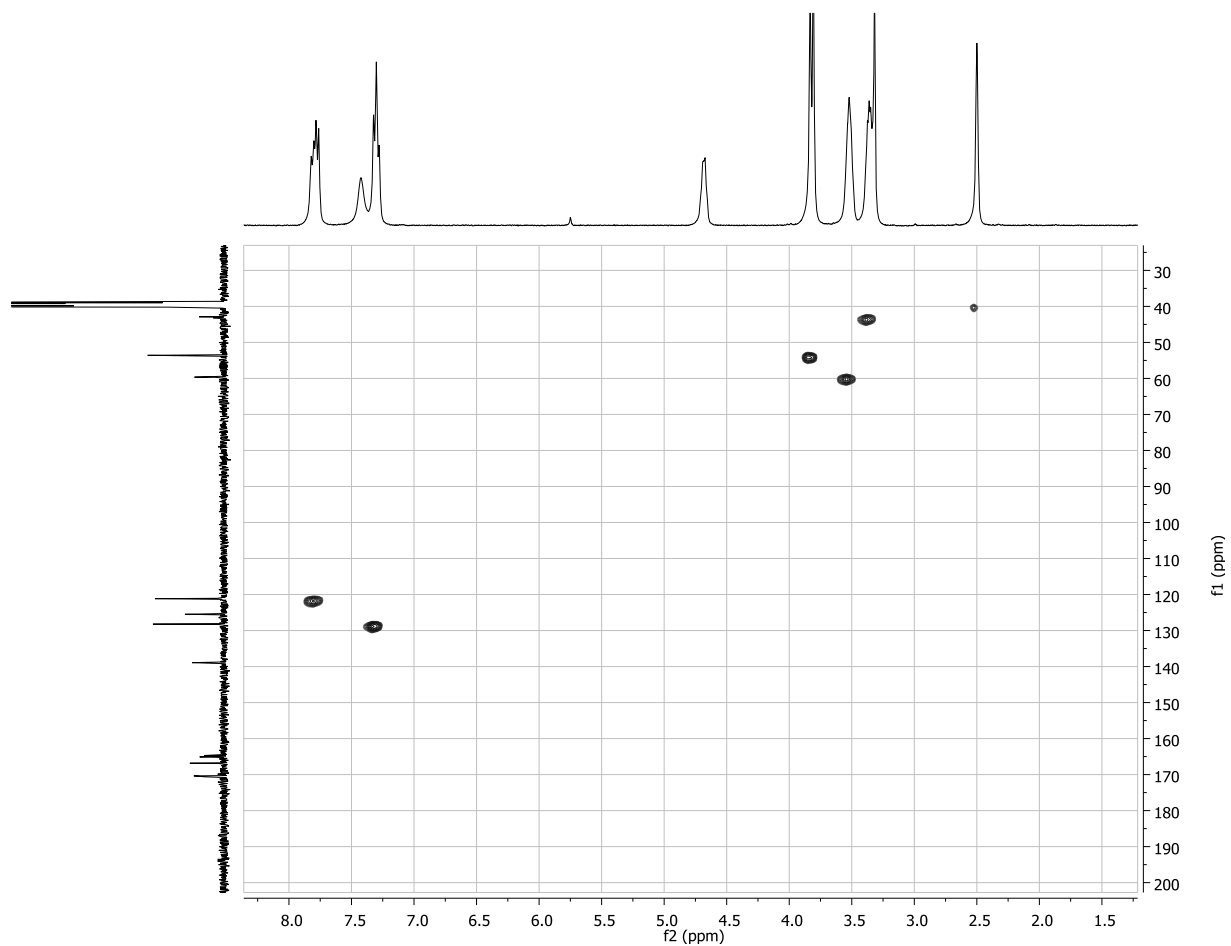
HRMS (ESI TOF) of **2.5**
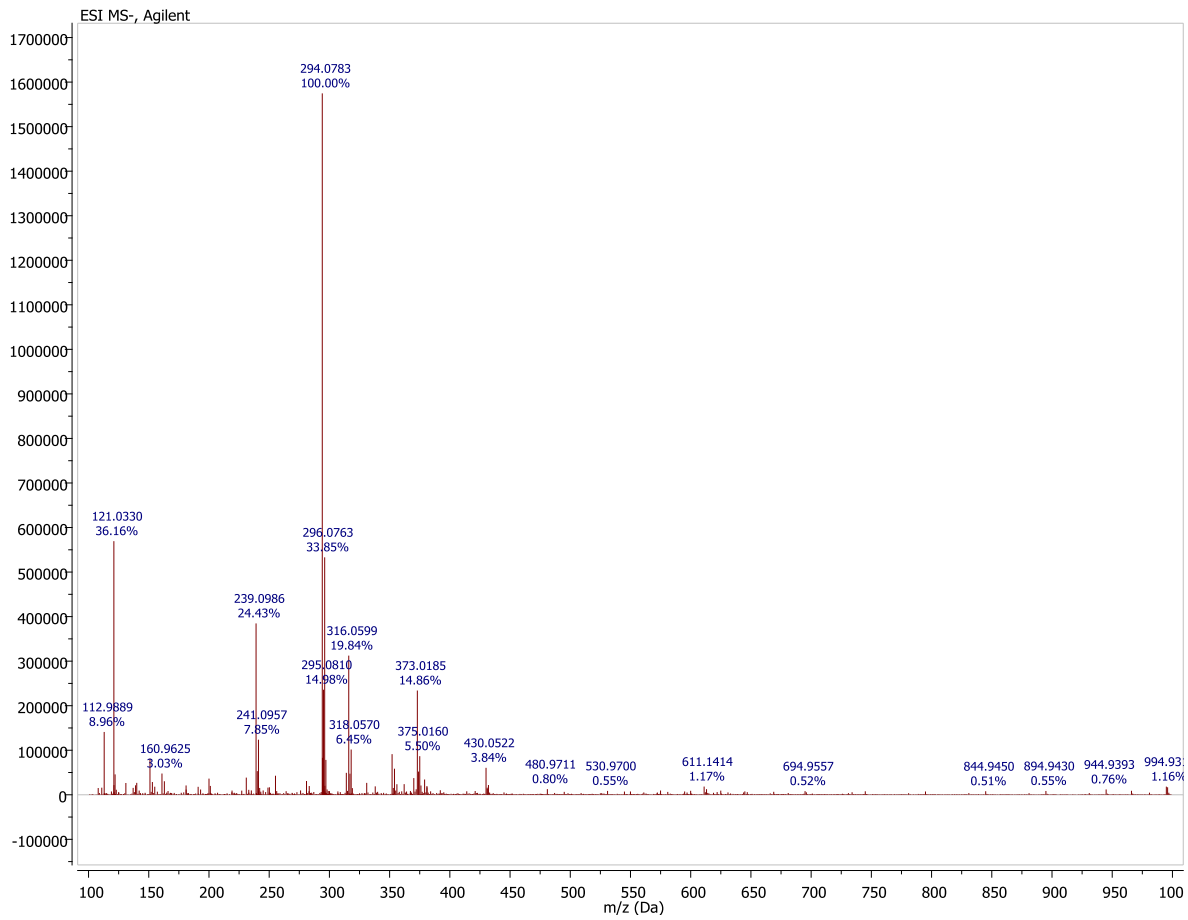
HPLC of **2.5**
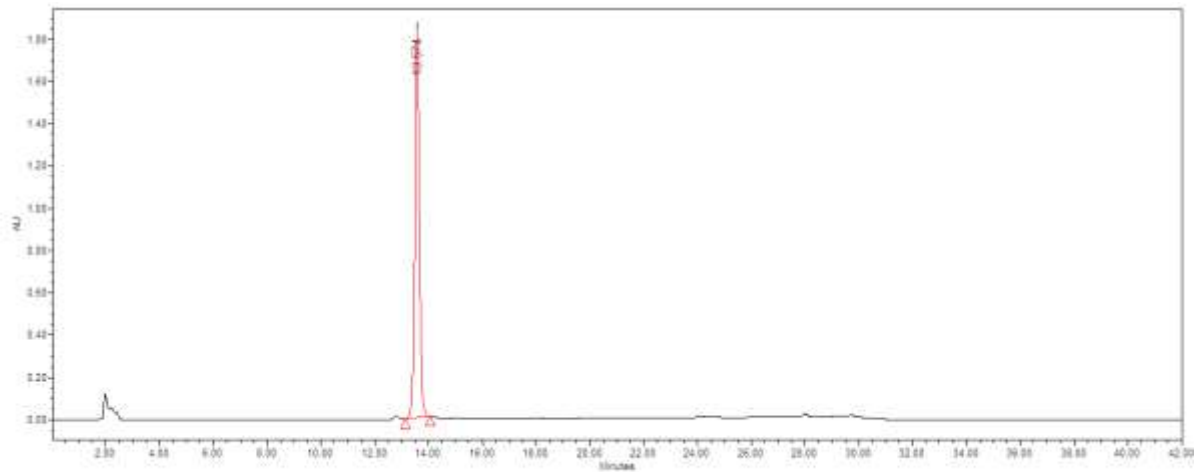
Retention time (min)	% Area
13.574	99.9
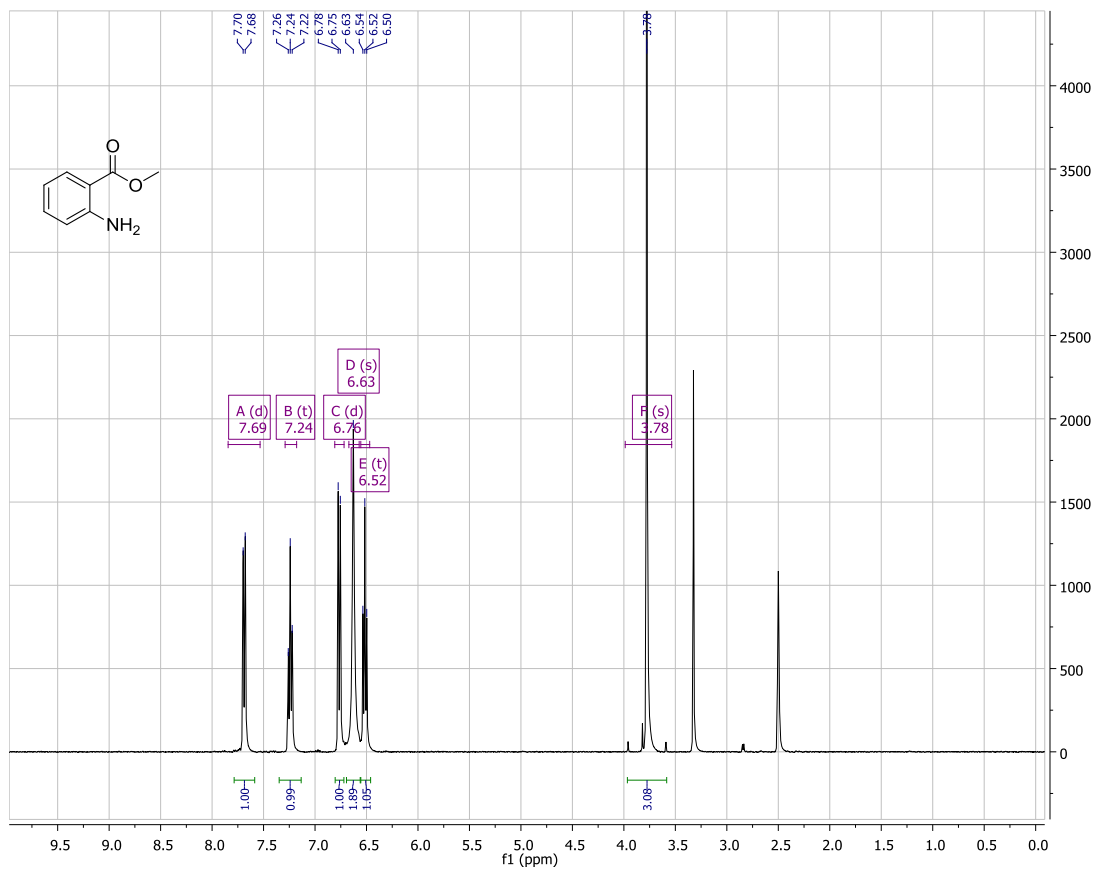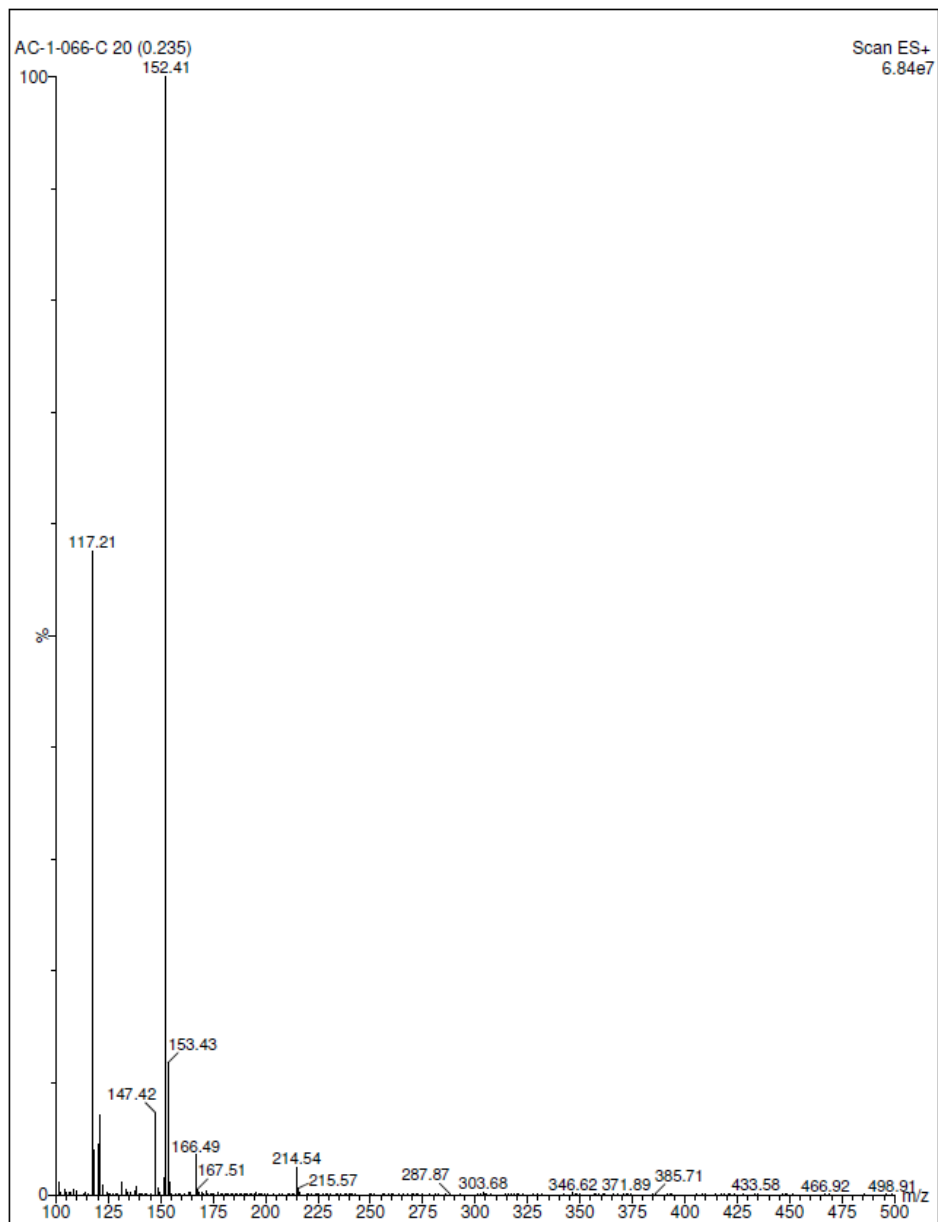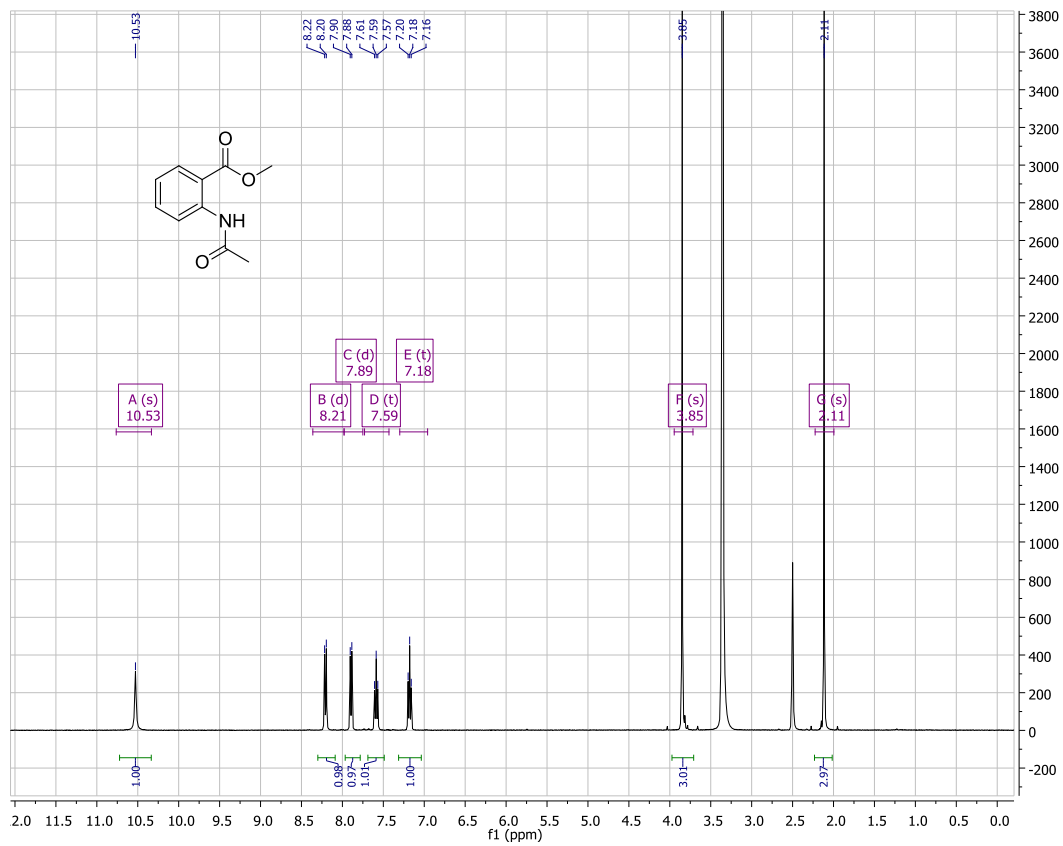
MS (ESI) of **3.9**
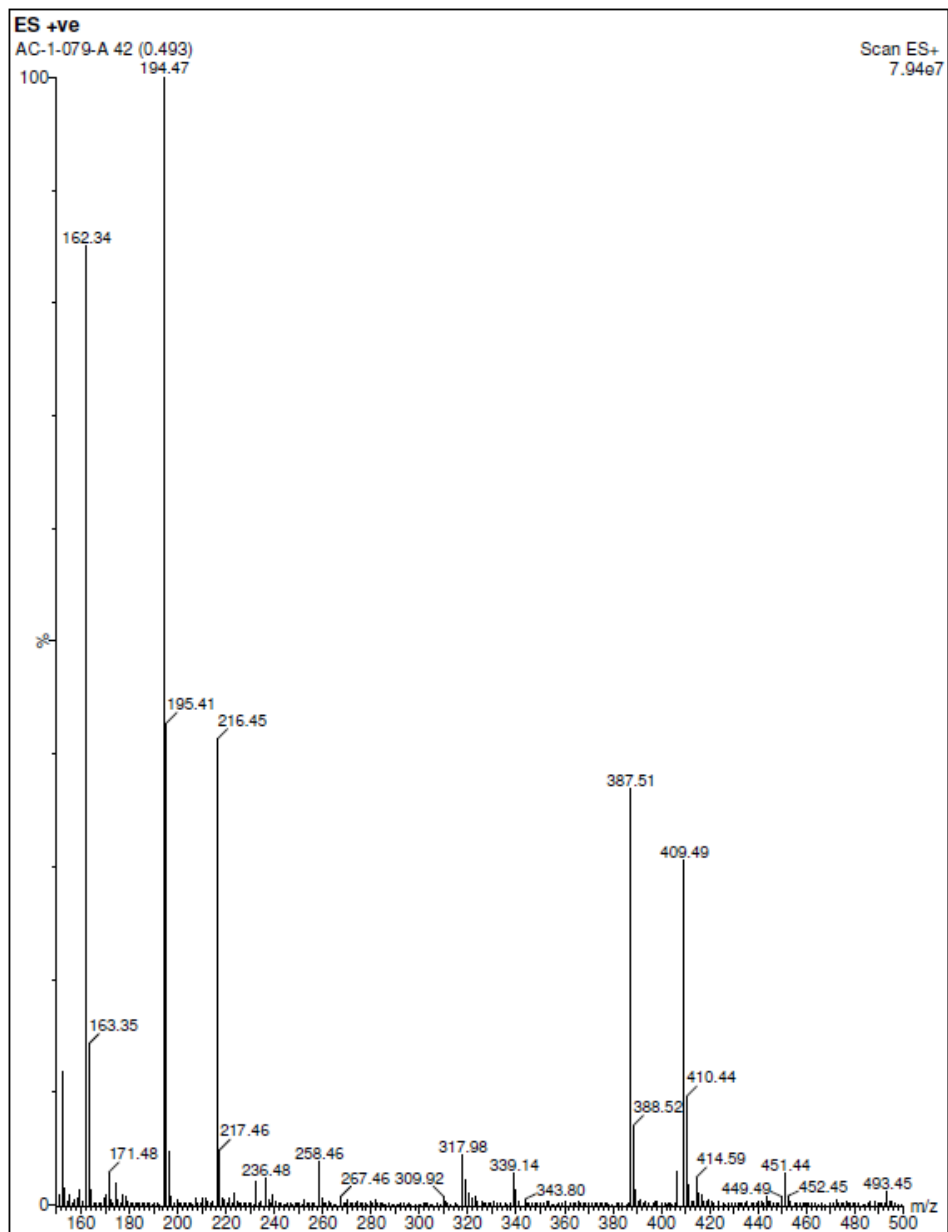
MS (ESI) of **3.10**

^{1}H NMR of **3.3**
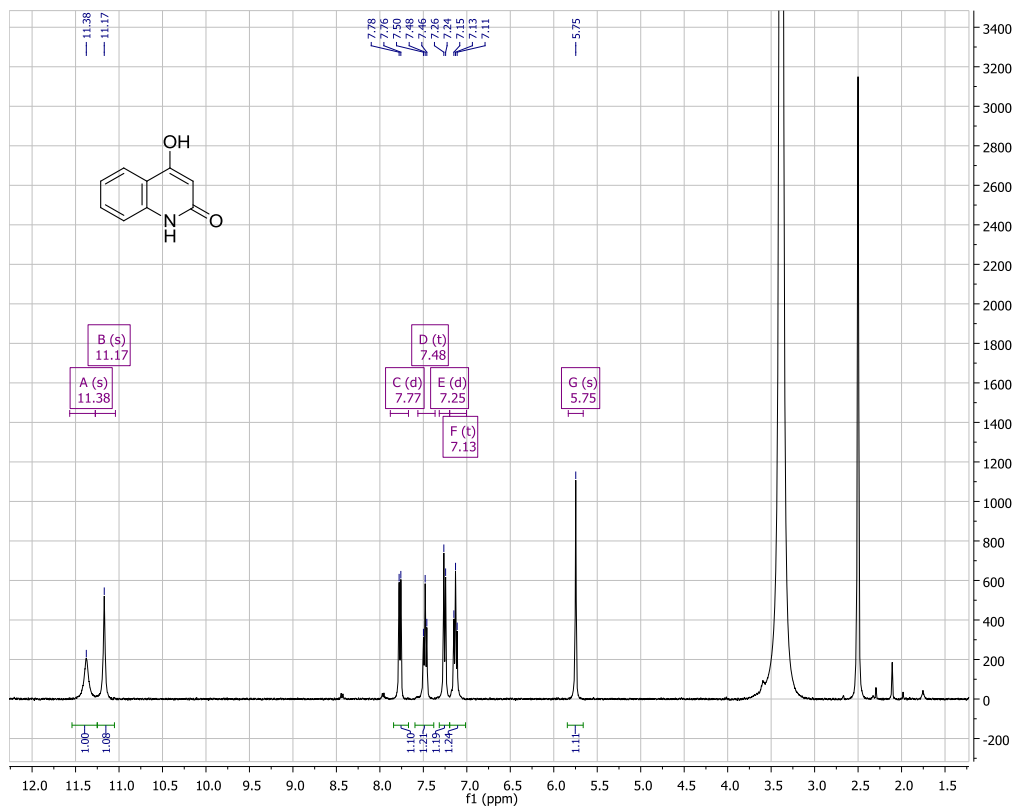
MS (ESI) of **3.3**
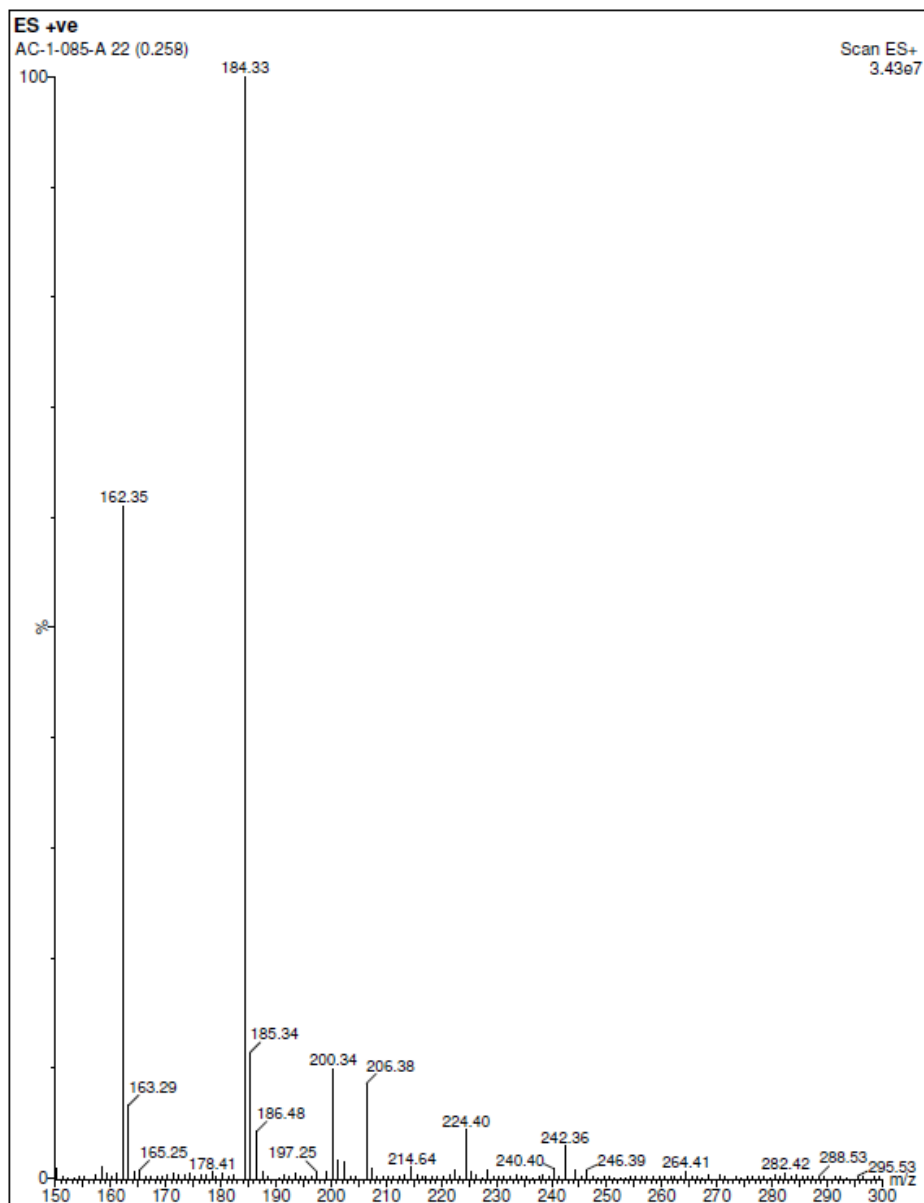
¹H NMR spectrum of **3.11**
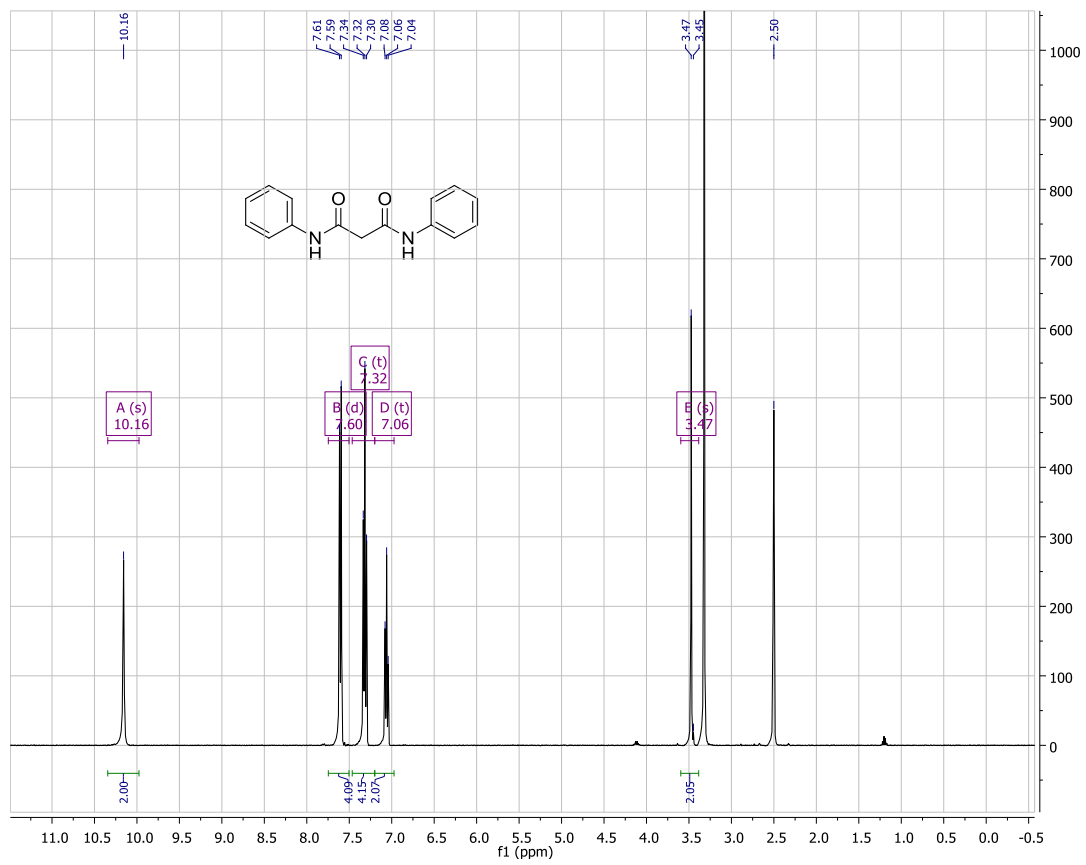
^{13}C NMR spectrum of **3.11**
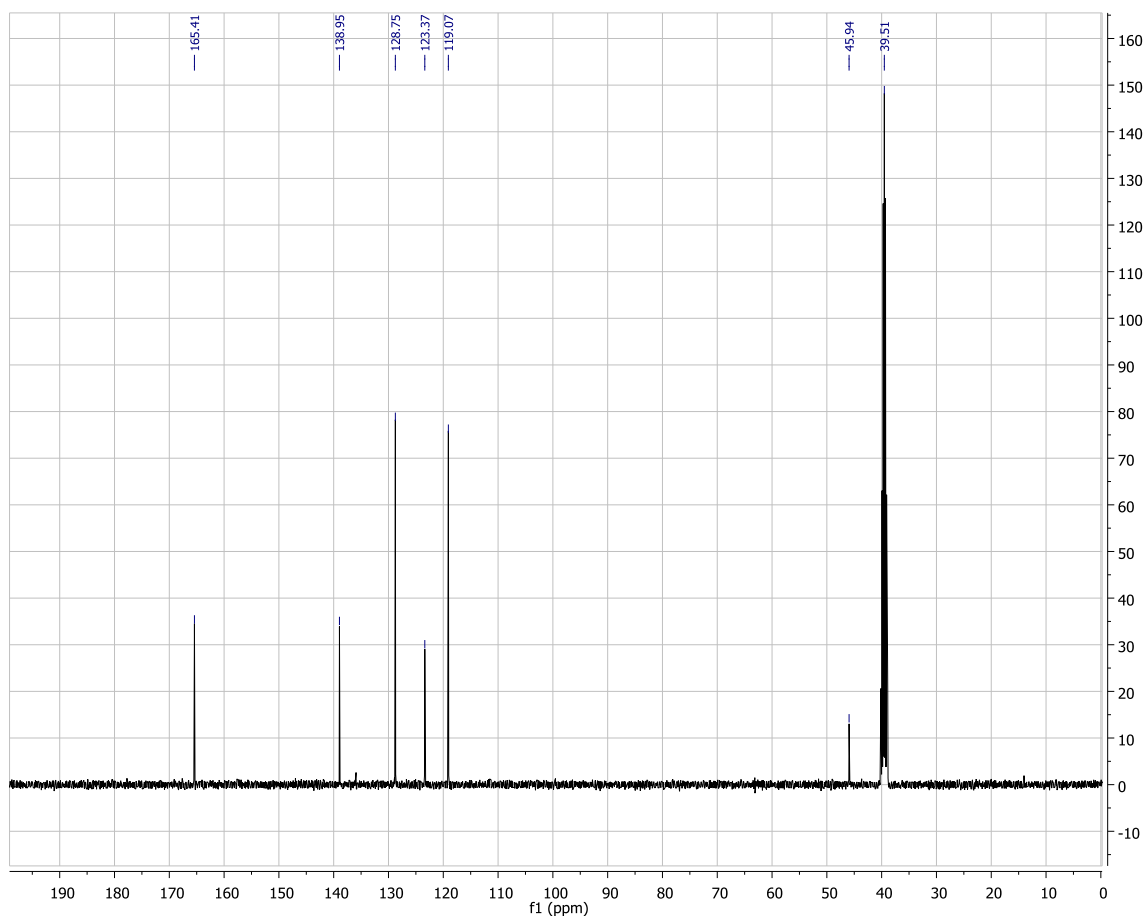
HRMS (TOF) of **3.11**

¹H NMR spectrum of **3.3**
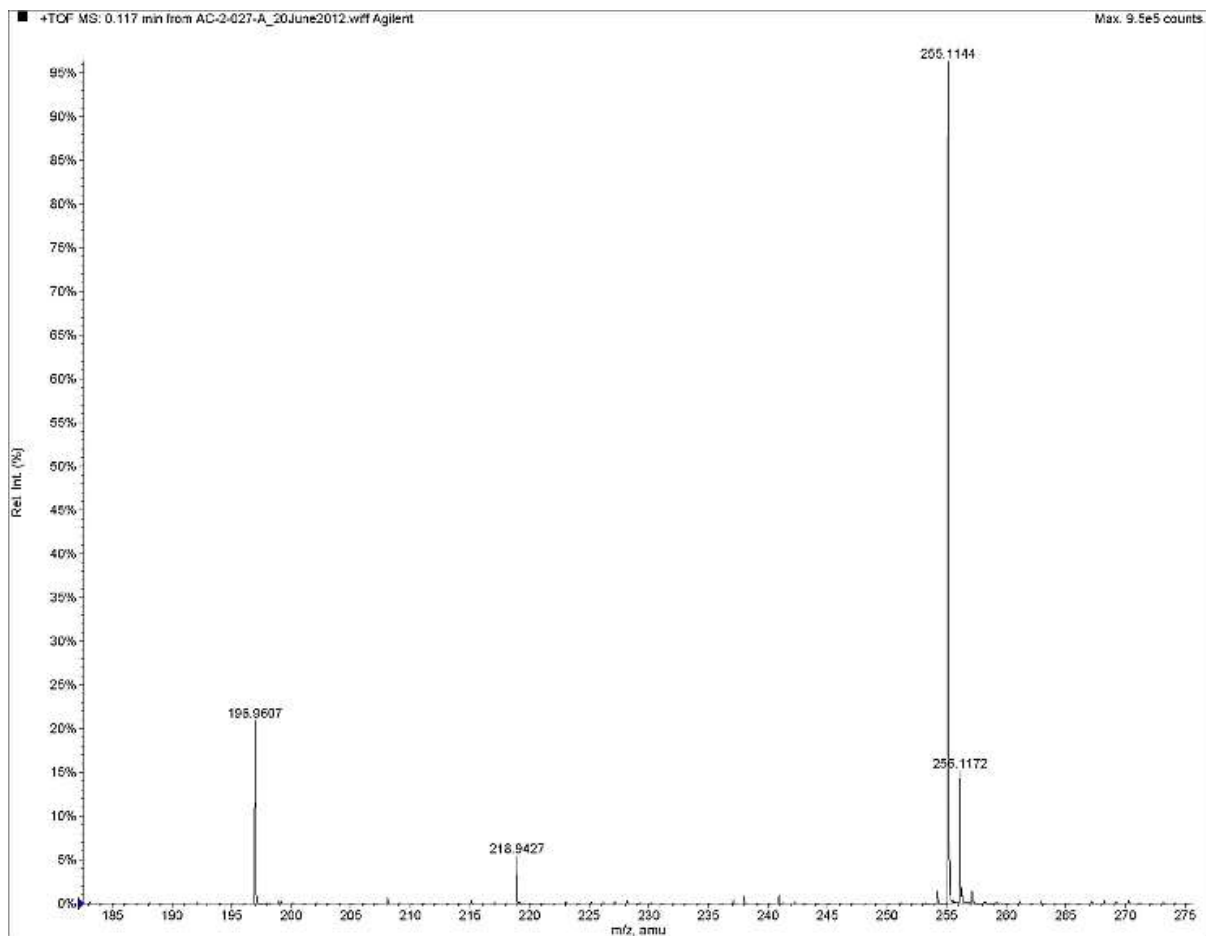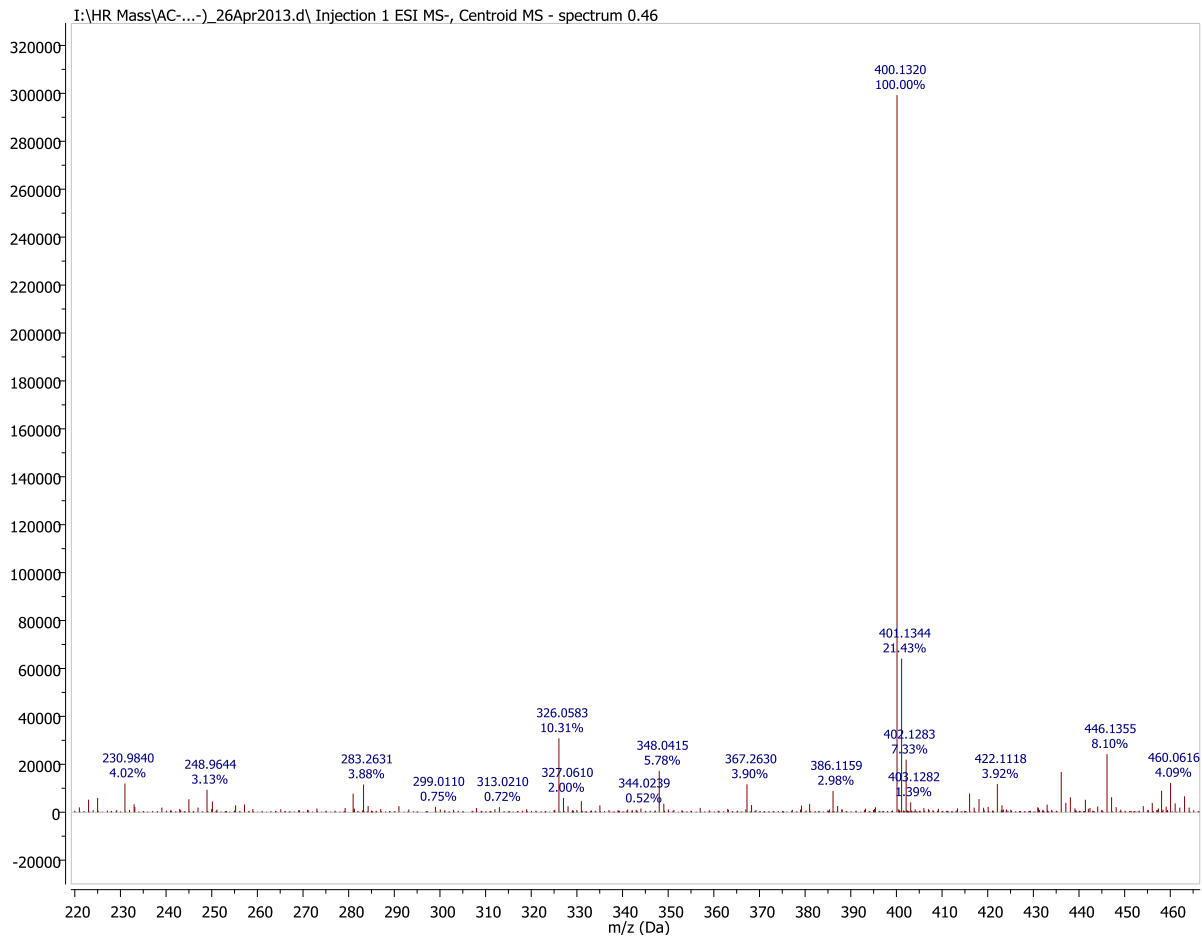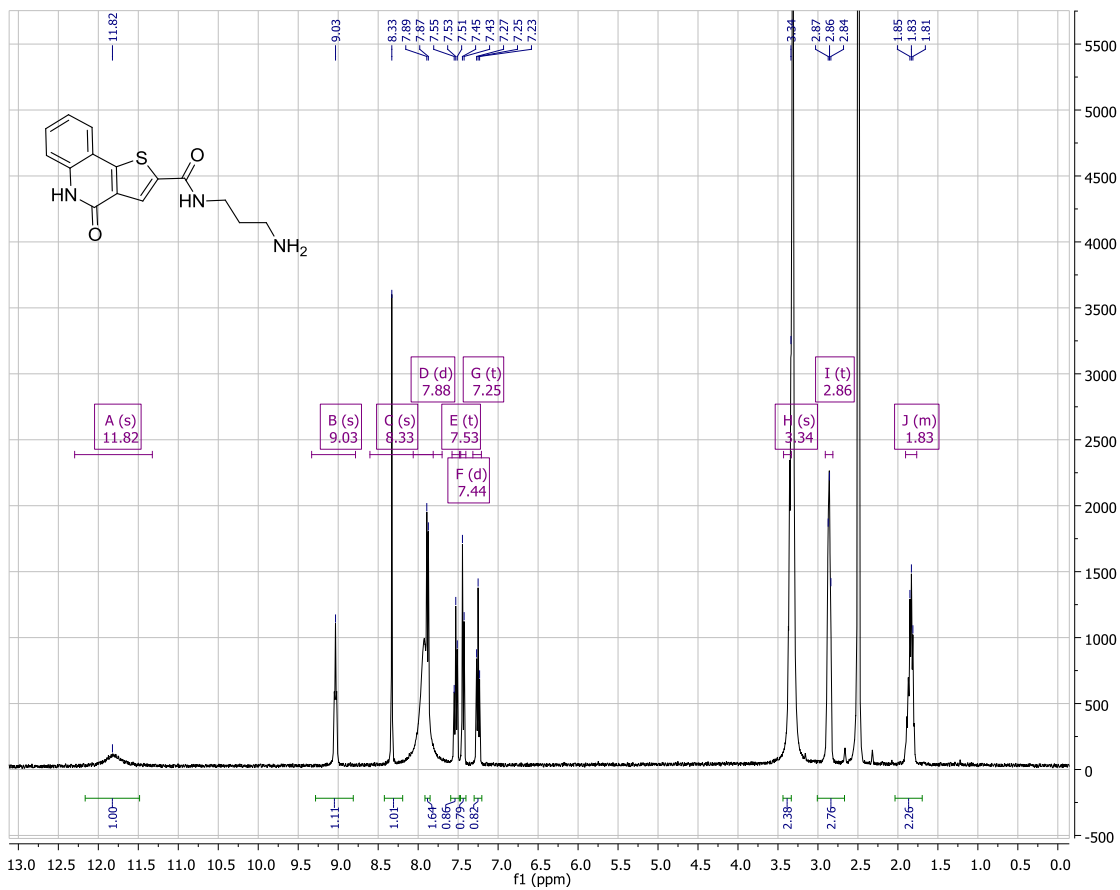
¹³C NMR spectrum of **3.3**
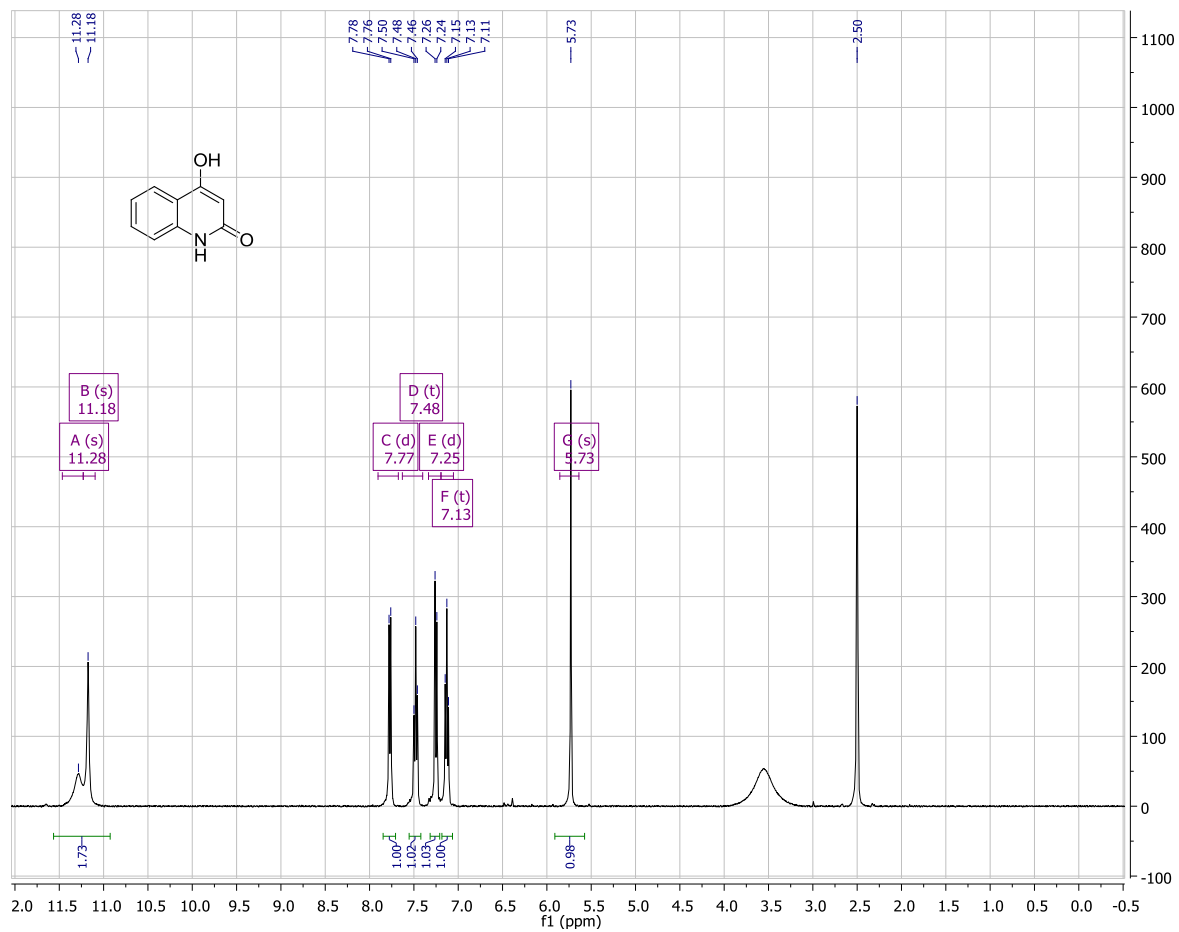
^{13}C NMR spectrum of **3.3**
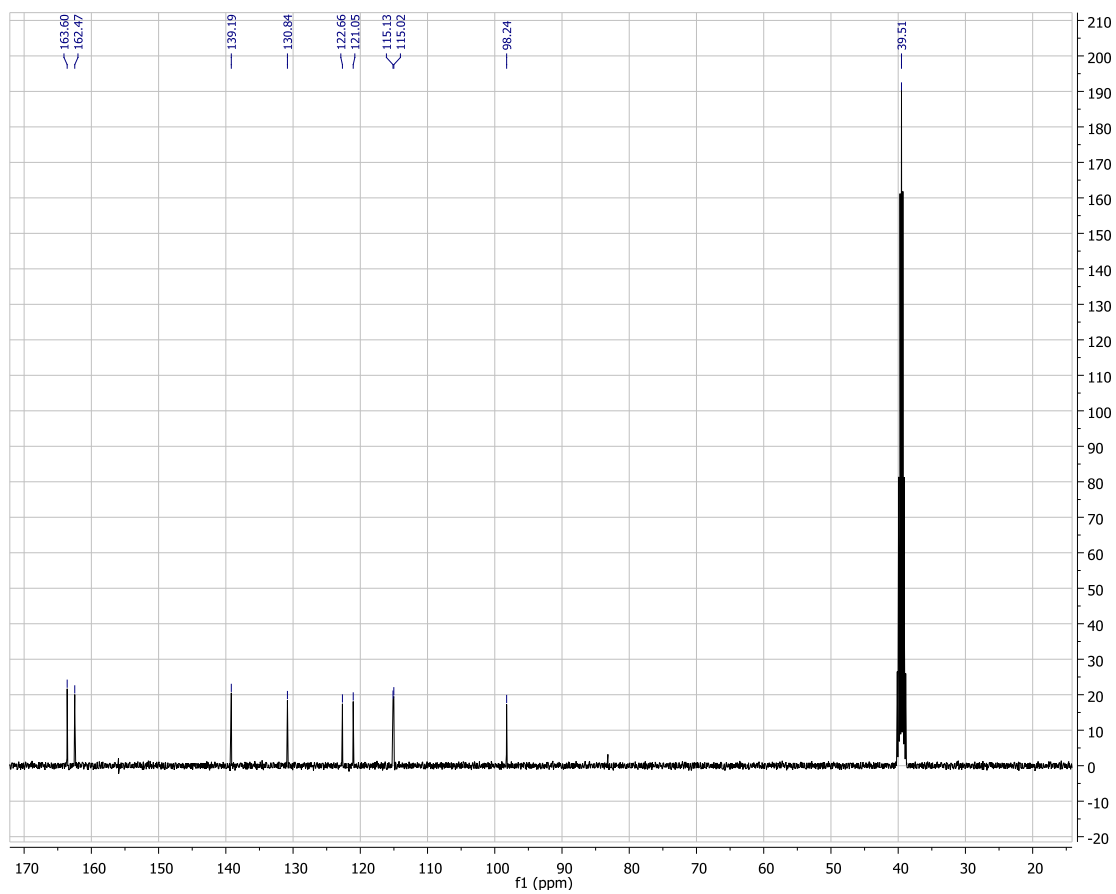
HRMS (TOF) of **3.3**
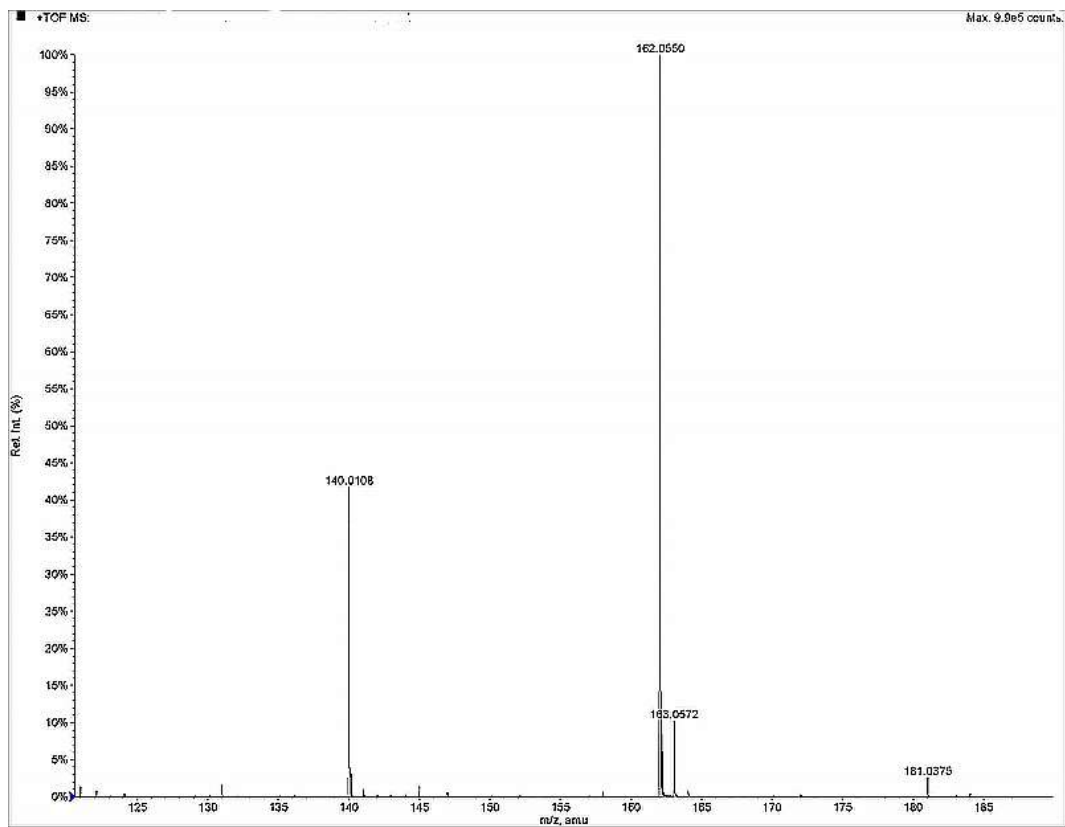
^{1}H NMR spectrum of **3.12**
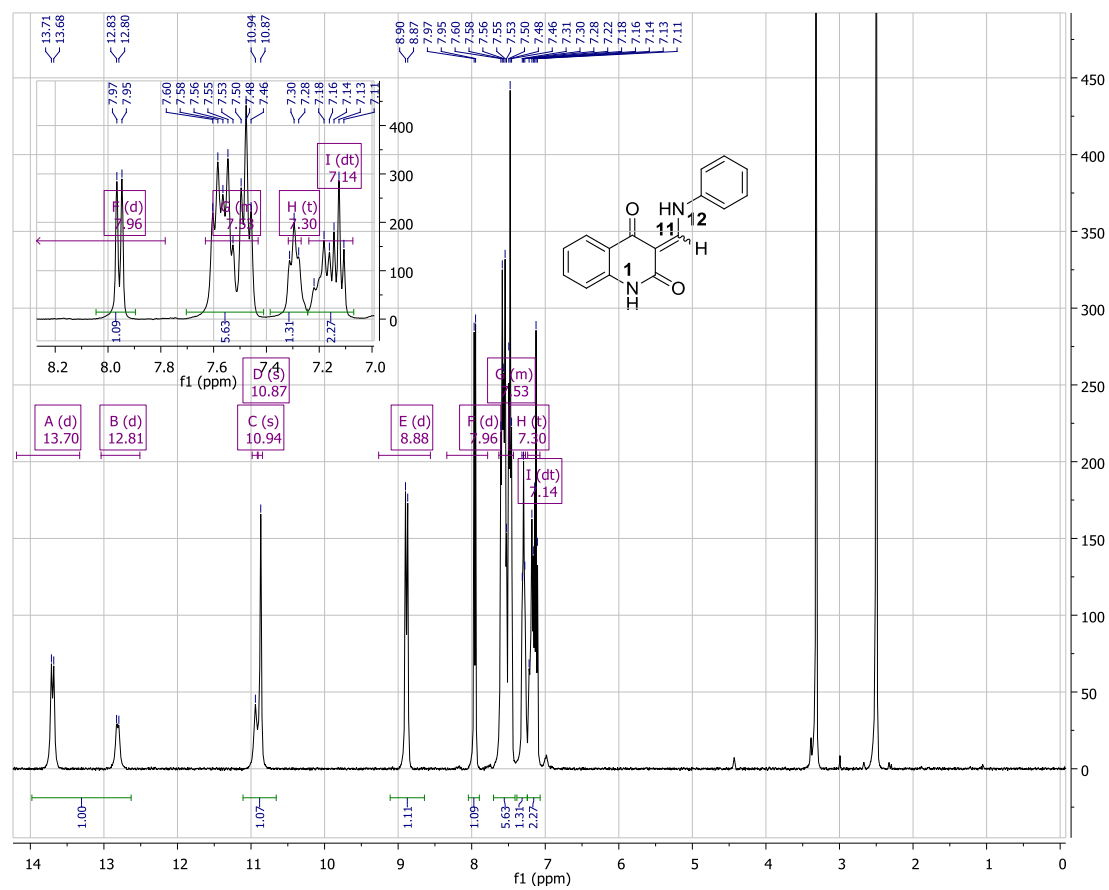
¹H NMR (D₂O wash) spectrum of **3.12**
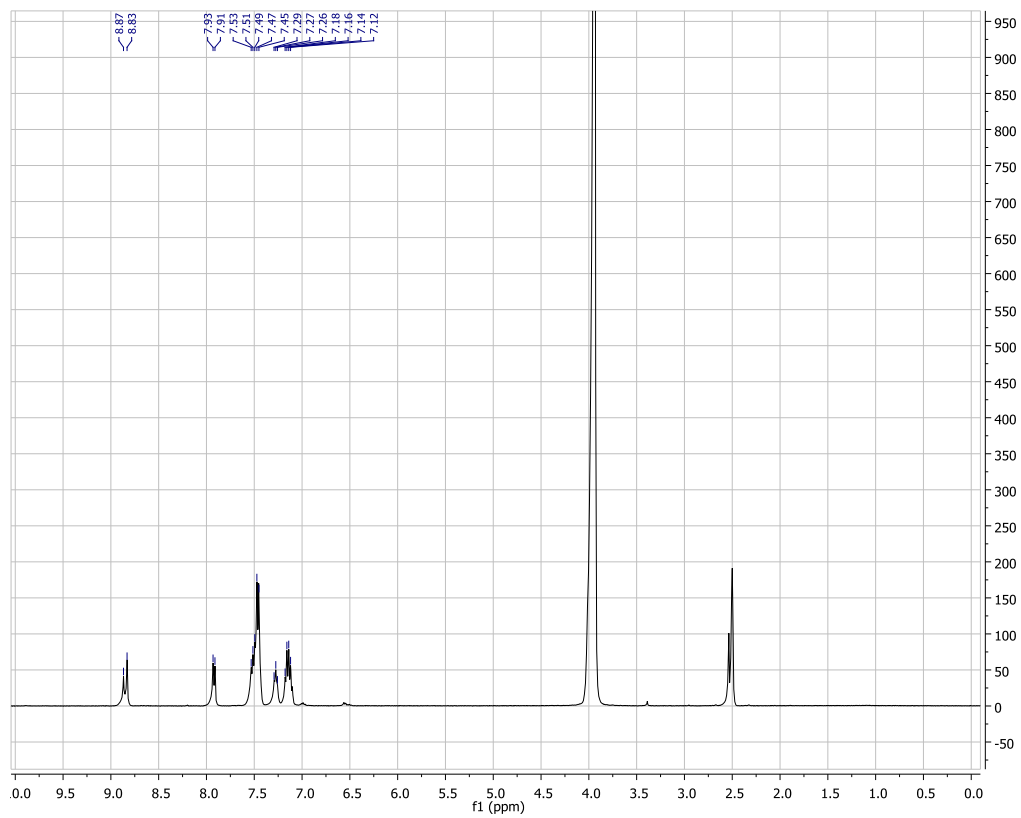
COSY spectrum of **3.12**
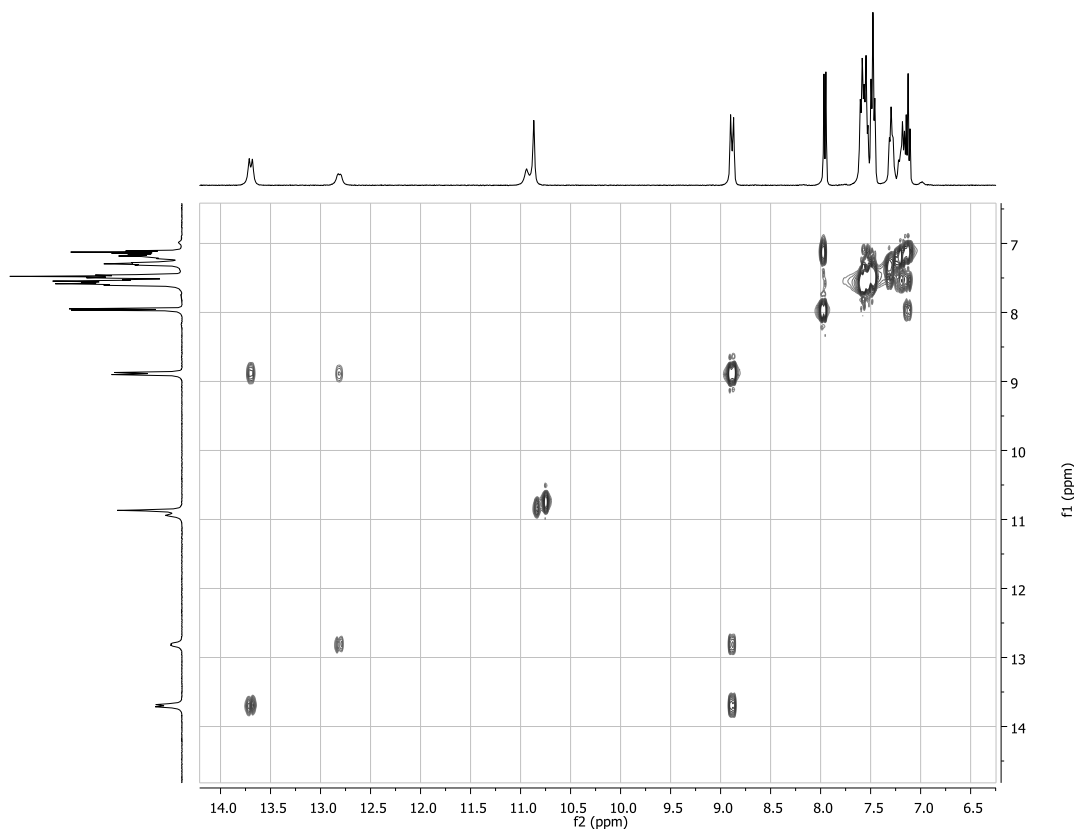
^{13}C spectrum of **3.12**
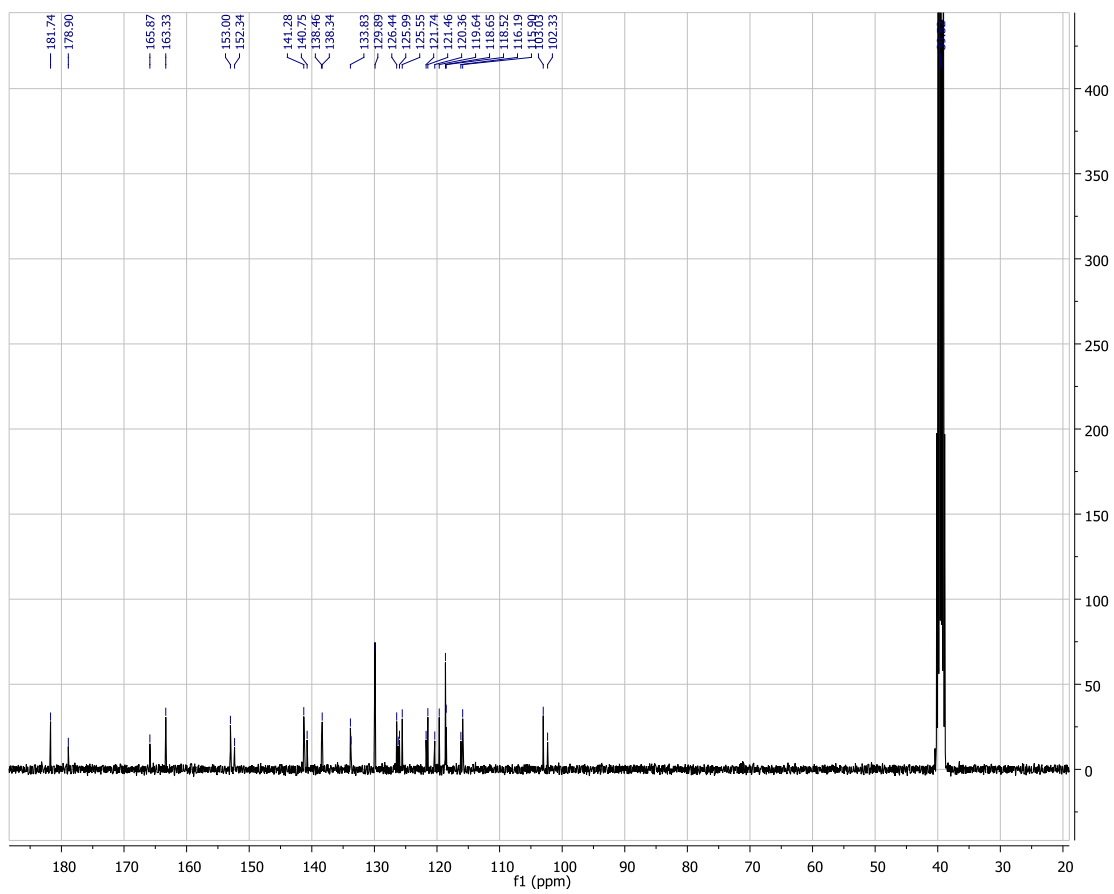
HRMS (TOF) of **3.12**
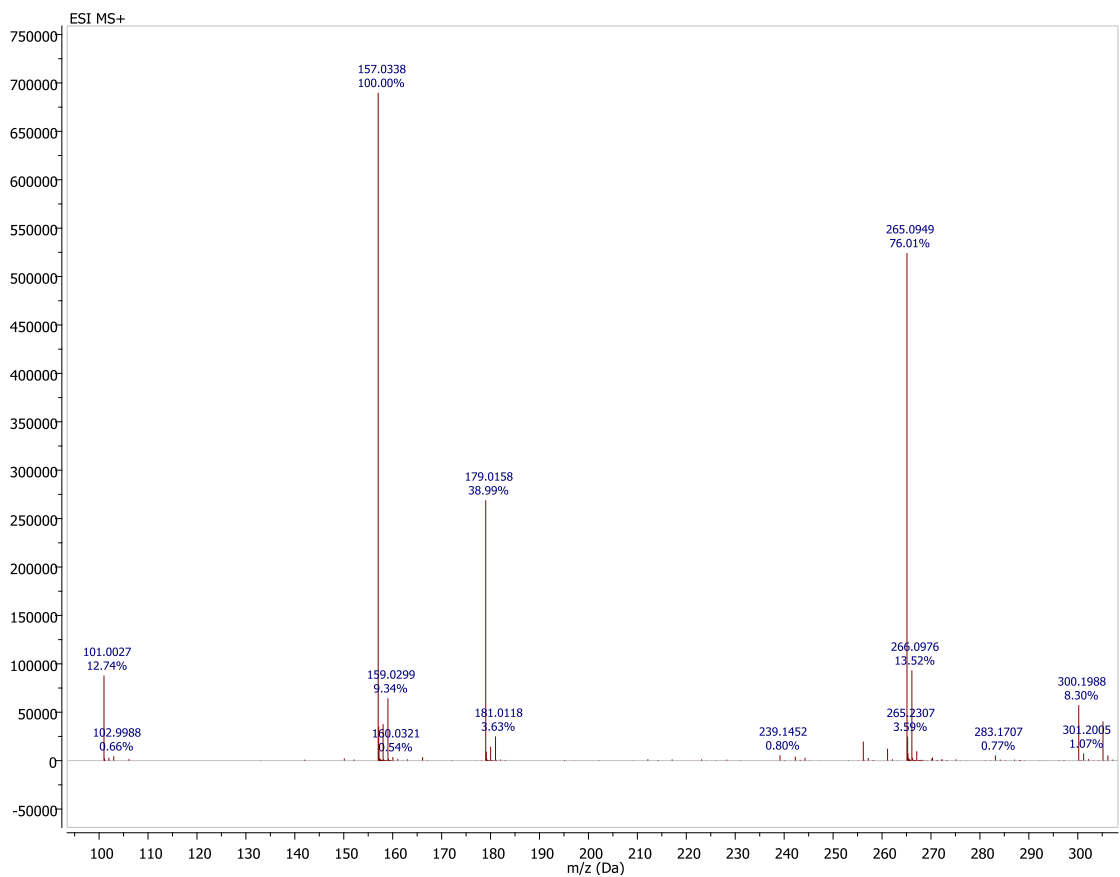
¹H NMR spectrum of **3.2**

¹³C NMR spectrum of **3.2**

189.33
160.37
146.27
139.54
134.12
126.66
123.33
122.71
117.43
115.92
39.51
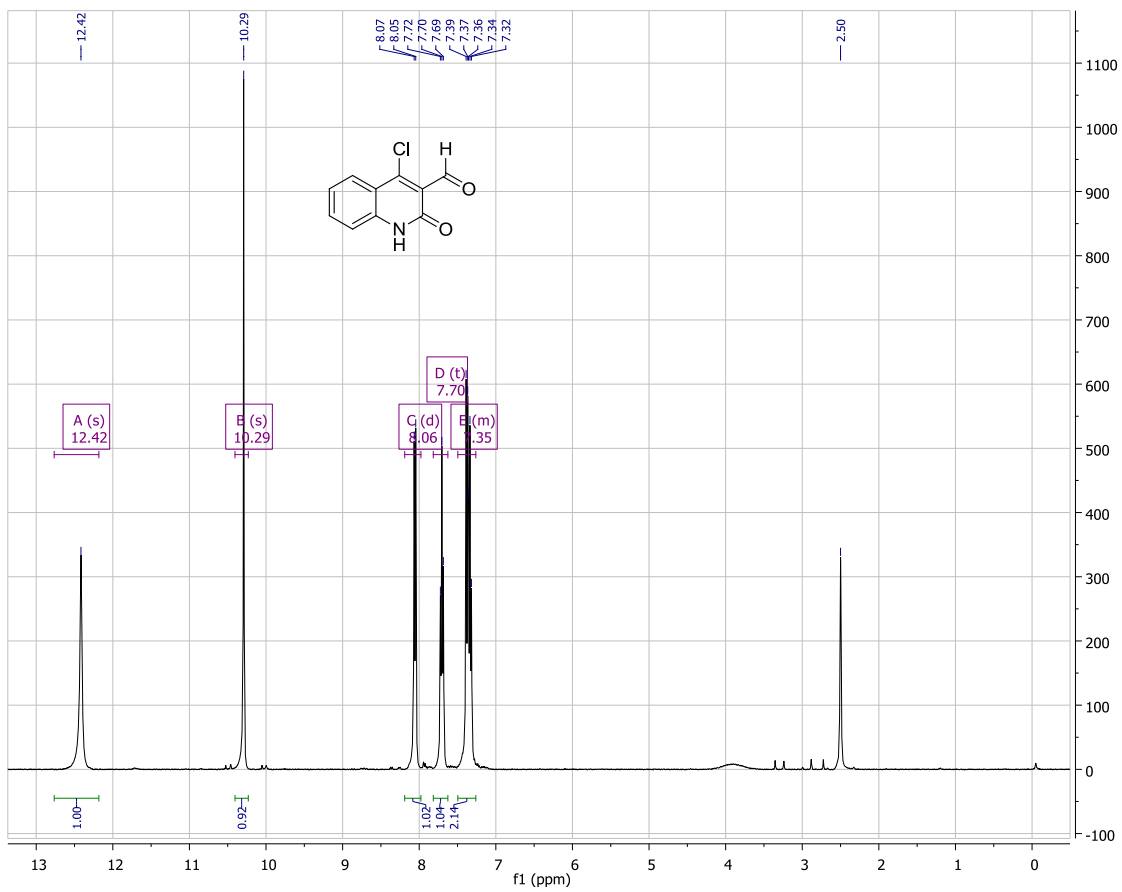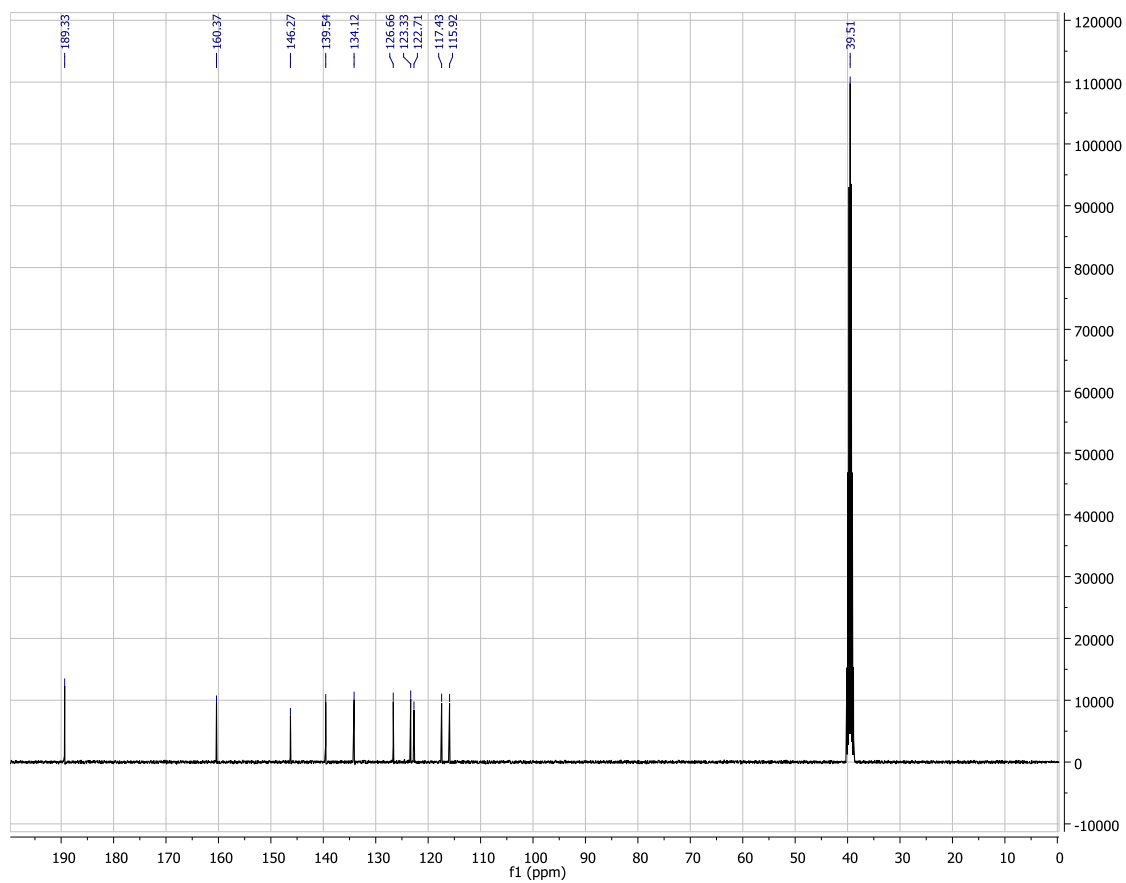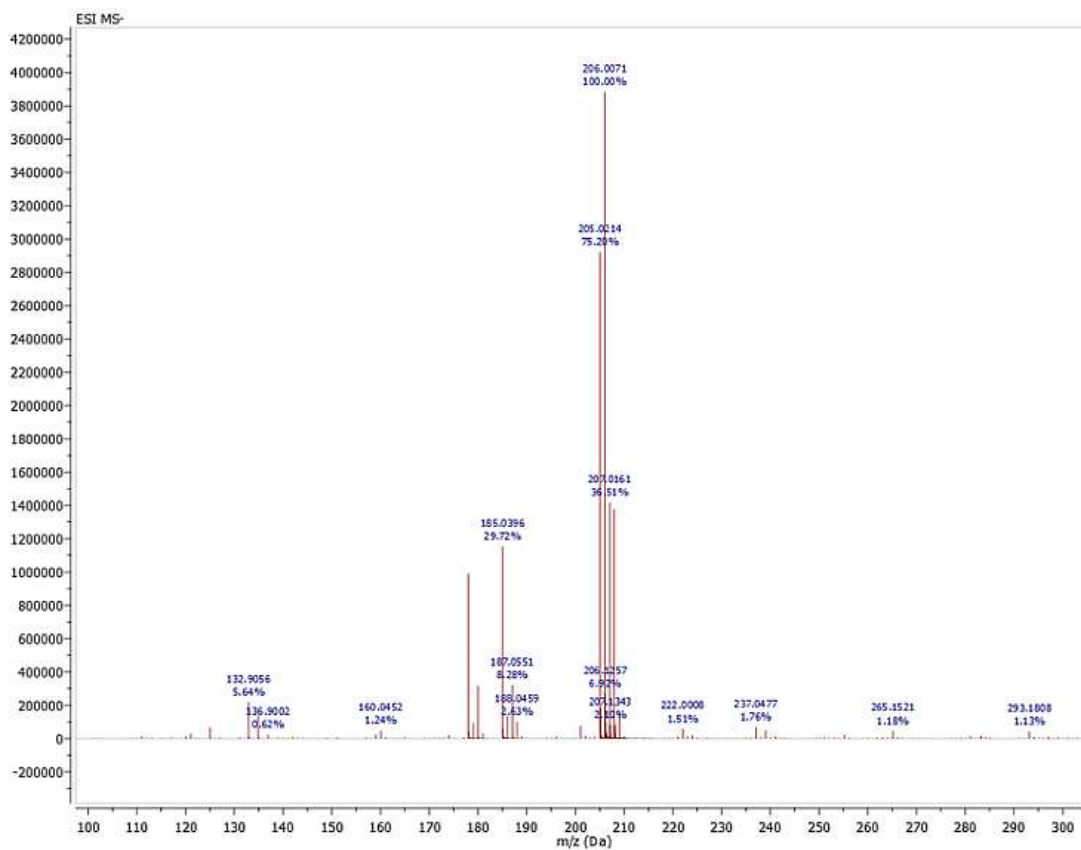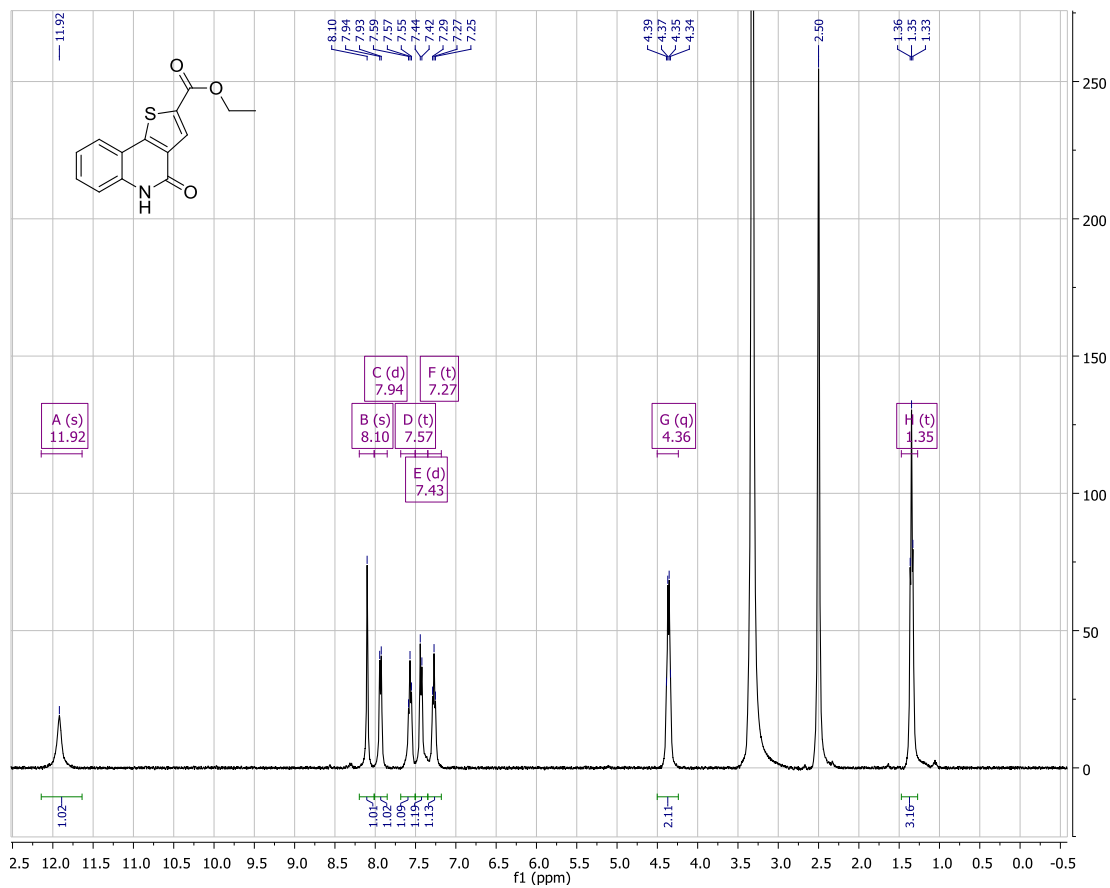
HRMS (TOF) of **3.2**

¹³C NMR spectrum of **3.14**
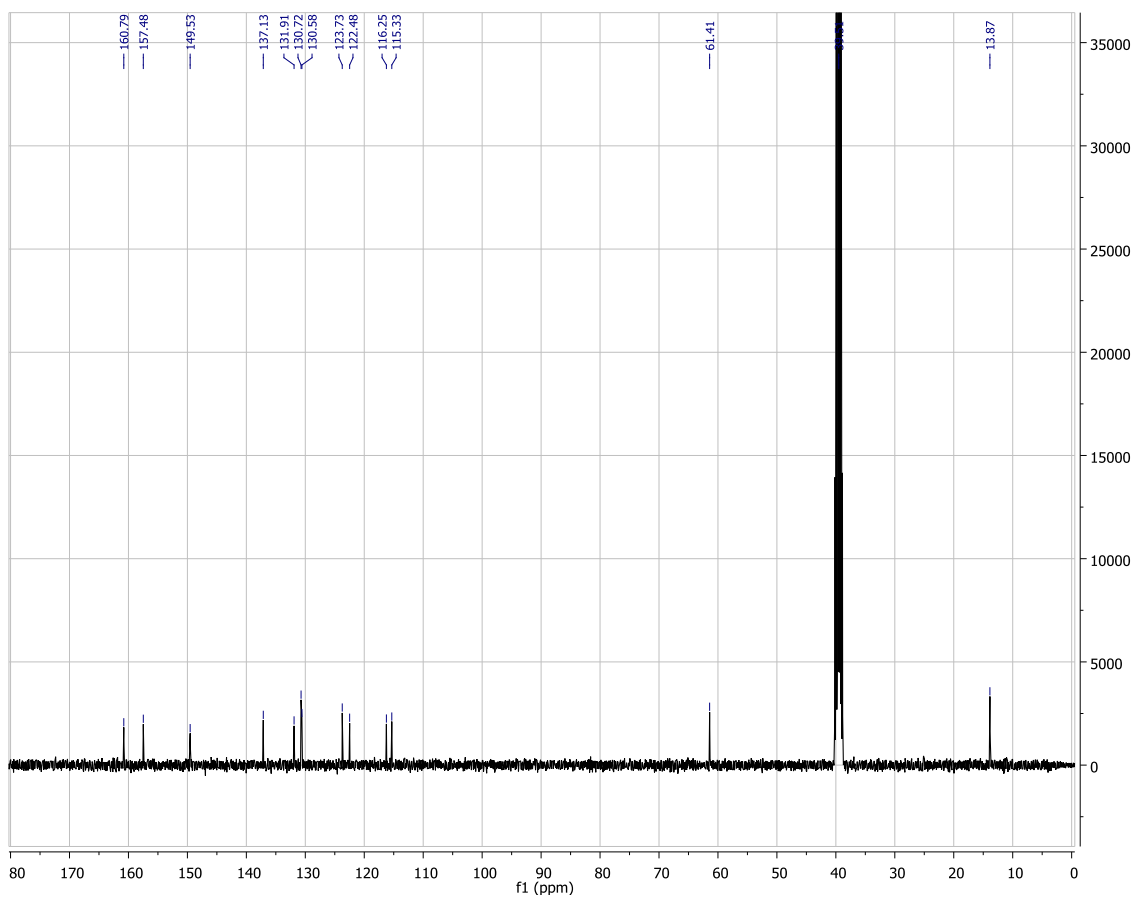
HRMS (TOF) of **3.14**
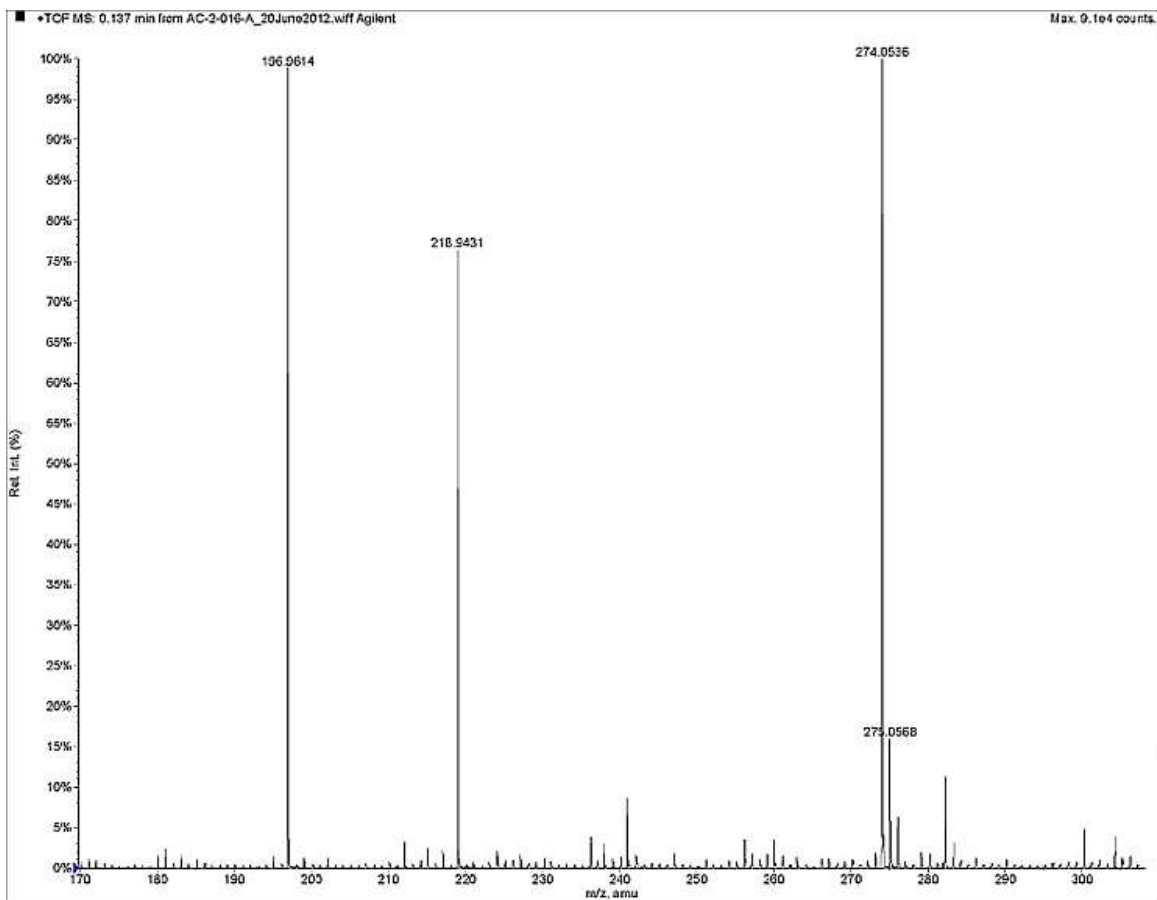
HPLC scan of **3.14**
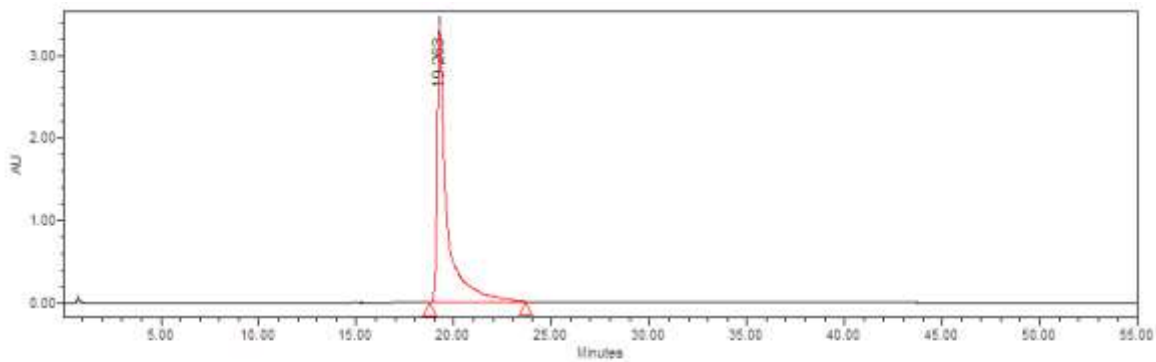
Retention time (min)	% Area
19.263	100
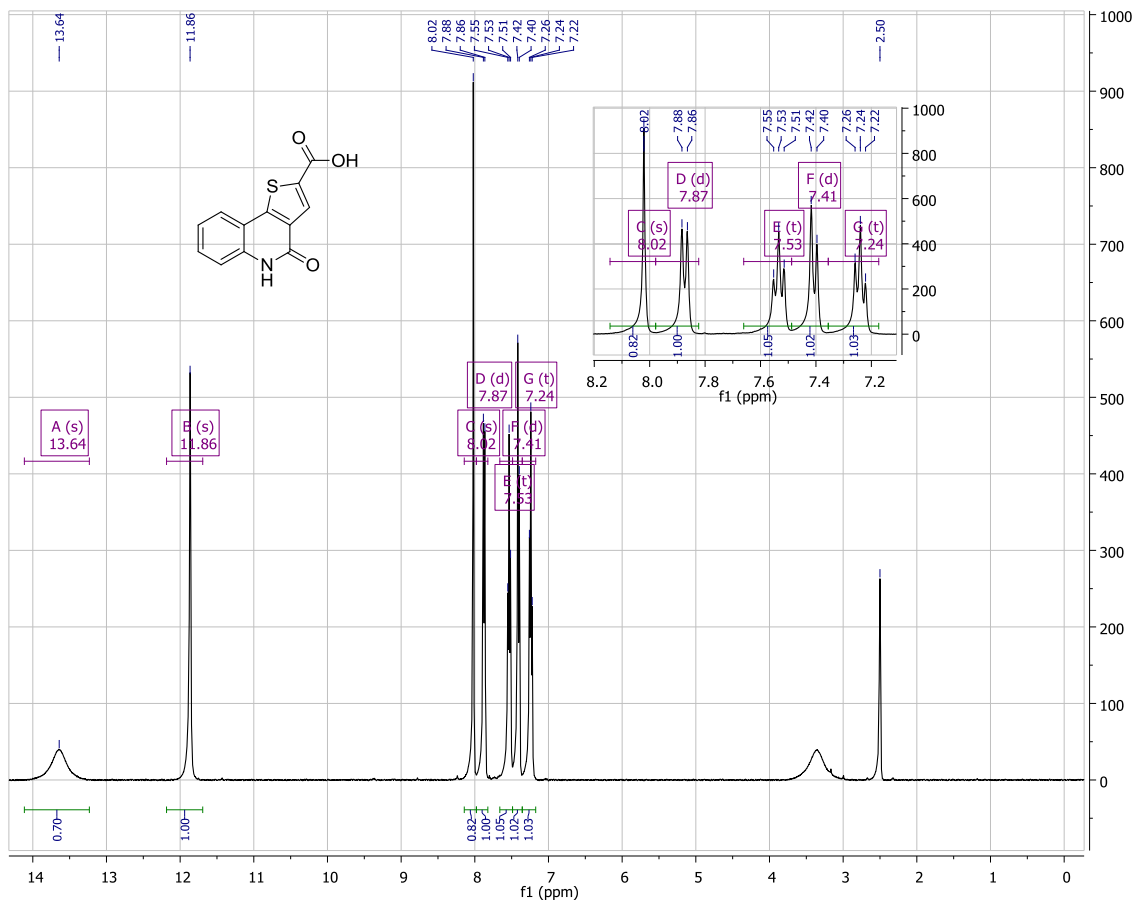
¹H NMR (D₂O wash) spectrum of **2.14**
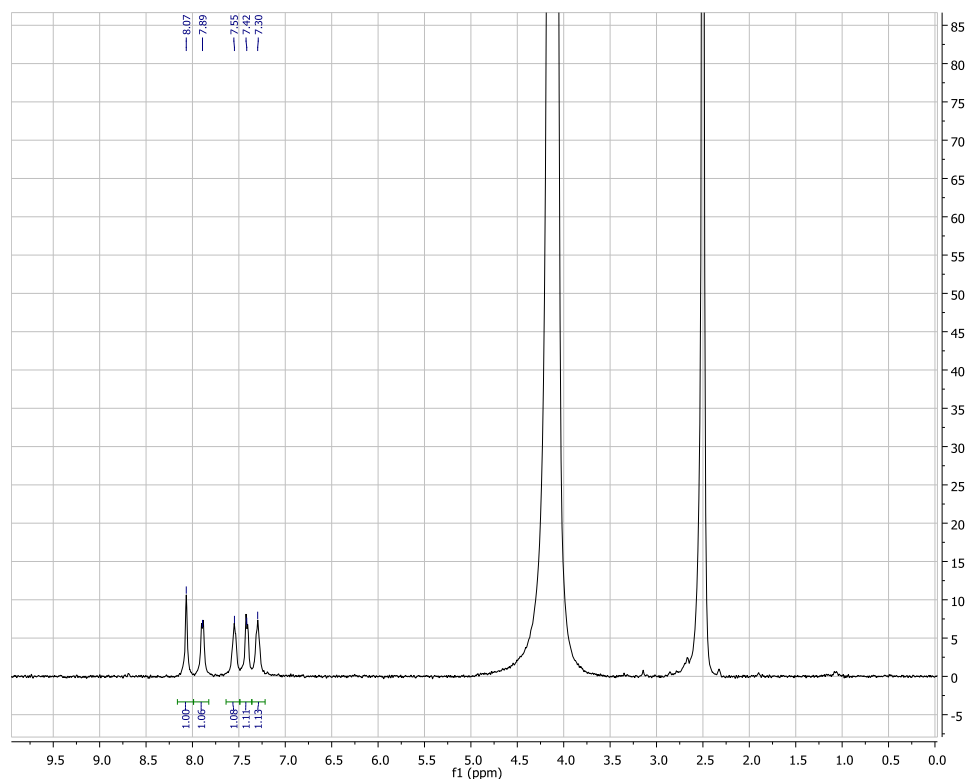
¹³C NMR spectrum of **2.14**
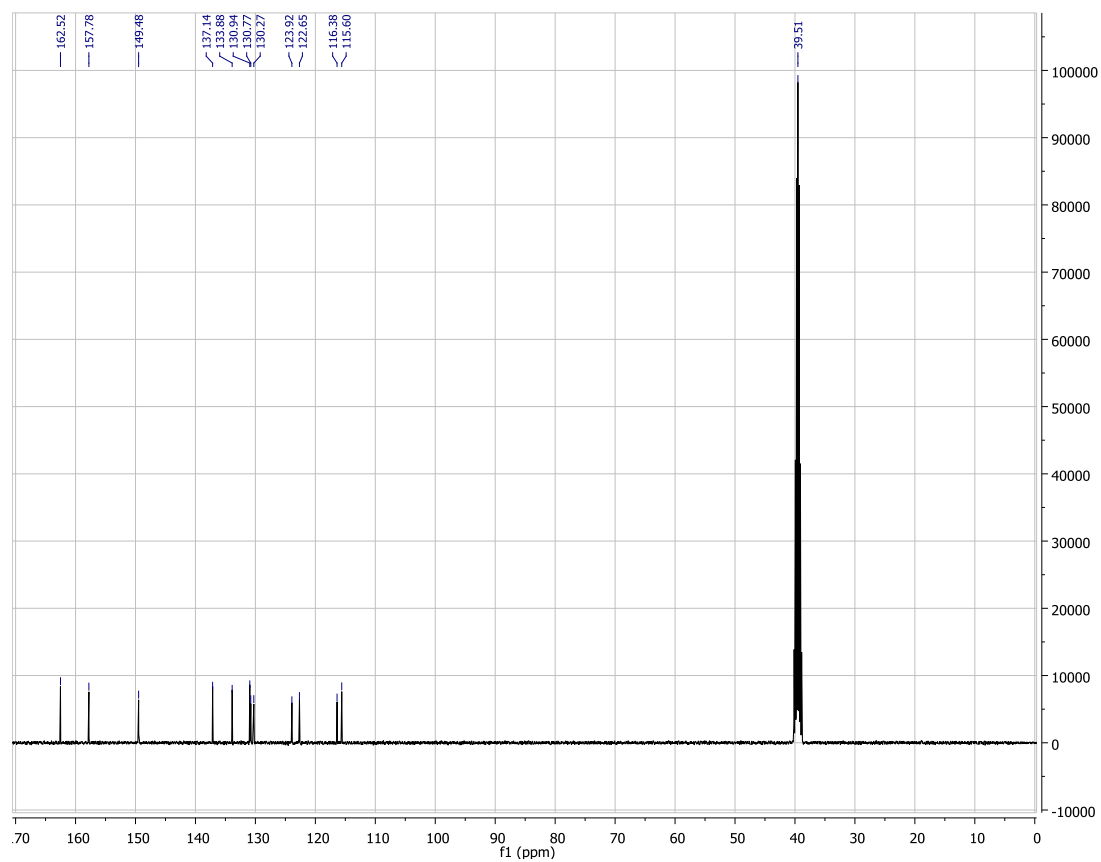
HSQC spectrum of **2.14**
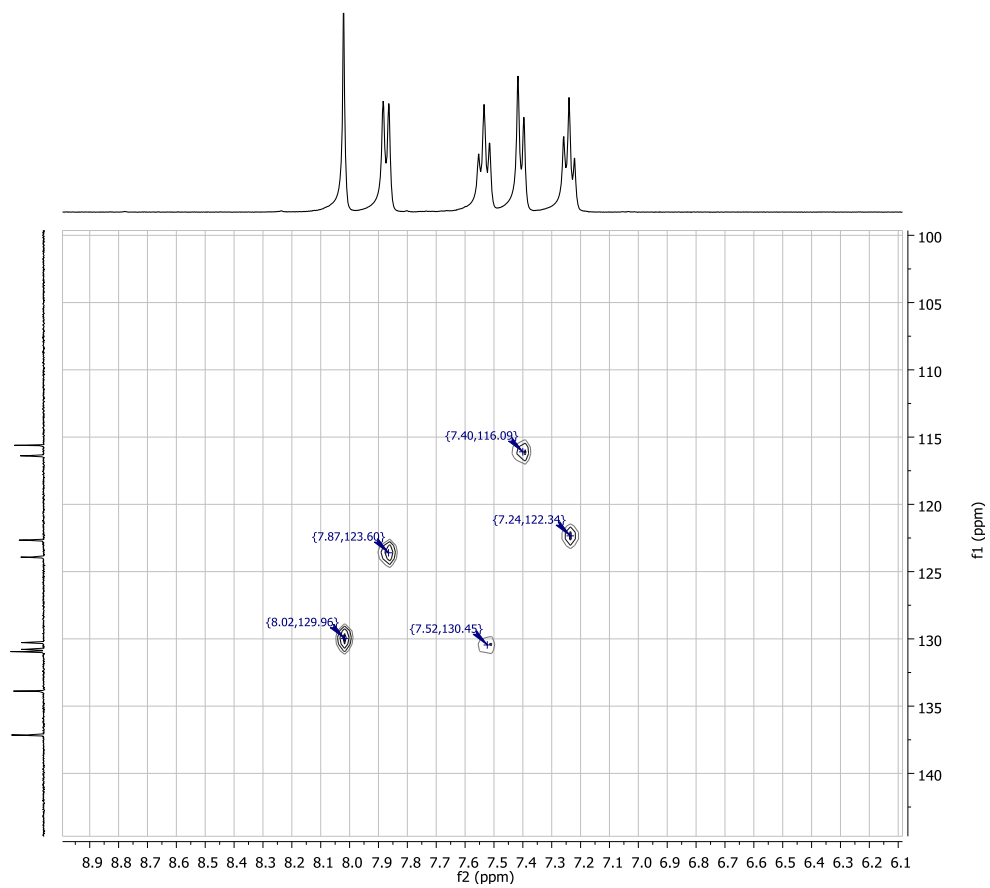
COSY spectrum of **2.14**
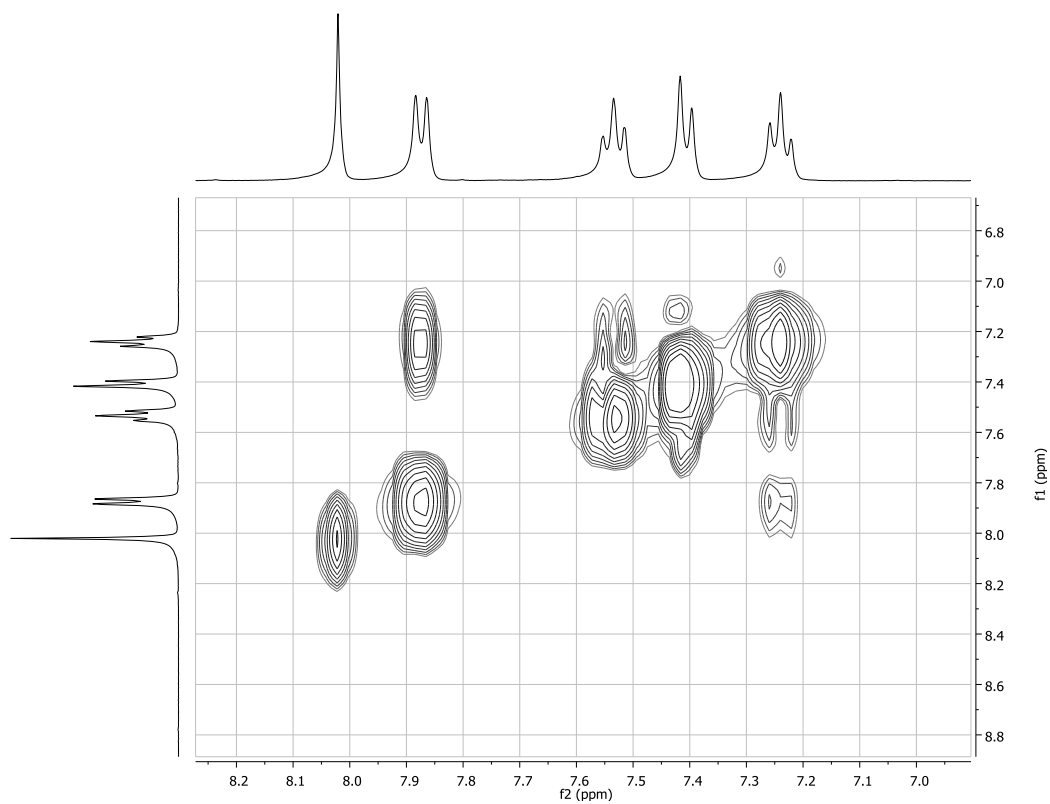
HMBC spectrum of **2.14**
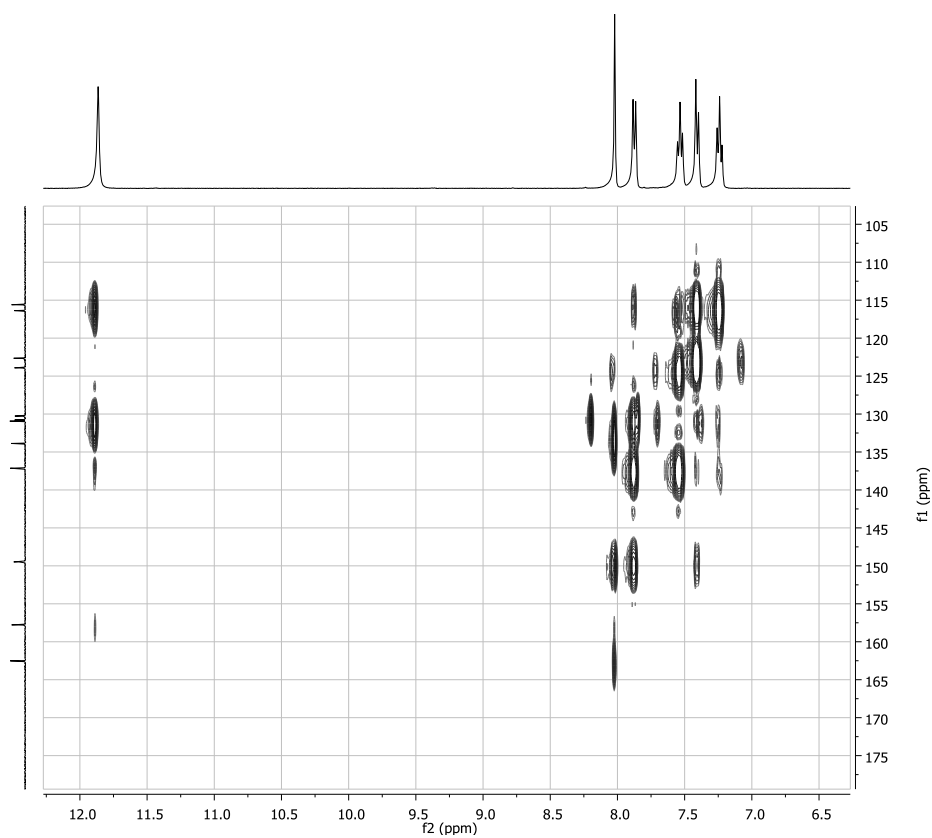
HRMS (TOF) of **2.14**
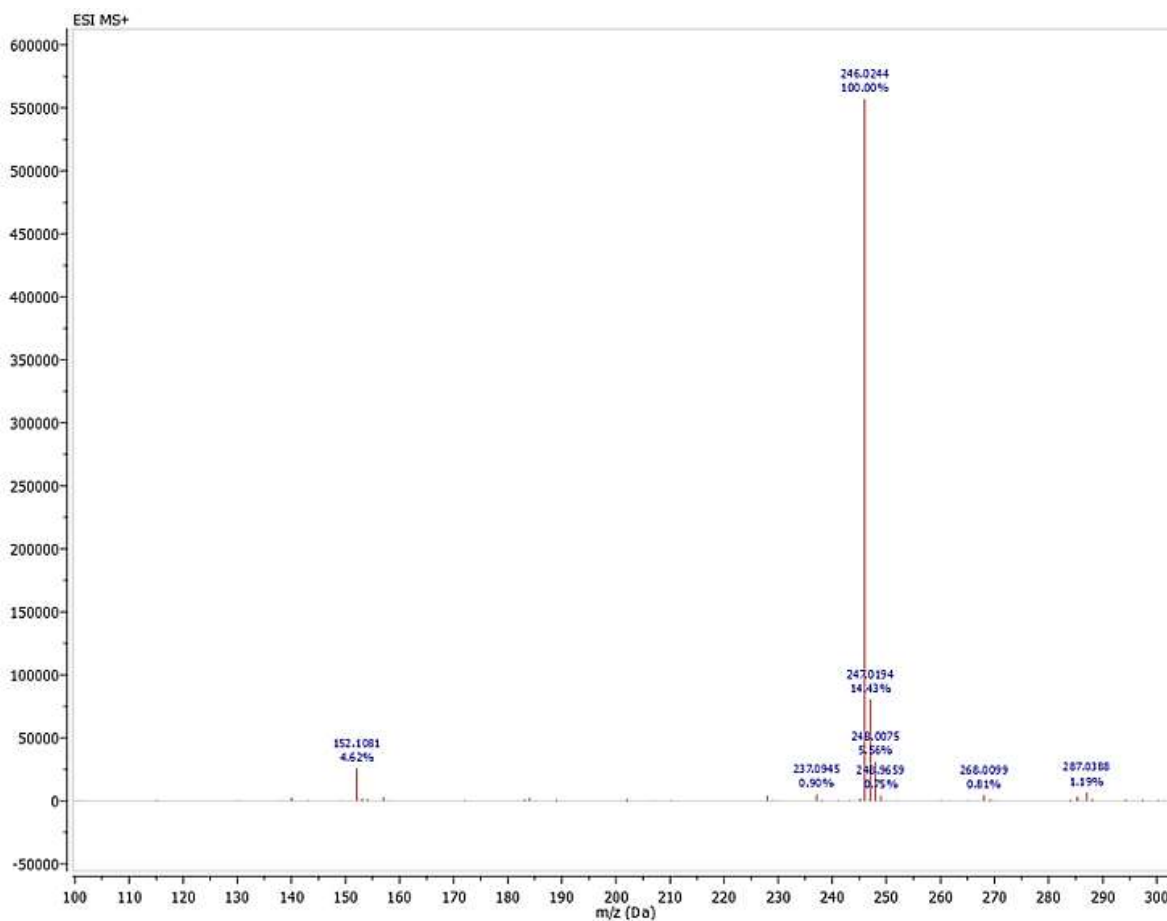
HPLC scan of **2.14**
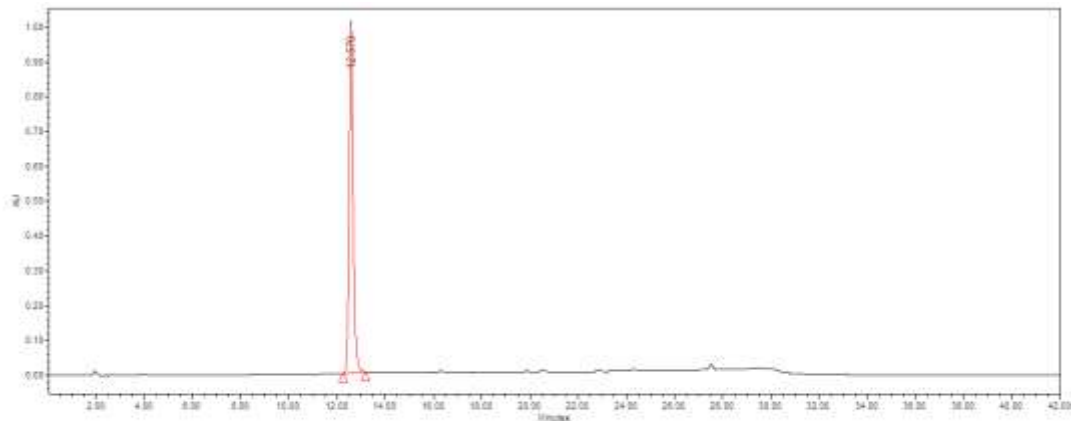
Retention time (min)	% Area
12.579	100

¹H NMR of 2.10
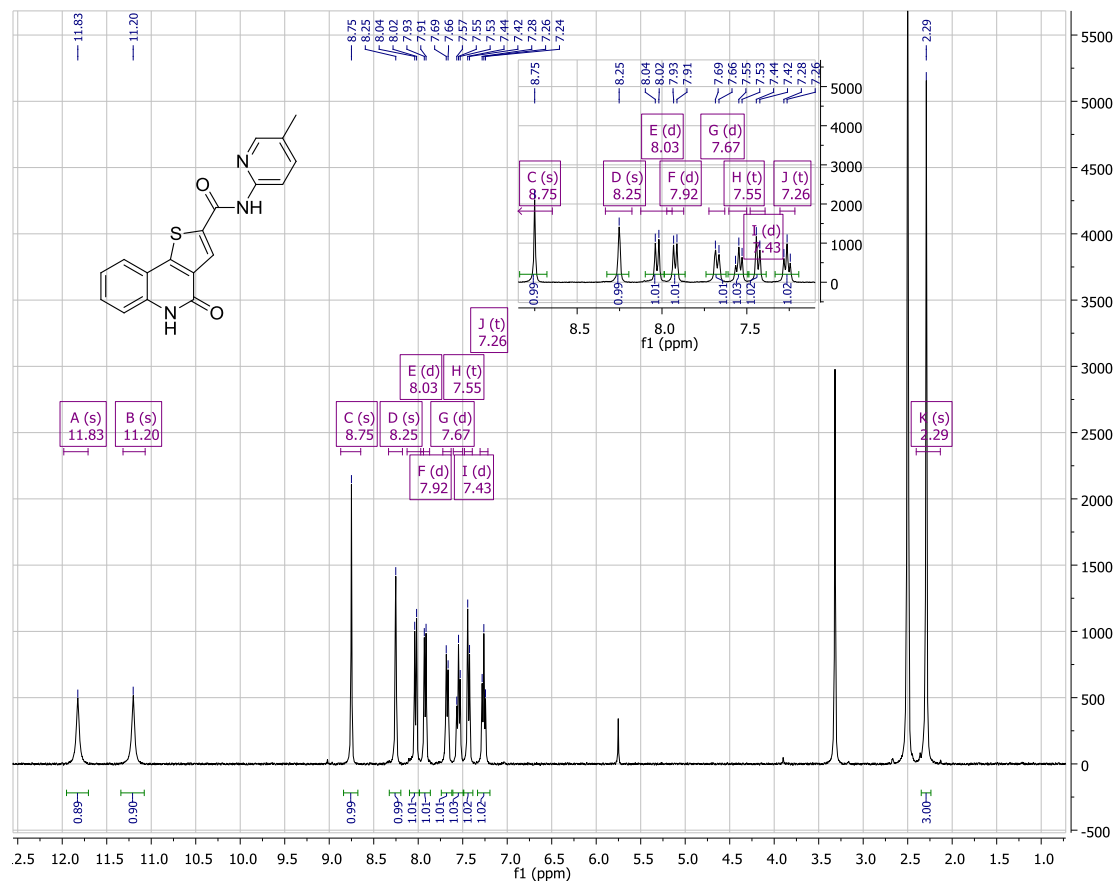
¹³C NMR of **2.10**
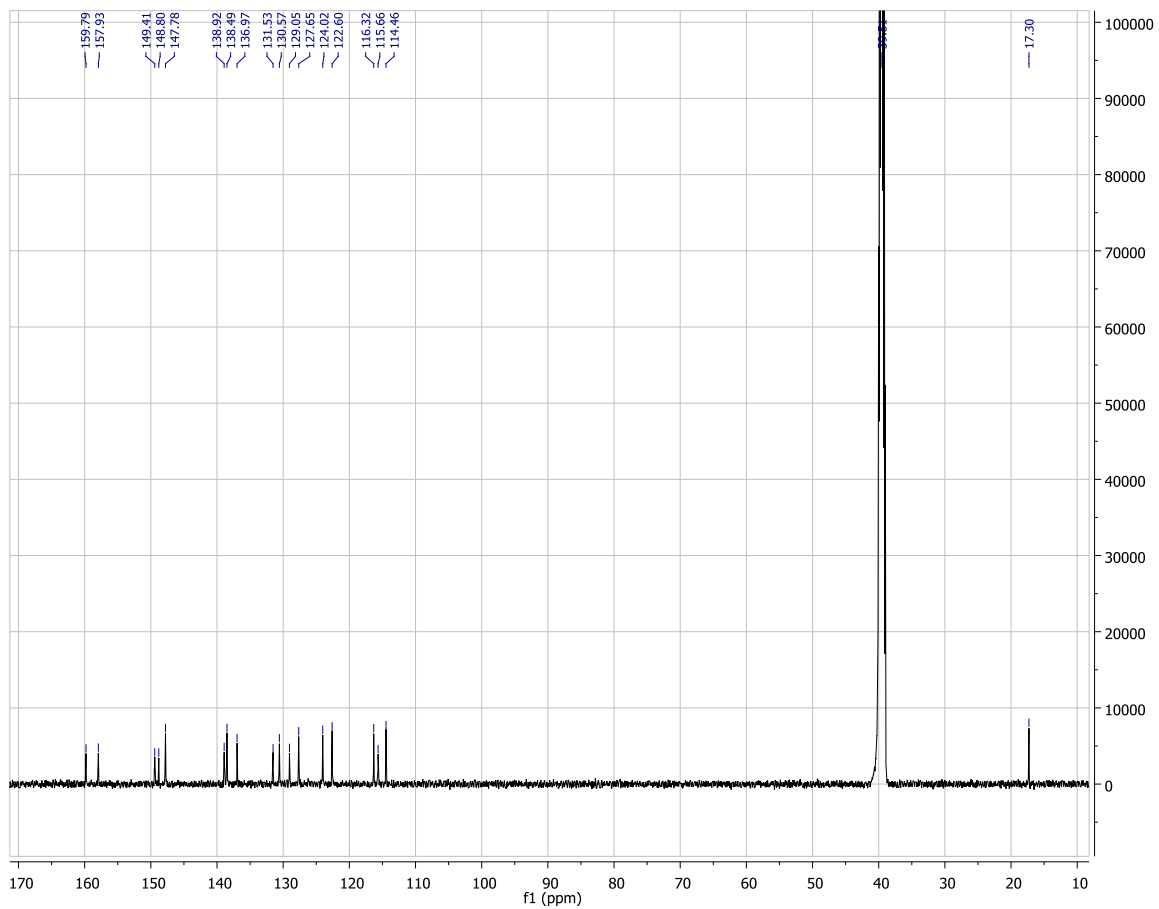
HSQC of **2.10**

HRMS (ESI TOF) of **2.10**

Generic Display Report (all)

+MS, 18.0-18.1min #(1177-1184)

336.0818

359.2422

301.0771 308.9772 318.0711

AC-2-040-A

Bruker Daltonics DataAnalysis 3.3   5/8/2012 6:50:46 PM   Page 1 of 1
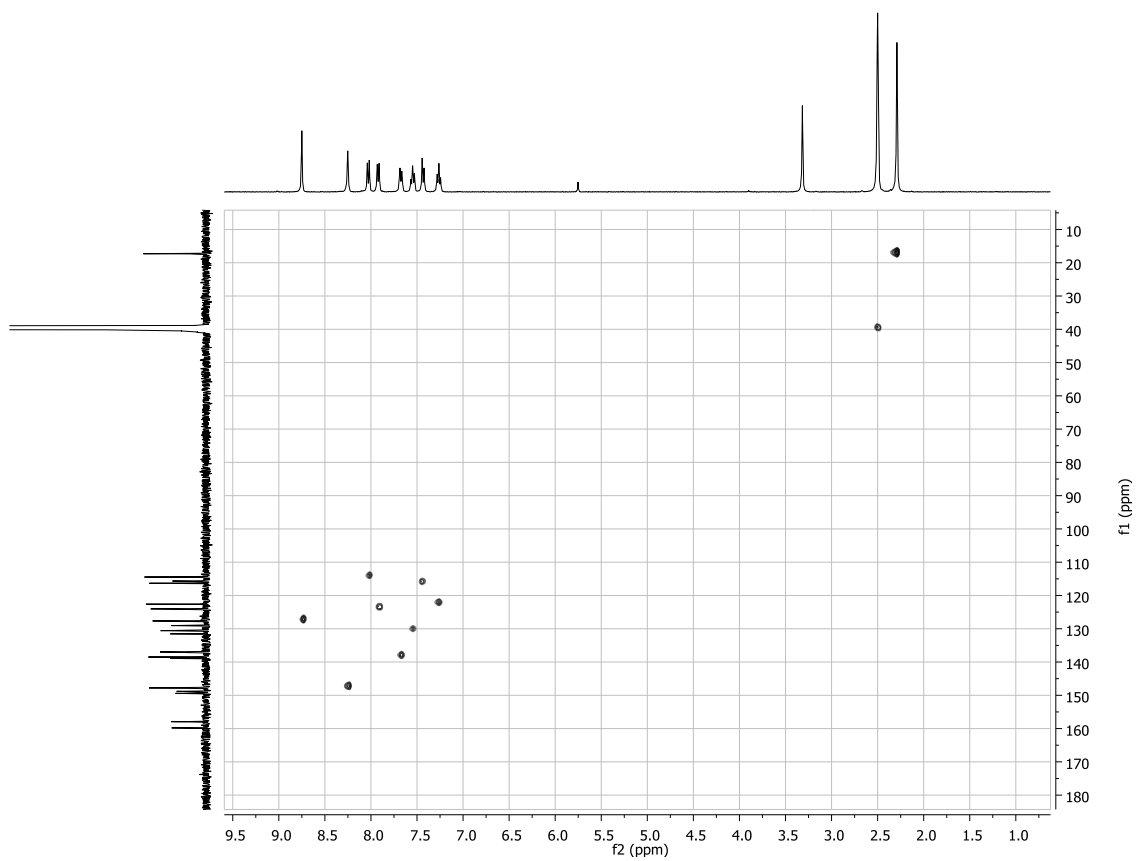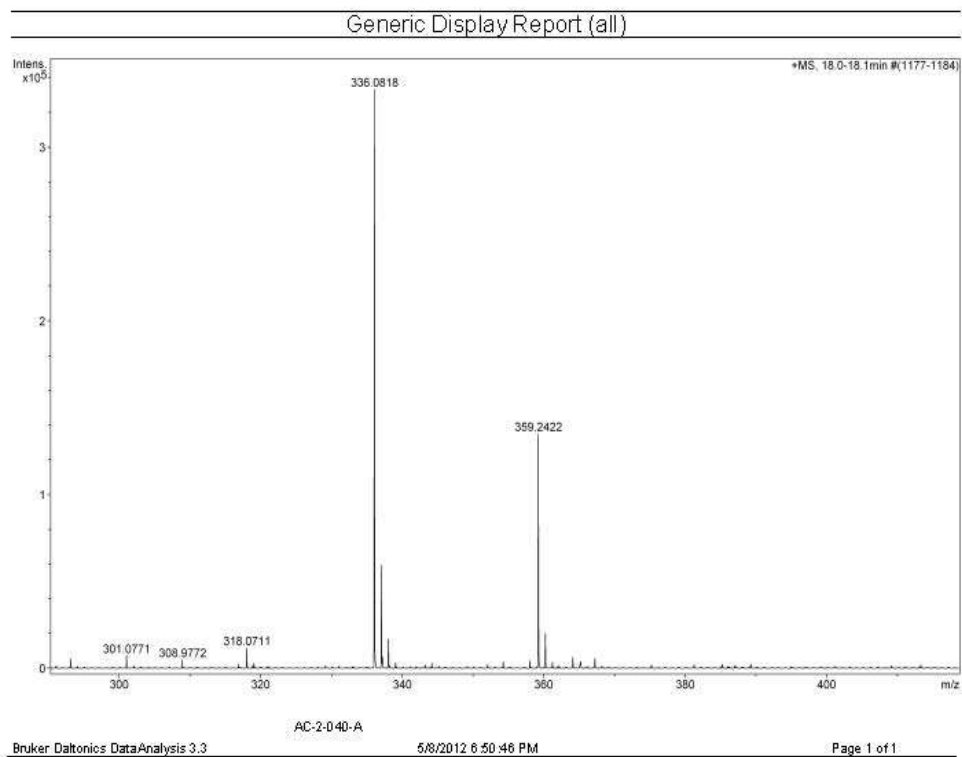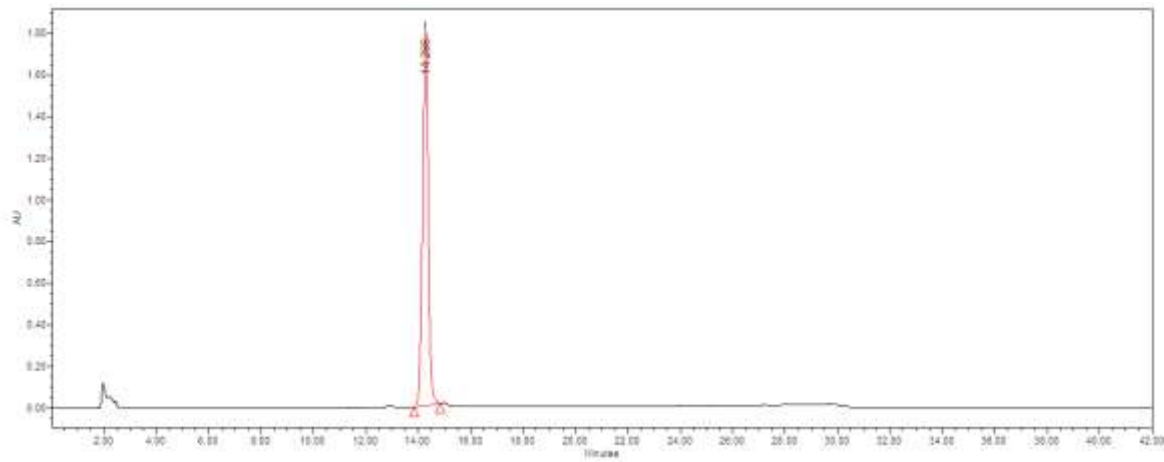
HPLC scan of **2.10**

Retention time (min)	% Area
14.286	100

¹H NMR spectrum of **3.15**
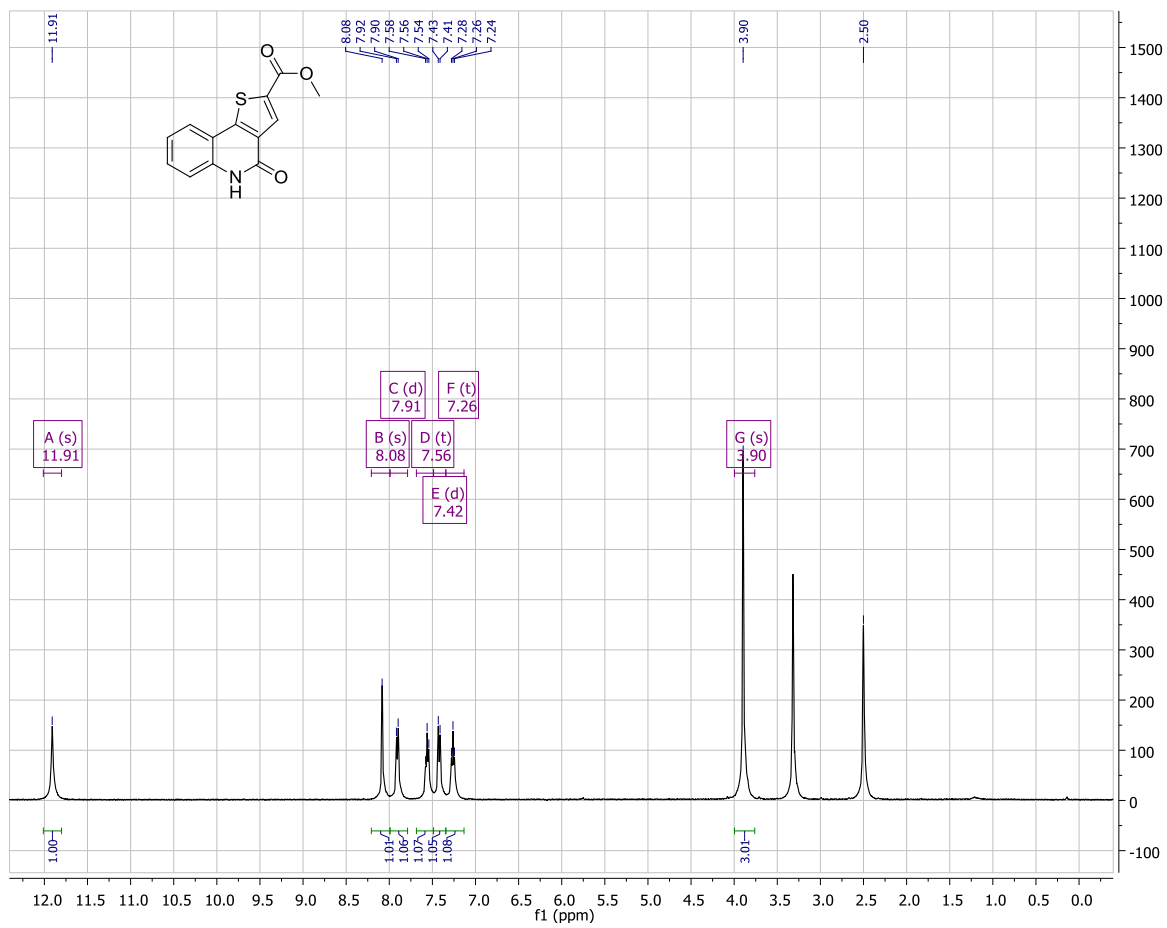
¹³C NMR spectrum of **3.15**
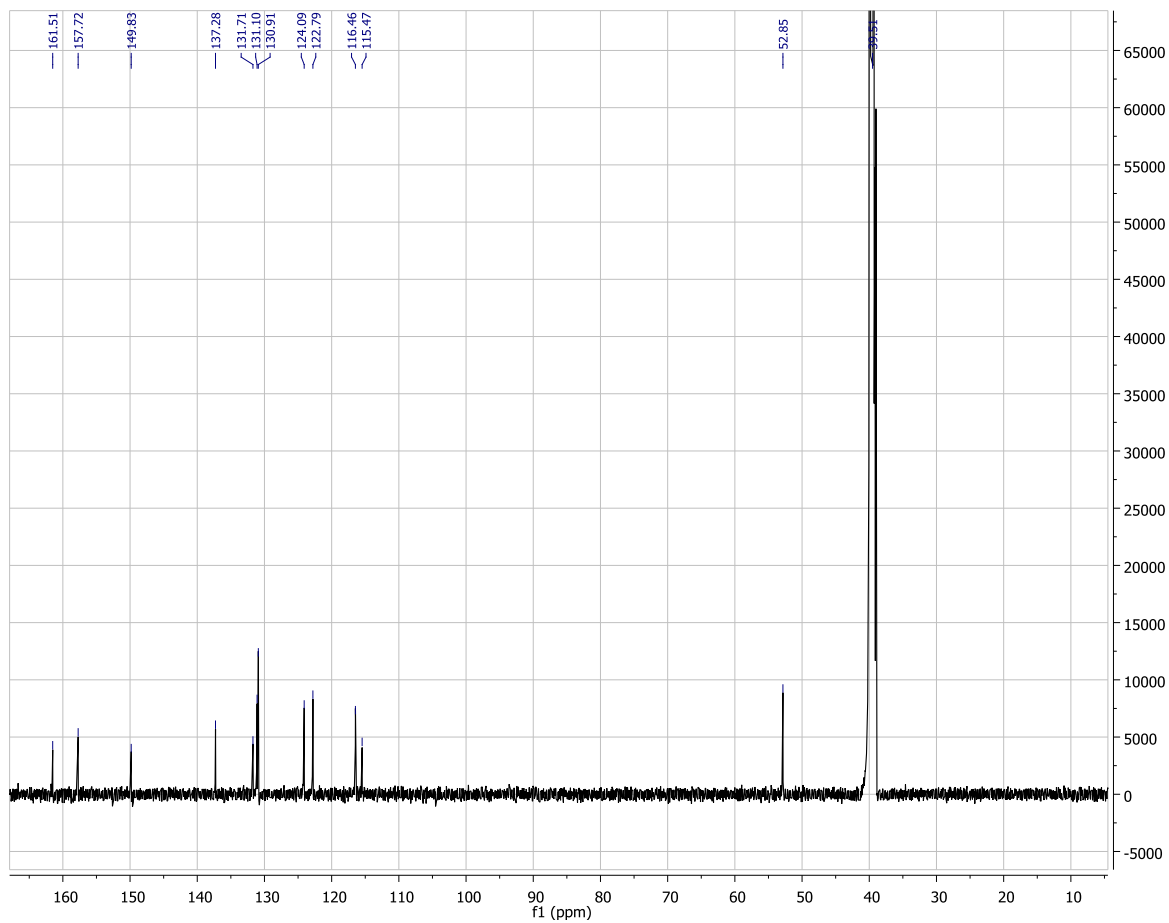
HRMS (TOF) of **3.15**
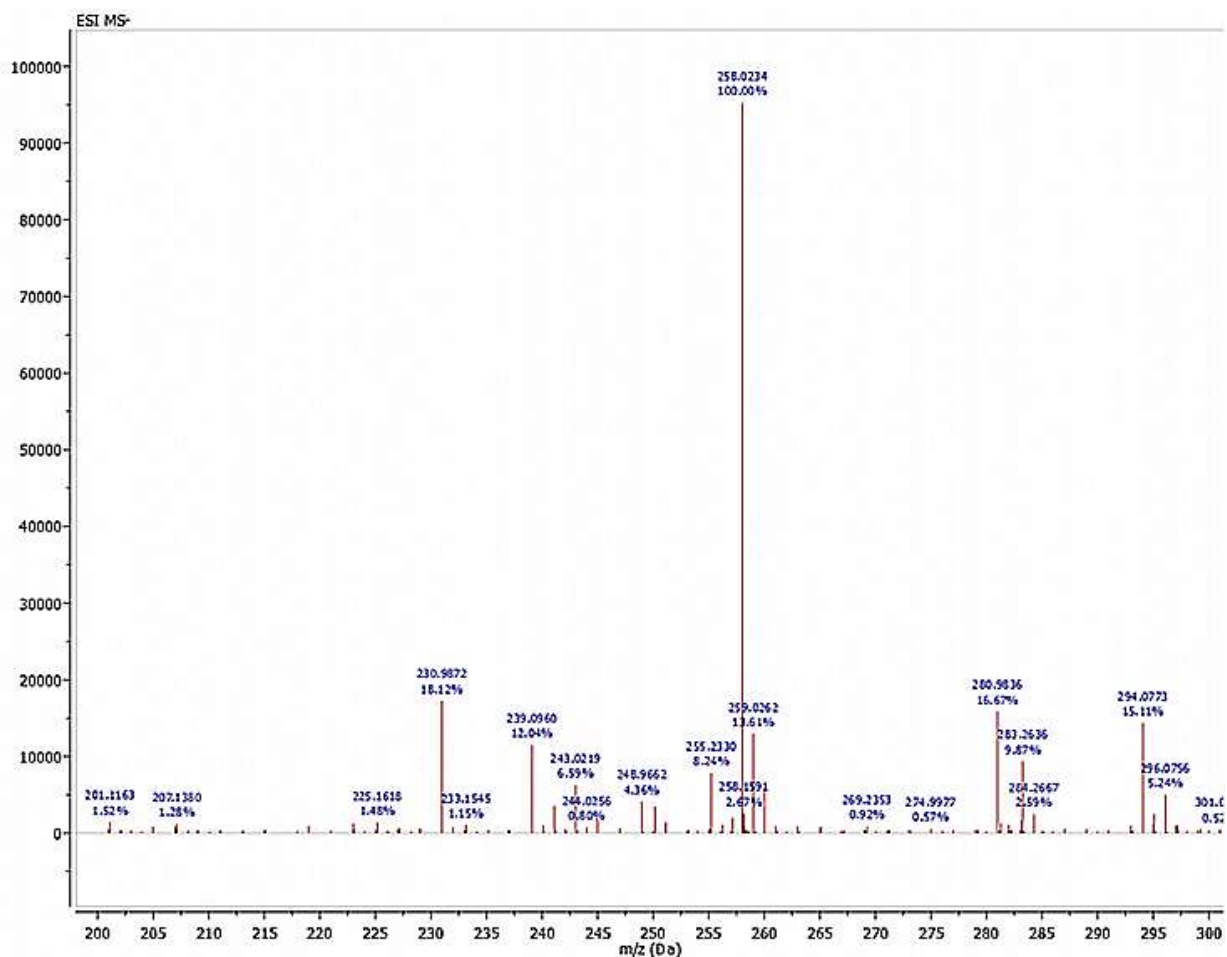
HPLC scan of **3.15**
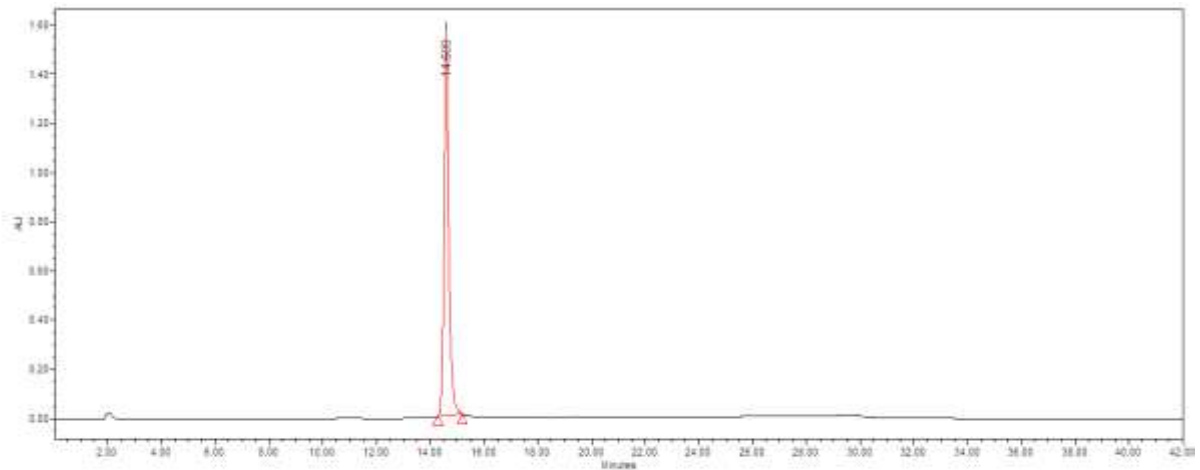
Retention time (min)	% Area
14.599	99.65
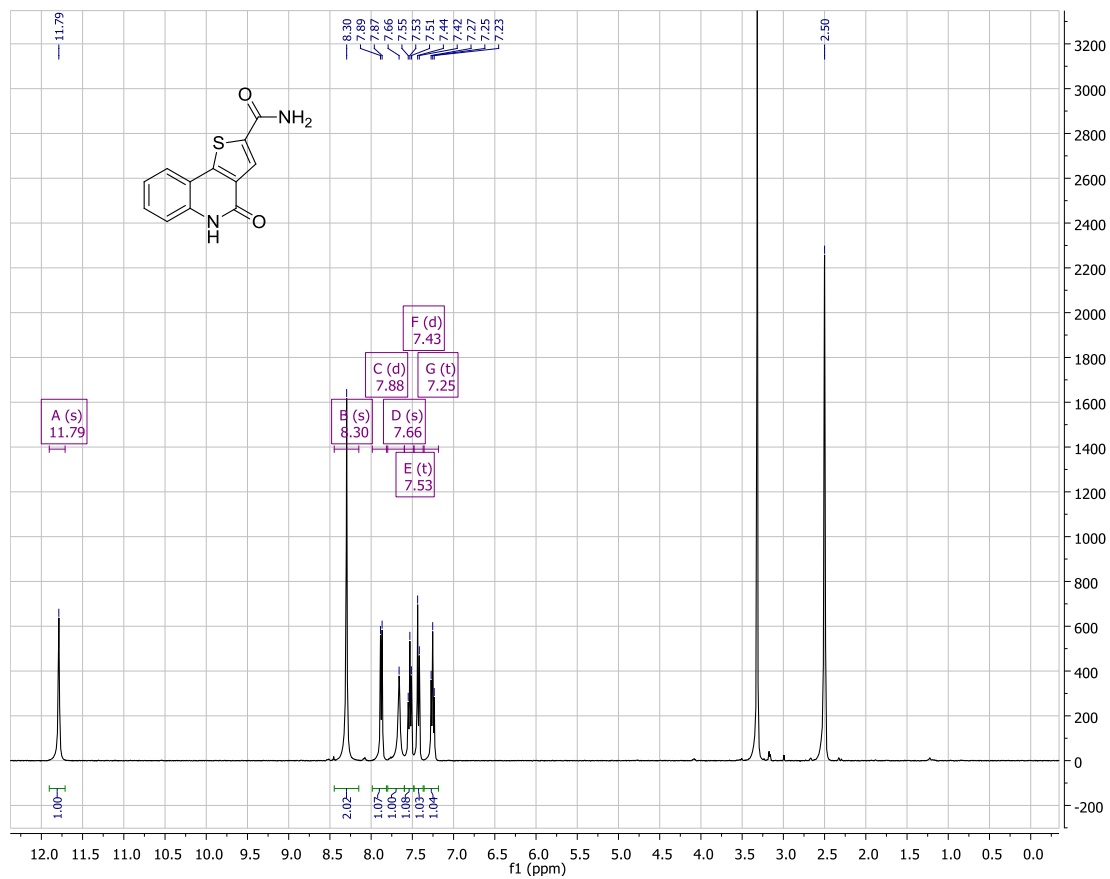
^{1}H NMR (D$_2$O wash) spectrum of **3.16**
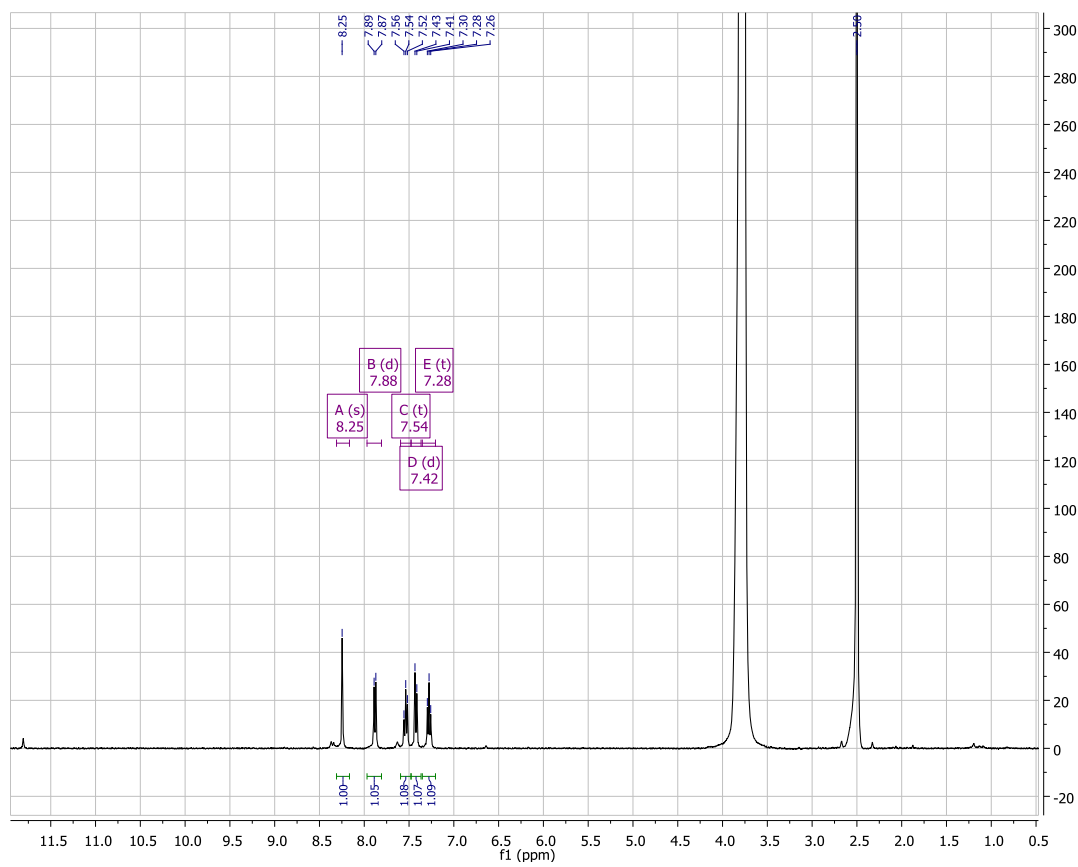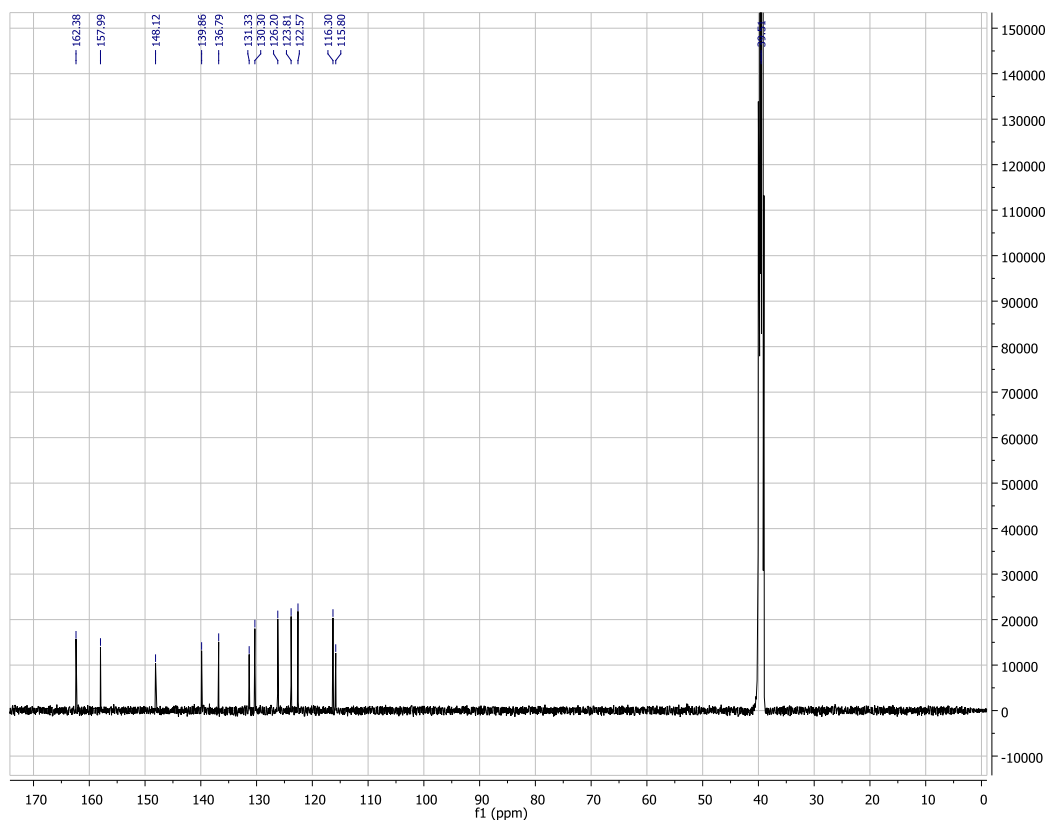
HRMS (TOF) of **3.16**
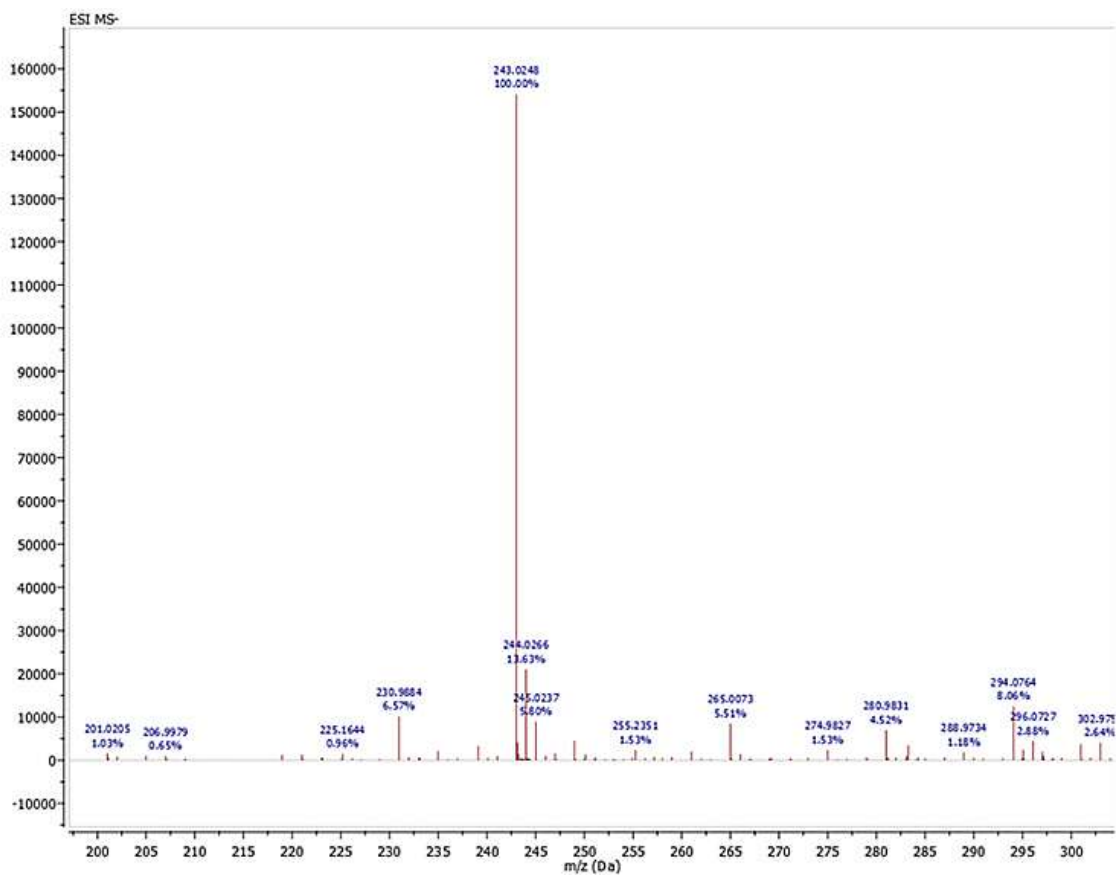
HPLC scan of **3.16**
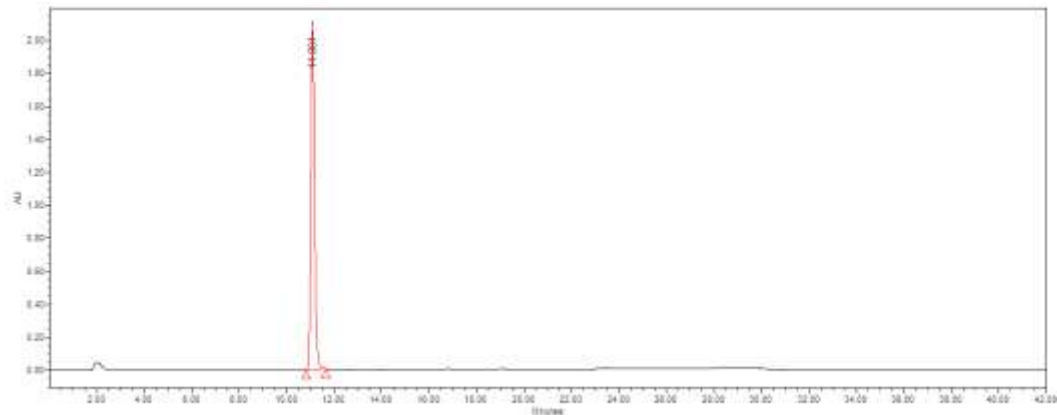
Retention time (min)	% Area
11.091	100

¹³C NMR spectrum of **3.17**
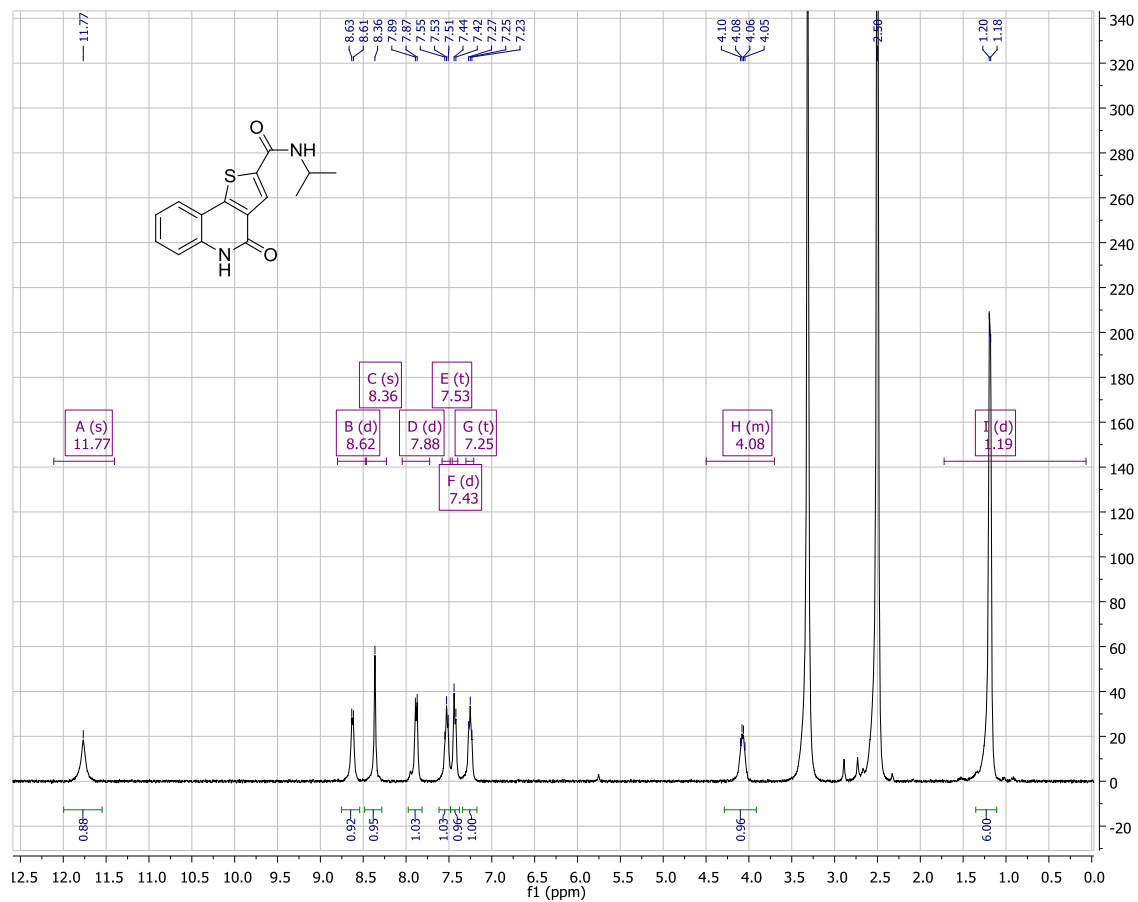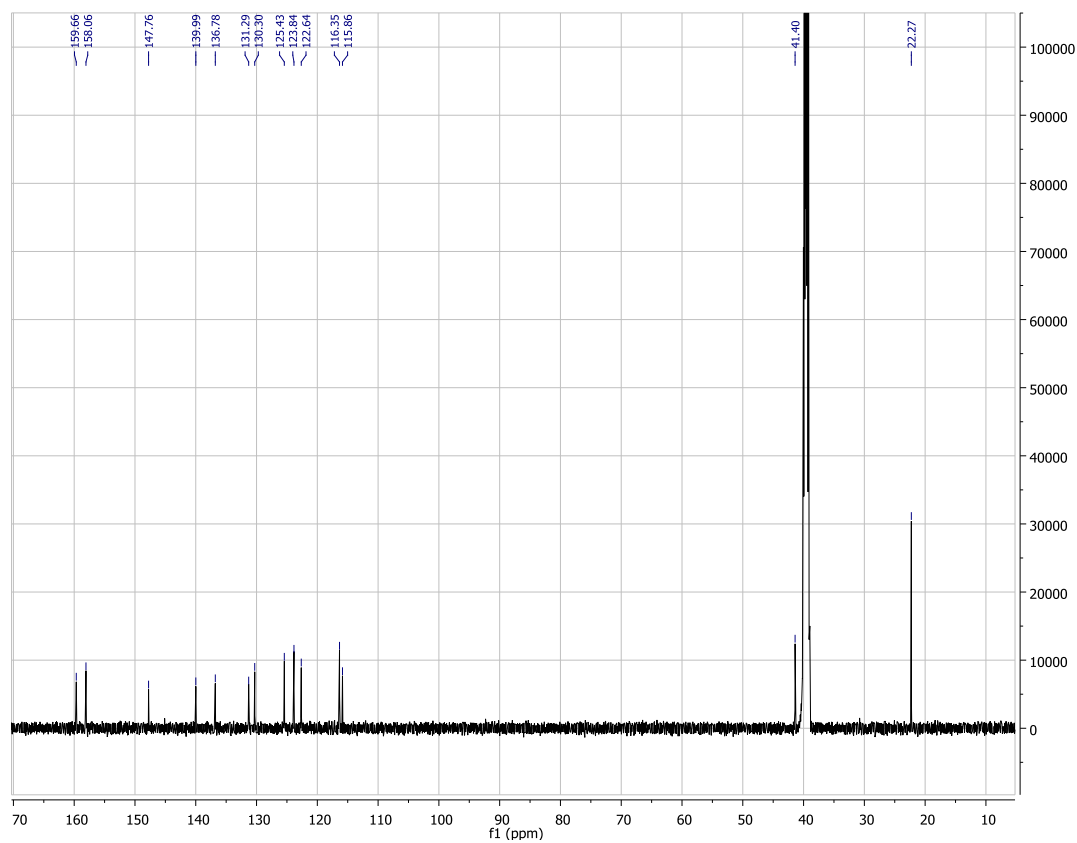
HRMS (TOF) of **3.17**
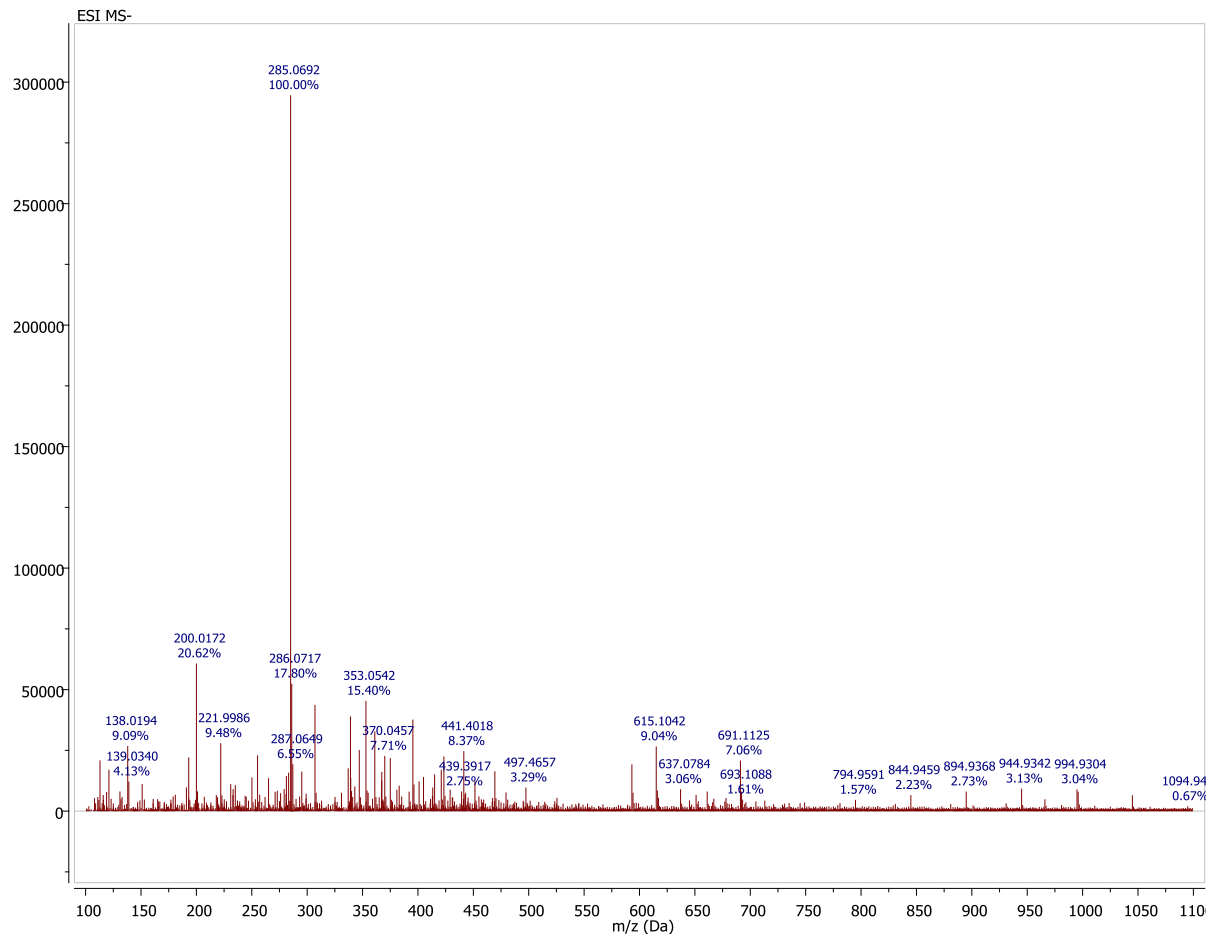
HPLC scan of **3.17**
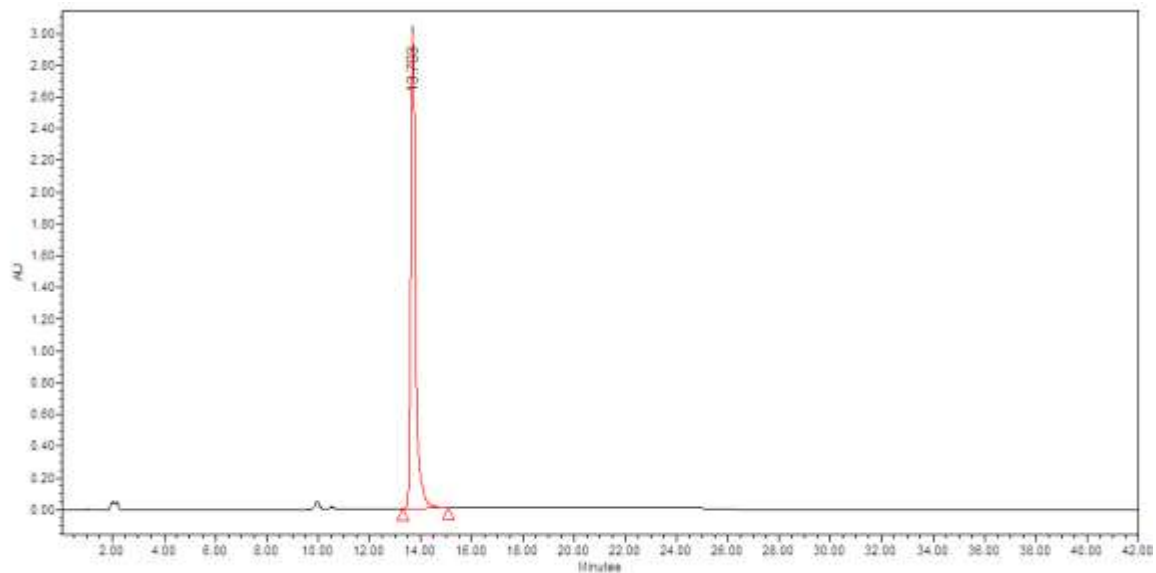
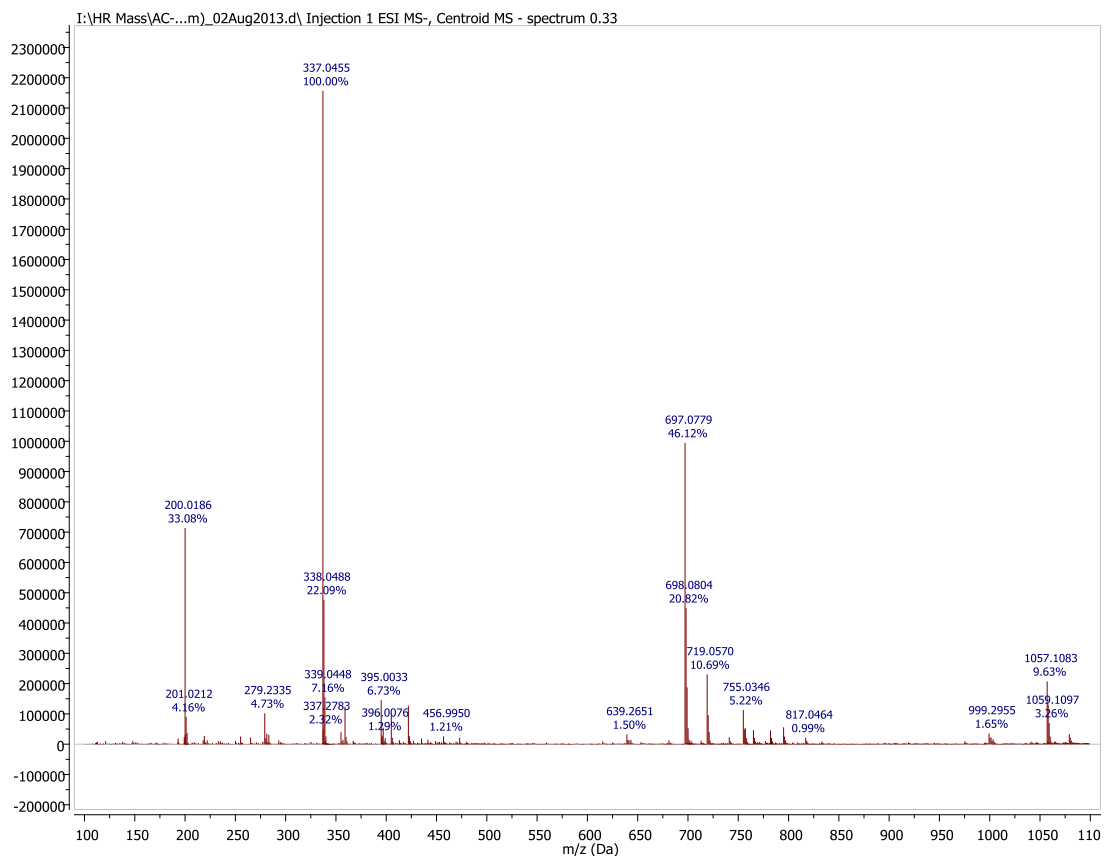| Retention time (min)	% Area
13.703	98.30

¹H NMR spectrum of **3.18**
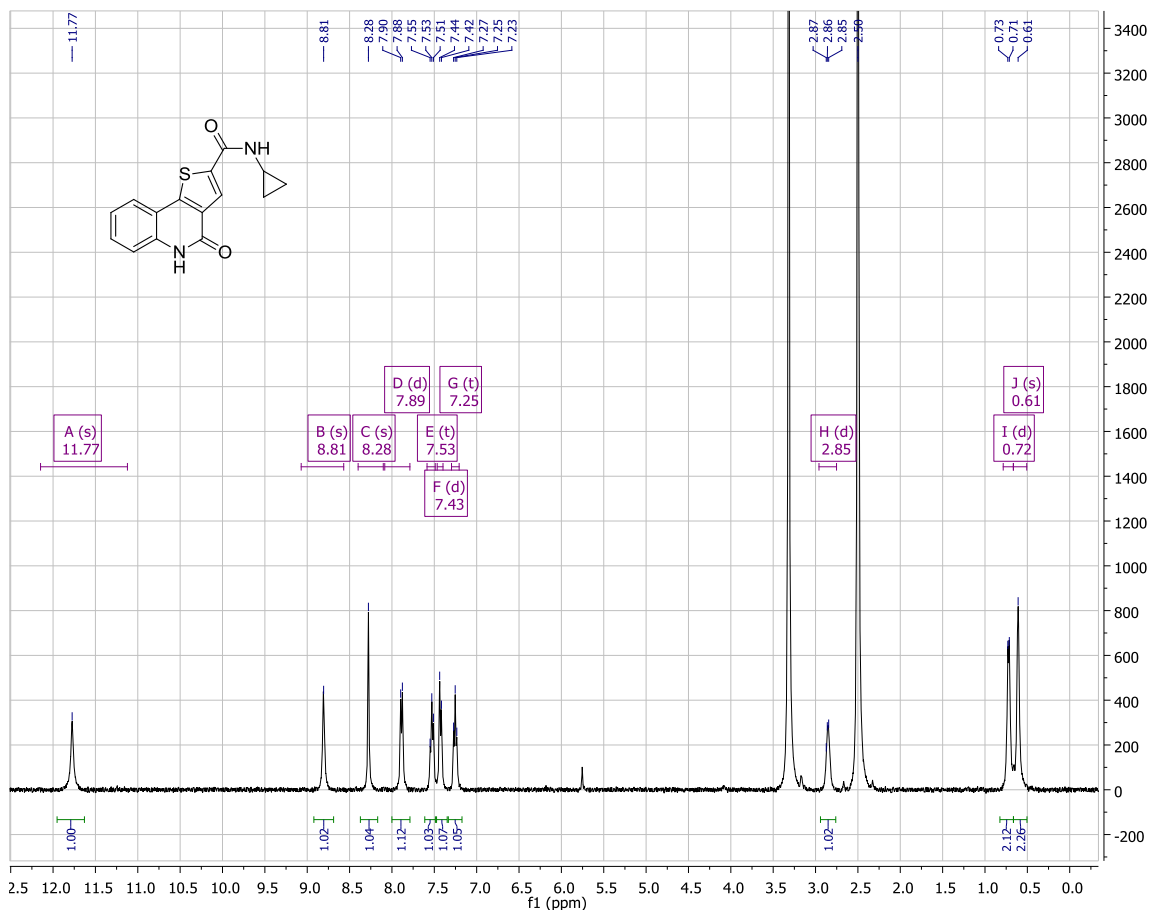
¹³C NMR spectrum of **3.18**
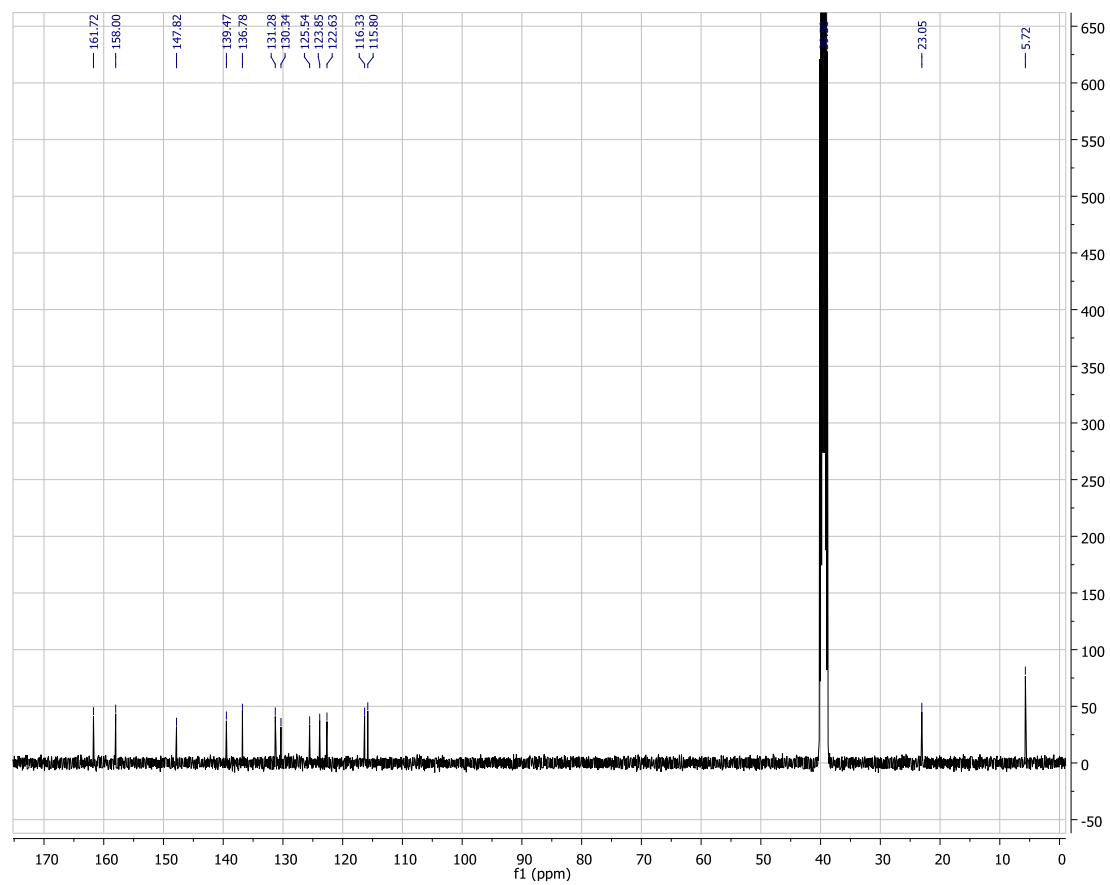
HRMS (TOF) of **3.18**
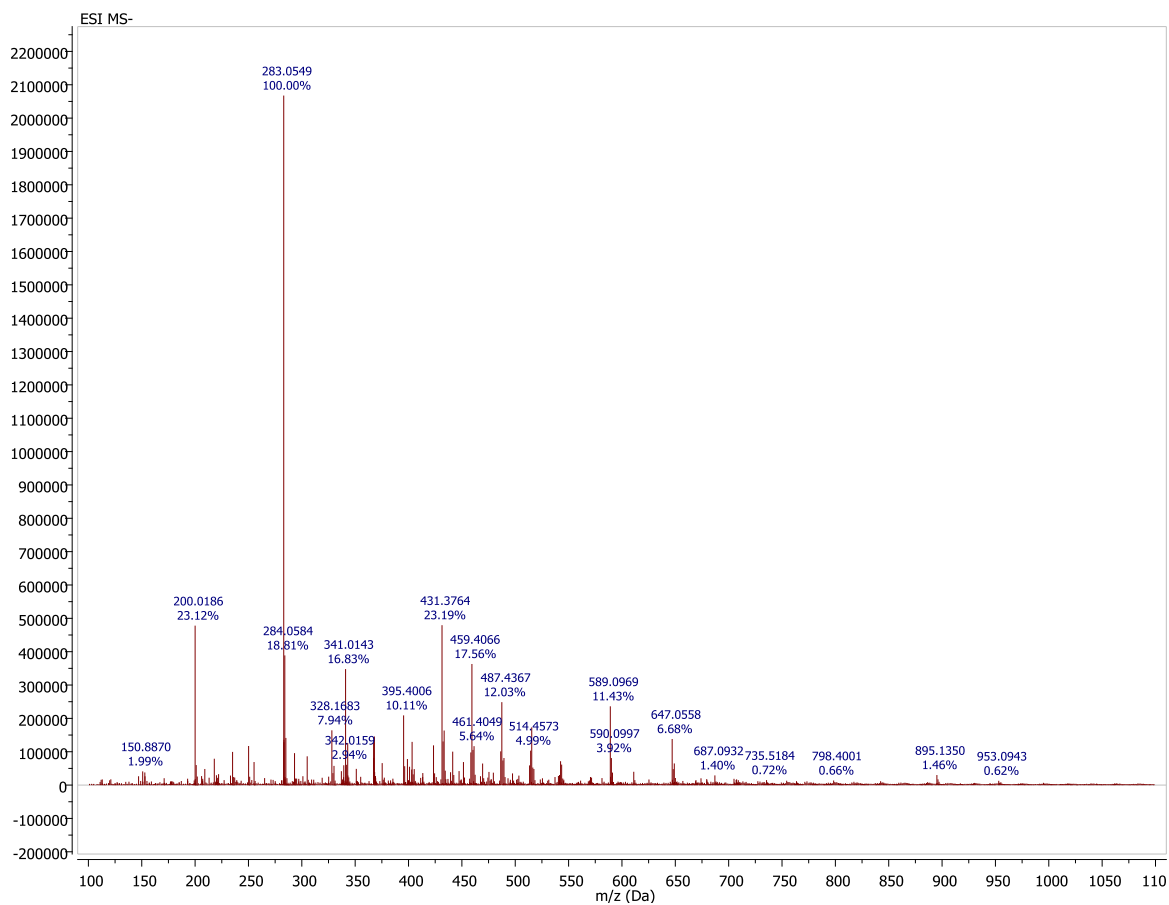
HPLC scan of **3.18**
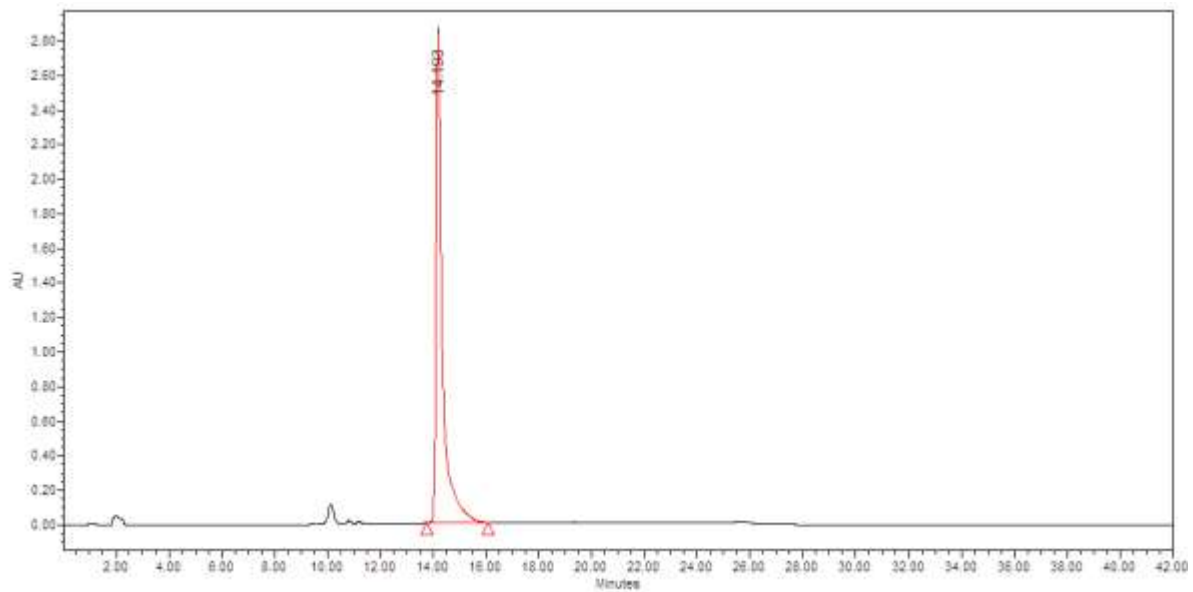
Retention time (min)	% Area
14.193	96.67

¹³C NMR spectrum of **3.19**
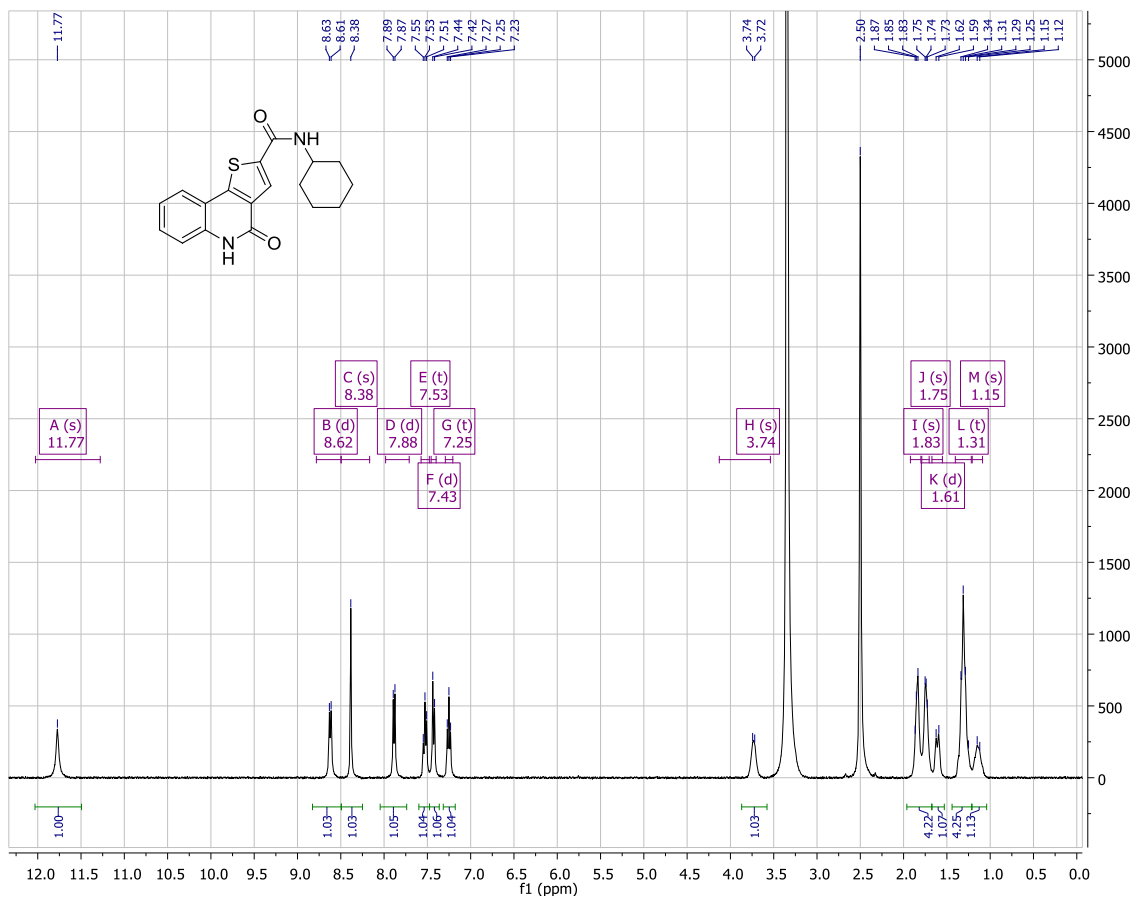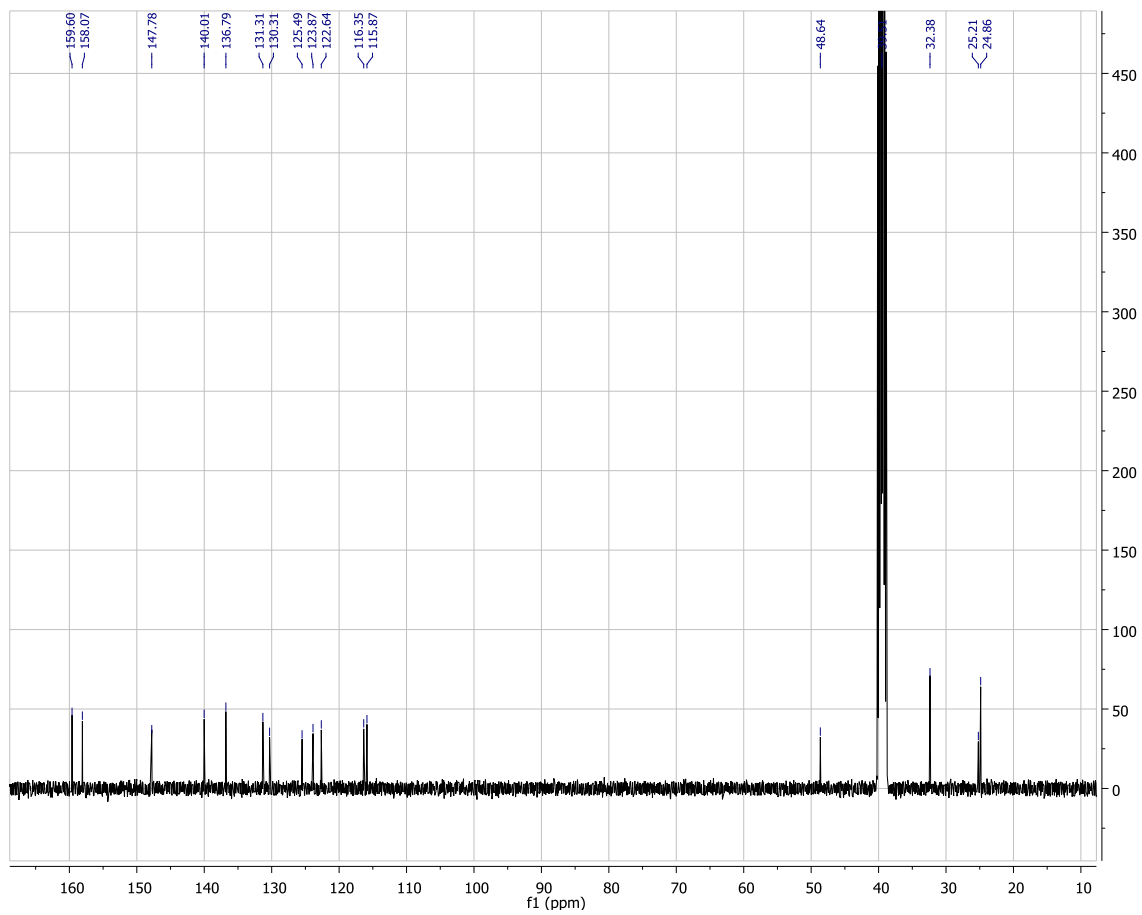
HRMS (TOF) of 3.19
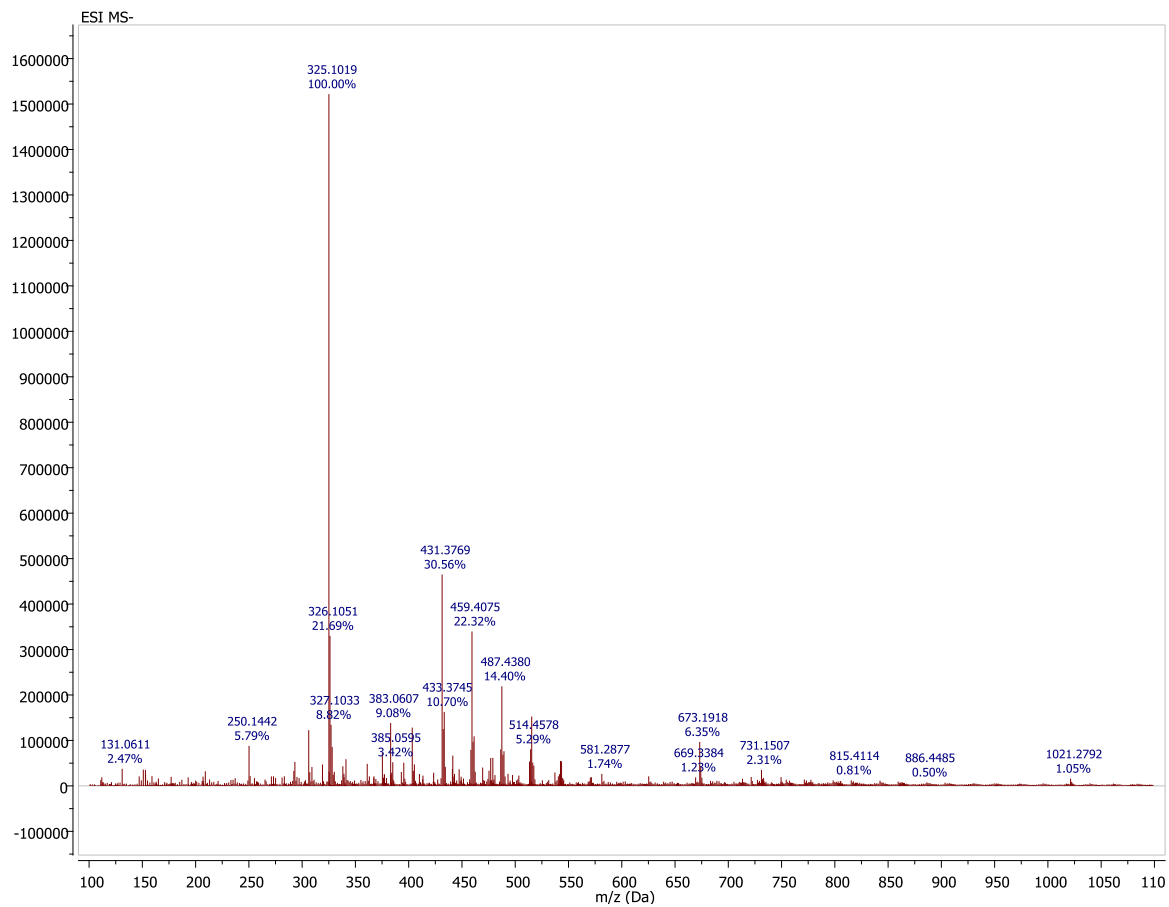
HPLC scan of 3.19
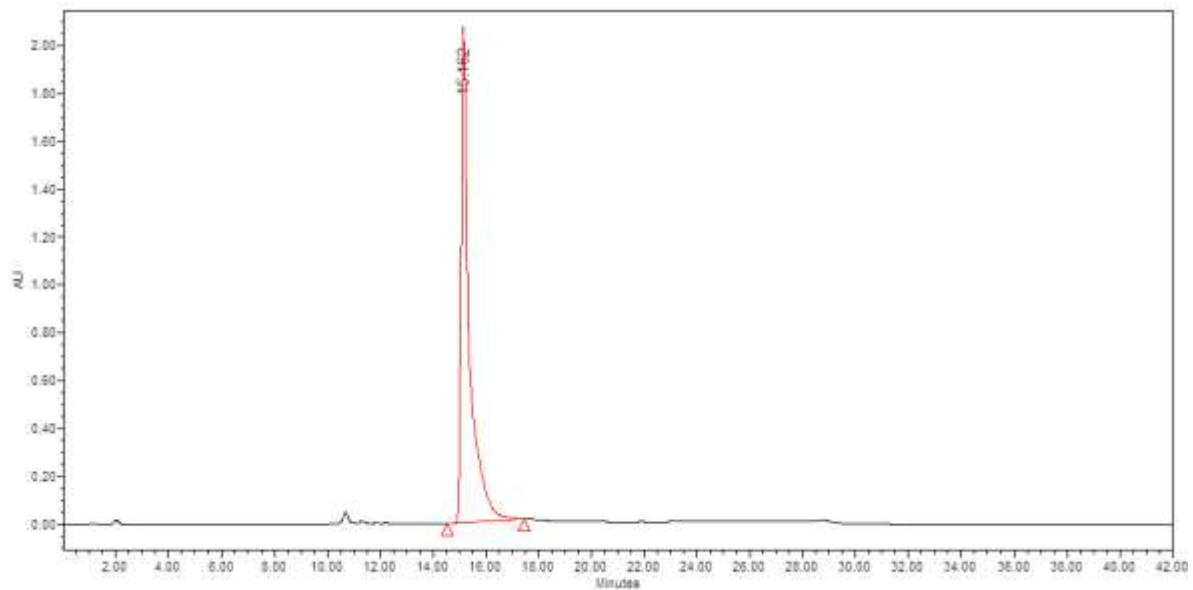
Retention time (min)	% Area
15.162	98.70

^{1}H NMR spectrum of **3.20**
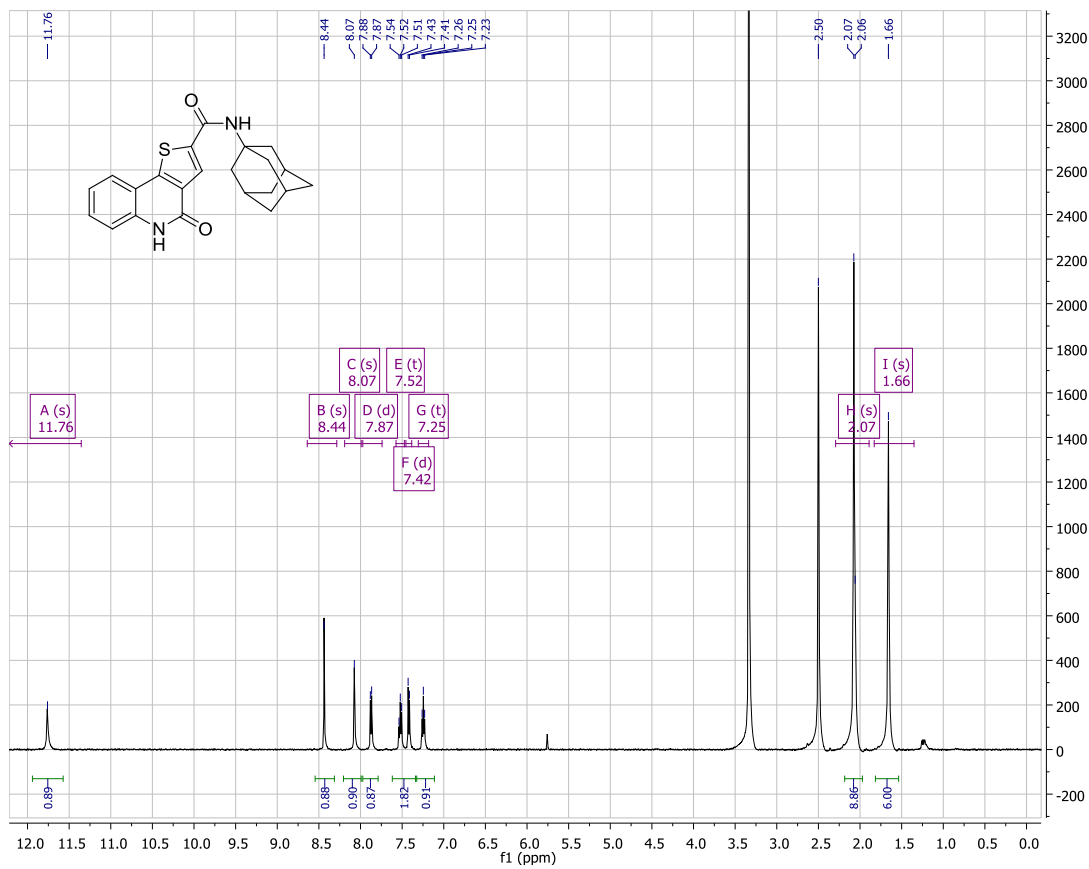
^{13}C NMR spectrum of **3.20**
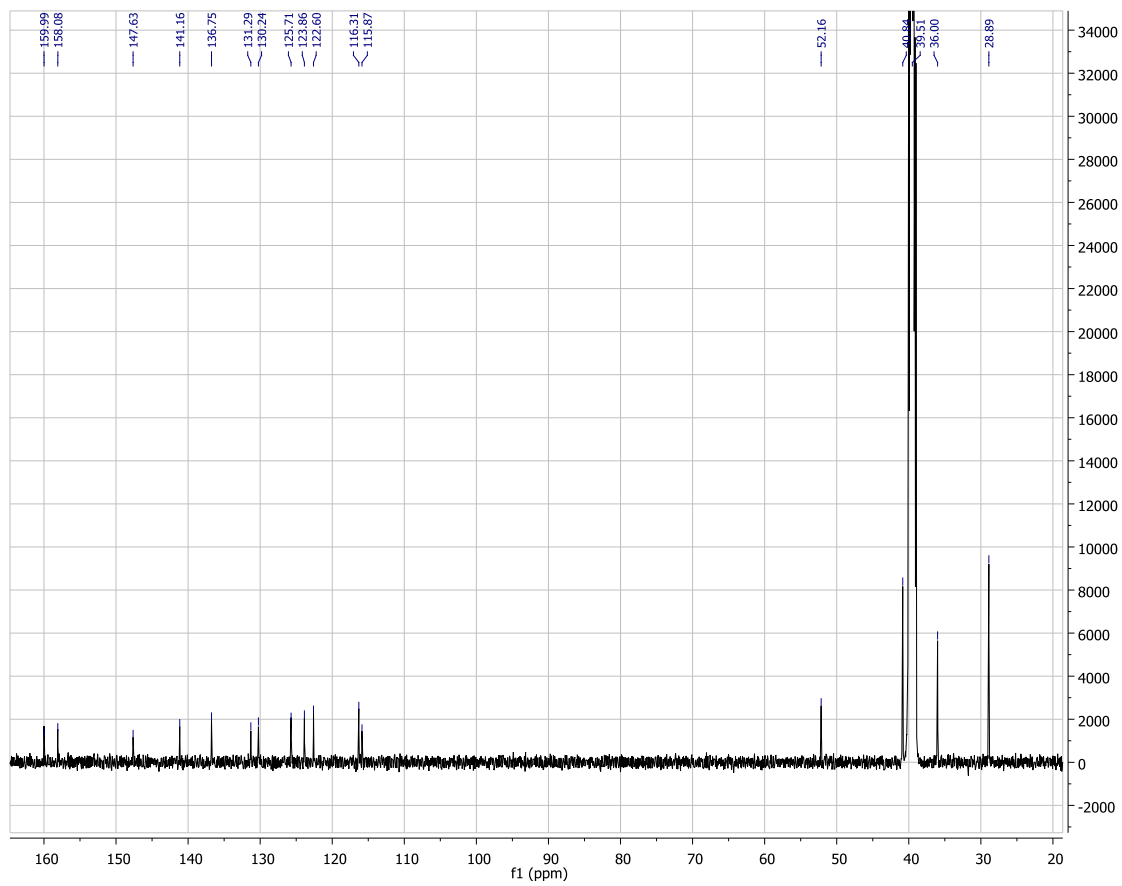
HRMS (TOF) of **3.20**
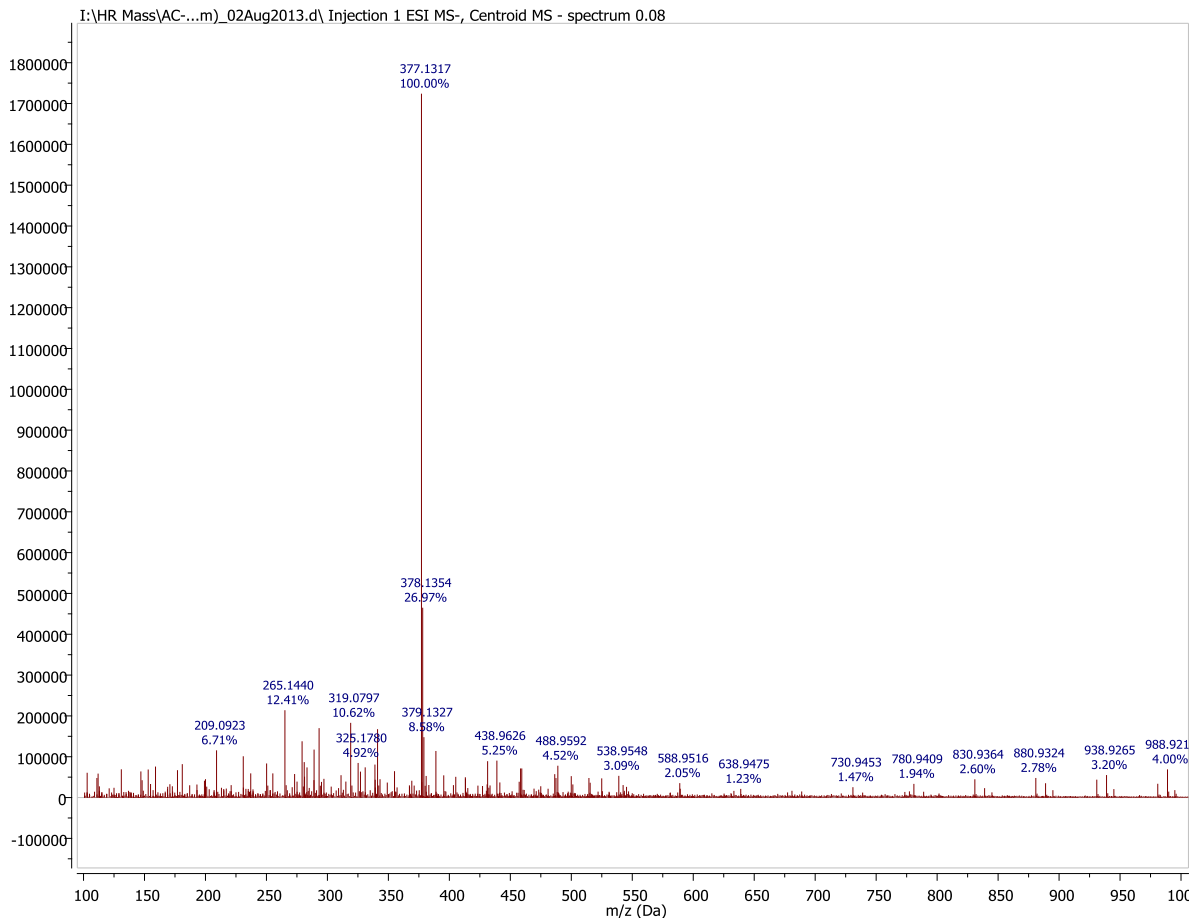
HPLC scan of 3.20
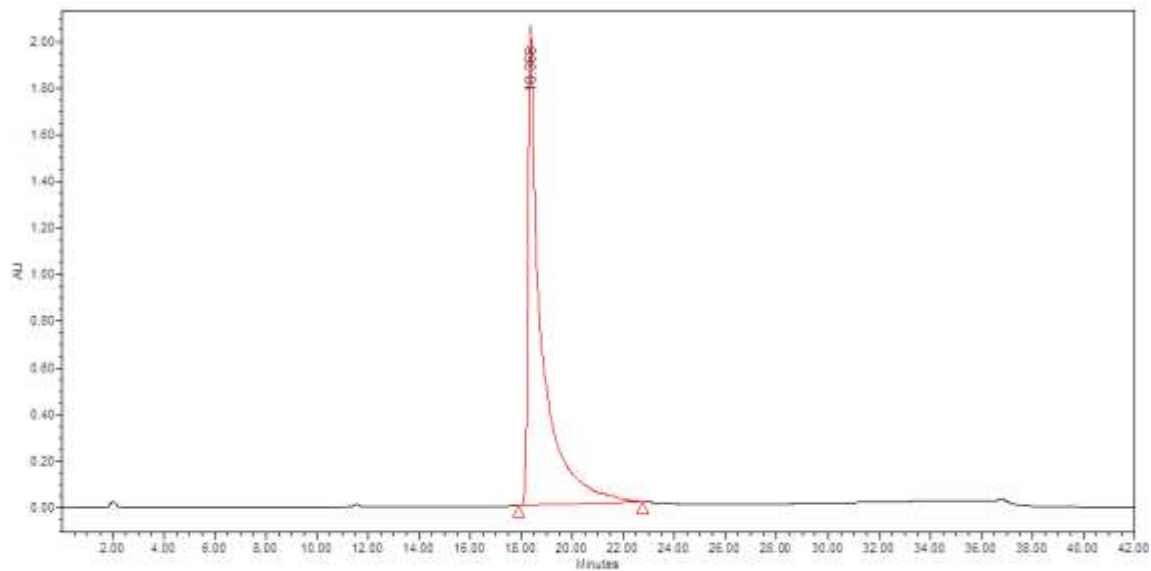
Retention time (min)	% Area
18.368	99.72

¹H NMR spectrum of **3.21**
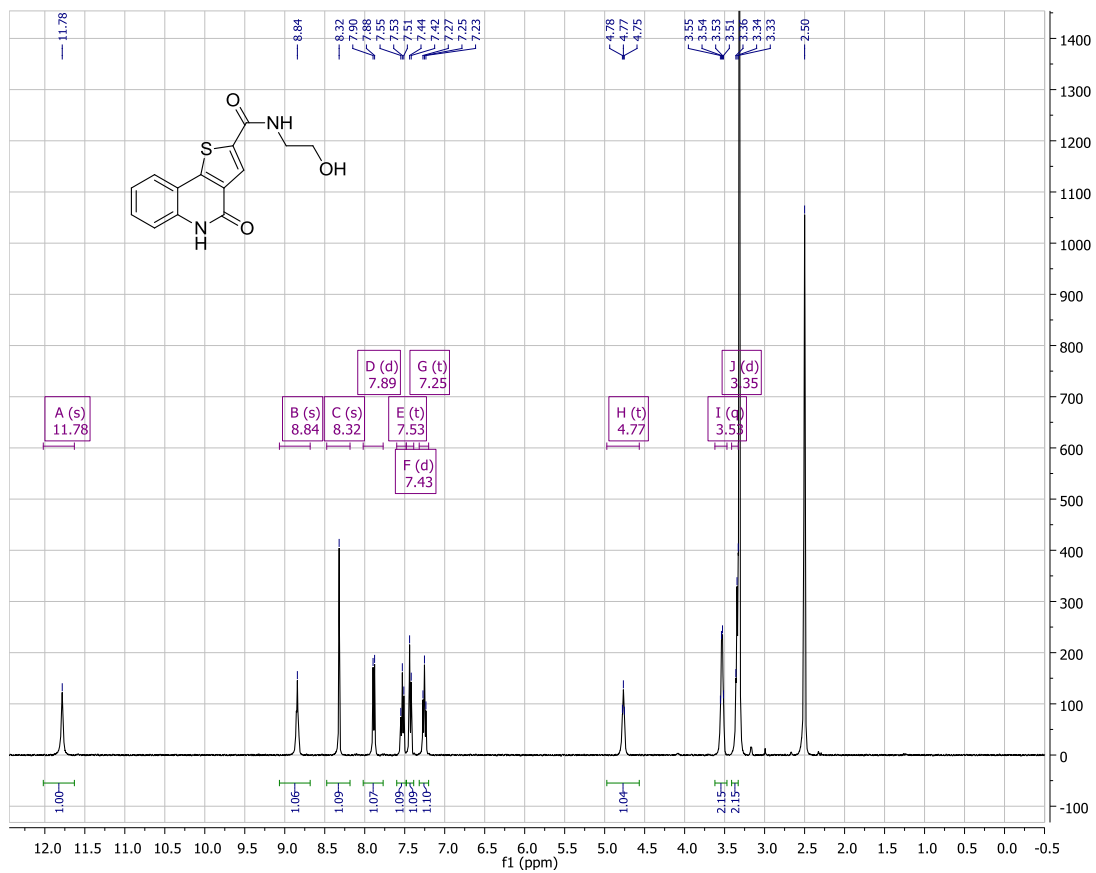
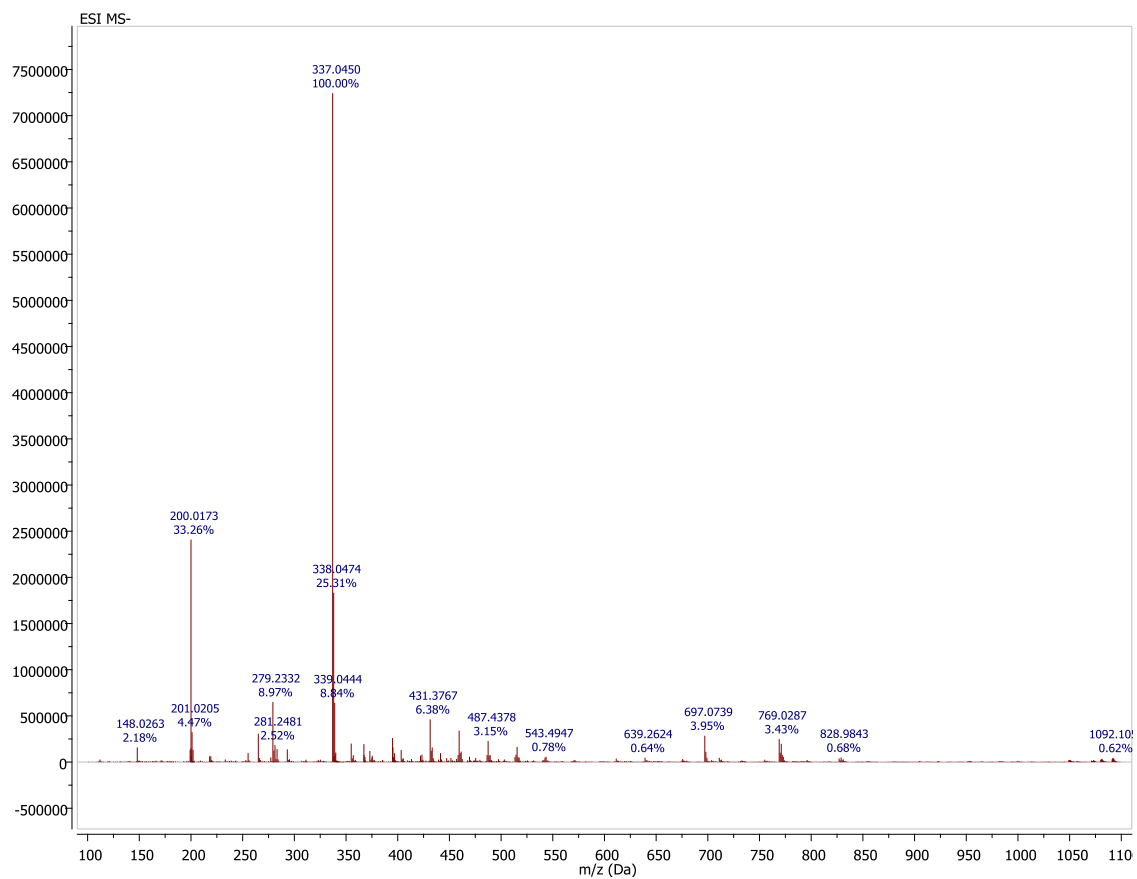¹³C NMR spectrum of **3.21**
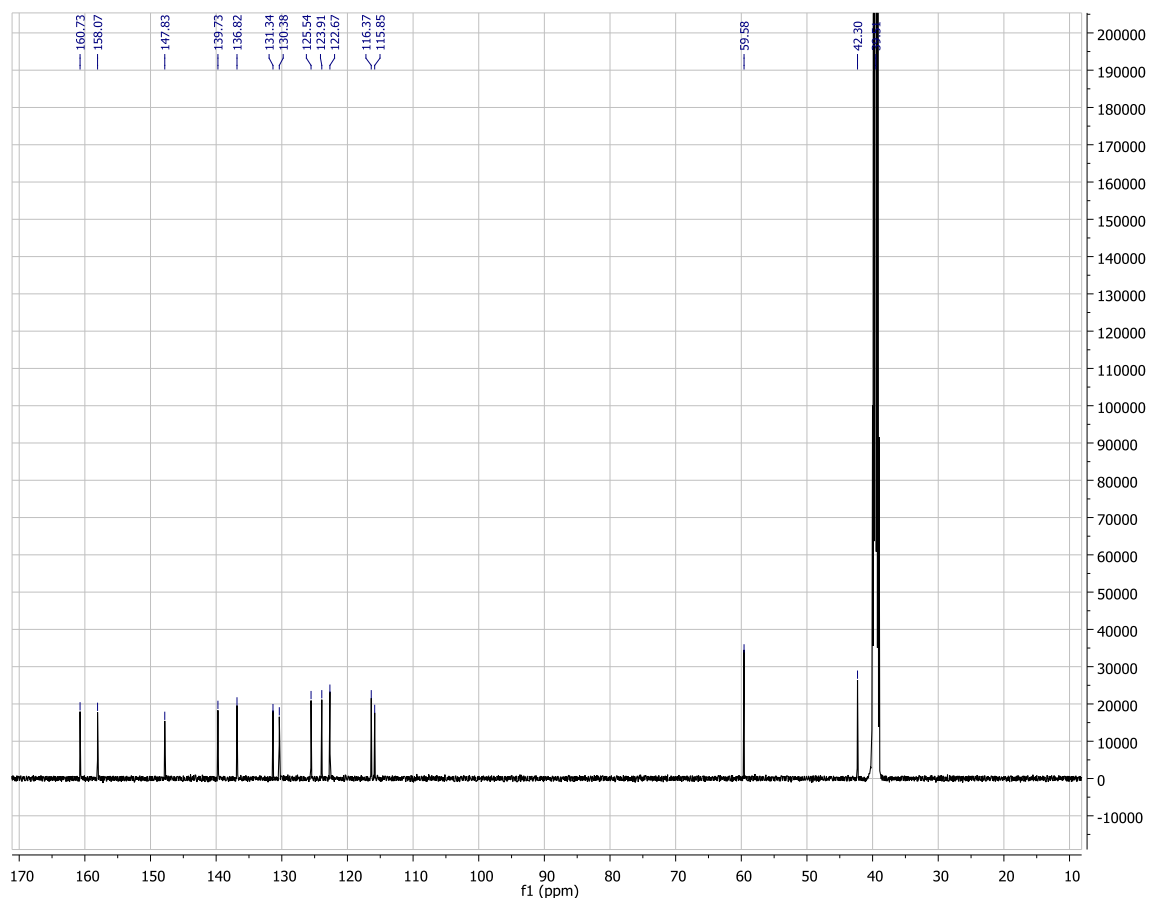
HRMS (TOF) of **3.21**
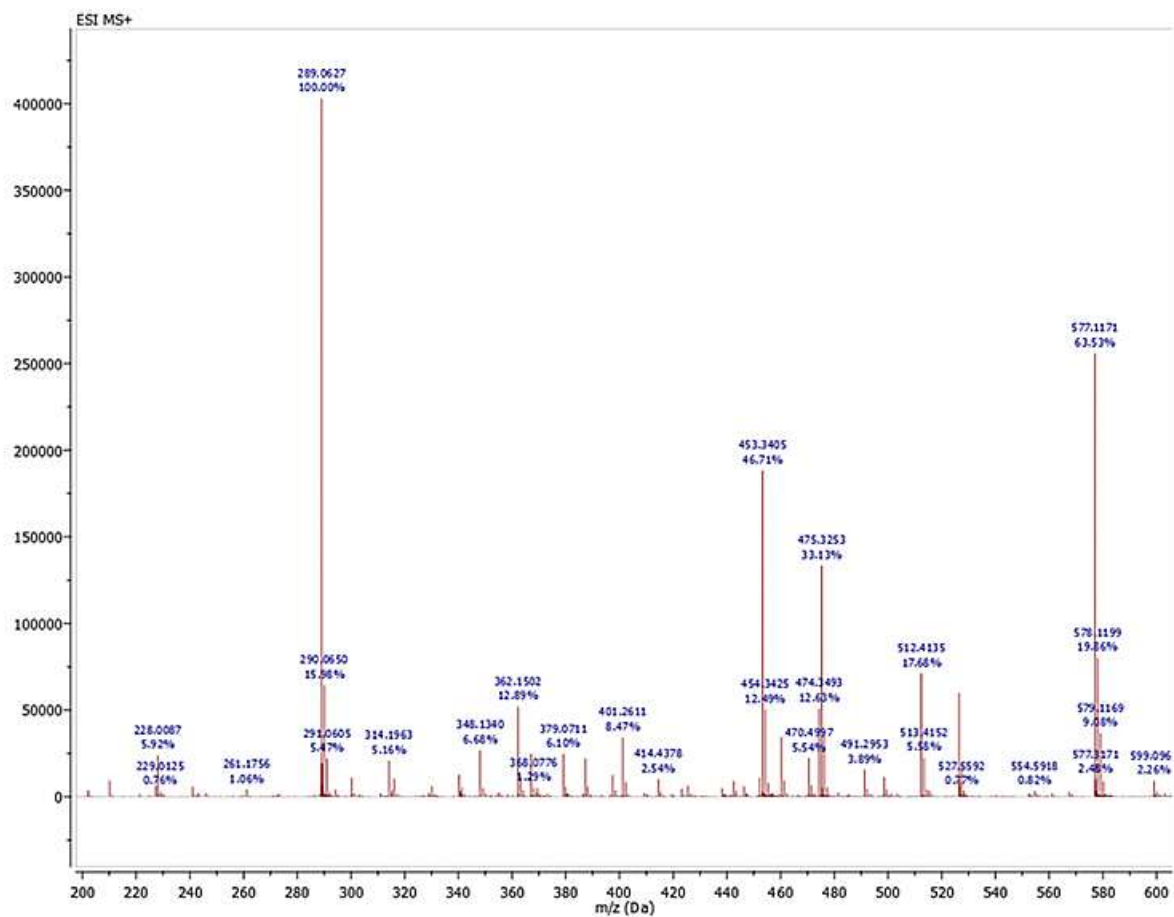
HPLC scan of **3.21**
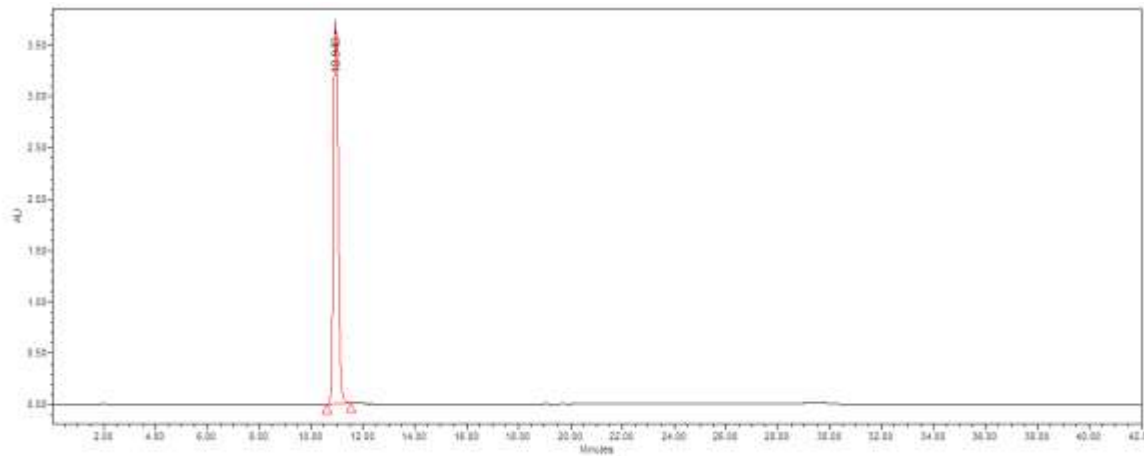
Retention time (min)	% Area
10.948	100

^{1}H NMR spectrum of **3.22**
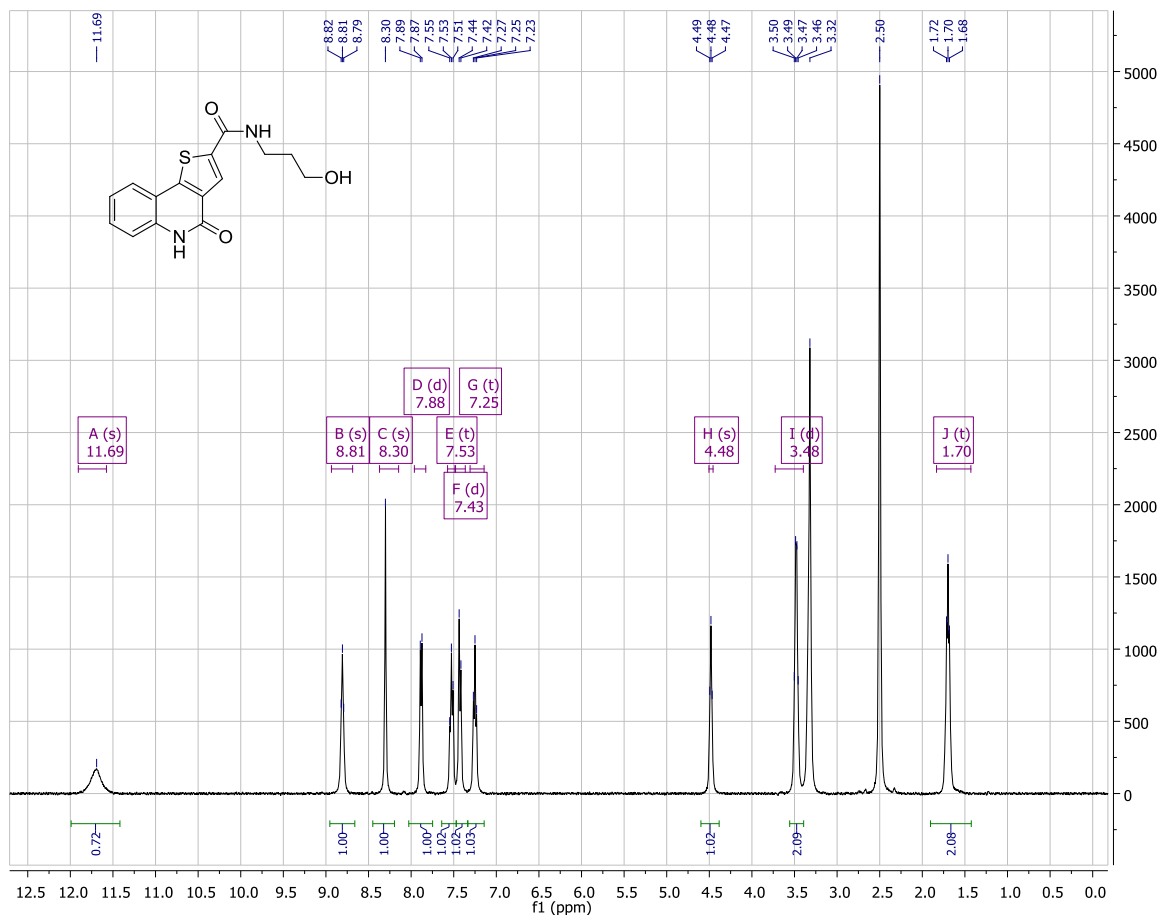
¹H NMR (D₂O wash) spectrum of **3.22**
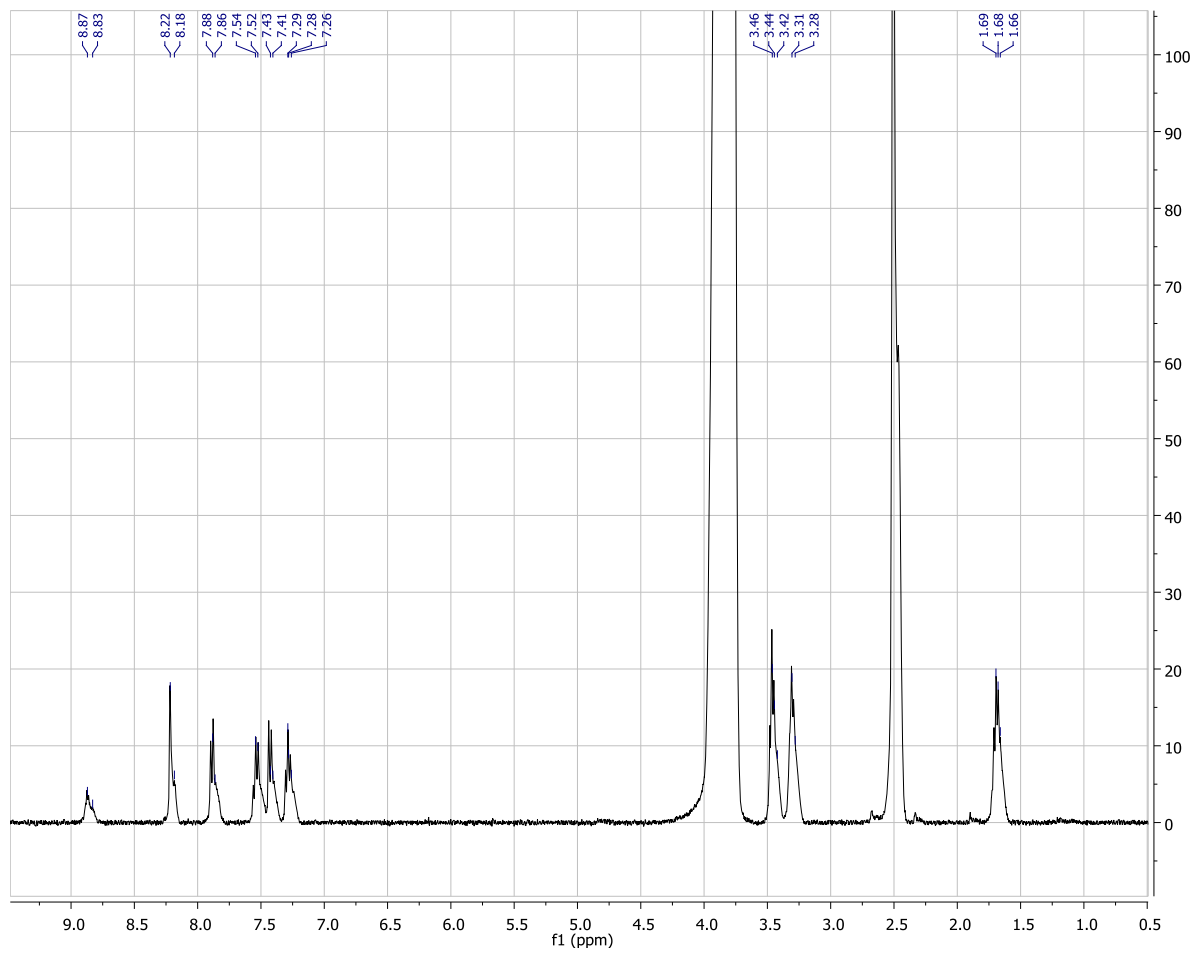
¹³C NMR spectrum of **3.22**
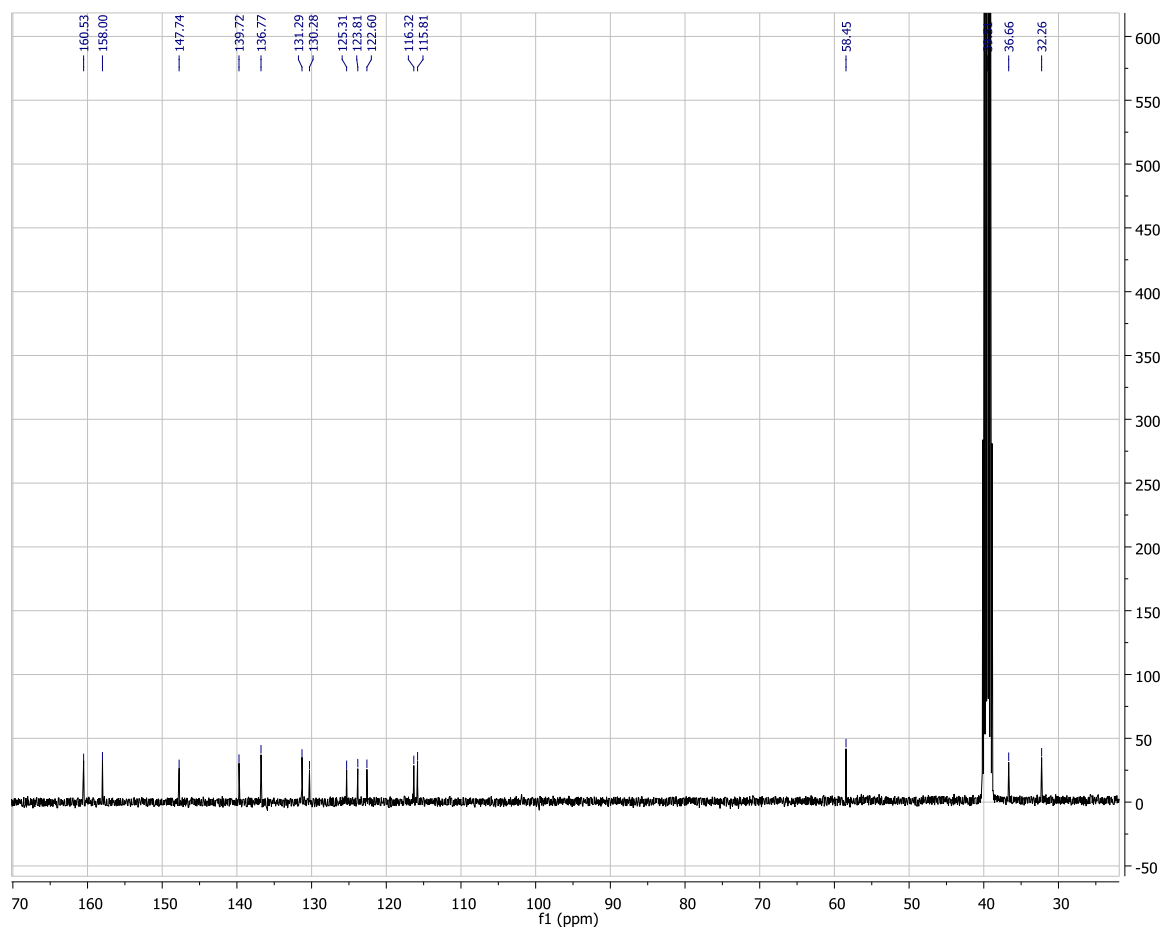
HRMS (TOF) of **3.22**
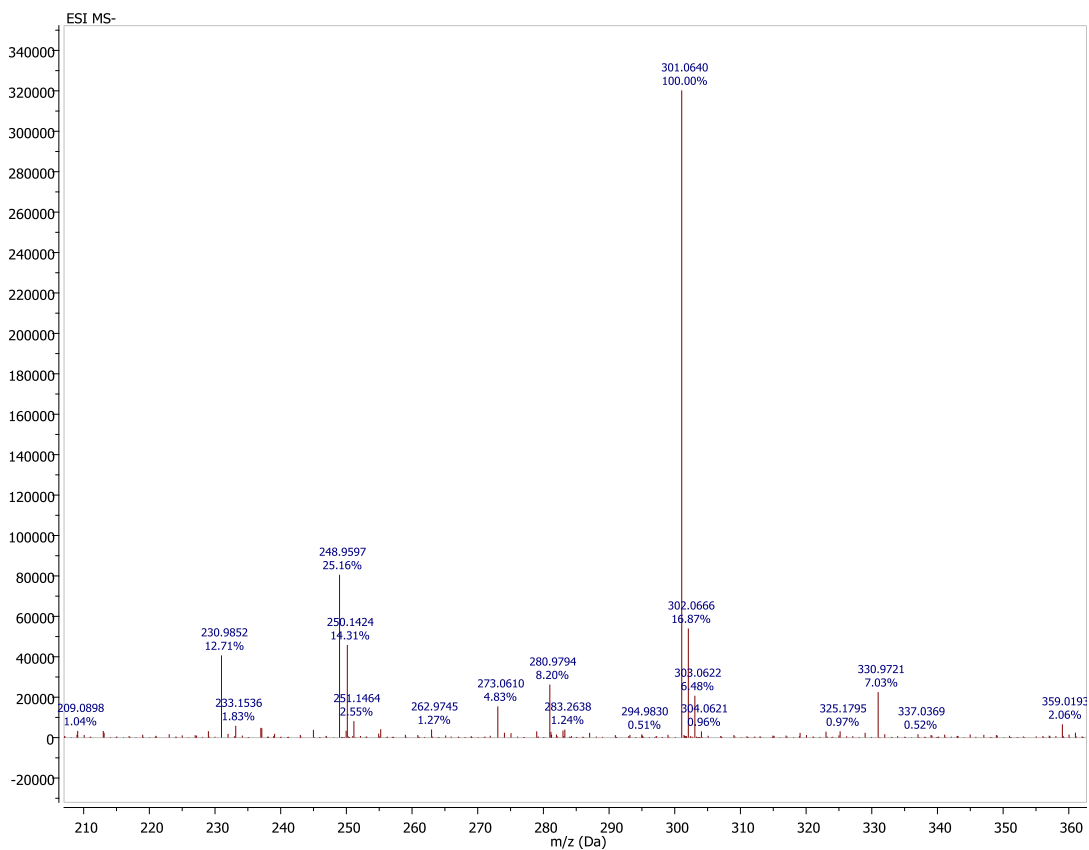
HPLC scan of **3.22**
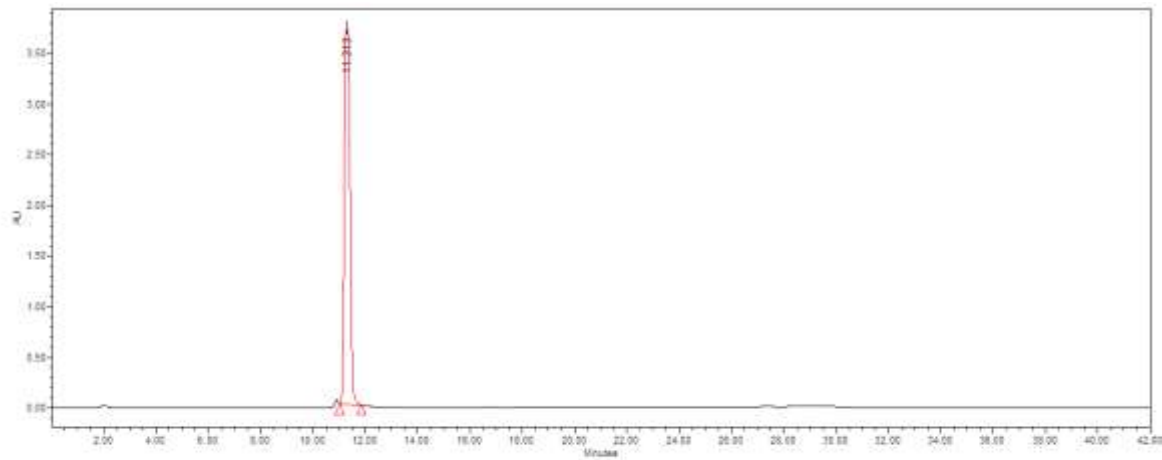
Retention time (min)	% Area
11.313	99.35

189
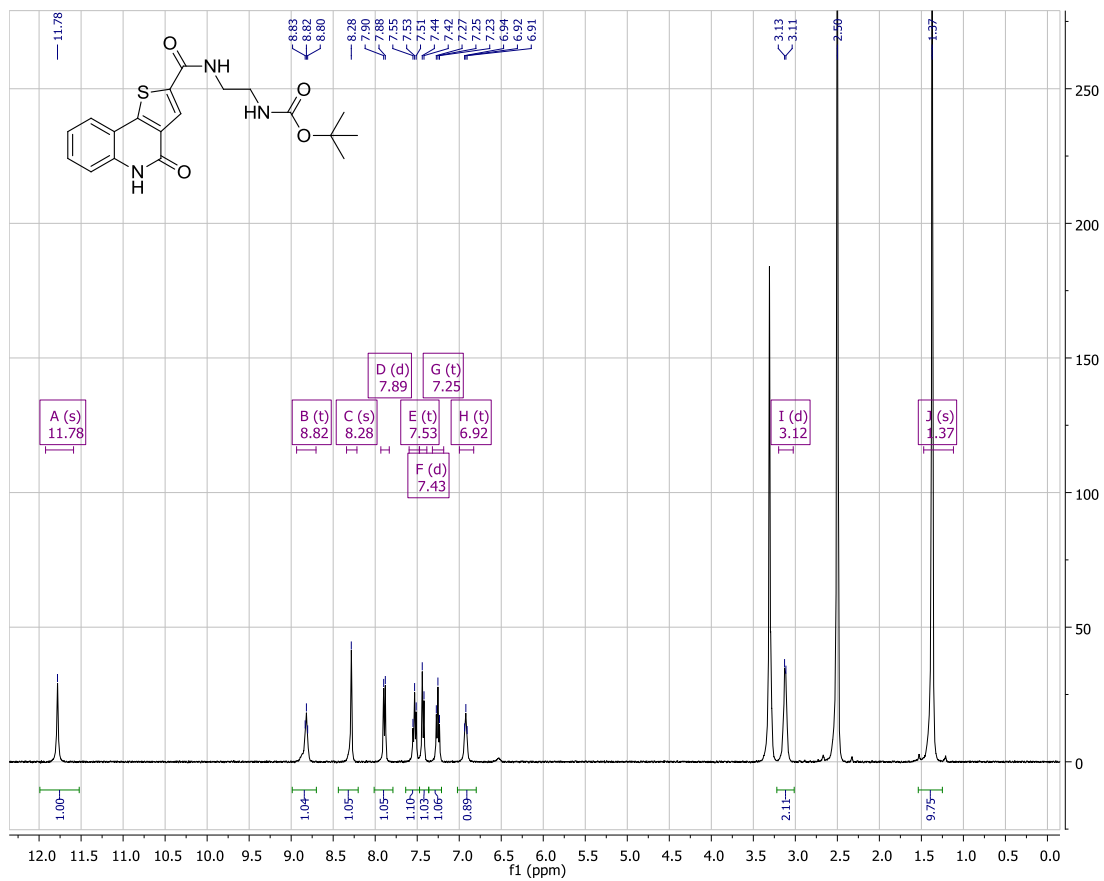
^{1}H NMR spectrum of **3.23**
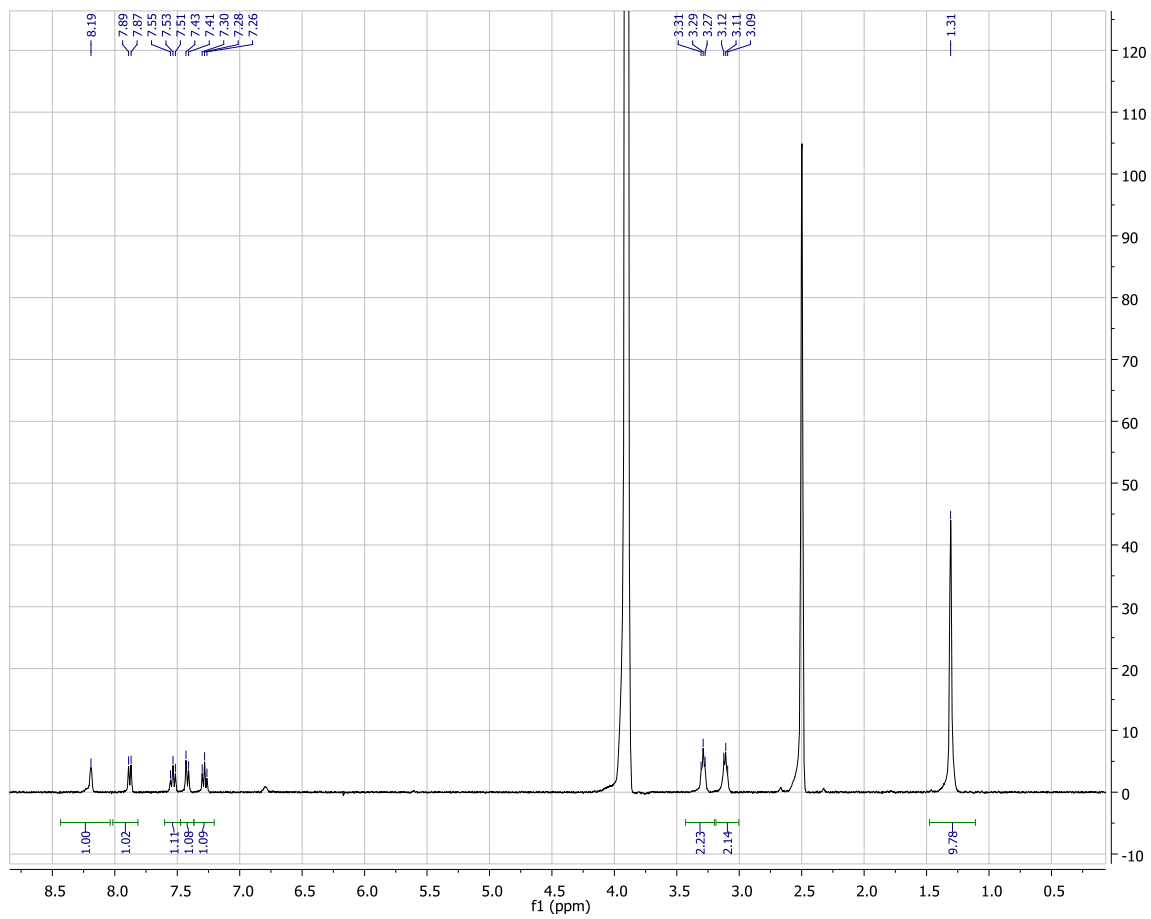
¹³C NMR spectrum of **3.23**
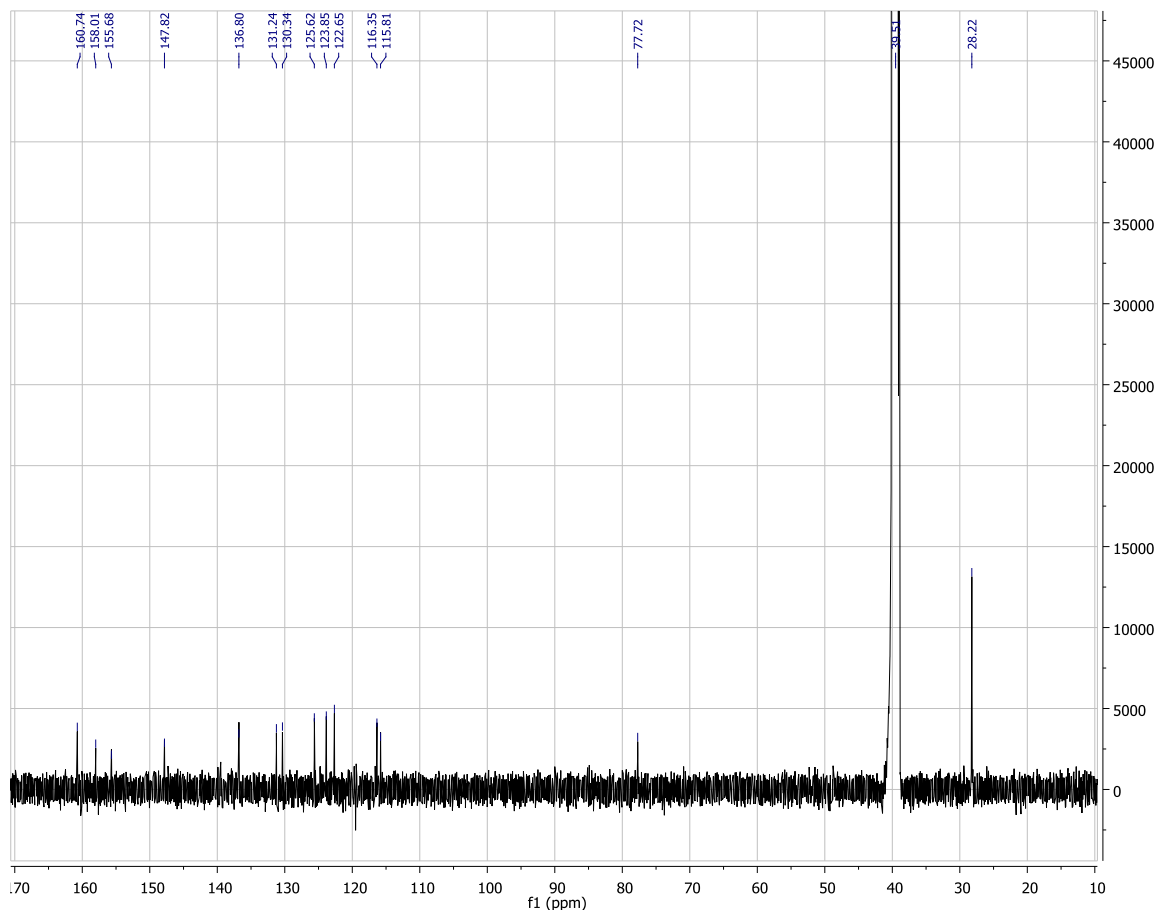
HSQC spectrum of **3.23**
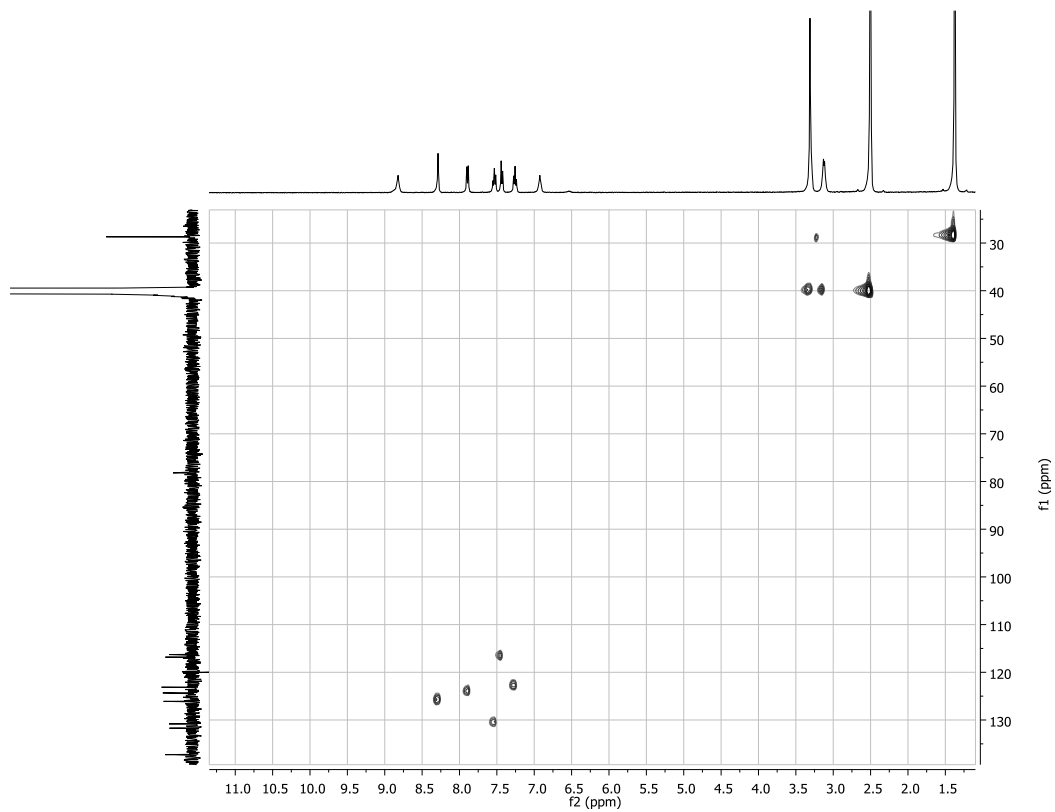
HRMS (TOF) of **3.23**
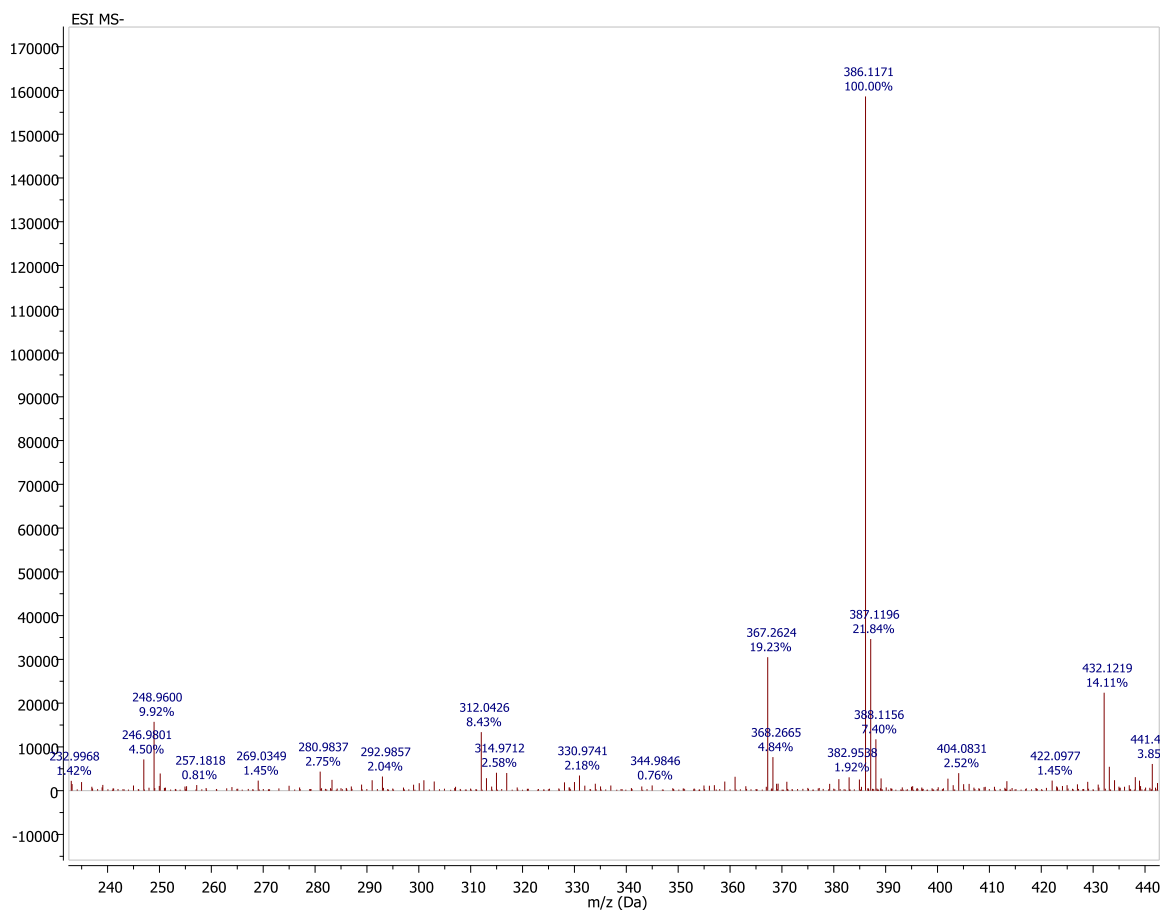
^{1}H NMR spectrum of **3.24**
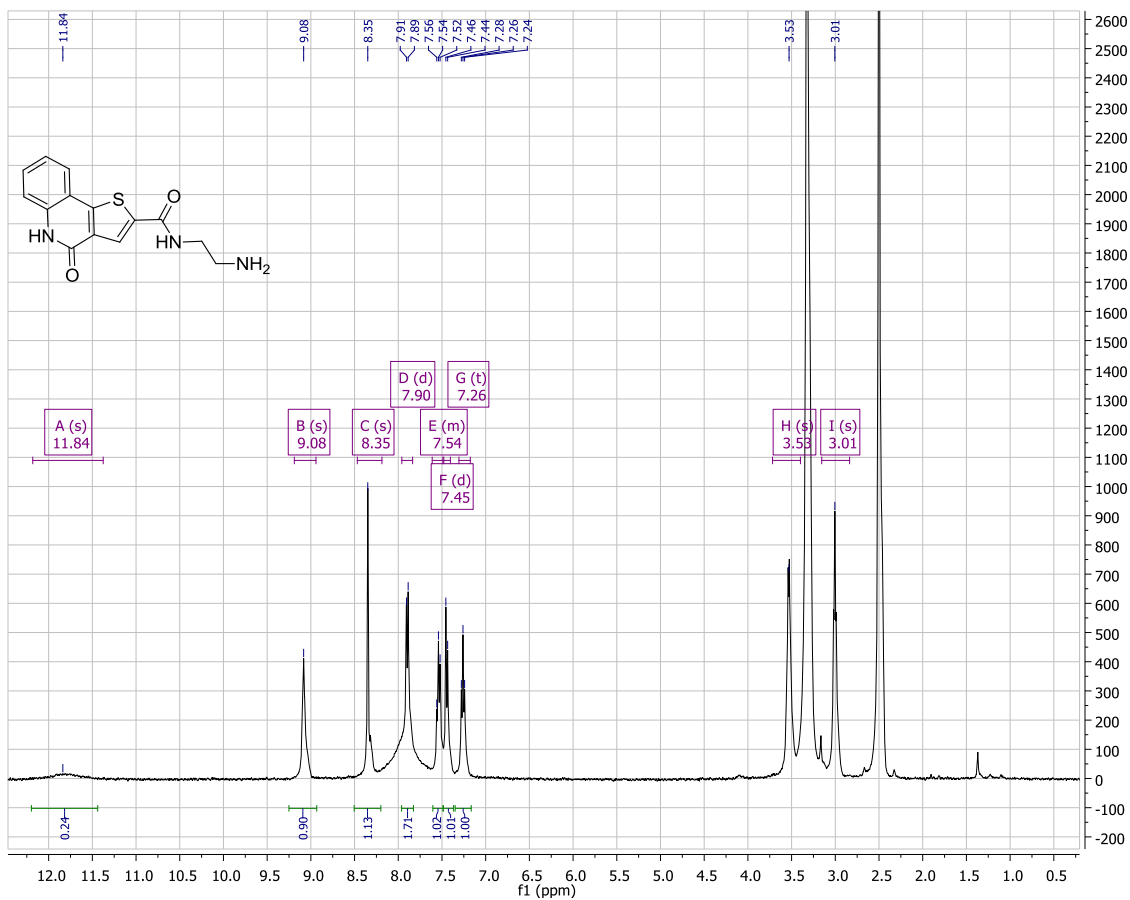
¹H NMR (D₂O wash) spectrum of **3.24**
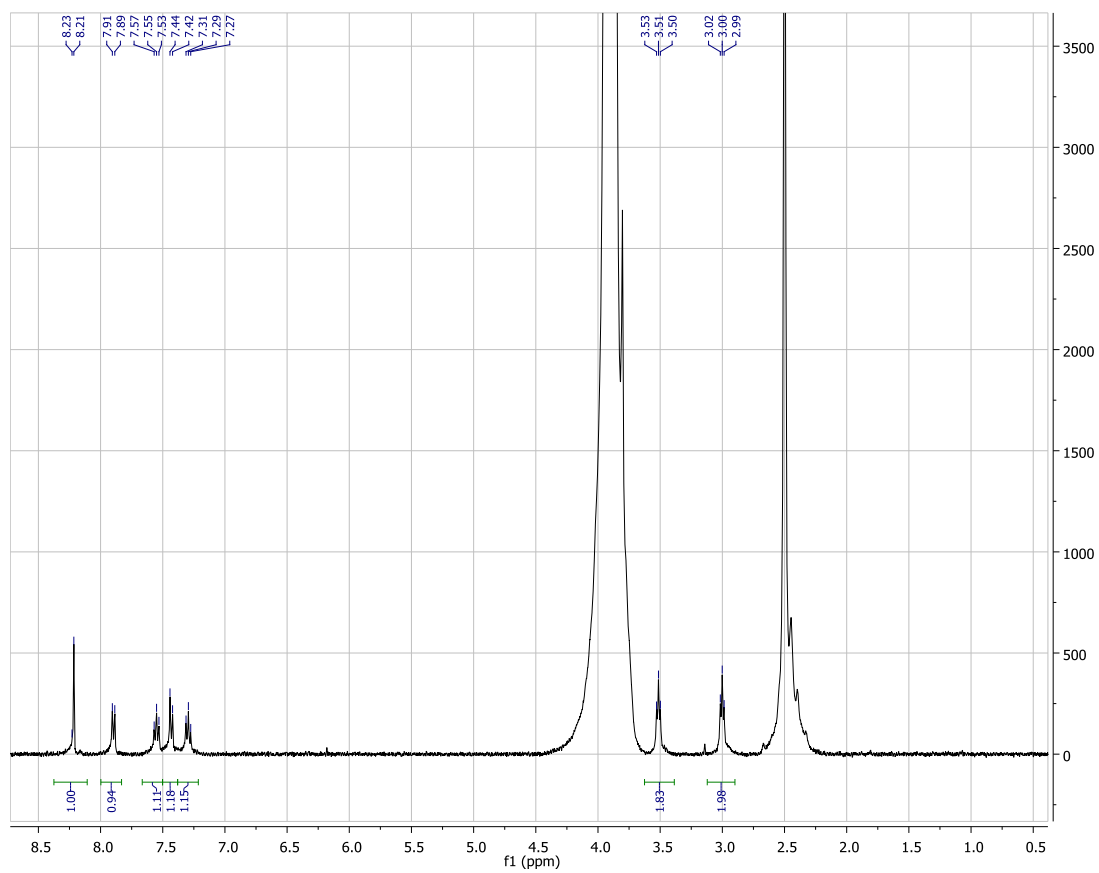
¹³C NMR spectrum of **3.24**
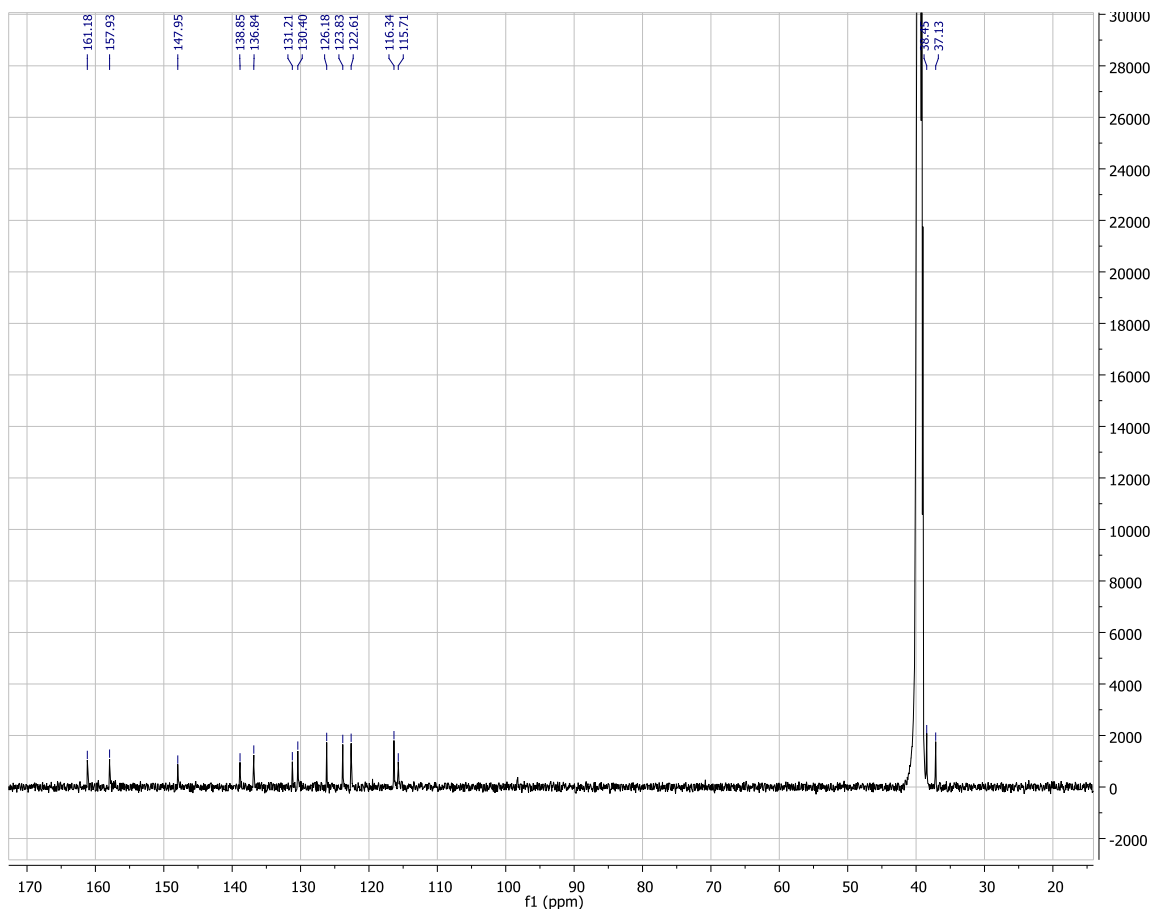
HRMS (TOF) of **3.24**
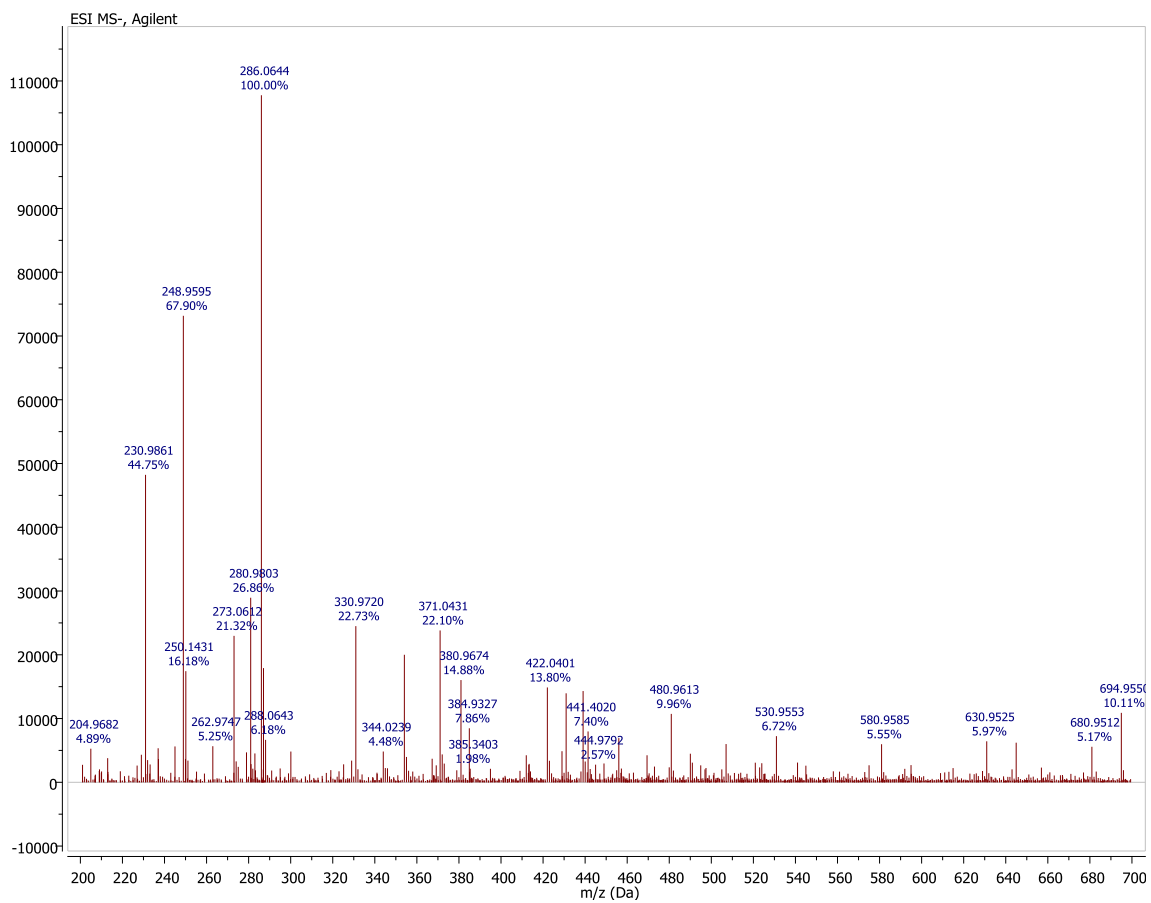
HPLC scan of **3.24**
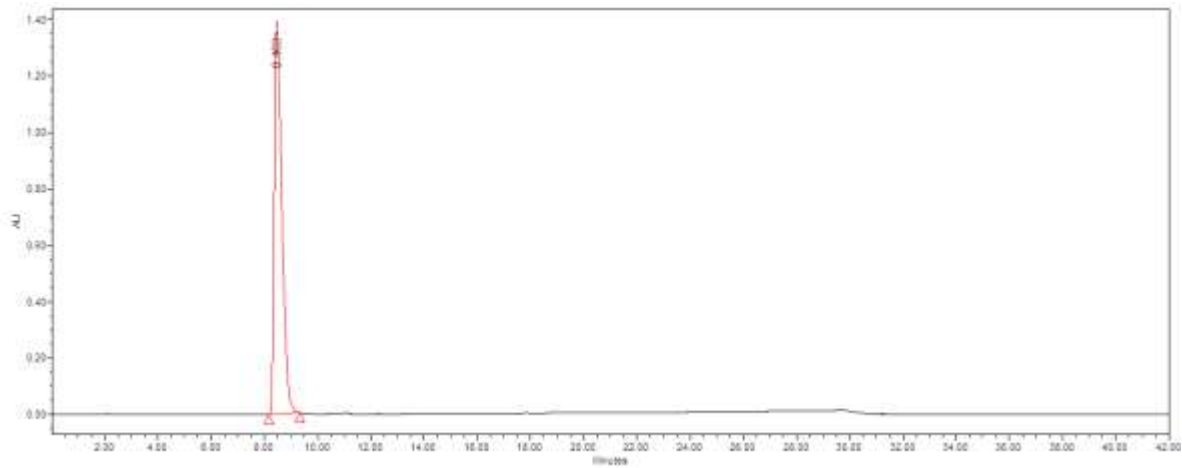
Retention time (min)	% Area
8.463	100

¹H NMR spectrum of **3.25**

¹³C NMR spectrum of **3.25**

160.51
158.00
155.57
147.78
139.59
136.79
131.28
130.31
125.37
123.82
122.62
116.33
115.81
77.48
29.51
37.73
37.14
29.39
28.24
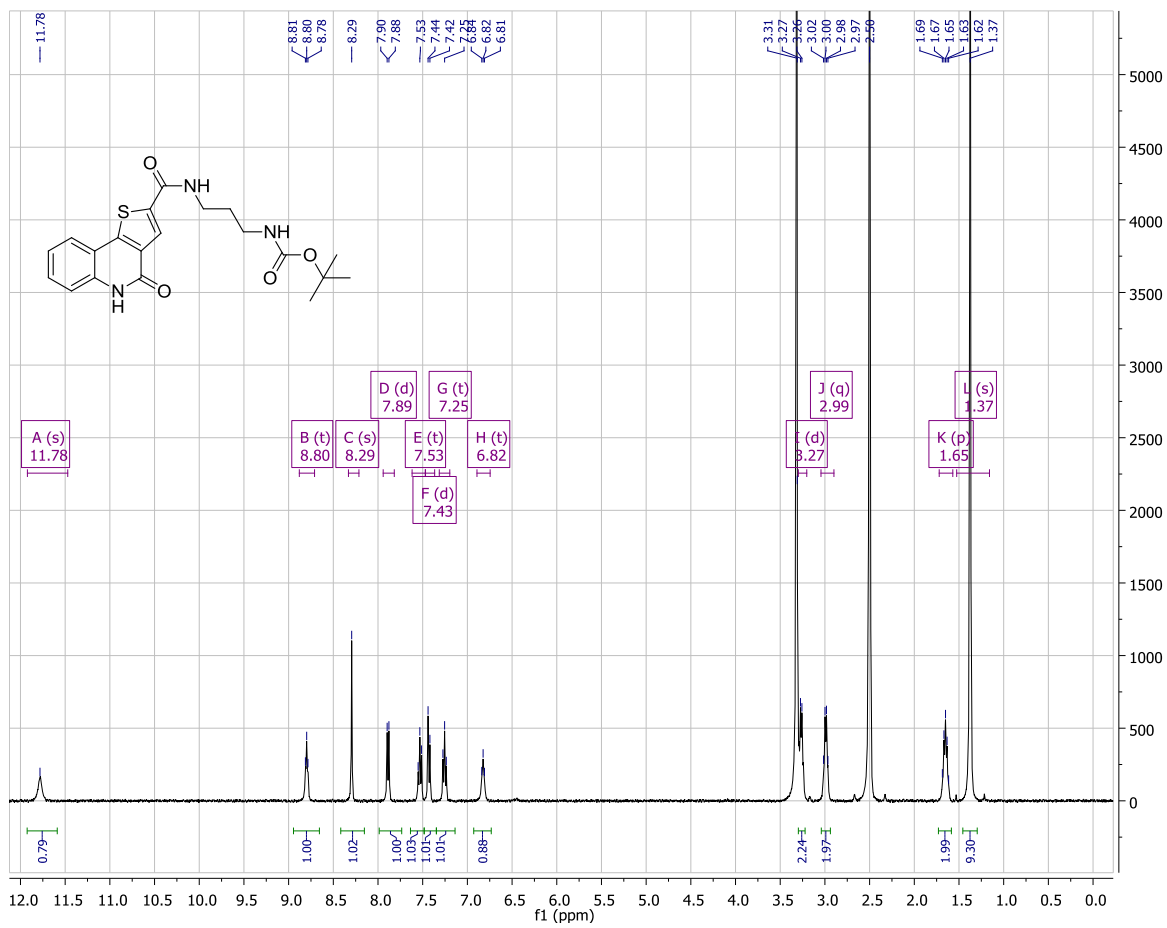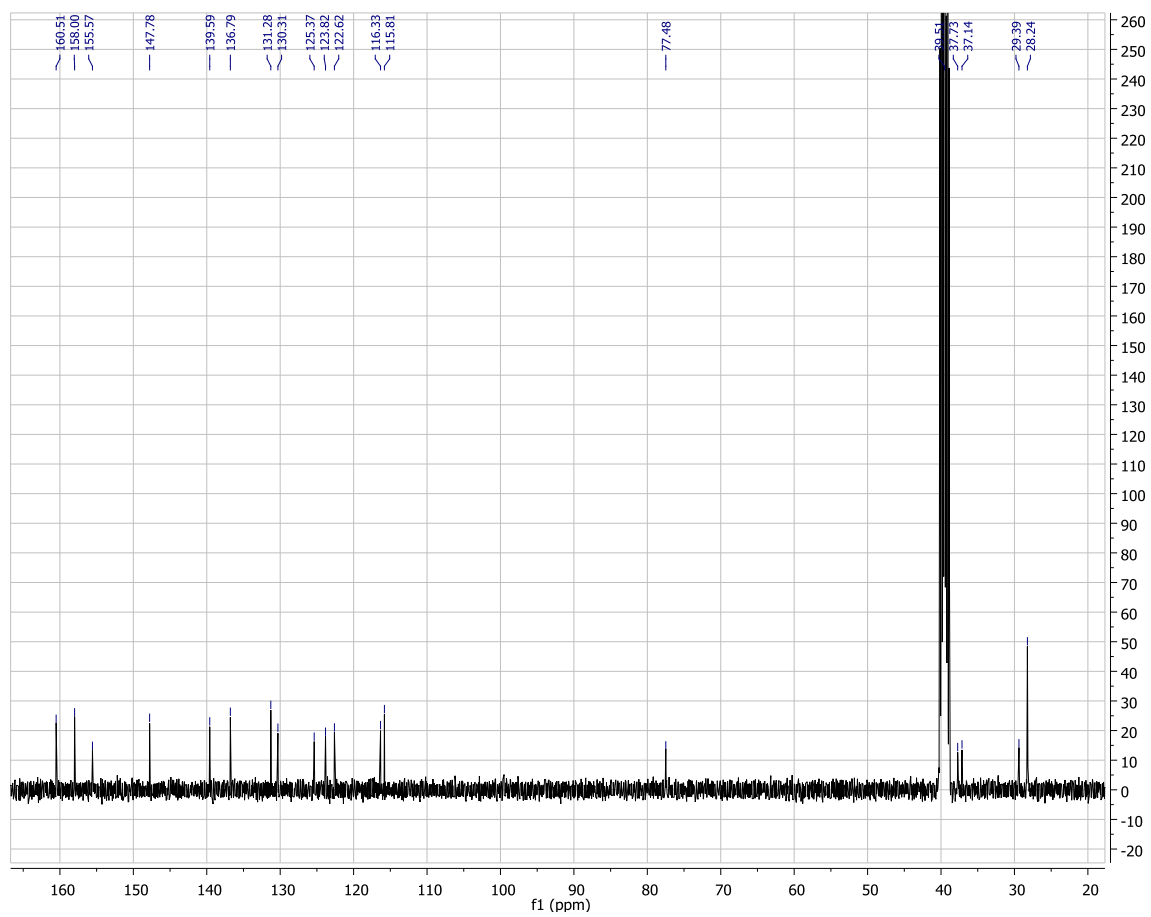
HRMS (TOF) of **3.25**

^{1}H NMR spectrum of **3.26**

¹H NMR (D₂O wash) spectrum of **3.26**
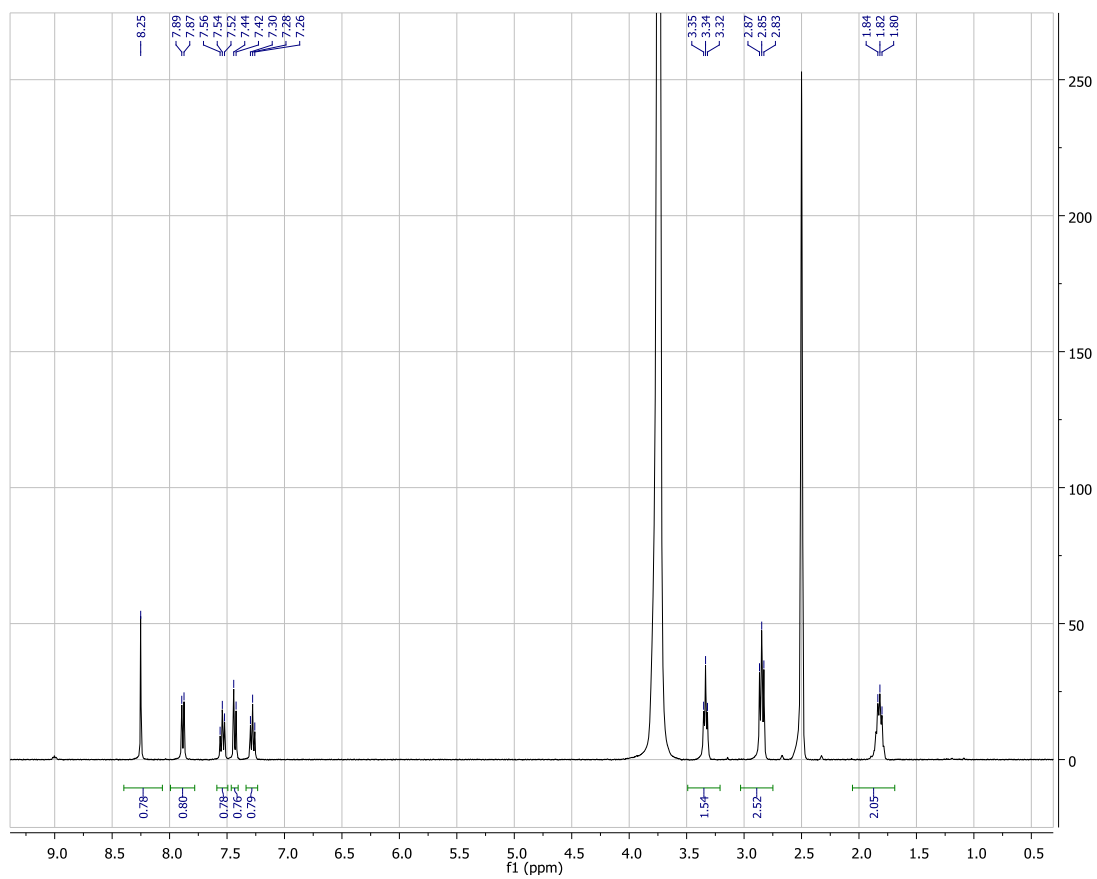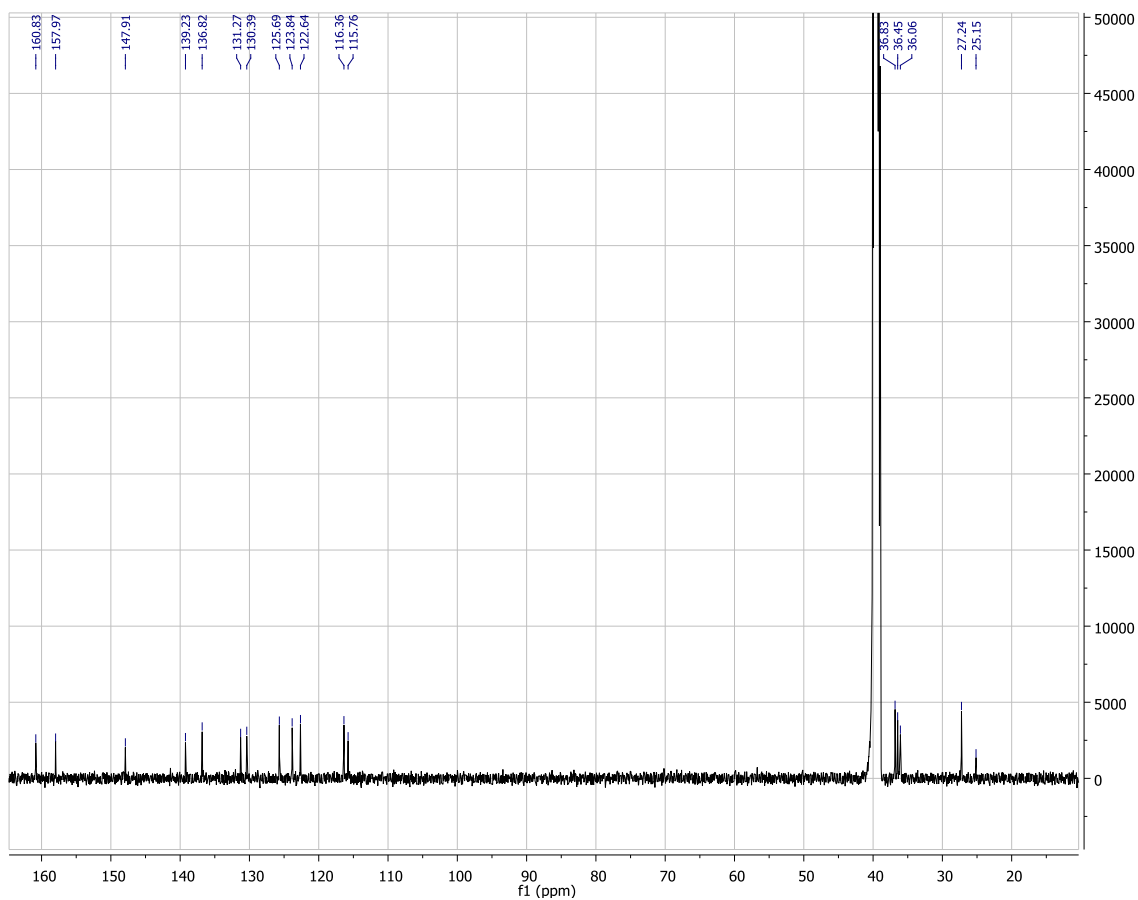
HSQC of **3.26**
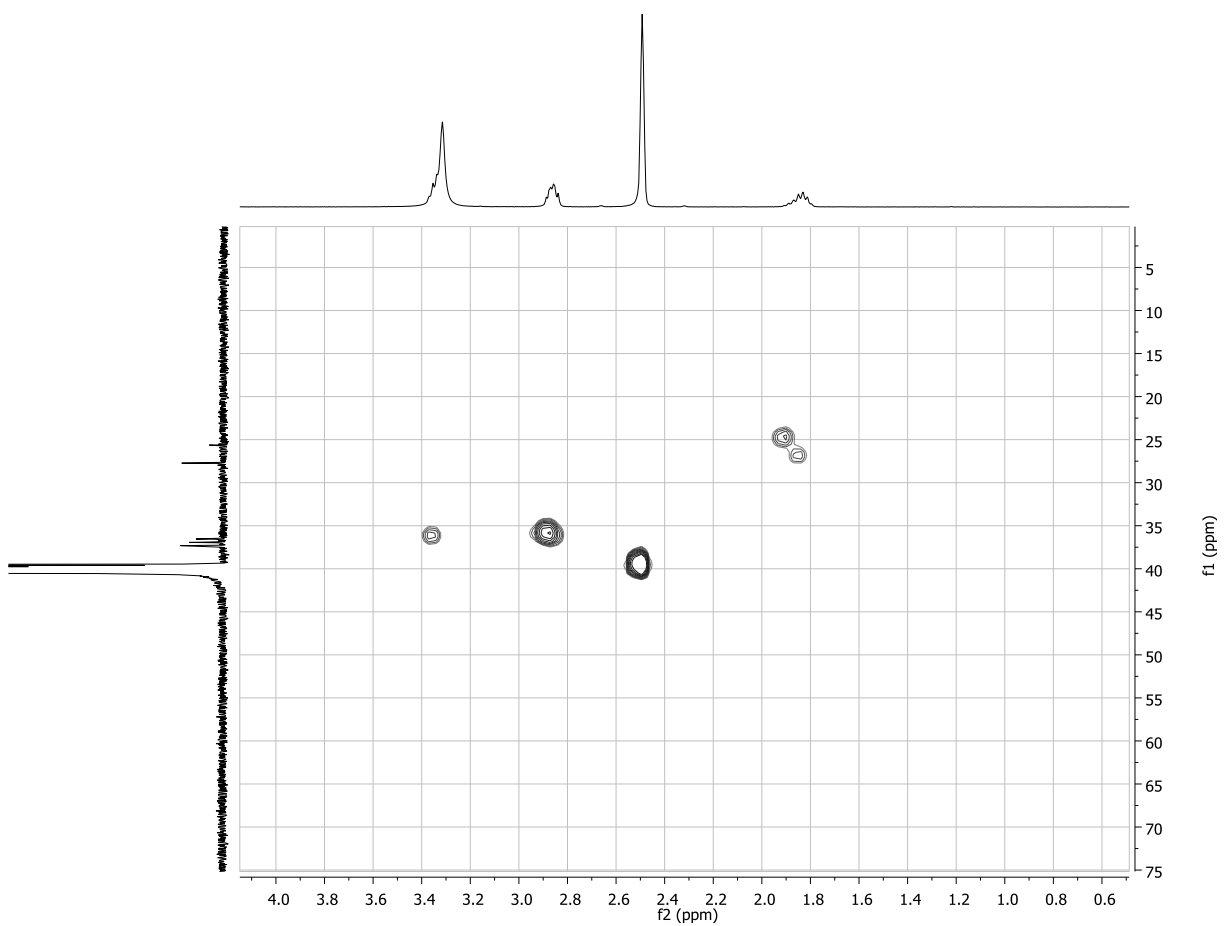
HRMS (TOF) of **3.26**
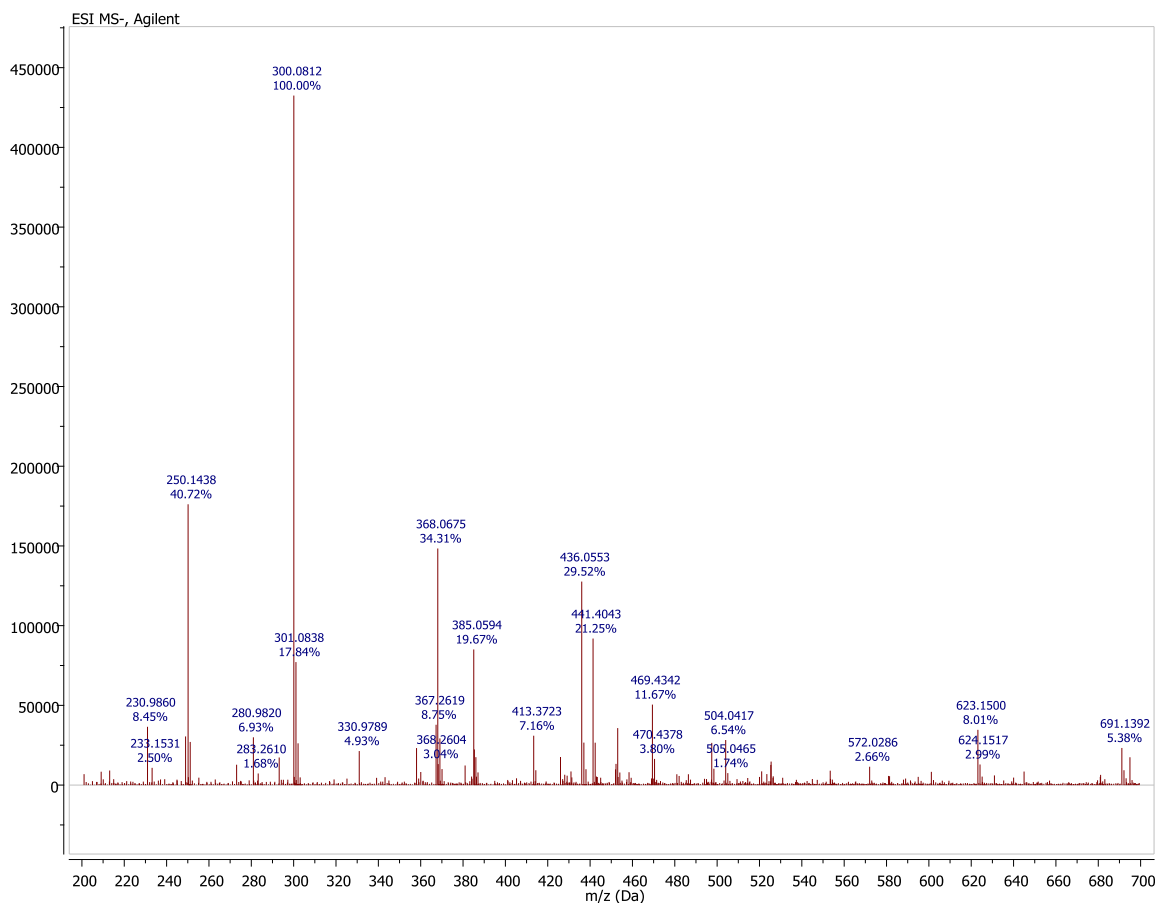
HPLC scan of **3.26**
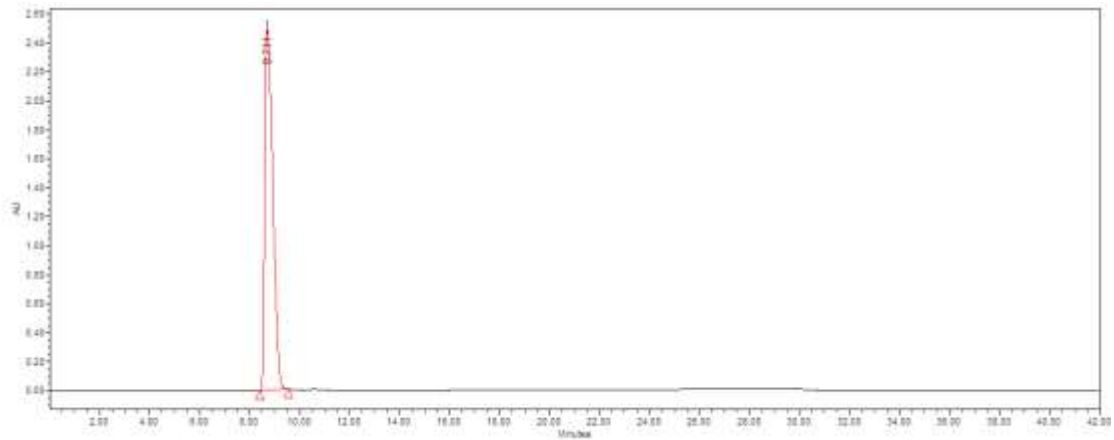
Retention time (min)	% Area
8.711	100

¹³C NMR spectrum of **3.27**

159.33
158.03
148.54
139.47
138.50
136.93
131.36
130.57
128.74
126.75
123.99
122.69
120.21
116.39
115.74
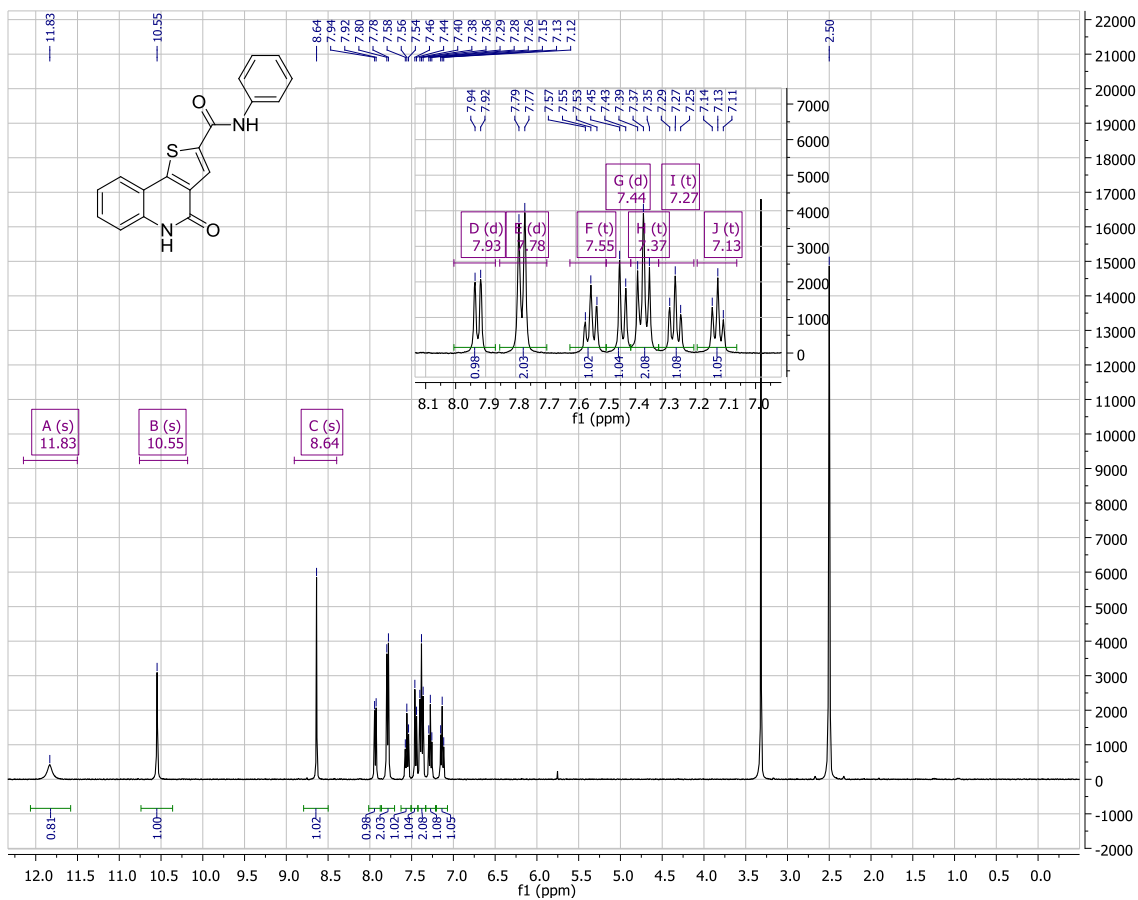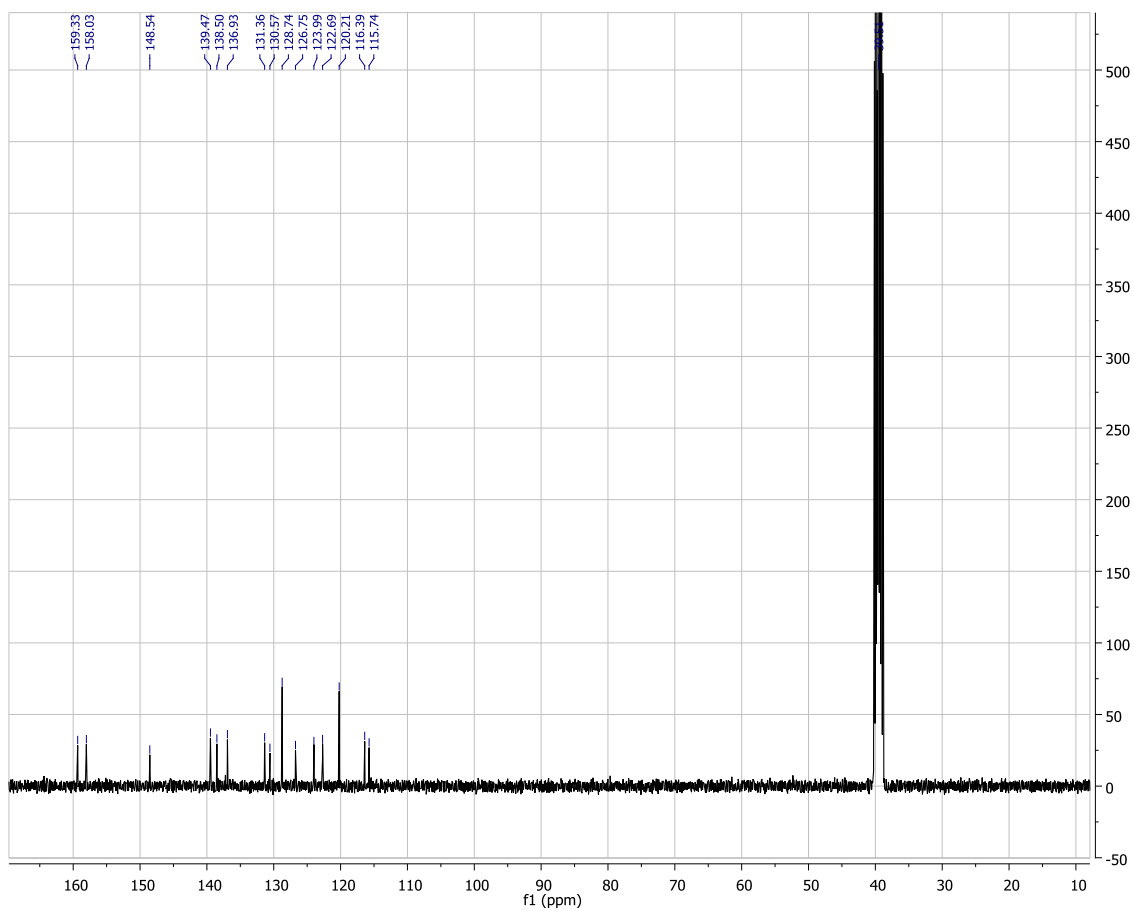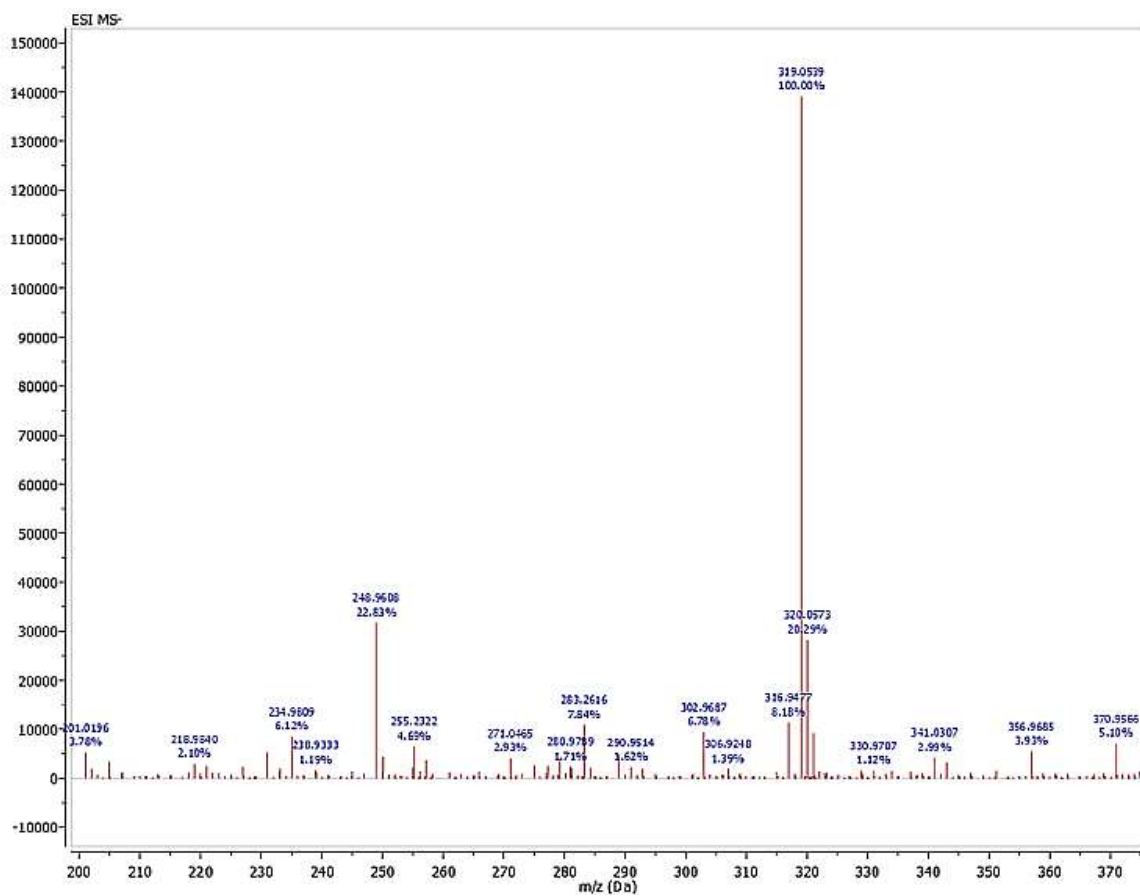
HRMS (TOF) of **3.27**

HPLC scan of **3.27**
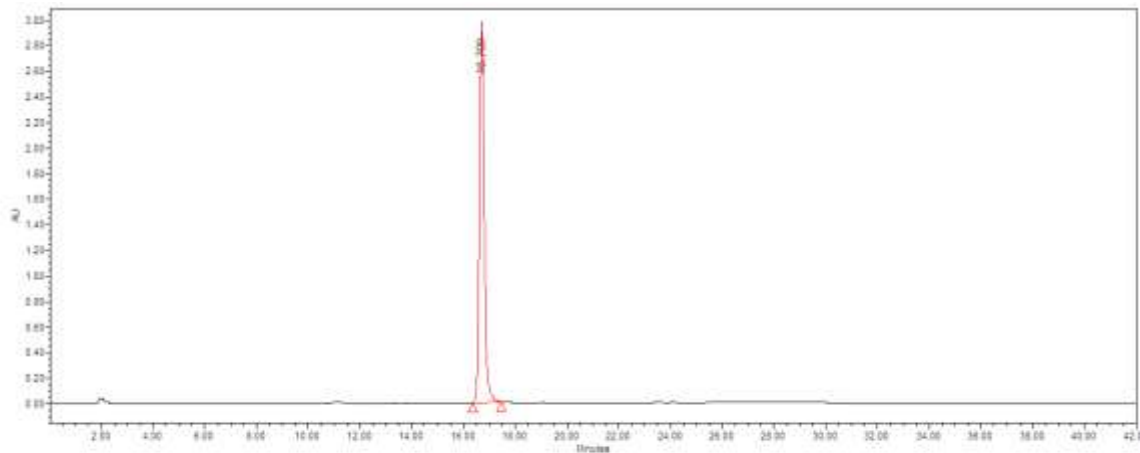
Retention time (min)	% Area
16.709	99.36

^{1}H NMR spectrum of **3.28**
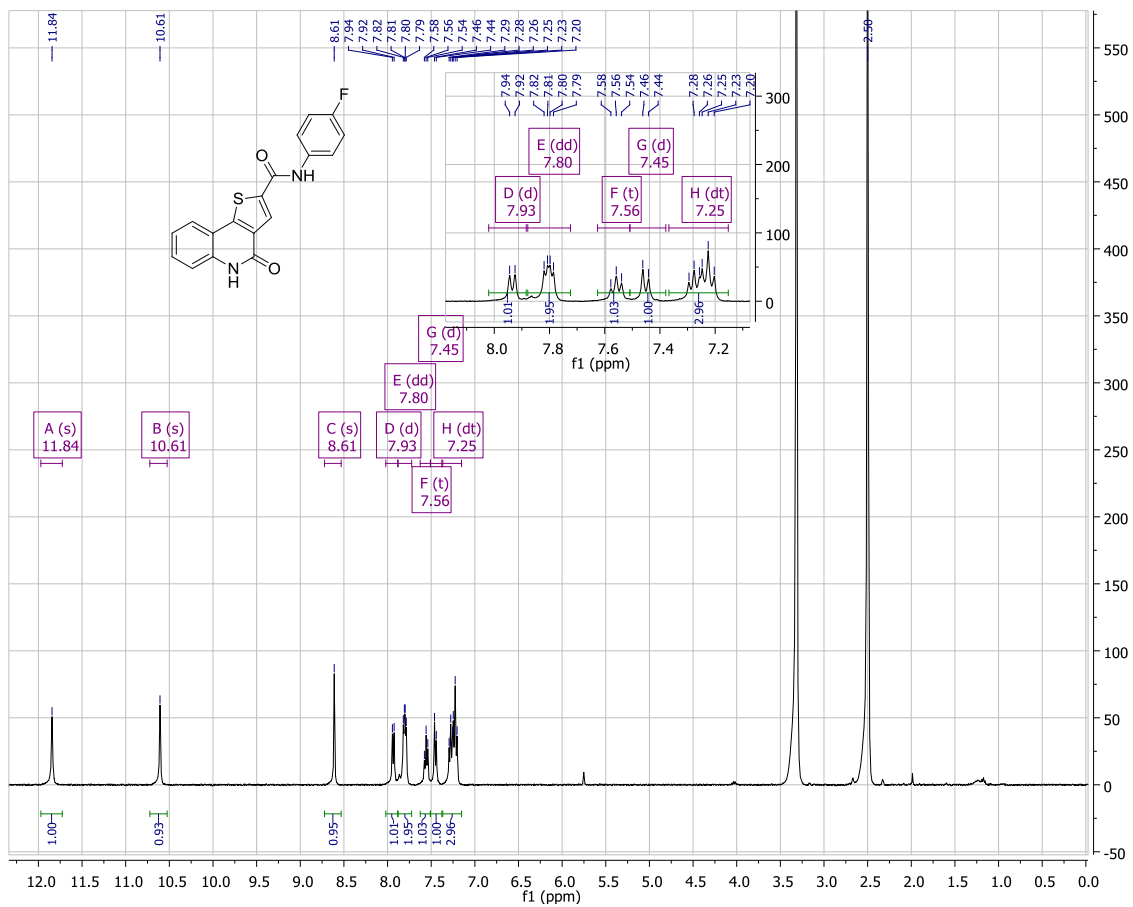
¹³C NMR spectrum of **3.28**
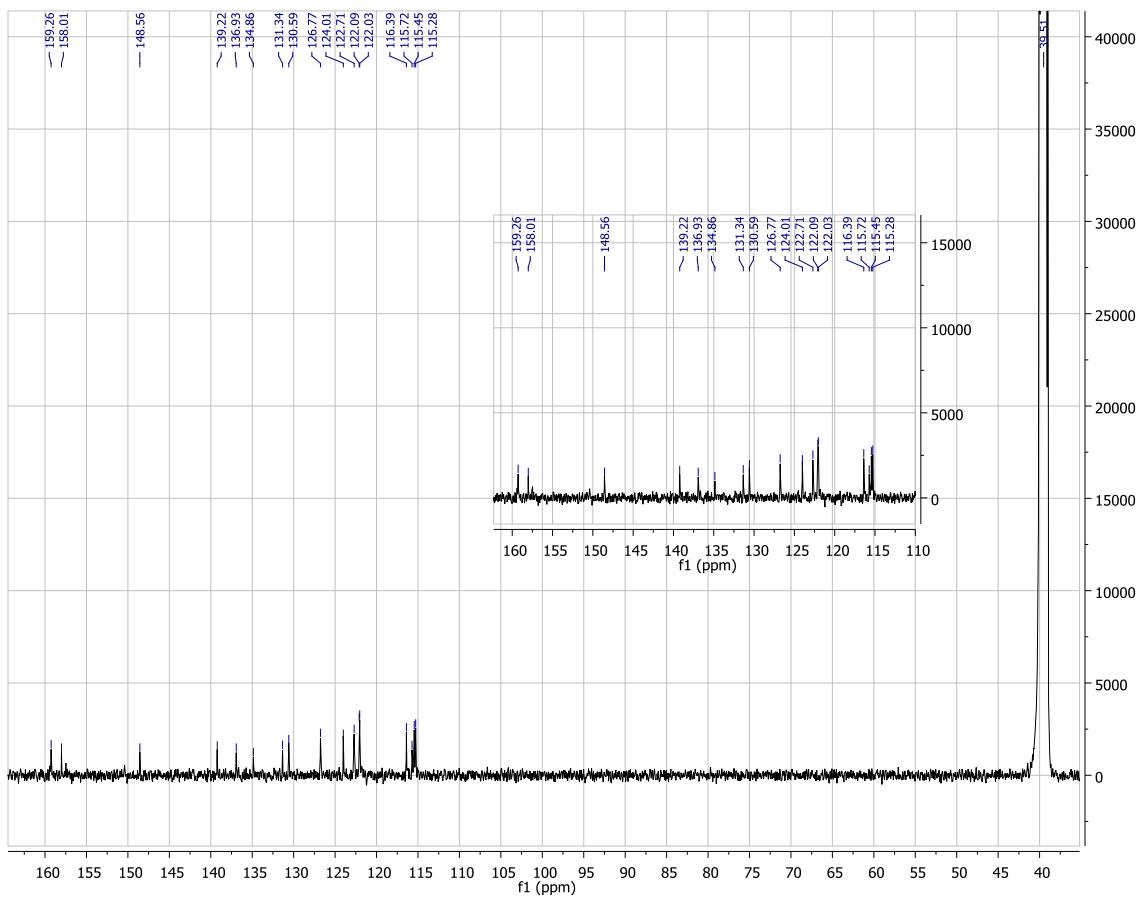
HRMS (TOF) of **3.28**

HPLC scan of **3.28**
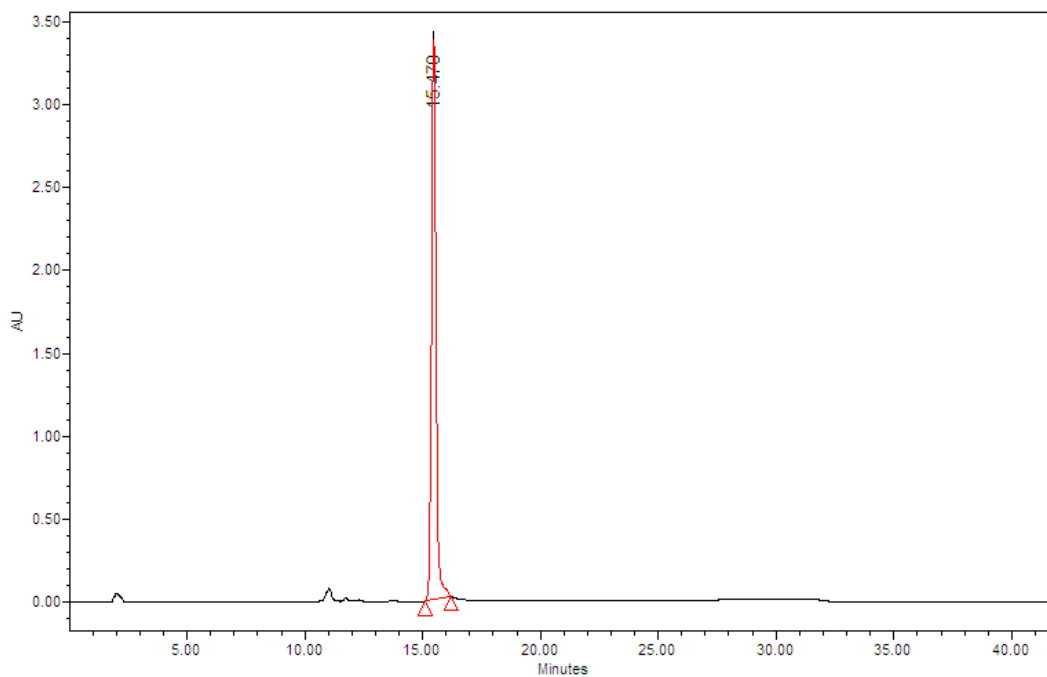
Retention time (min)	% Area
15.470	97.5

¹H NMR spectrum of **3.29**
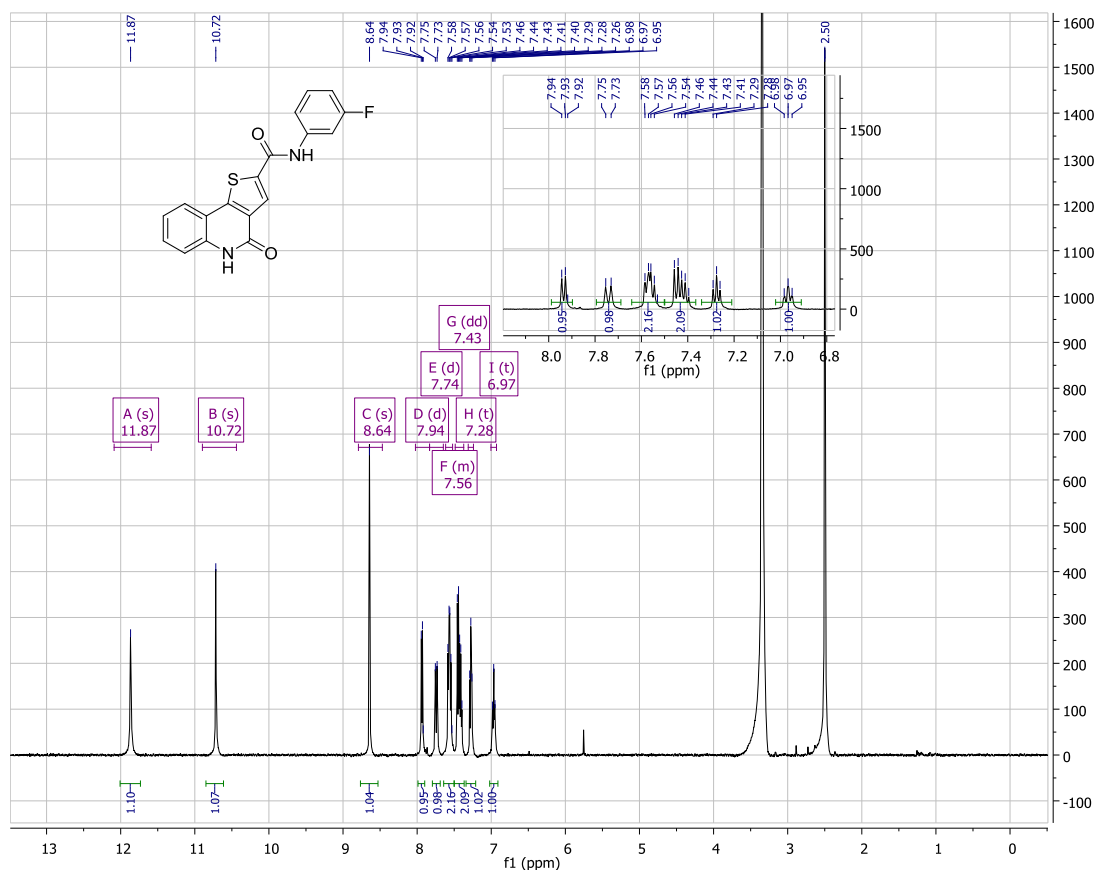
¹³C NMR spectrum of **3.29**
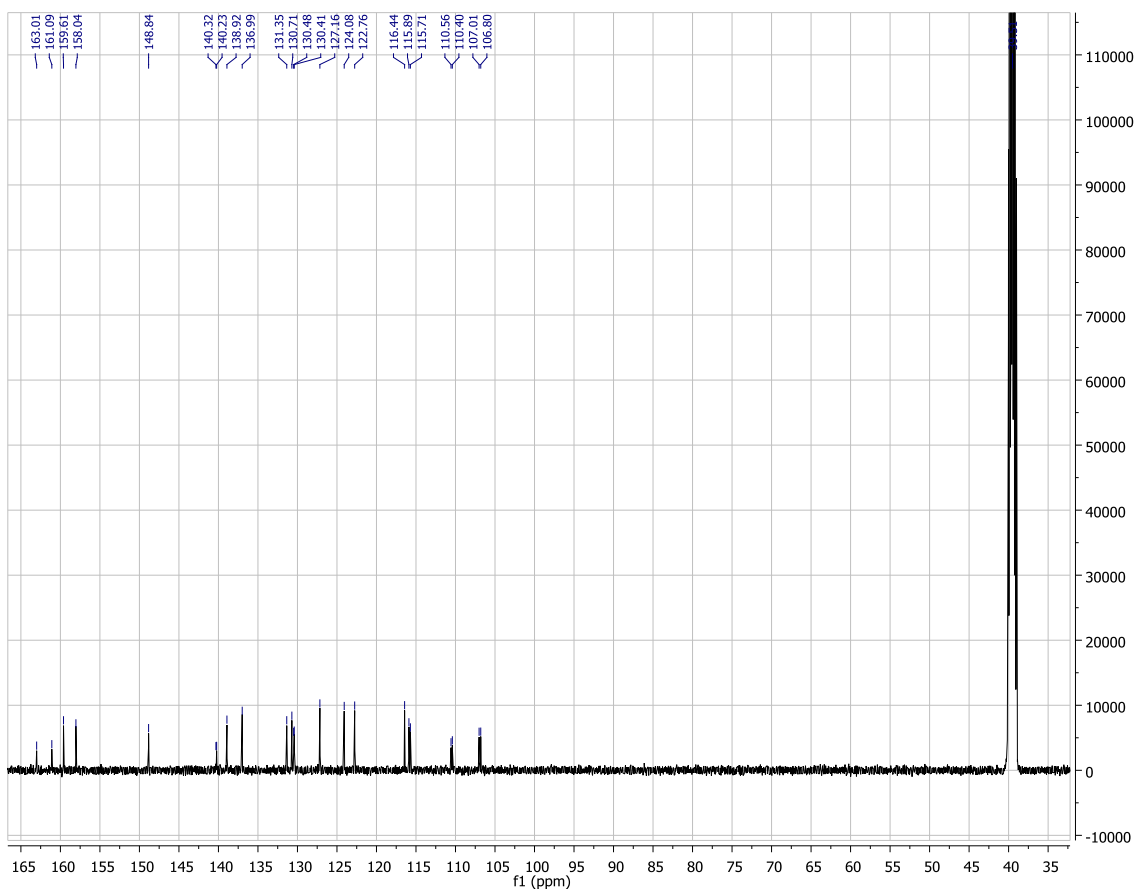
HRMS (TOF) of **3.29**

HPLC scan of **3.29**
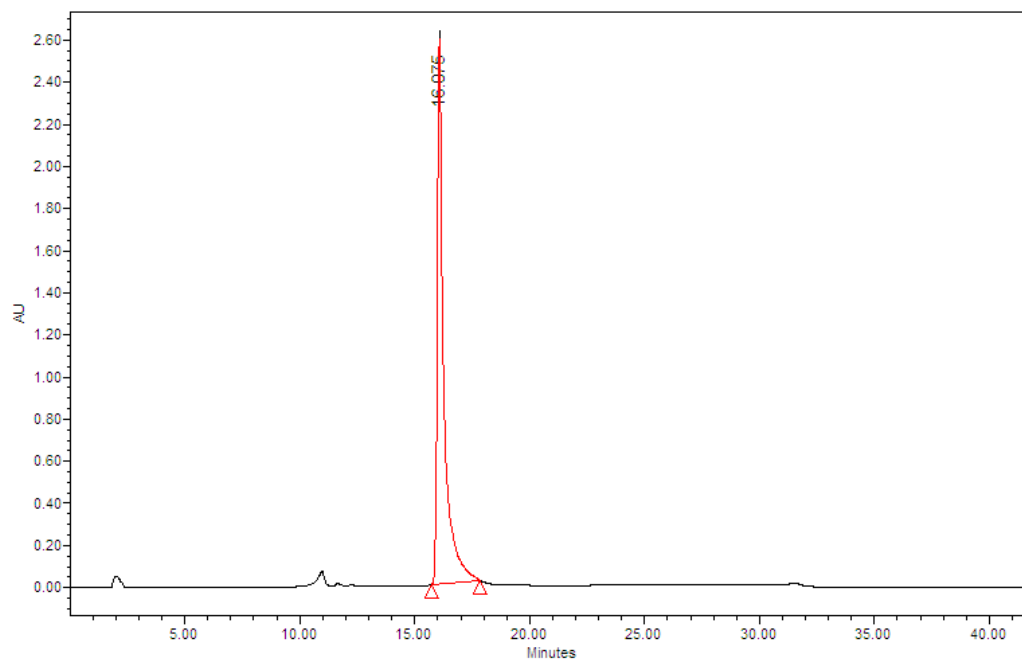
Retention time (min)	% Area
16.076	97.19

^{1}H NMR spectrum of **3.30**
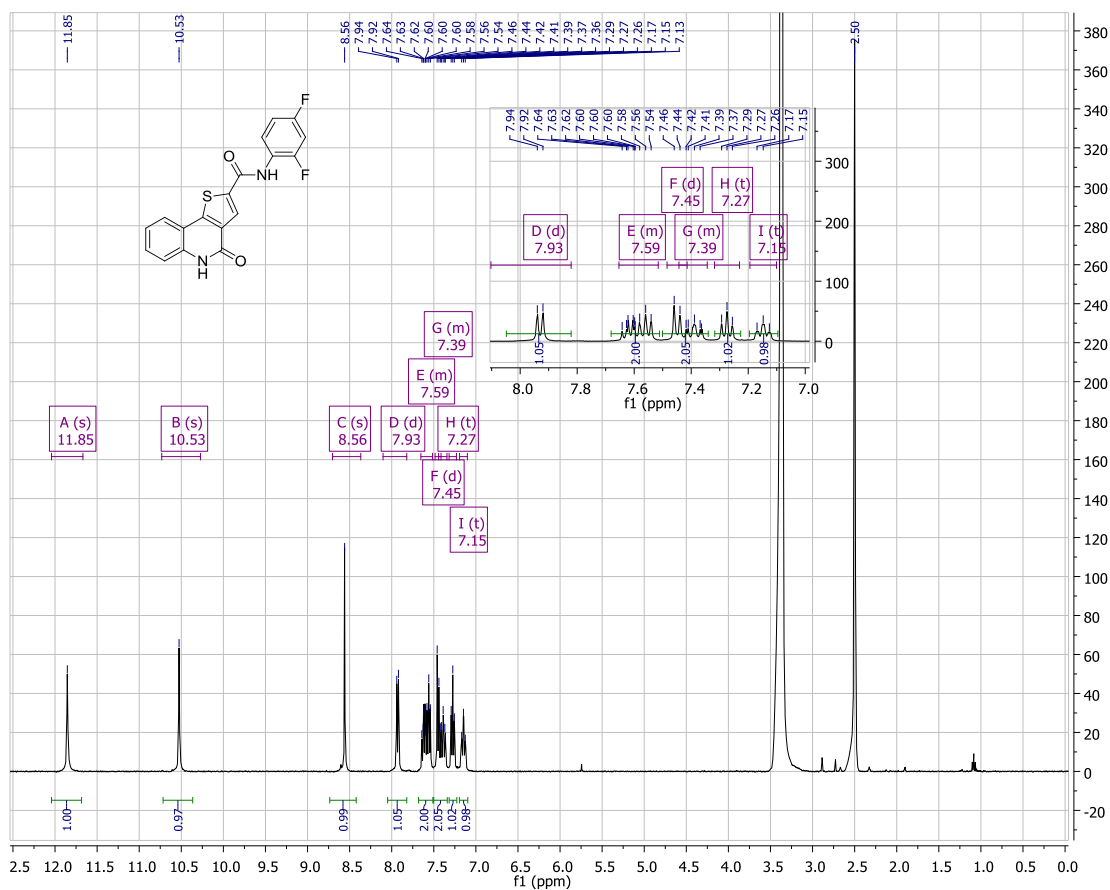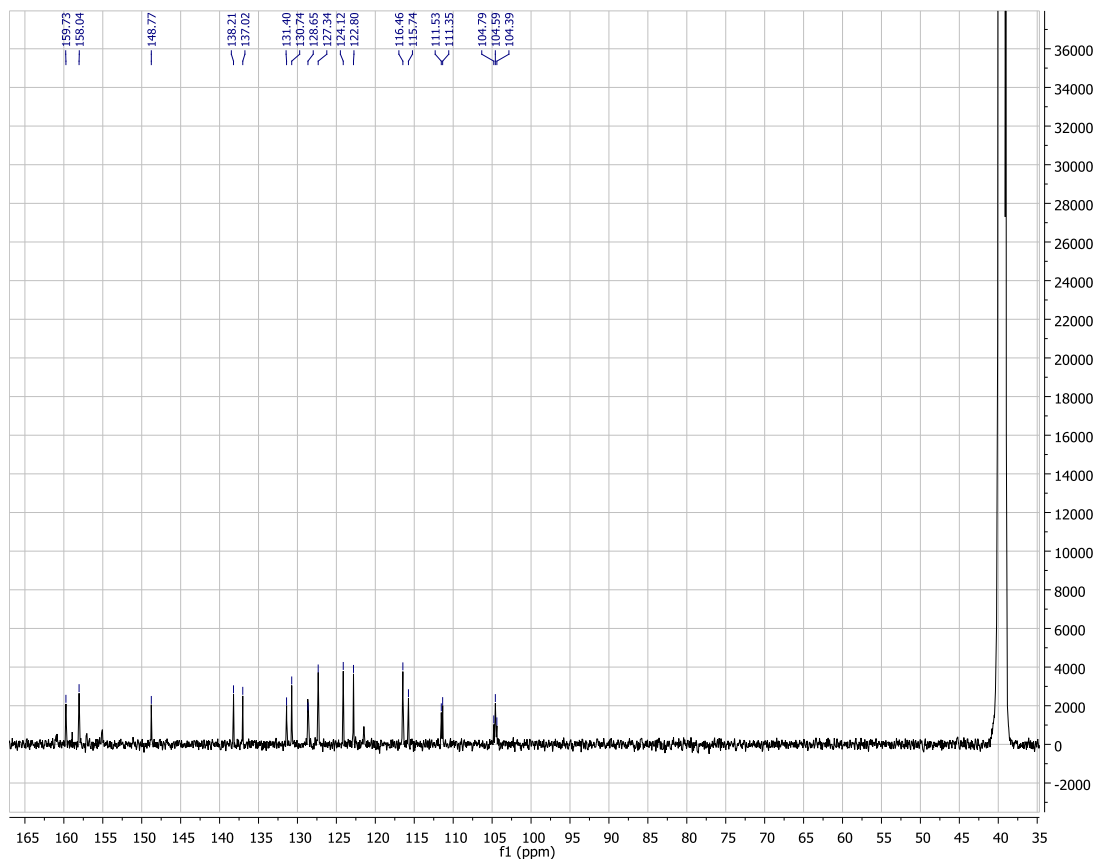
HRMS (TOF) of **3.30**
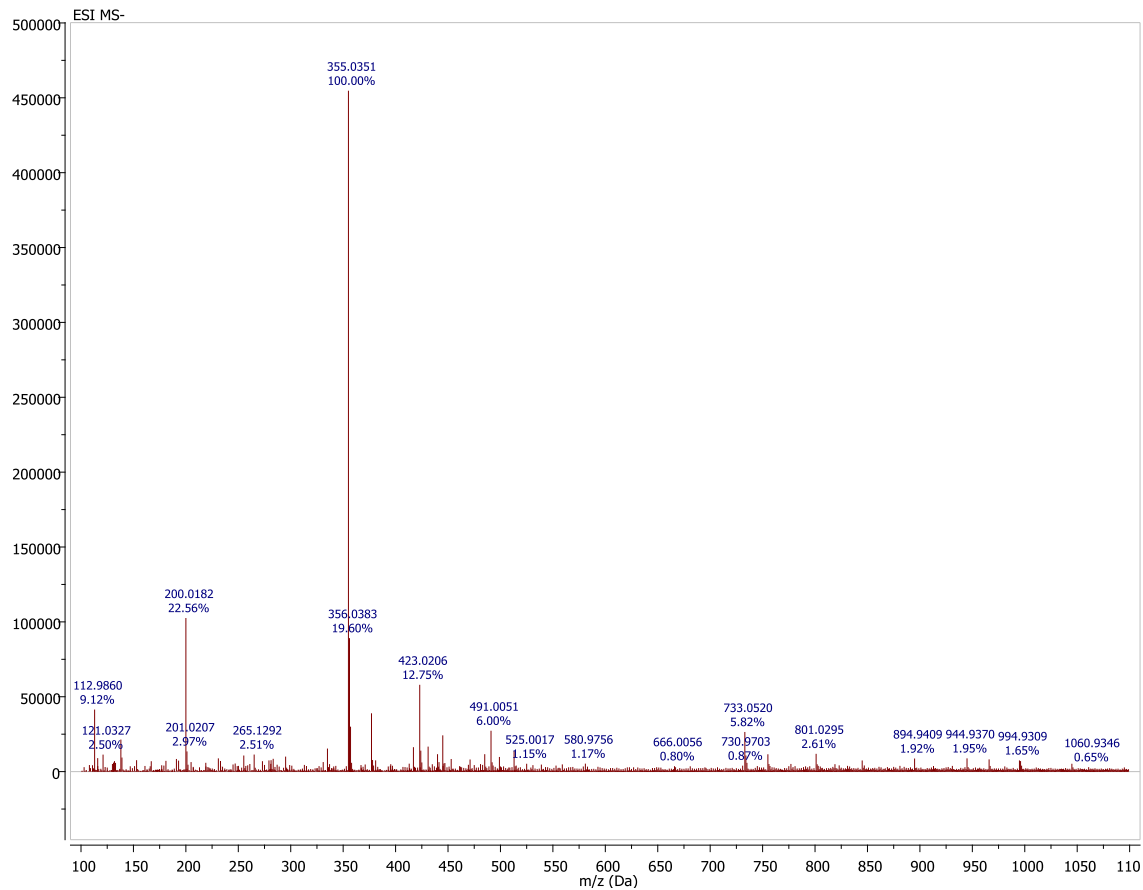
HPLC scan of **3.30**
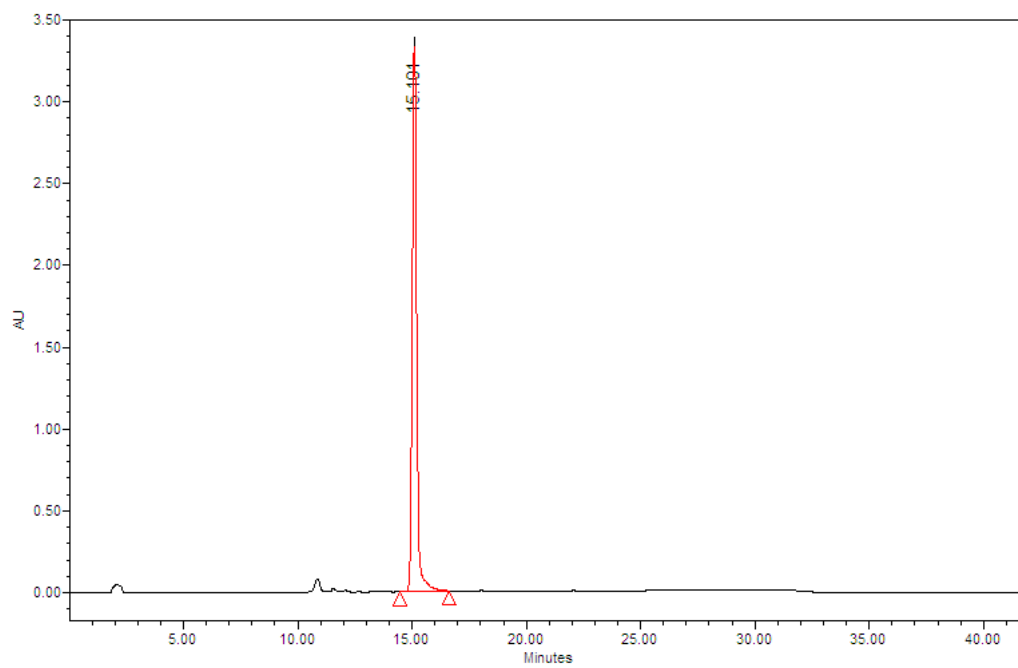
Retention time (min)	% Area
15.101	97.29

¹³C NMR spectrum of **3.31**

160.65
158.02
148.02
139.33
139.10
136.86
131.35
130.42
128.39
127.38
126.96
125.74
123.91
122.67
116.38
115.81
42.75
39.5
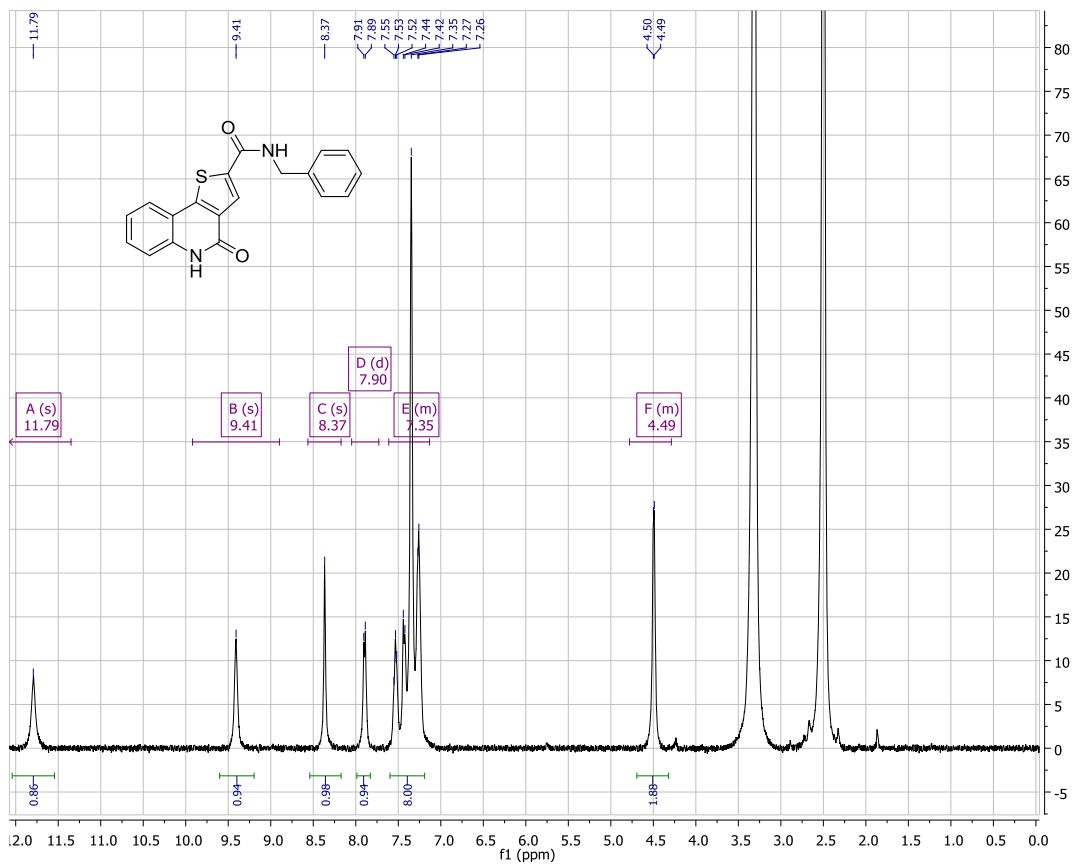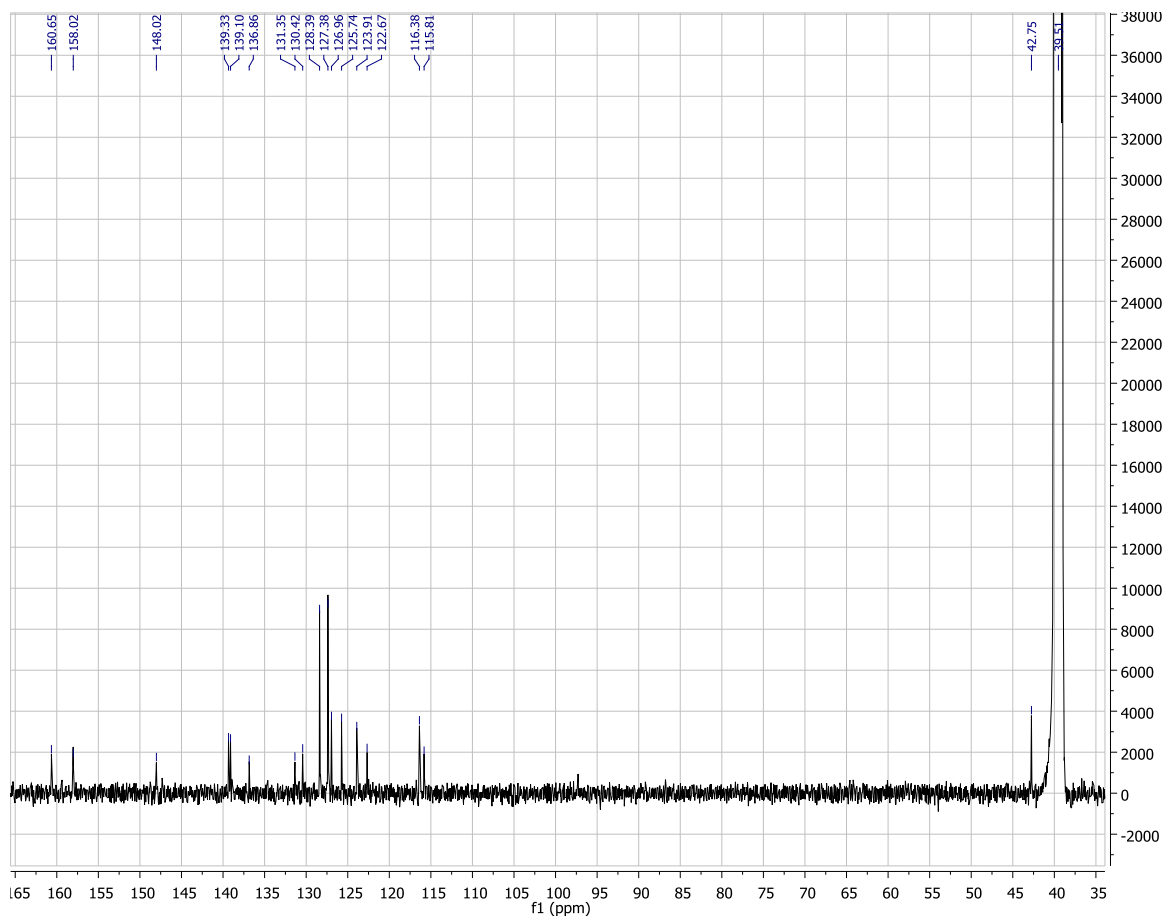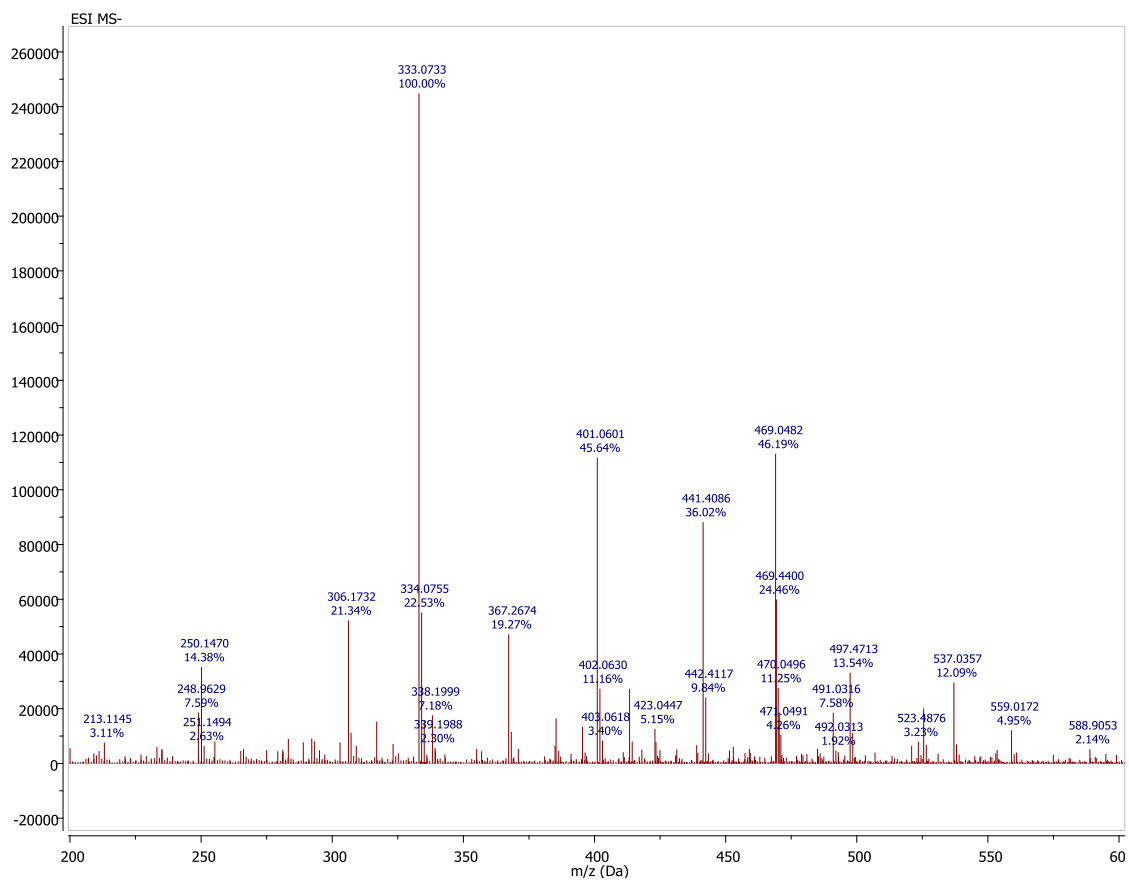
HRMS (TOF) of **3.31**

HPLC scan of **3.31**
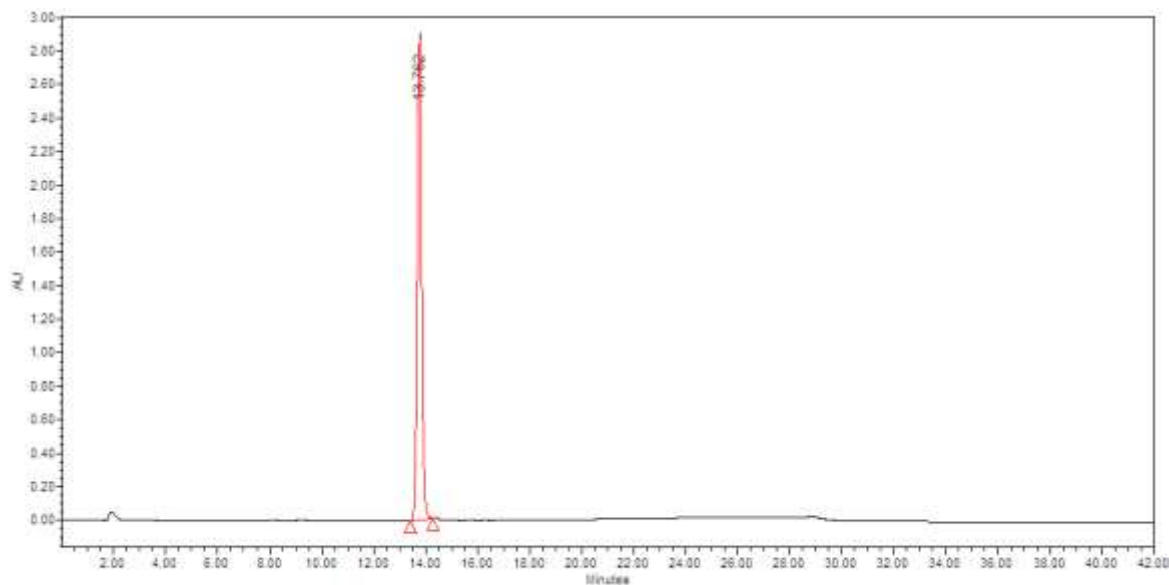
Retention time (min)	% Area
13.762	100

¹³C NMR spectrum of **3.32**
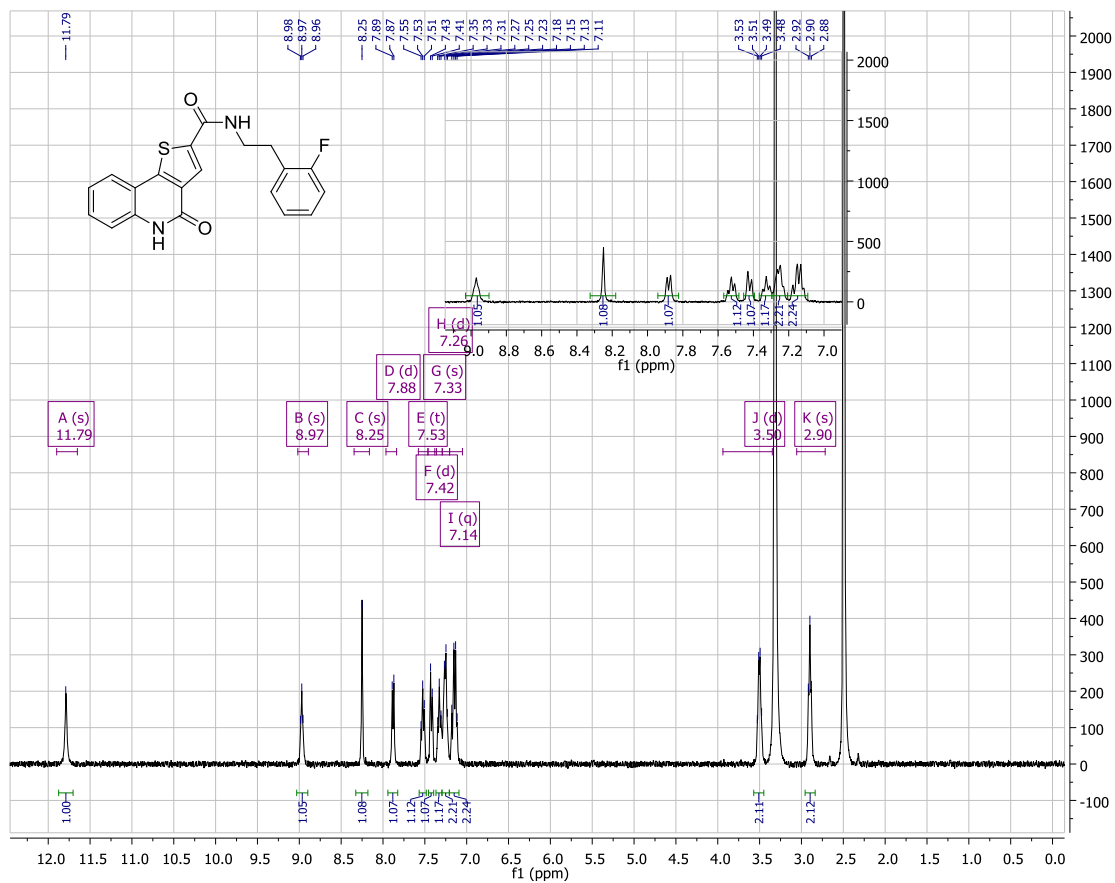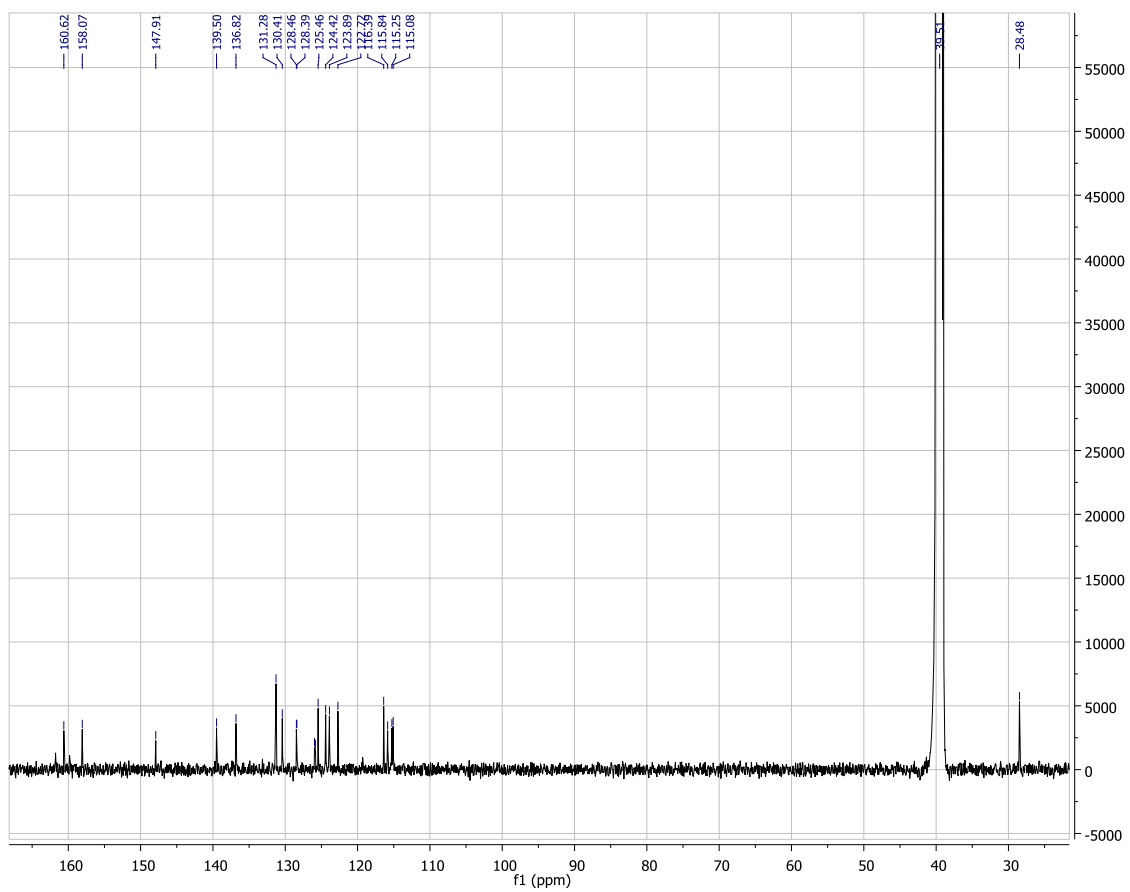
HRMS (TOF) of **3.32**
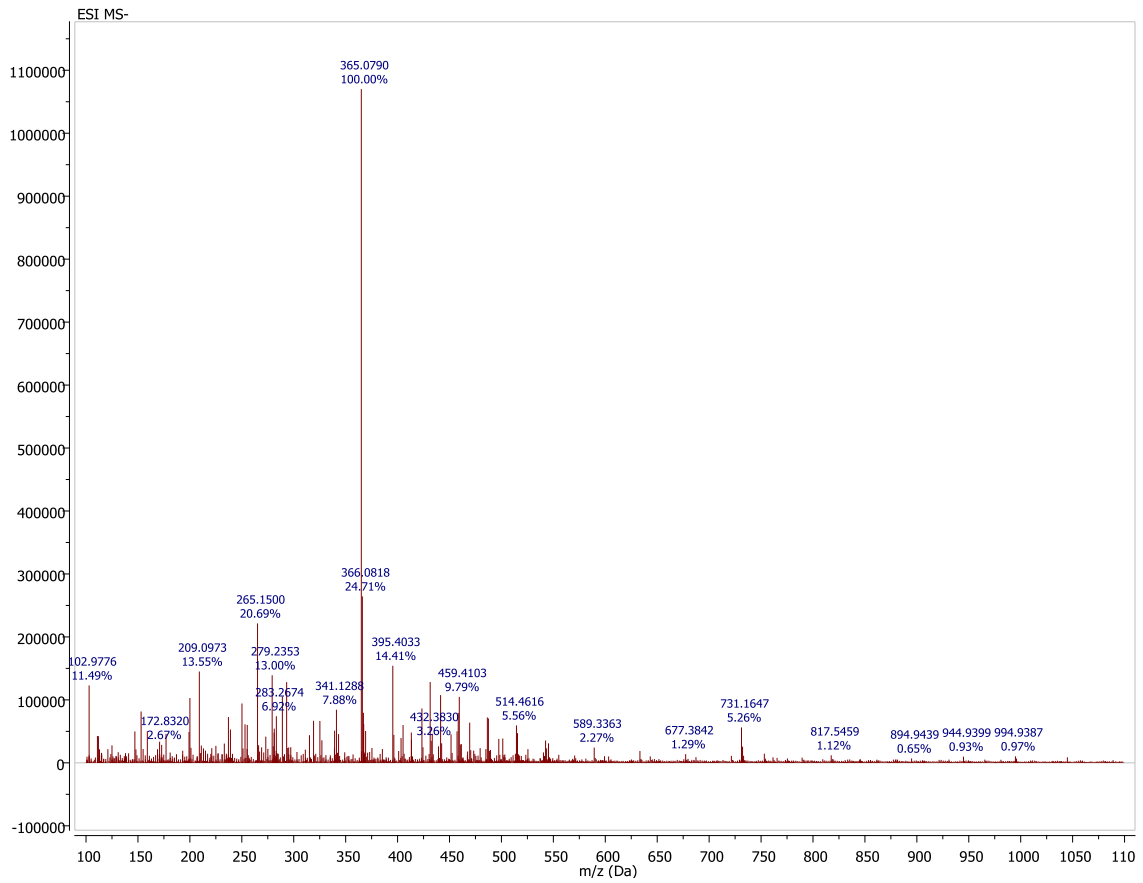
HPLC scan of **3.32**
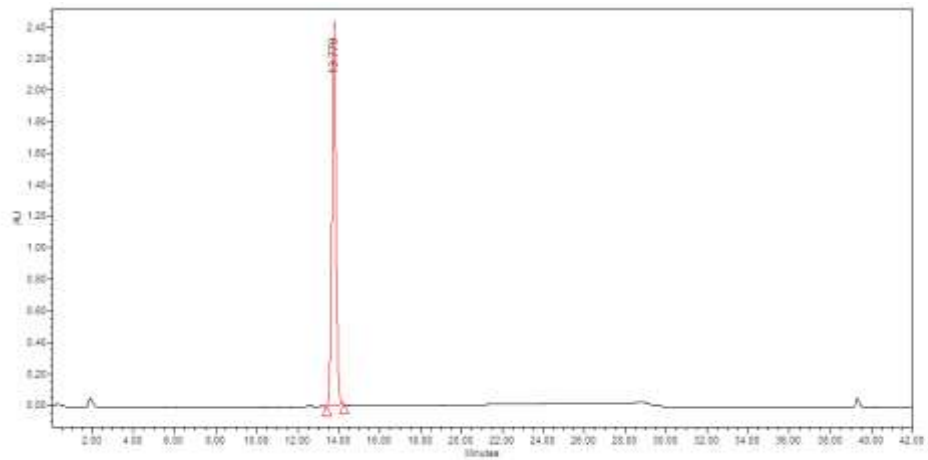
Retention time (min)	% Area
13.779	99.64

¹H NMR spectrum of **3.33**

¹³C NMR spectrum of **3.33**

234

HRMS (TOF) of **3.33**

ESI MS-, Agilent
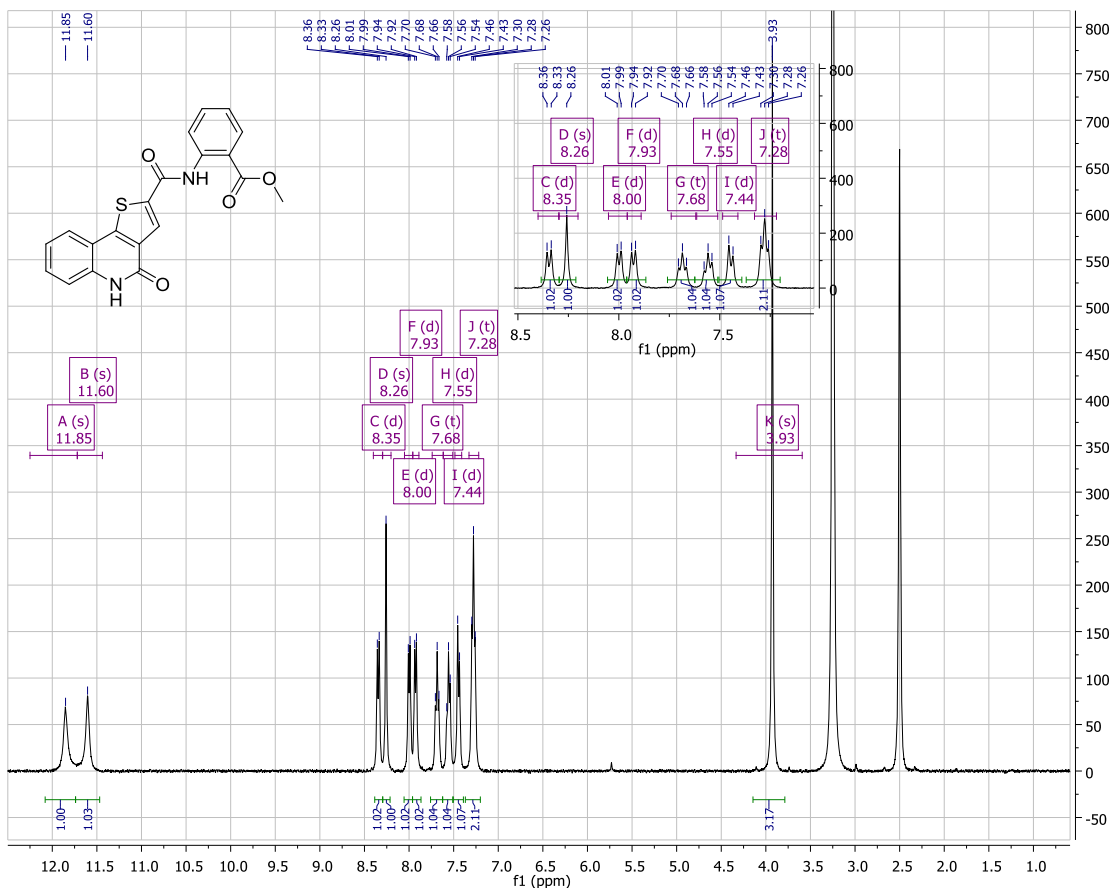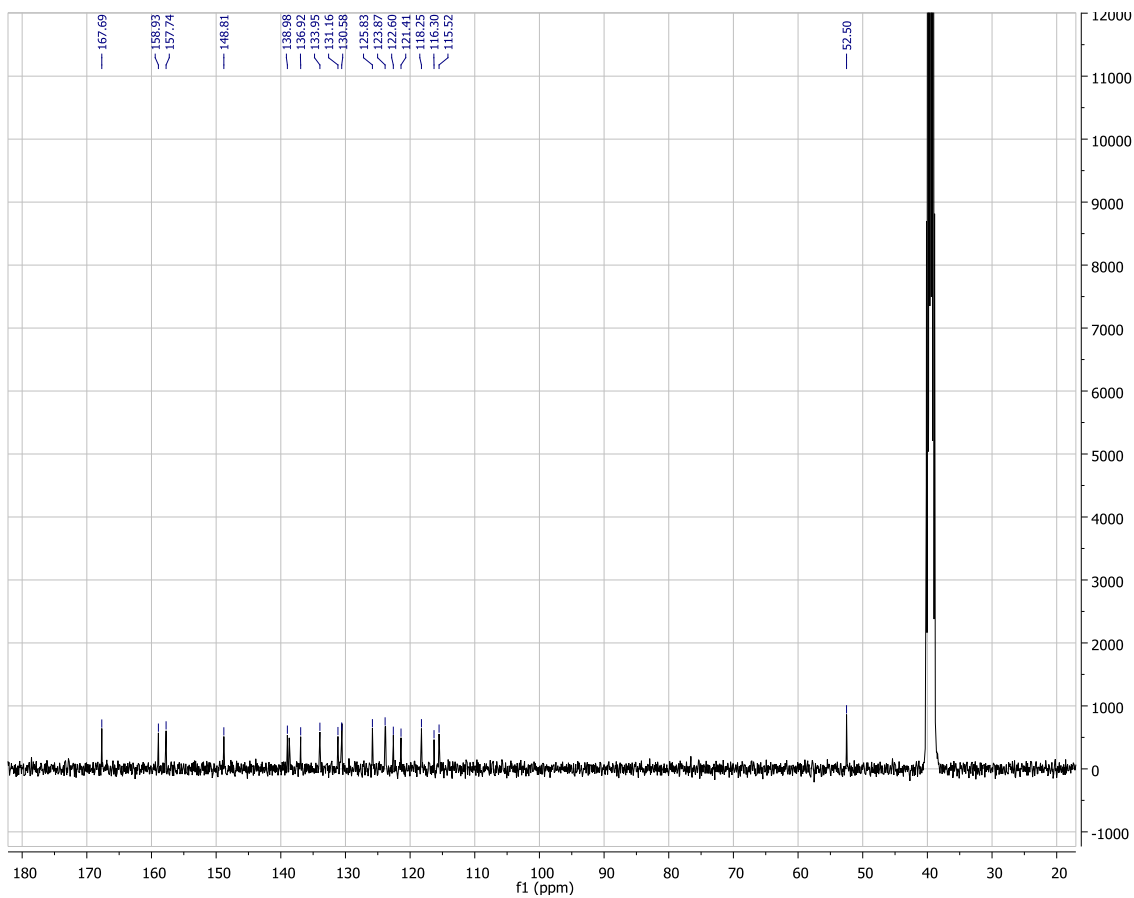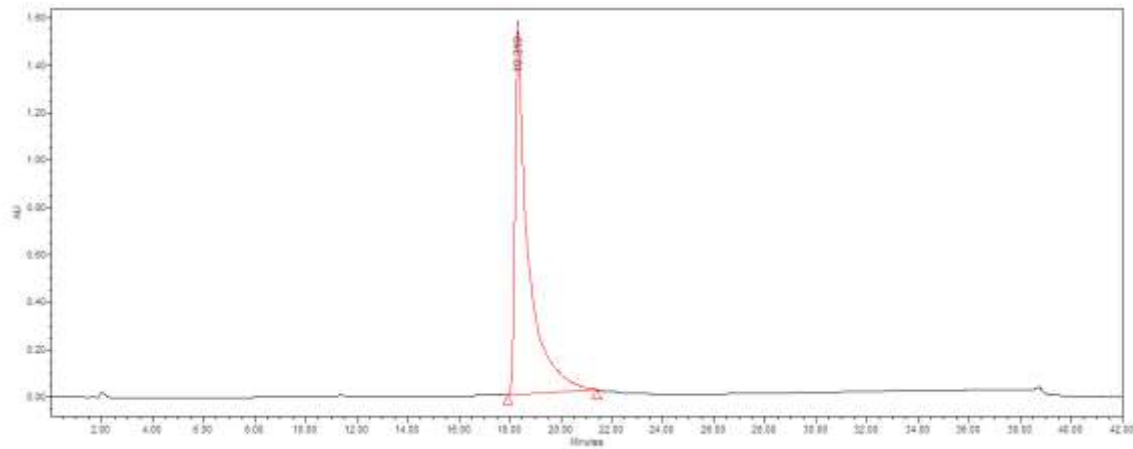
HPLC scan of **3.33**

Retention time (min)	% Area
18.319	100

^{1}H NMR spectrum of **3.34**
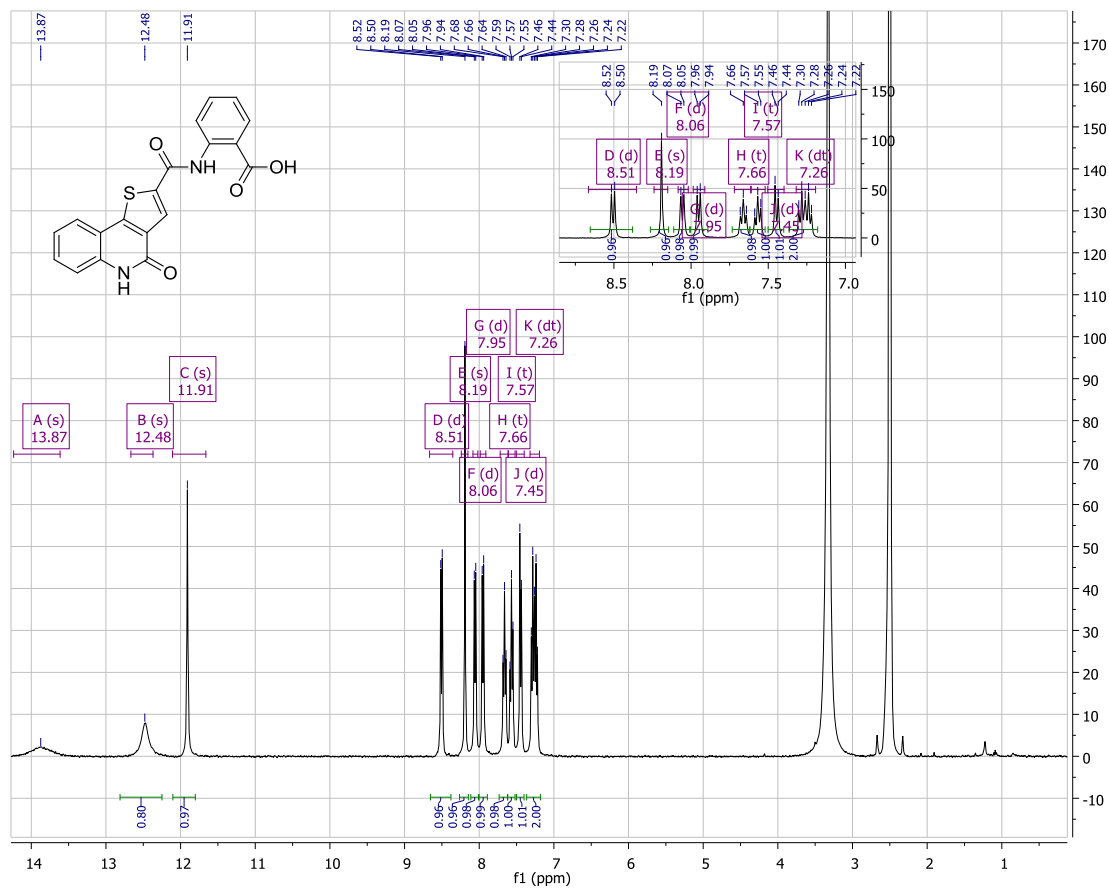
¹³C NMR spectrum of **3.34**
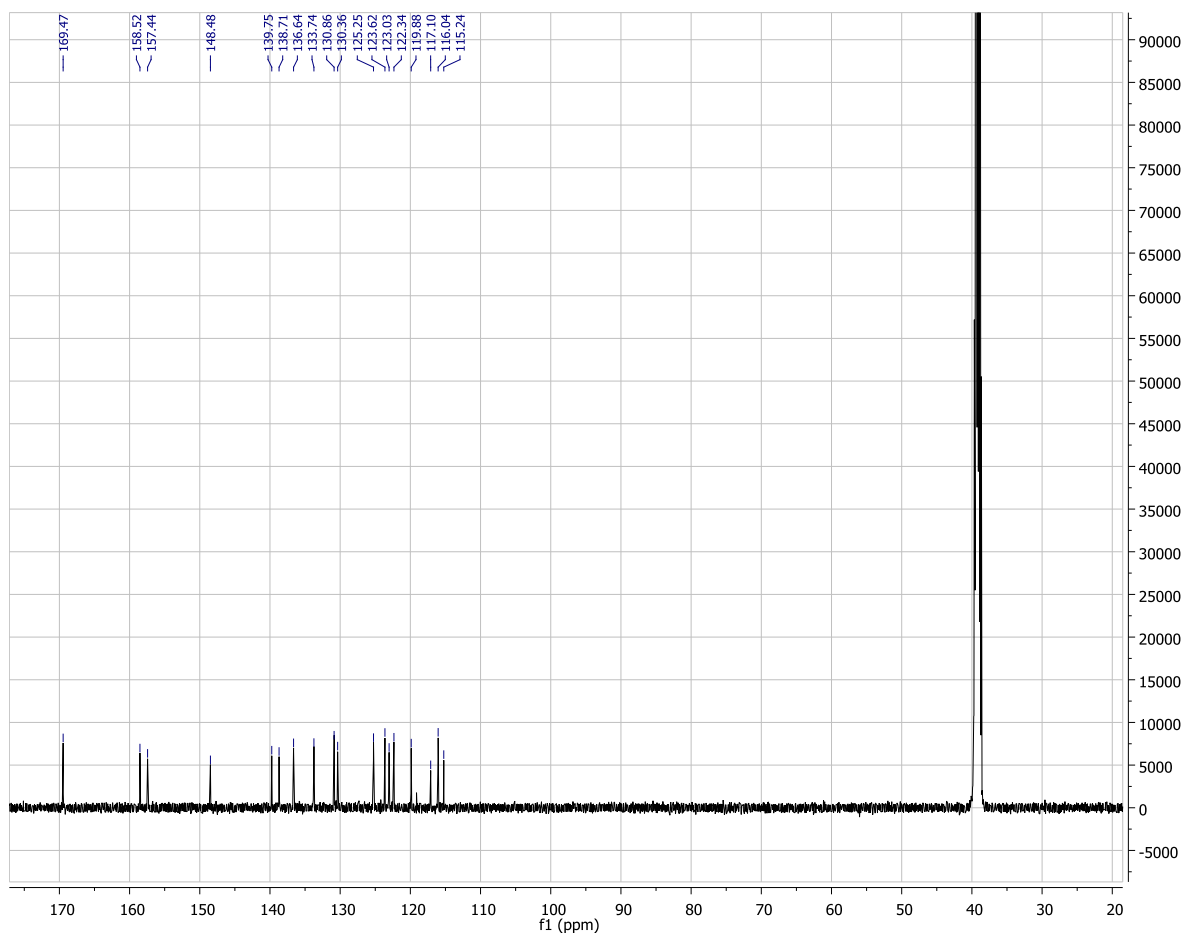
HRMS (TOF) of **3.34**

HPLC scan of **3.34**
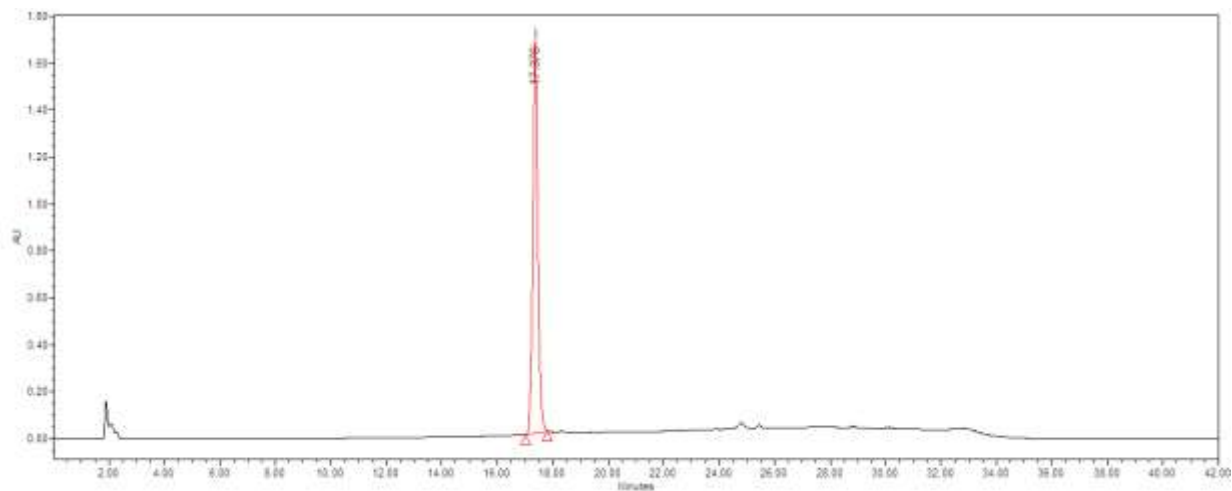
Retention time (min)	% Area
17.376	100

^{1}H NMR spectrum of **3.35**
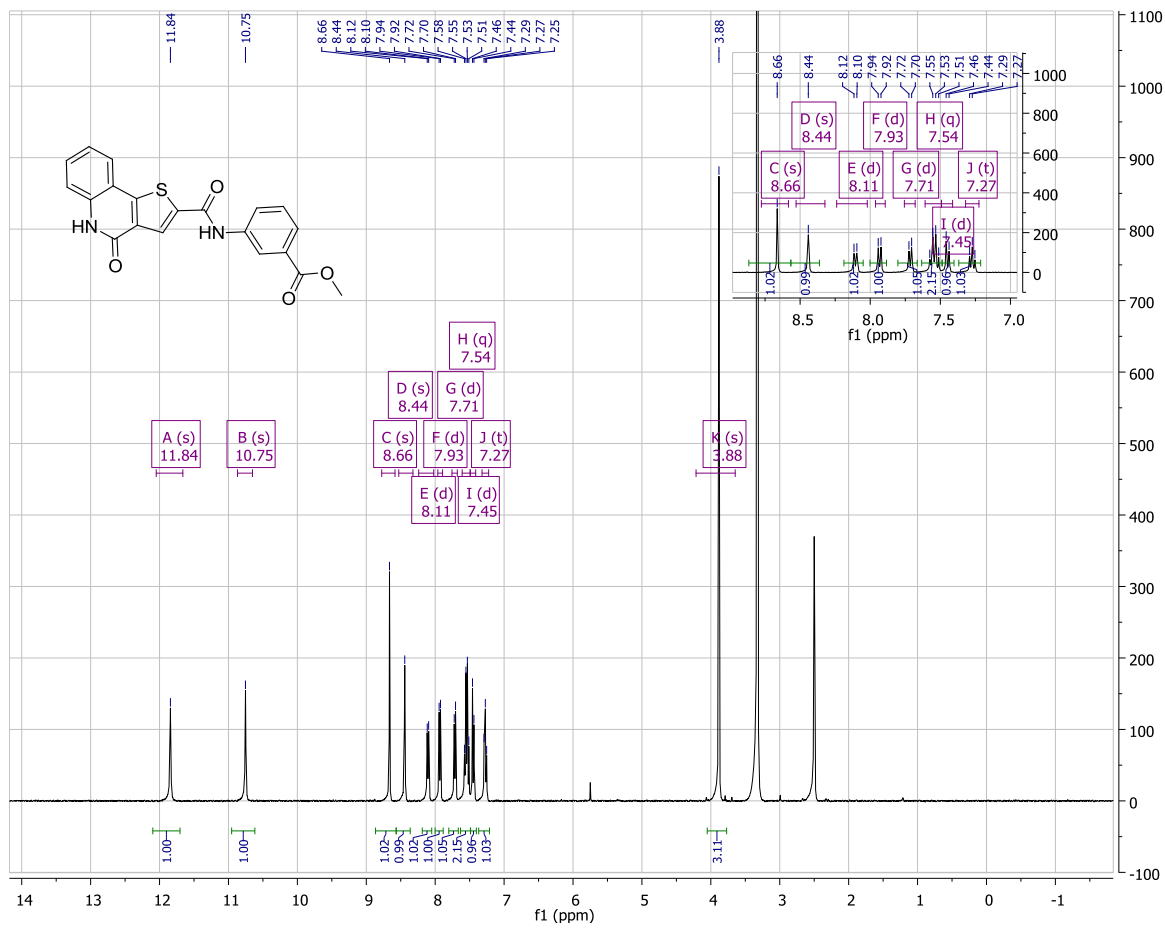
¹³C NMR spectrum of **3.35**

HRMS (TOF) of **3.35**

ESI MS-, Agilent
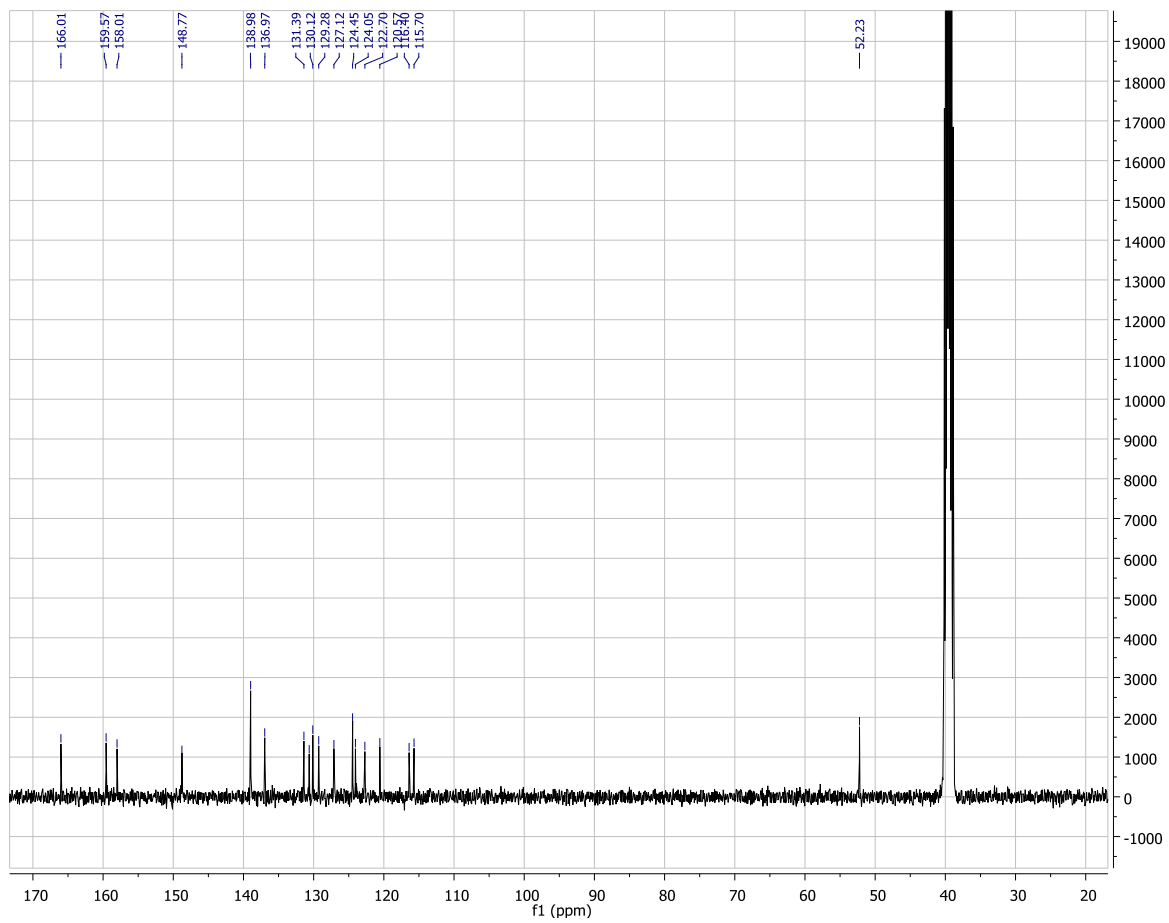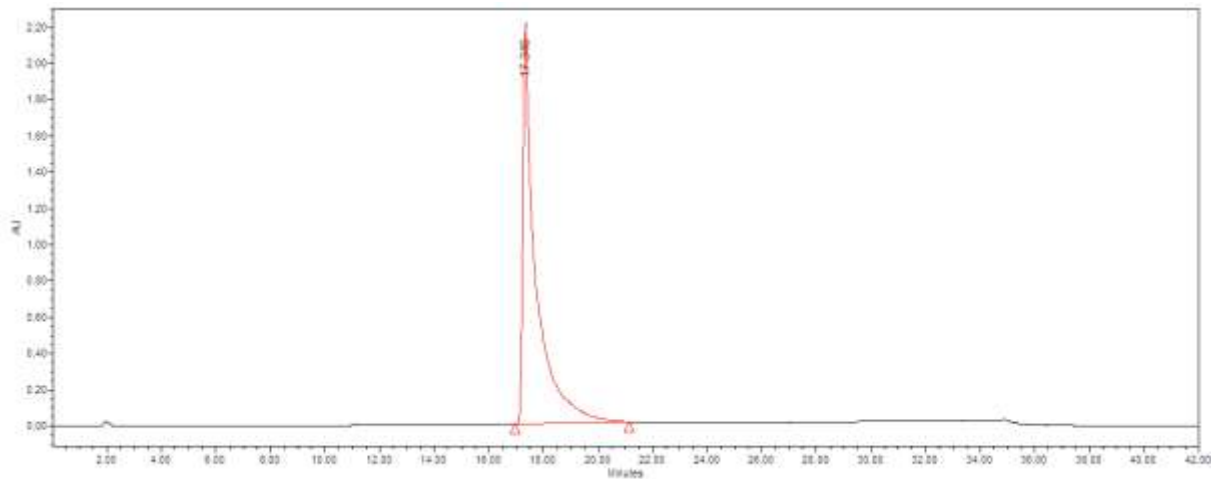
HPLC scan of **3.35**

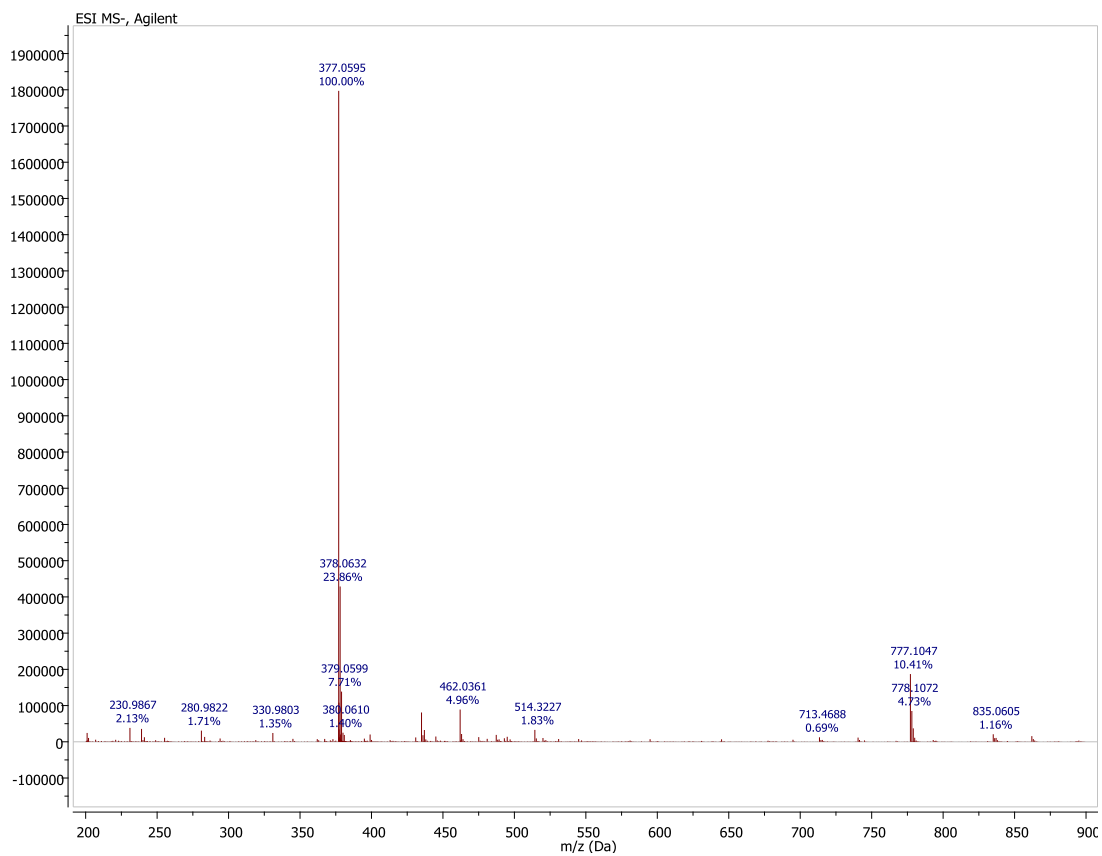| Retention time (min)	% Area
17.346	100

¹H NMR spectrum of **3.36**
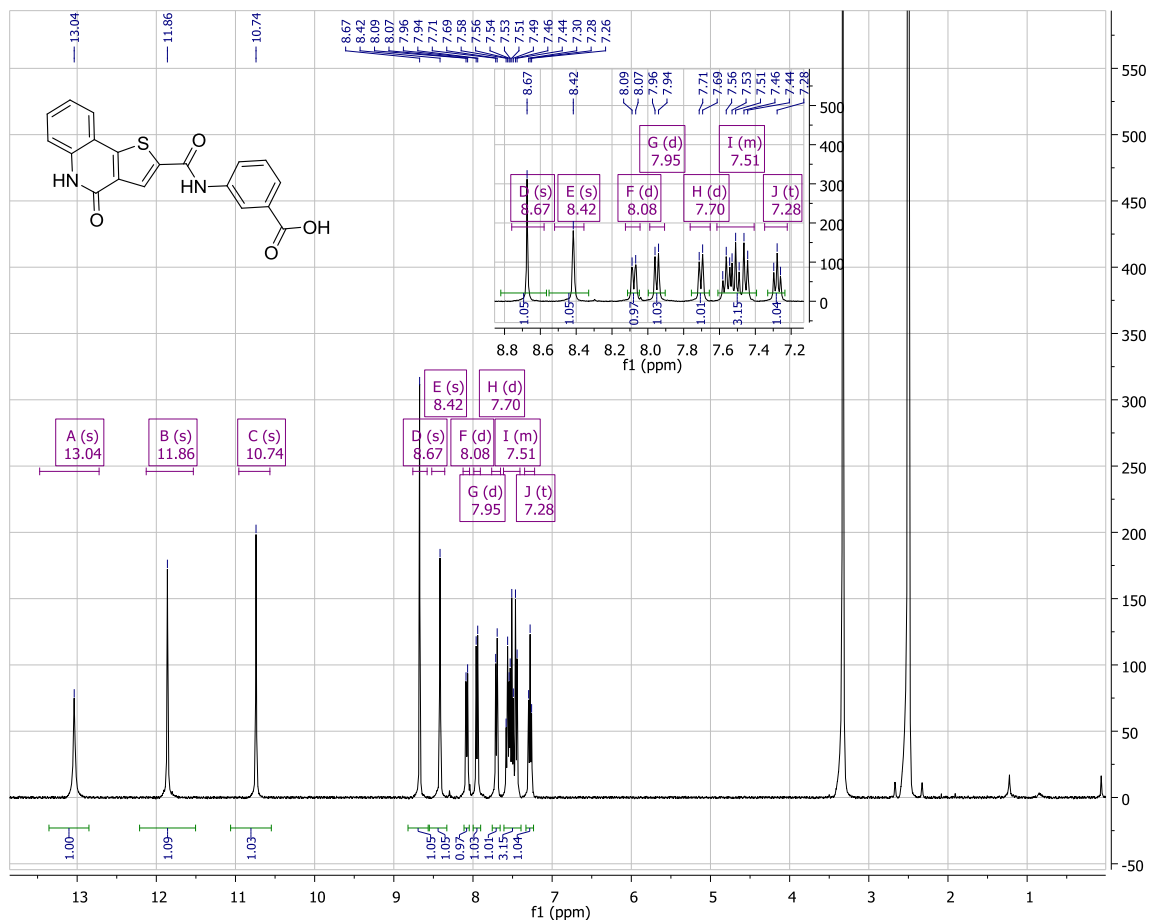
^{13}C NMR spectrum of **3.36**
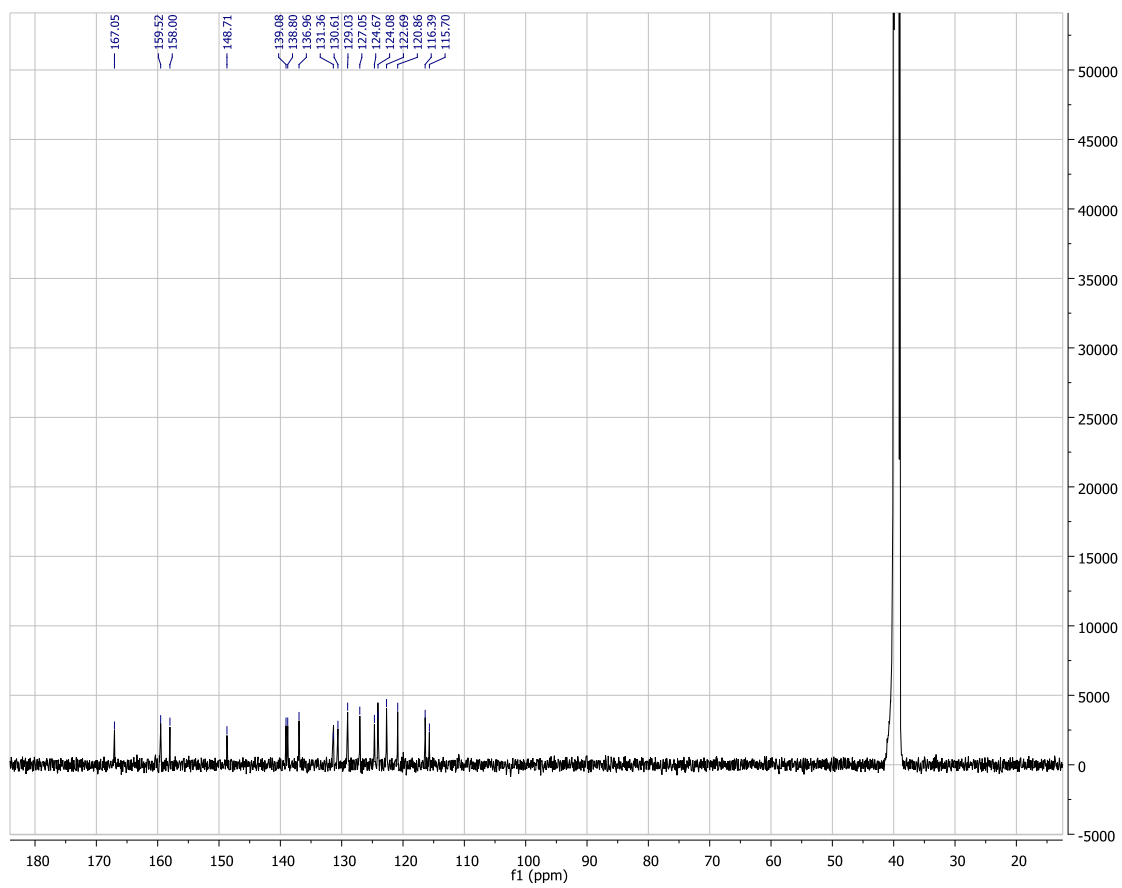
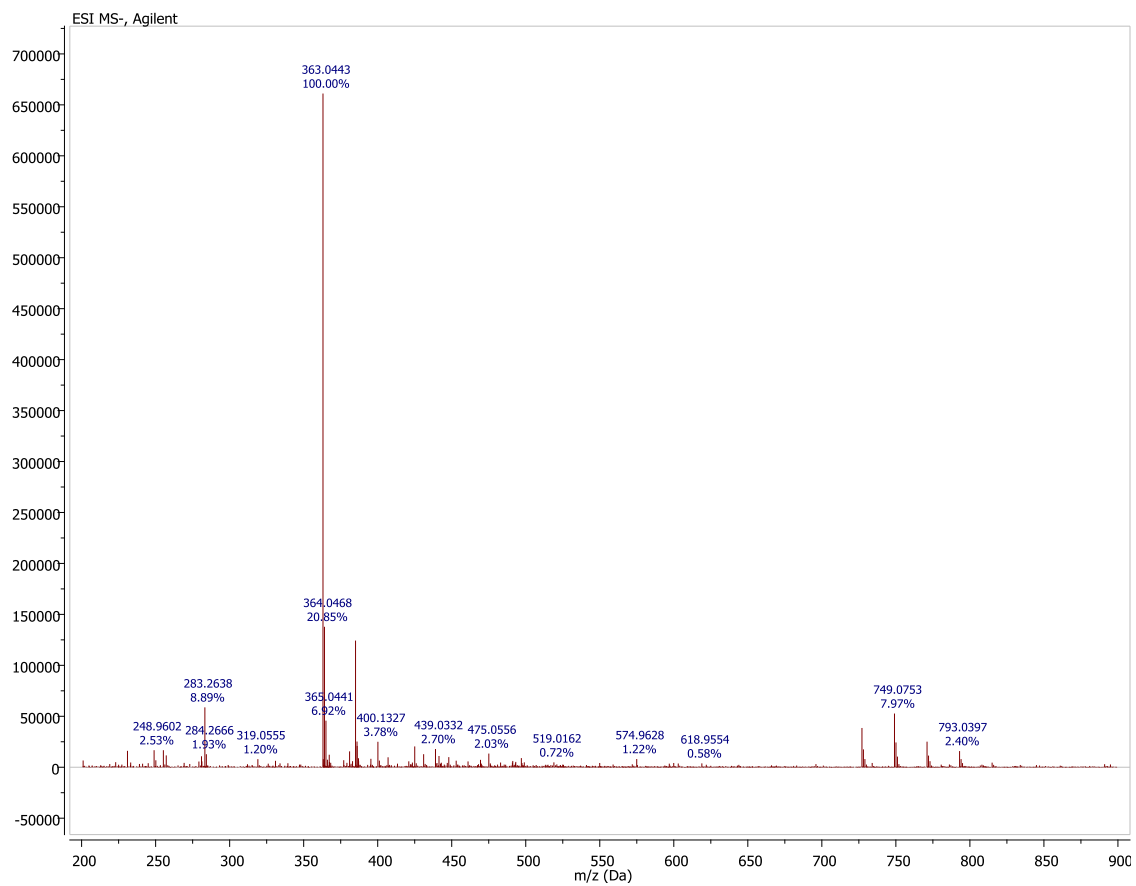HRMS (TOF) of **3.36**
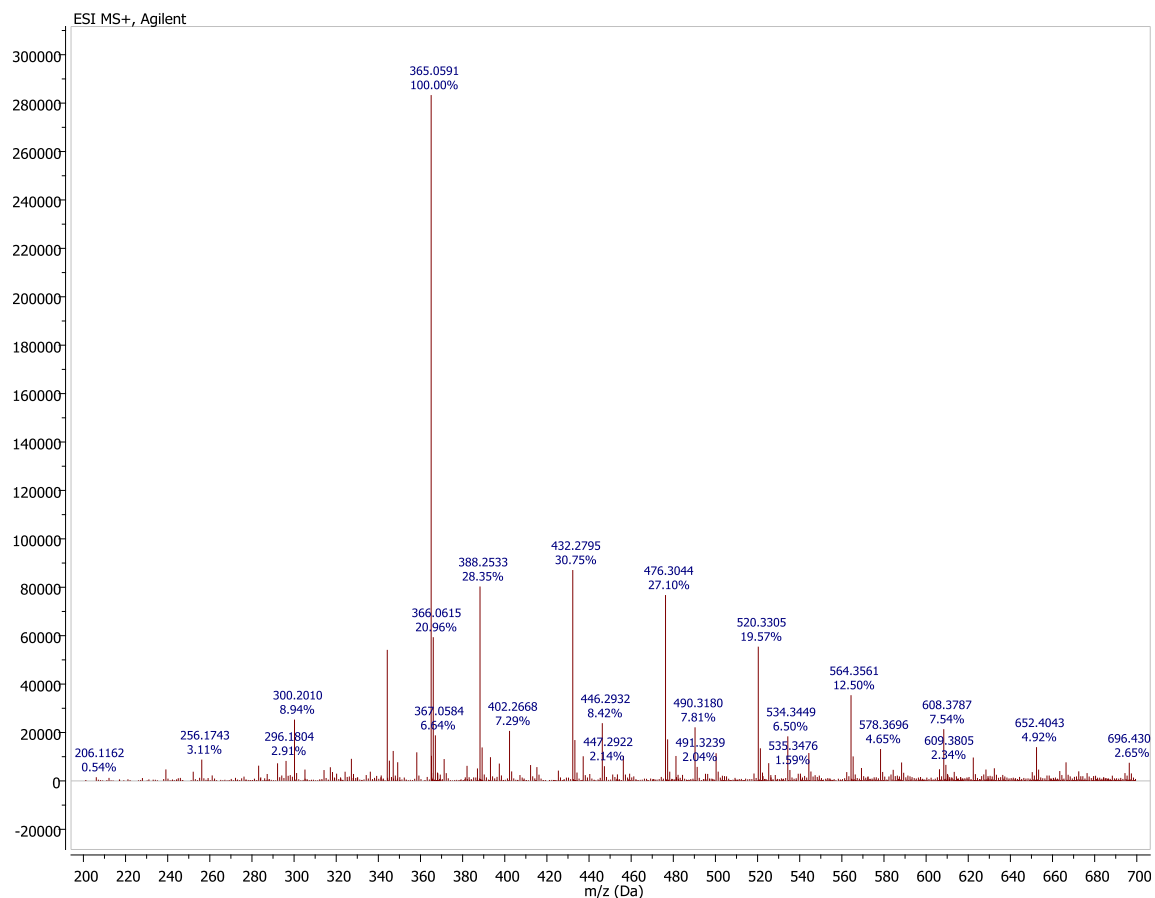
HPLC scan of **3.36**
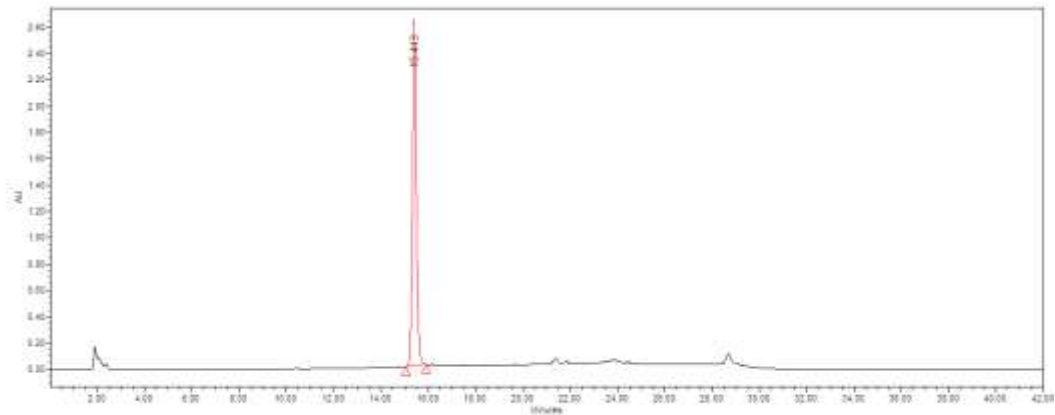
Retention time (min)	% Area
15.413	100

¹H NMR spectrum of **3.37**

¹³C NMR spectrum of **3.37**
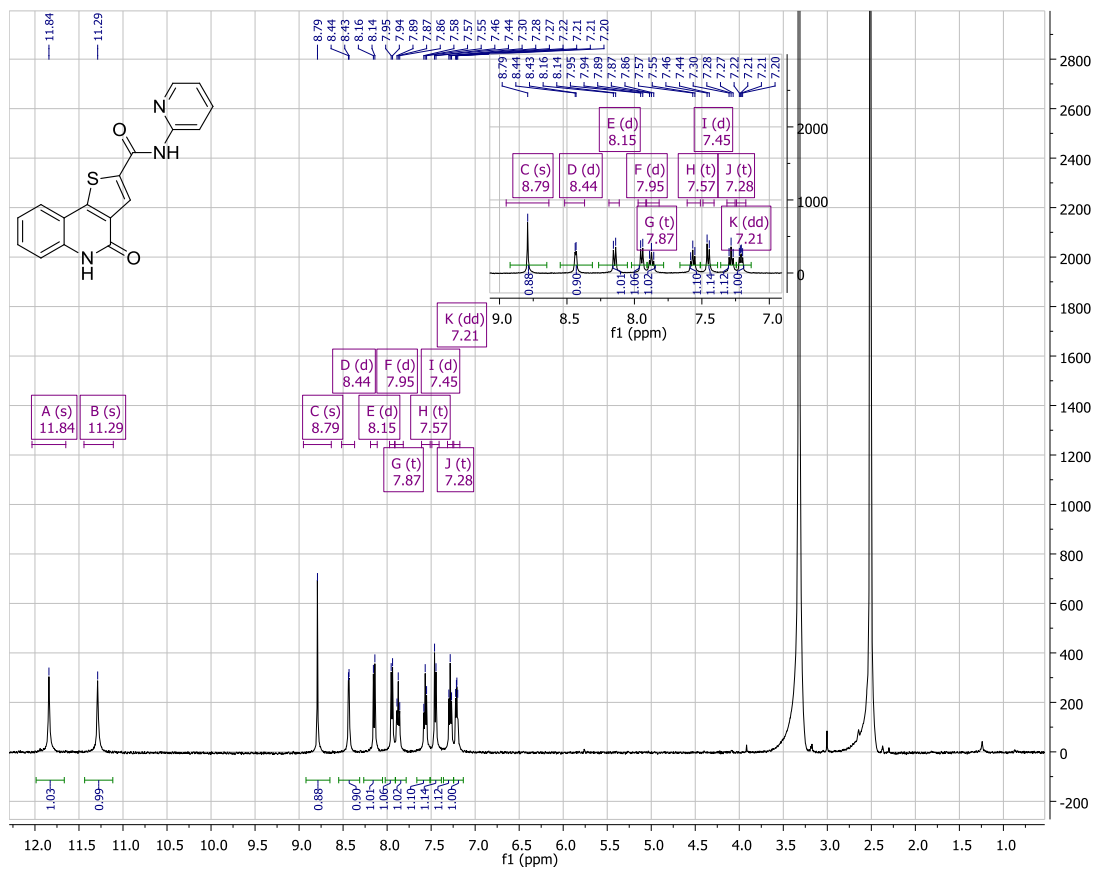
^{13}C NMR spectrum of **3.37**

HRMS (TOF) of **3.37**

ESI MS-, Agilent
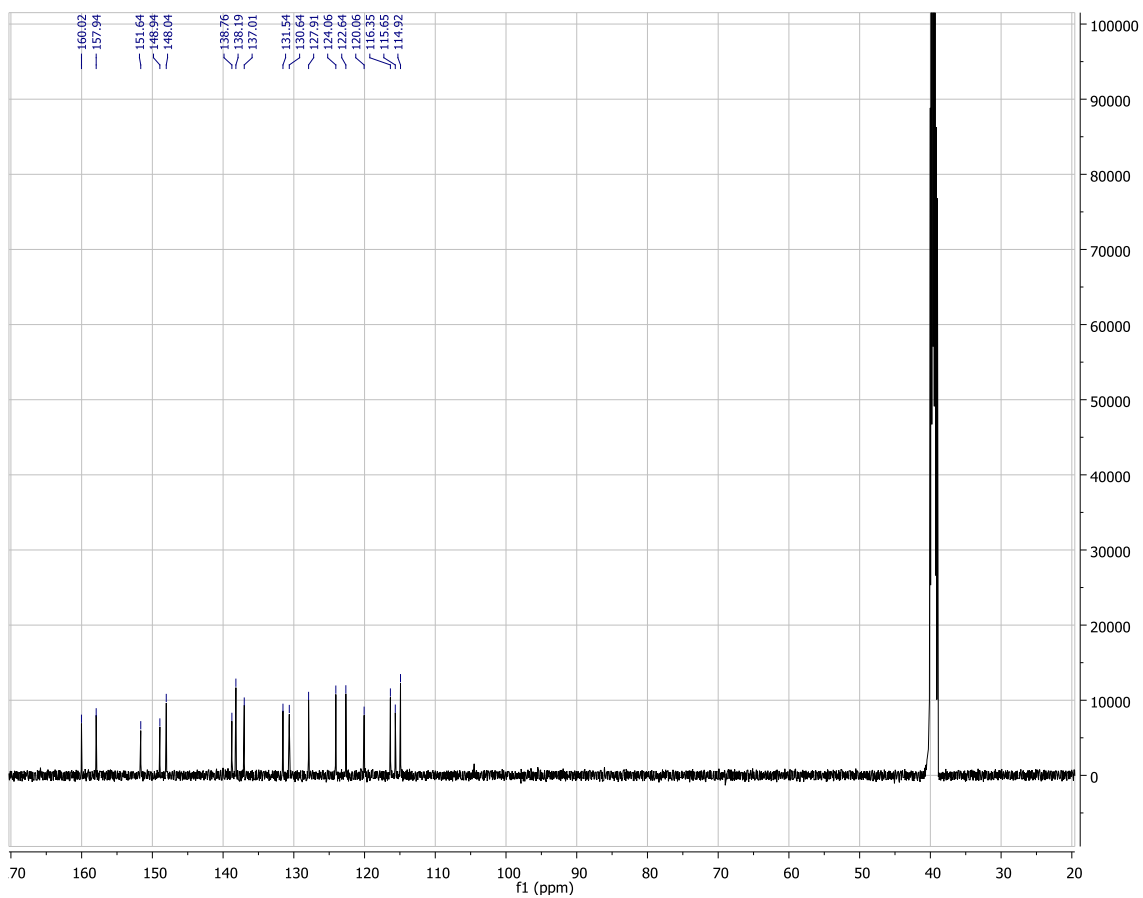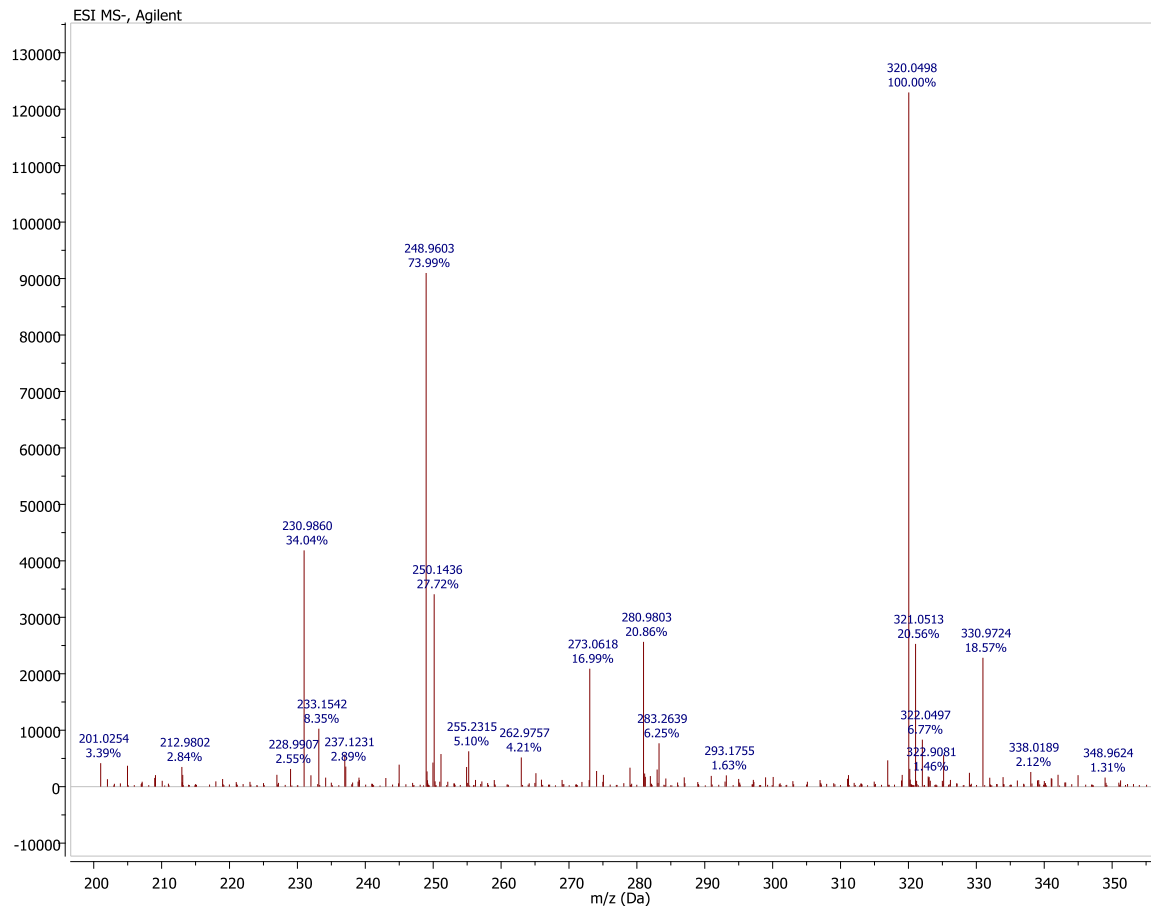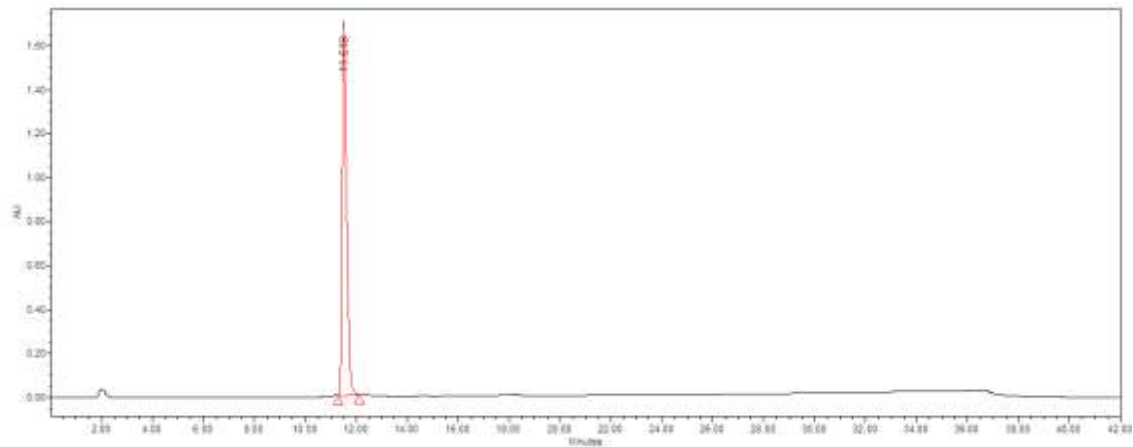
HPLC scan of **3.37**

Retention time (min)	% Area
11.518	100

^{1}H NMR spectrum of **3.38**
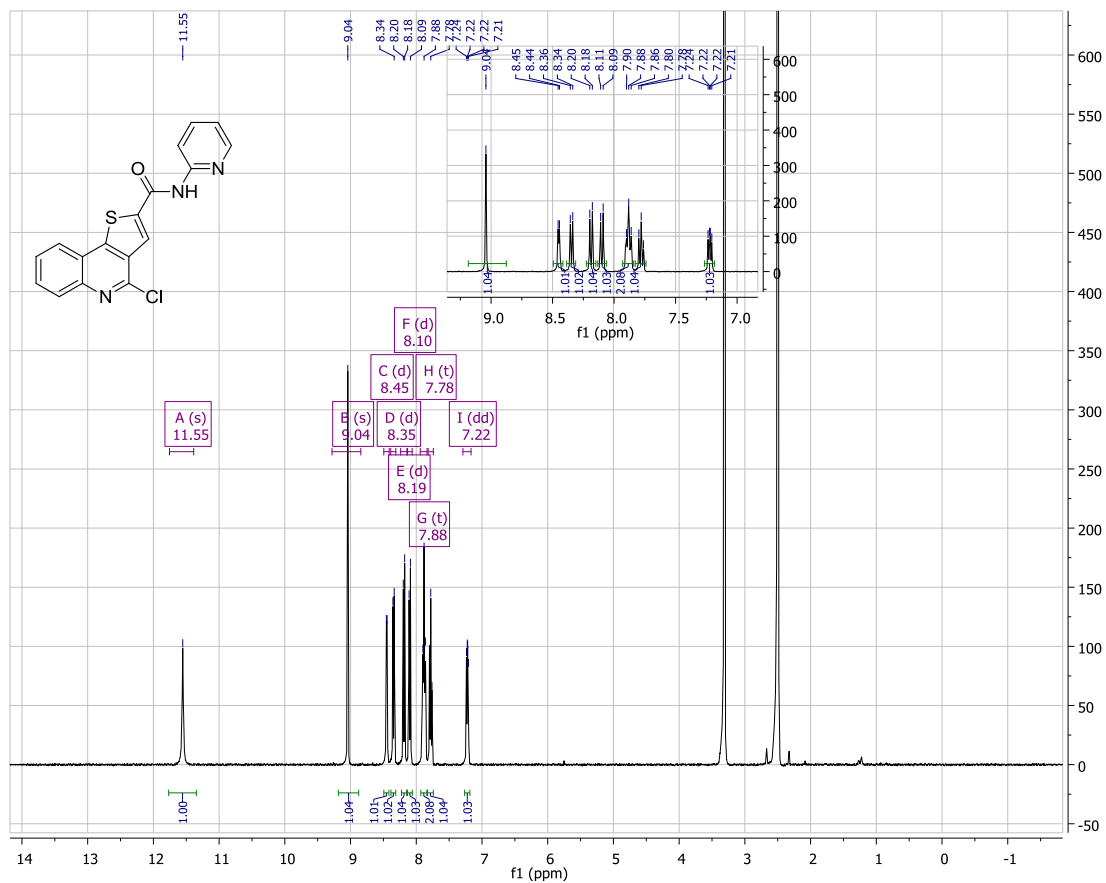
COSY spectrum of **3.38**
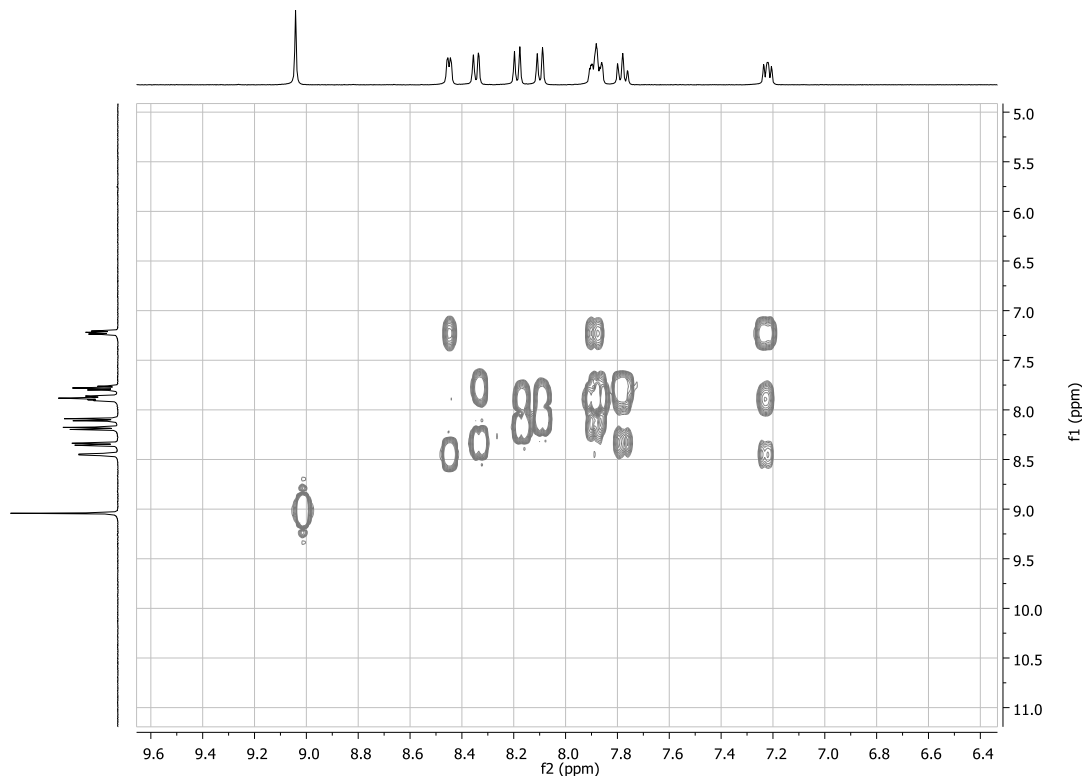
^{13}C NMR spectrum of **3.38**
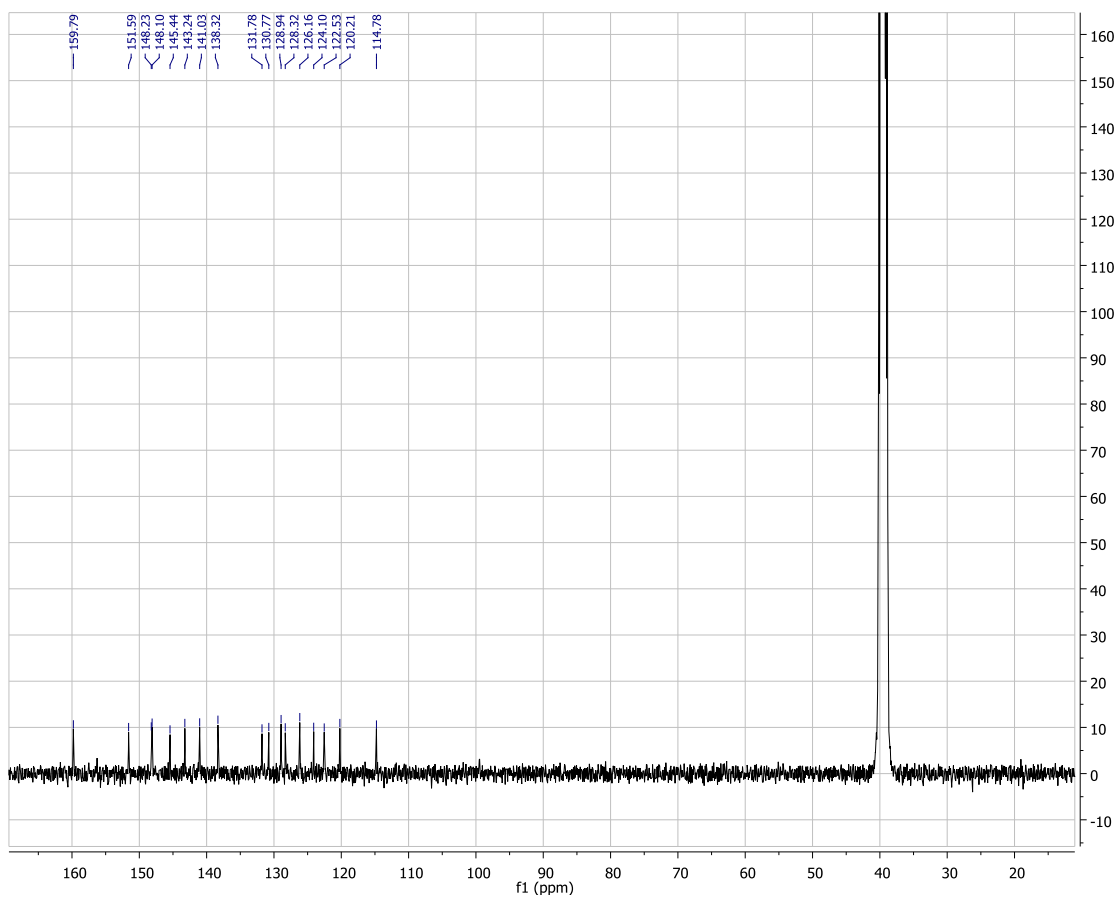
HRMS (TOF) of **3.38**
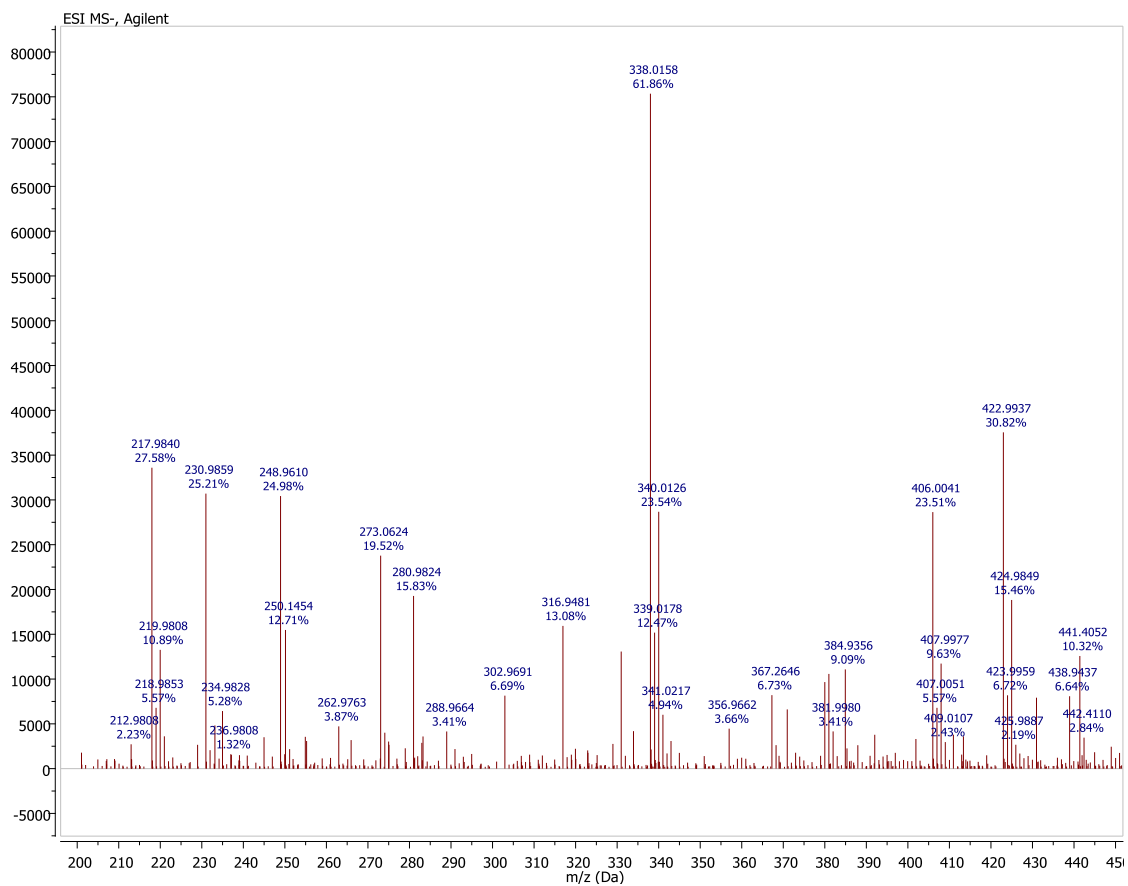
HPLC scan of **3.38**
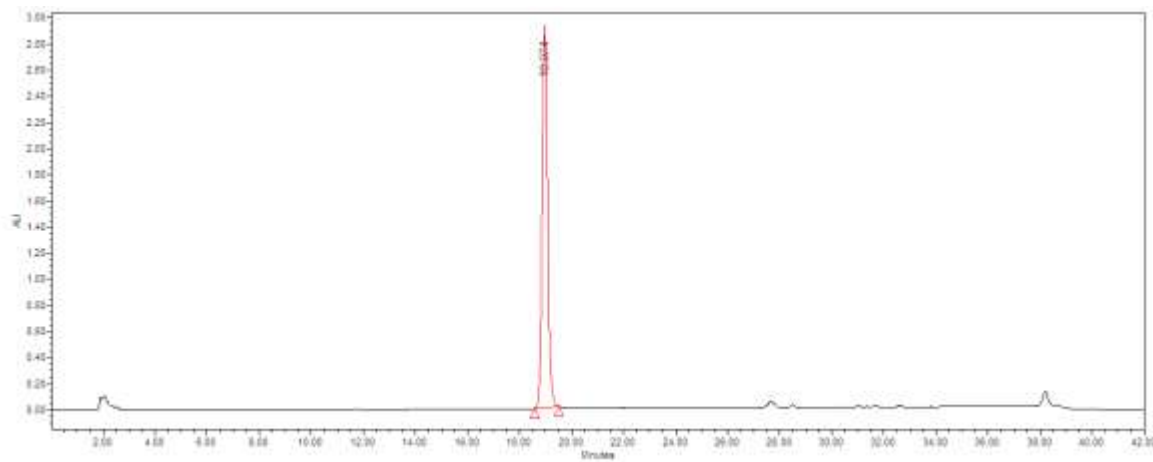
Retention time (min)	% Area
18.974	97.52

^{1}H NMR spectrum of **3.39**
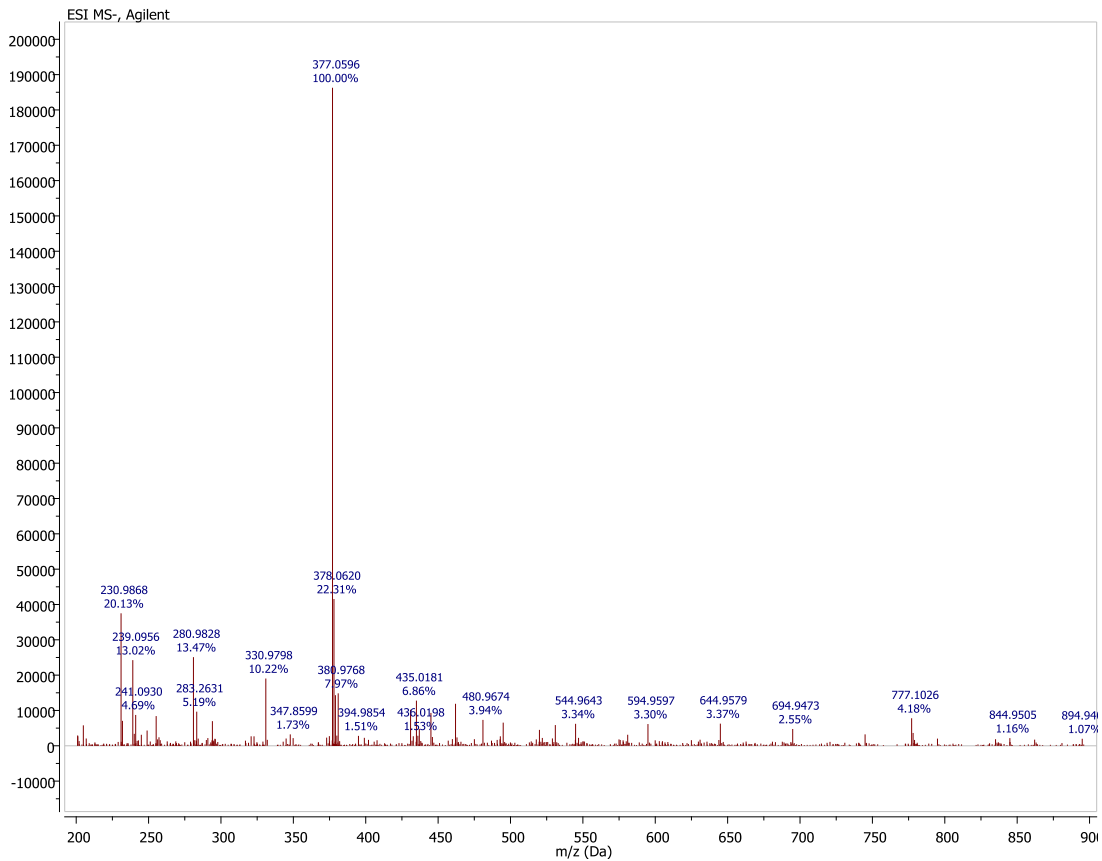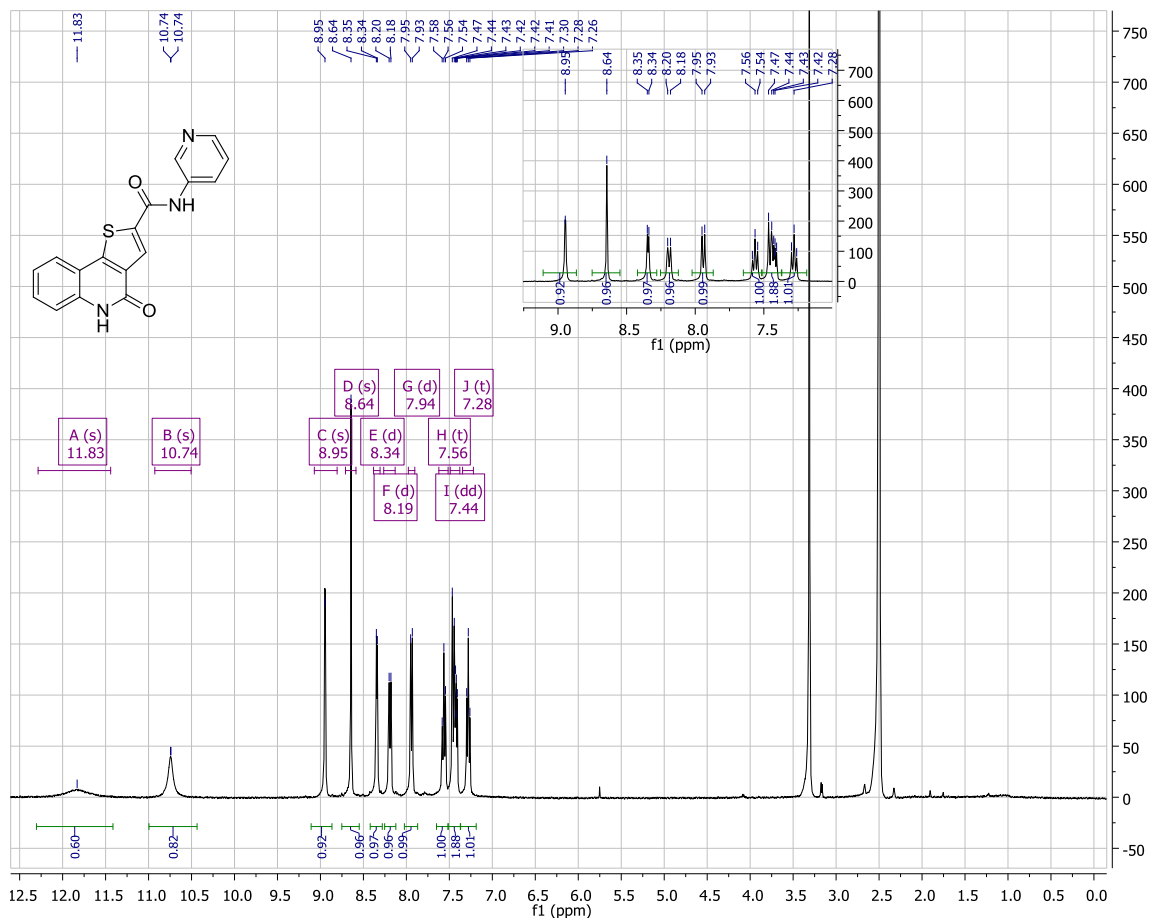
¹³C NMR spectrum of **3.39**
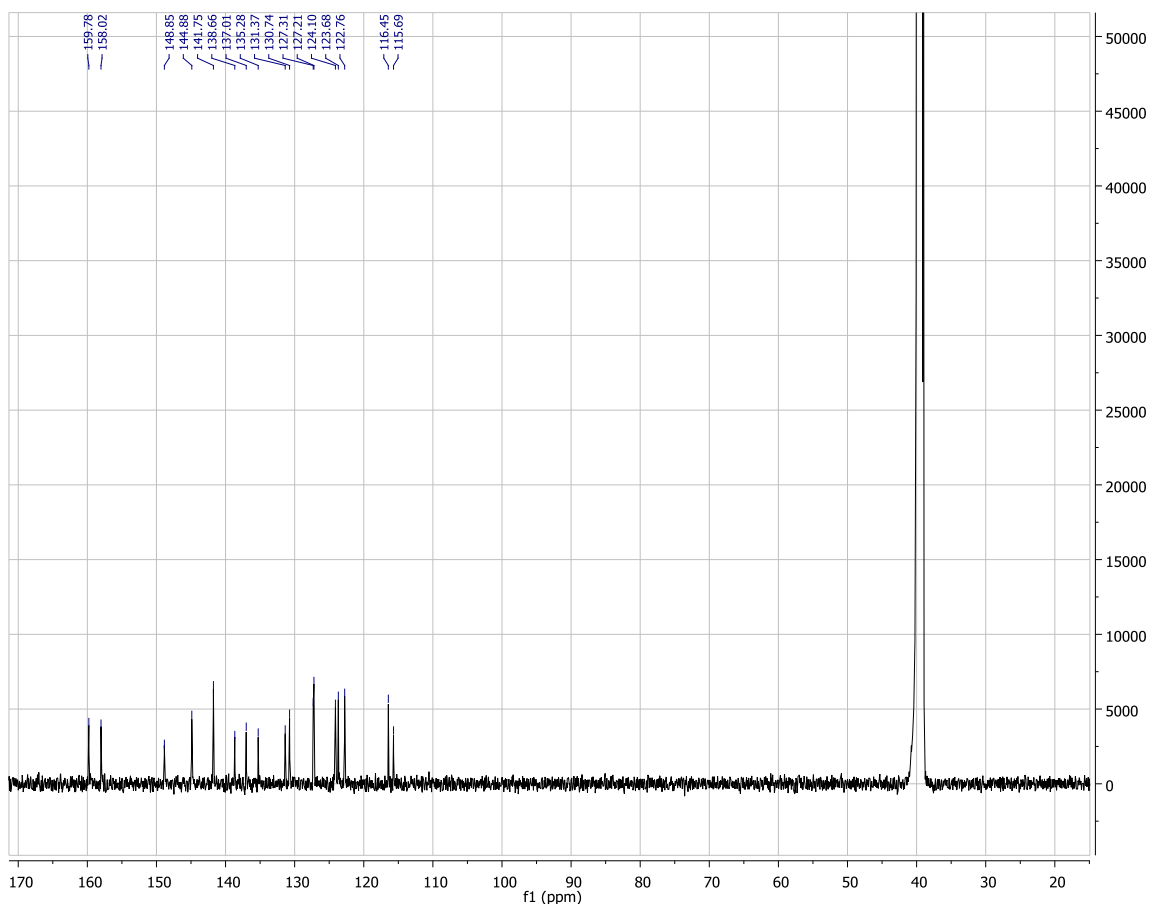
HRMS (TOF) of **3.39**
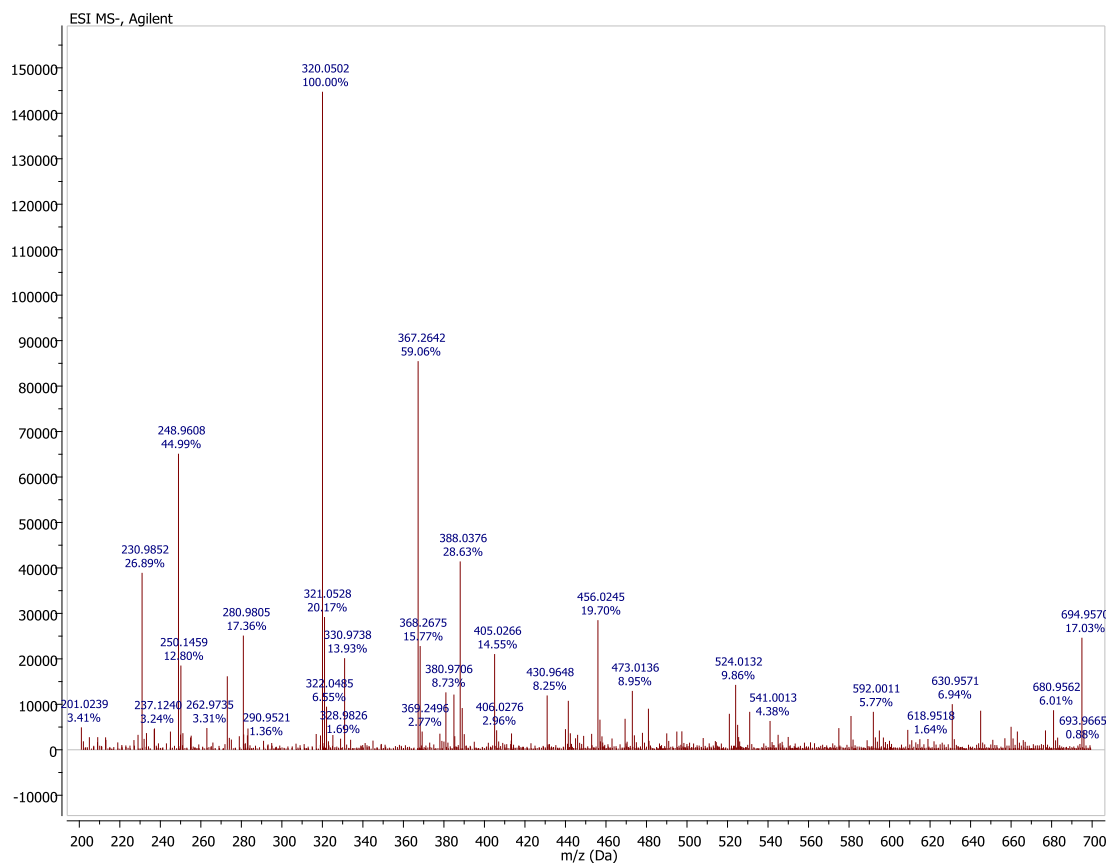
HPLC scan of **3.39**
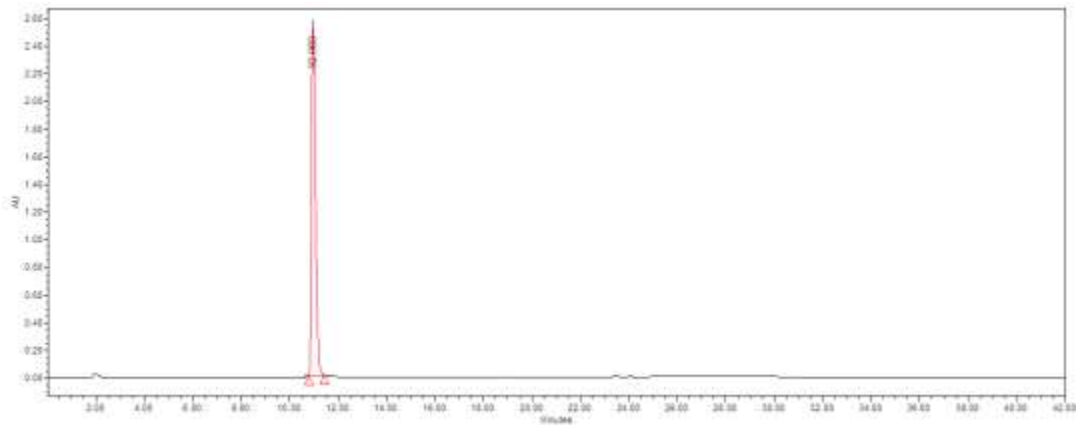
Retention time (min)	% Area
10.969	100

APPENDIX B: LIST OF PUBLICATIONS FROM DISSERTATION

Portion of the dissertation is published as:

Chatterjee, A.; Cutler, S.J.; Khan, I.A.; Williamson, J.S. "Efficient synthesis of 4-oxo-4,5-dihydrothieno[3,2-c]quinoline-2-carboxylic acid derivatives from aniline", *Mol. Diversity*, (in press), DOI: 10.1007/s11030-013-9476-4, **2013**

Portion of the dissertation is submitted for publication as:

Chatterjee A., Cutler, S. J., Doerksen, R. J., Khan, I. A., Williamson, J. S. "Discovery of novel thienoquinolone derivatives as selective and ATP non-competitive CDK5/p25 inhibitors by structure-based virtual screening."

VITAE

Department of Medicinal Chemistry
School of Pharmacy, University of Mississippi,
University, MS 38677
chatterjee.arindam@yahoo.com

EDUCATION

PhD in Pharmaceutical Sciences with a major in Medicinal Chemistry
School of Pharmacy, University of Mississippi
November, 2013
Dissertation "Molecular Modeling and SAR studies of CDK5/p25 Selective Inhibitors"

MS in Pharmaceutical Sciences with a major in Medicinal Chemistry
School of Pharmacy, University of Mississippi
August, 1994
Thesis "Design and Synthesis of Photoactive (9'-azido-) taxol - A Probe for Establishing the Taxol Binding Site/s with Tubulin".

Bachelor of Technology in Pharmaceutical Technology
University of Calcutta, India
August, 1989

Bachelor of Science (Honors)
University of Calcutta, India
June, 1985

SCIENTIFIC METHODOLOGY EXPERIENCE

Synthetic Chemistry Strategy: Basic organic synthetic strategies, oxidation, reduction, hydrogenation, HWE reactions, organo-lithium reactions, Grignard's reaction, organo boron chemistry, Weinreb amide chemistry, Pictet Spengler, cyclo-addition chemistry, Vilsmeier-Haack reaction; microwave assisted chemistry; asymmetric synthesis, Evan's chiral auxiliary, Sharpless epoxidation; complex heterocyclic syntheses, hetero Diels Alder chemistry, Menisci reaction; transition metal mediated coupling, Heck, Suzuki, Stille, Buchwald, Negishi and Ullmann; solution phase parallel synthesis; multi step natural product synthesis, synthesis of photoreactive taxol; reductive amination using different borohydride reagents; multi step customized synthesis of radio-labeled compounds (^{3}H, ^{14}C)

Separation & Spectroscopic Proficiency: Chromatographic purification techniques (TLC, gravity columns, flash, chromatotron, MPLC), HPLC (normal and reverse phases, preparative); interpretation and operation of UV, IR, NMR (1D and 2D); mass spectral data interpretation of LC-MS, GC-MS

Modeling and Software packages: Computational model building; structure based virtual screening; proficiency in Schrodinger Maestro, Canvas, Phase, Prime; PyMol

Symyx electronic notebook; Chemdraw; Reaxys and Scifinder Search
Biological Assay
CDK5 and CDK2 assay development using FRET based techniques.

PROFESSIONAL EXPERIENCE

University of Mississippi
Department of Medicinal Chemistry
2010 – Present   *Graduate Research Assistant*

Eli Lilly & Company, Indianapolis, IN 46285
2008 - 2010   *Associate Consultant*
2001 - 2008   *Assistant Sr. Organic Chemist*
Responsibilities included design, synthesis, purification and characterization of different classes of organic compounds as potential therapeutic inhibitors for kinases
Experienced in working at hit to lead and lead optimization phases
Part of a team, which developed a candidate for P-38 inhibitor
Part of a team, which developed a candidate for JAK-2 inhibitor
Designed and executed a facile synthesis of dihydropyrrolopyrazole core
Designed and synthesized several key compounds in MLK-7 project for cardiovascular disease

Pfizer Global Research and Development (Formerly Parke-Davis Pharmaceutical Research, Division of Warner Lambert), Ann Arbor, MI 48105
1999 – 2001   *Sr. Associate Scientist*
1997 – 1999   *Associate Scientist*
Responsibilities included design, synthesis, purification and characterization of various classes of organic compounds as potential therapeutic agents for neurological disorder
Designed and synthesized novel targets in calcium channel project for stroke,
Developed SAR for novel cdk-5 inhibitors for Alzheimer's disease
Synthesized novel targets for neuro-immunophilins used as a target for neuro-restoration
Designed and synthesized compounds in SAR for 5HT-7-receptor antagonists
Developed SAR for BACE inhibitors as therapeutic target for Alzheimer's disease

American Radiolabeled Company Inc., St. Louis, MO 63146
1995 - 1997   *Production Chemist*
1994 - 1995   *Chemist I*
Responsibilities included multi-step synthesis of ^{3}H and ^{14}C labeled compounds of biological interest.

HONORS/AWARDS

Graduate Fellowship from Graduate School 5/2013
Dissertation Fellowship from Graduate School, University of Mississippi, 9/ 2012
Employee recognition spotlight award at Eli Lilly on 3/2010
Employee recognition spotlight award at Eli Lilly on 3/2009
Employee recognition spotlight award at Eli Lilly on 11/2008

Employment Recognition Award on 1/2000 at Parke-Davis
Employment Recognition Award on 12/1999 at Parke-Davis
Employment Recognition Award on 3/1999 at Parke-Davis
Grant-in-Aid of Research, 1992 from Sigma Xi, The Scientific Research Society for the project entitled "Photoaffinity Labeling of Taxol Binding Site(s) of Tubulin"

LIST OF PUBLICATIONS

Chatterjee, A.; Cutler, S.J.; Khan, I.A.; Williamson, J.S. "Efficient synthesis of 4-oxo-4,5-dihydrothieno[3,2-c]quinoline-2-carboxylic acid derivatives from aniline", *Mol. Diversity*, (in press), DOI: 10.1007/s11030-013-9476-4, **2013**.

Chatterjee A., Cutler, S. J., Doerksen, R. J., Khan, I. A., Williamson, J. S. "Discovery of novel thienoquinolone derivatives as selective and ATP non-competitive CDK5/p25 inhibitors by structure-based virtual screening", *Submitted for publication*.

Mader, M.; de Dios, A.; Shih, C.; Bonjouklian, R.; Li, T.; White, W.; Lopez de Uralde, B.; Sanchez-Martinez, C.; del Prado, M.; Jaramillo, C.; de Diego, E.; Martin Cabrejas, L.M.; Dominguez, C.; Montero, C.; Shepherd, T.; Dally, R.; Toth, J.E.; **Chatterjee, A.**; Pleite, S.; Blanco-Urgoiti, J.; Perez, L.; Barberis, M.; Lorite, M.J.; Jambrina, E.; Nevill, C.R.; Lee, P.A.; Schultz, R.C.; Wolos, J.A.; Li, C.; Campbel, R.M.; Anderson, B.D. "Imidazolyl Benzamidazoles and Imidazo [4, 5-b] pyridines As Potent P38 α MAP Kinase Inhibitors with Excellent in vivo Antiinflammatory Properties", *Bioorg. Med. Chem. Lett.*, *18,* (1), 179-183, **2008**.

Li, H.-Y.; Wang, Y.; McMillen, W.T.; **Chatterjee, A.**; Toth, J.E.; Mundla, S.R.; Voss, M.; Boyer, R. D.; Sawyer, J.S. "A Concise Synthesis of Quinazolinone TGF-β RI Inhibitor through One-Pot Three-Component Suzuki-Miyaura/Etherification and Imidate-Amide Rearrangement Reactions", *Tetrahedron, 63*, (47), 11763-11770, **2007**.

Hudack, R.A., Jr.; Barta, N.S.; Guo, C.X.; Deal, J.G.; Dong, L.; Fay, L.K.; Caprathe, B W.; **Chatterjee, A.**; Vanderpool, D.; Bigge, C.F.; Showalter, R.; Bender, S.L.; Augelli-Szafran, C.E.; Lunney, E.; Hou, X. "Design, Synthesis and Biological Activity of Novel Polycyclic Aza-Amide FKBP12 Ligands", *J. Med. Chem., 49*, (3), 1202-1206, **2006**.

Wang, X.; Mader, M.M.; Toth, J.E.; Yu, X.; Jin, N.; Campbell, R.M.; Smallwood, J.K.; Christe, M.E.; **Chatterjee, A.**; Goodson, T., Jr.; Vlahos, C.J.; Matter, W.F.; Bloem, L.J. "Complete Inhibition of Anisomycin and UV Radiation but Not Cytokine Induced JNK and p38 Activation by an Aryl substituted Dihydropyrrolopyrazole Quinoline and Mixed Lineage Kinase 7 Small Interfering RNA", *J Biol. Chem., 280*, (19), 19298-19305, **2005**.

Hu, L.-Y.; Ryder, T.R.; Rafferty, M.F.; Siebers, K.M.; Malone, T.; **Chatterjee, A.**; Feng, M.R.; Lotarski, S.M.; Rock, D.M.; Stoehr, S.J.; Taylor, C.P.; Weber, M.L.; Miljanich, G.P.; Millerman, E.; Szoke, B.G. "Neuronal N-Type Calcium Channel Blockers: A series of 4-piperidinylaniline Analogs with Analgesic Activity", *Drug Des. Discovery*, *17*, 85-93, **2000**.

Bhattacharyya, S.; **Chatterjee, A.**; Williamson, J.S., "Reductive Amination with Zinc Borohydride. Efficient, Safe Route to Fluorinated benzylamines", *Syn. Comm*., *27*, (24), 4265-4274, **1997.**

Bhattacharyya, S.; **Chatterjee, A.**; Williamson, J.S. "An Efficient, Safe and Convenient One-Step Synthesis of β-Phenethylamines via Reductive Amination Reaction Utilizing Ti(OiPr)$_4$ and NaBH$_4$", *Synlett*, *10*, 1079-1080, **1995**.

Chatterjee, A.; Bhattacharyya, S.; McChesney, J.D.; ElSohly, H.N.; Williamson, J.S. "Preparation of 7-Triethylsilylbaccatin III Using A Regioselective Reductive Deacetylation", *Nat. Prod. Lett.*, *6*, 139-145, **1995**.

Bhattacharyya, S.; **Chatterjee, A.**; Duttachowdhury, S.K. "Use of Zinc Borohydride in Reductive Amination : An Efficient Method for *N*-Methylation of Amines", *J. Chem. Soc., Perkin Trans. 1*, 1-2, **1994**.

Chatterjee, A.; Williamson, J.S.; Zjawiony, J.K.; Peterson, J.R. "Synthesis of A Photoreactive Taxol Side Chain", *Bioorg. Med. Chem. Lett.*, *2*, (1), 91-94, **1992**.

PATENTS

Chatterjee, A.; Goodson, T. Jr.; Mader, M. M.; Toth, J. E.; "Mixed Lineage Kinase Modulators**",** WO 2004048383 (**2004**).

Guo, C. X.; Augelli-Szafran, C. E.; Barta, N. S.; Bender, S. L.; Bigge, C. F.; Caprathe, B. W.; **Chatterjee, A.**; Deal, J. G.; Dong, L.; Fay, L. K.; Hou, X.; Hudack, R. A. " Preparation of diazabicyclo[3.3.1]nonane derivatives as FKBP-Binding Ligands" WO 2002089806 (**2002**).

Booth, R. J.; **Chatterjee, A**.; Malone, T. "Preparation of 2-amino-8H-pyrido[2,3-d]pyrimidin-7-ones as cyclin dependent kinase inhibitors for treatment of neurodegenerative disease" WO 2001055148 (**2001**).

POSTERS AND ORAL PRESENTATIONS

Chatterjee, A.; Cutler, S. J.; Doerksen, R. J.; Khan, I. A.; Williamson, J. S. "Identification of novel, selective CDK5/p25 inhibitor: Structure based virtual screening, synthesis, biological evaluation and SAR studies", poster presentation at ACS Fall National Meeting, Indianapolis, Indiana, September, **2013**

Chatterjee, A.; Doerksen, R.J.; Cutler, S.J.; Khan, I. A.; Dasmahapatra, A.; Williamson, J. S. "Synthesis and Binding Studies of A Photoactive Taxol Derivative", oral presentation at MALTO Meeting, Louisiana, May **2011**

Hu, L.Y.-; Ryder, T.R.; Rafferty, M.F.; Malone, T.; Song, Y.; **Chatterjee, A.**; Taylor, C.P.; Feng, M.R.; Lotarski, S.M.; Schmidt, J.J.; Rock, D.M.; Siebers, K.M.; Stoeher, S.J.; Weber, M.L.; Miljanich, G.P.; Millerman, E.; Szoke, S.G.; Wang, Y.-X. "Design and Synthesis of Orally

Active N-Type Calcium Channel Blockers with Analgesic Activity" oral presentation at Midwest ACS Regional Meeting, St. Louis, MO, October **2000**

Chatterjee, A.; Malone, T.; Wang, K.; Caprathe, B.; Nath, R.; Probert, A.; Dutta, S.; Augelli-Szafran, C.; Hamilton, H.; Gogliotti, R.; Lunney, B. "A Novel Benzothiophene Series of Selective CDK5 Inhibitors: Analogs of PD 0177817", poster presentation at 5th annual Drug Discovery Symposium, Ypsilanti, MI, October **2000**

Barta, N. S.; Bigge, C.; Caprathe, B.; Carroll, R.; **Chatterjee, A.**; Fay, L.; Hudack, Jr., R. A.; Lunney, E.; Bender, S.; Deal, J.; Dong, L.; Guo, C.; Hou, X.; Kissinger, C.; Pelletier, L.; Schachtschabel, U.; Showalter, R.; Vanderpool, D.; Villafranca, E. "Structure-Activity Relationship of Novel Tetracyclic Azaamide Neuroimmunophilins", poster presentation at 5th annual Drug Discovery Symposium, Ypsilanti, MI, October **2000**

Chatterjee, A.; Geer, J.; Malone, T. C.; Rafferty, M. F. "Diazabicyclic Derivatives as N-type Calcium Channel Blockers", poster presentation at 4th annual Drug Discovery Symposium, Ypsilanti, MI, October **1999**

Chatterjee, A.; Booth, J.; Brogly, L.; Campbell, G.; Cody, W.; Geer, J. J.; He, J.; Hu, L.-Y.; Lescosky, L.J.; Malone, T.; Miljanich, G.; Nadasdi, L.; Rafferty, M.F.; Rock, D.; Sercel, A.; Silva, D.; Stoehr, S.; Song, Y.; Szoke, B.G.; Hornoch, K. T.; Taylor, C.; Urge, L.; Weber, M.; Vartanian, M. "PD151307 Analogs: Investigation of Tyrosine (OBn) Modified Derivatives as N-Type Calcium Channel Blockers" poster presentation at 217 national meeting of American Chemical Society, Anaheim, California, March, **1999**

Chatterjee, A.; Bhattacharyya, S.; McChesney, J.D.; ElSohly, H.N.; Williamson, J.S. "Production of 7-Triethylsilylbaccatin III Using A Regioselective [$CH_3(CH_2)_3$]NBH_4 Reducing System", poster presentation at 46th Southeast Regional Meeting of American Chemical Society, Birmingham, AL, October **1994**

Chatterjee, A.; Zjawiony, J.K.; Williamson, J.S. "Synthesis and Tubulin Activity of A Photoactive Taxol Derivative", oral presentation at Joint Meeting of the South Central Branch, American Society for Microbiology and the Mid-South Biochemists, Starkville, MS, November **1992**

Chatterjee, A.; Peterson, J.R.; Zjawiony, J.K.; ElSohly, H.N.; Williamson, J.S. "Synthesis and Binding Studies of A Photoactive Taxol Derivative", oral presentation at MALTO Meeting, Arkansas, May **1992**

Chatterjee, A.; Williamson, J.S.; Zjawiony, J.K.; Peterson, J.R. "Design and Synthesis of A Photoreactive Taxol Analog - A Chemical Probe for Establishing the Taxol Binding Site(s) with Tubulin", poster presentation at American Association of Pharmaceutical Scientists Annual Meeting, Washington D.C., November **1991**

Chatterjee, A.; Williamson, J.S.; Zjawiony, J.K.; Peterson, J.R. "Design and Synthesis of A Photoactive (9'-azido-) Taxol - A Probe for Establishing the Taxol Binding Site(s) with Tubulin", oral presentation at MALTO Meeting, New Orleans, Louisiana, May **1991**